STRENGTHENING OF CONTAINER GLASSES AND RELATED COMPOSITIONS

by

Kajal K Mallick

A thesis submitted for the degree of

Doctor of Philosophy

of the

University of Warwick

Department of Physics

University of Warwick

April 1995

PAGE NUMBERING AS ORIGINAL

To my family

SUMMARY

Several methods of strengthening, including surface precipitation of low solubility particles, vapour treatment, ion-exchange, chemical vapour deposition (CVD) and combination treatments, have been investigated to improve the pristine strength of commercially available container and related glass compositions; their relative applicability in container manufacture has also been evaluated and discussed. As a part of this, a wide range of soda lime silica compositions, that includes typical container glass specifications, have been investigated to study their crystallisation behaviour in terms of the effect of nucleating agent, viscosity, time and temperature.

Significant flexural strength enhancement of 16 to 163 % has been achieved for the processes studied, with a maximum of ~ 500 MPa and ~ 400 MPa for glasses using lithium ion exchange and exposure to LiBr and/or $AlBr_3$ vapour respectively. Treatment times are short, compared to those currently used in industry. The mechanism of strengthening relies on surface compression by production of a glass skin or surface crystallised phase(s) having a low thermal expansion coefficient than the bulk of the glass.

The physical properties of the glasses have been characterised by differential thermal analysis (DTA) and X-ray diffraction (XRD) as well as other methods such as high temperature viscometry and dynamic secondary ion mass spectroscopy (SIMS).

CONTENTS

LIST OF TABLES AND FIGURES

TABLES

FIGURES

ACKNOWLEDGEMENTS

In presenting this thesis, I would particularly like to thank Dr Diane Holland for her supervision, invaluable advice and continual encouragement throughout the course of this investigation.

My sincere thanks are due to Professor Harold Rawson, Dr S P Jones of Emhart (UK) Limited and Dr B Hamilton of Rockware Glass Limited for their contribution both as co-ordinators of the IPGR (International Partners in Glass Research) programme and for stimulating discussions on a number of occasions; Mr C Hamlin of Rockware Glass Limited for providing a steady supply of glass containers.

Assistance from Dr A Chew of Loughborough Consultancy for providing SIMS profiles is gratefully acknowledged as are GPD Laboratory Services of ACI, Australia for feasibility data on selected glasses.

I would also like to thank Mr R Lamb (Bob) and Mr H Mathers (Harold) for their tremendous help and co-operation in building various in-house apparatus required for this work.

The International Partners in Glass Research (IPGR) is acknowledged for the Research Fellowship for the duration of the project and for granting permission to publish the research findings.

Finally, my special thanks extend to my wife for her patience, loving support and encouragement throughout the course of this work.

DECLARATION

This thesis is submitted to the University of Warwick in support of my application for the degree of Doctor of Philosophy. It contains an account of my own research carried out at the Department of Physics during the period April 1985 to August 1988. It is presented according to the guidelines of the Department of Physics, Phys/PG3. The work described in this thesis is the result of my own research, except where specifically acknowledged in the text.

Chapter 1

INTRODUCTION

1.1 HISTORICAL PERSPECTIVE

Although glass always existed as naturally occurring minerals, it was not until around 6000 years ago in Mesopotamia and Egypt that man-made oxide glasses appeared in the form of decorative glazes. The development of the thriving art of glass making, since the first century AD, spread throughout the countries of the Roman empire and the many archaeological artefacts of Venetian origin are a fine testament to this endeavour. Control of glass compositions, during this era, was entirely empirical and most pre-seventeenth century glass articles were made of mainly silica/alkali/lime with coloured glasses containing oxides of cobalt, iron or chromium. This situation greatly improved with the understanding of the chemistry of the elements and, from 1670 onwards, more and more scientific and technological advances were made in the control of the composition and properties of glasses, thus extending the diversity of glass usage which continues today. This is illustrated in an excellent review by Rawson[1]. In recent times however, glasses have become used in many diverse and far-reaching applications that include architecture, transportation, engineering, electronics, telecommunications and aerospace industries. An example of a most notable present day success is found in its use as optical fibres which has revolutionised the telecommunications industry and the general field of optoelectronics. Glass is now recognised as one of the most important materials known. The typical compositions of some commercially available glasses are shown in Table 1.1. On a more day-to-day basis, container glass forms one of the most widely

manufactured types of glass. Its appeal is due primarily to its excellent transparency, its potential to be formed in various types, forms and colours so as to be aesthetically pleasing, its chemical durability and relatively low cost of manufacture. In recent years the glass container industry has had to respond to intense competition from other packaging materials such as polymers, papers and metals. Consequently, the industry has focused to offset, in particular, the high cost of transportation, as well as the risk of breakage during on-line handling, by improving the *lightweighting* or strength to weight ratio of container glasses. This adds to its other cost advantages, such as cheap raw materials and ease of

TABLE 1.1
TYPICAL COMPOSITIONS OF SOME COMMERCIAL GLASSES
(after Rawson[1])

wt %	SiO_2	Al_2O_3	B_2O_3	MgO	CaO	BaO	ZnO	PbO	Na_2O	K_2O	TiO_2	La_2O_3	Ta_2O_5	ThO_2	Others
1	72.2	1.9	-	1.5	9.6	-	-	-	14.6	-	-	-	-	-	0.2
2	72.0	1.3	-	3.5	8.2	-	-	-	14.3	-	-	-	-	-	0.7
3	71.5	2.0	-	2.8	6.6	-	-	-	15.5	1.0	-	-	-	-	0.6
4	56.0	-	-	-	-	-	-	29.0	2.0	13.0	-	-	-	-	-
5	75.5	2.6	16.0	-	-	-	-	-	3.7	1.7	-	-	-	-	0.5
6	61.3	0.2	2.2	-	4.6	-	-	2.9	14.4	7.0	-	-	-	-	0.4
7	29.2	2.5	-	-	-	-	-	63.3	0.5	-	4.0	-	-	-	0.5
8	-	-	20.0	-	-	-	-	-		-	-	36.0	28.0	16.0	-
9	5.5	17.5	16.0	-	9.0	52.0	-	-		-	-	-	-	-	-
10	5.0	-	17.0	-	-	-	14.0	64.0		-	-	-	-	-	-

1. Container glass
2. Window glass
3. Lamp bulbs
4. Lead crystal
5. Tungsten sealing
6. Optical glass - low refractive index
7. Optical glass - high refractive index (1.78)
8. Optical glass-high refractive index (1.85) with very low dispersion
9. Sodium vapour resistant
10. Solder glass

recycling, over other packaging materials. However, in order to maintain cost effectiveness and market lead, the prerequisites to manufacture lightweight glass containers are

- to maintain the forming conditions essentially the same as current industrial practice
- to ensure that any strengthening technique developed does not sacrifice an already existing and well established process which is both fast and efficient
- to retain the recyclability of glass containers

To this end, most research effort to date is concerned with a number of strengthening techniques, described in later chapters. Most significantly however, in 1985 an US based multinational consortium, known as International Partners in Glass Research (IPGR), of the major glass container industry companies worldwide was formed. Their aim was to pool all the expertise available in the field of glass science and technology in order to solve, cost effectively, the common problems faced by the industry. The target of this multi-million dollar research programme was to develop glass containers that will be ten times stronger and half the weight of those currently in use and also to reverse the trend towards increasing use of plastic, metal and composites in food and beverage packaging by shifting the competitive edge back to glass. The research work described in this thesis formed a major part of the IPGR programme in the UK.

Although thermally-toughened glass production methods are widely used, another form of strengthening in the container and float glass industry is that primarily achieved by exchange of K^+ For Na^+ and Na^+ for Li^+, carried out in a molten salt bath, resulting in a surface compression layer. Unfortunately, such processes are difficult to introduce in a production line and are of limited practical utility as most of the glass compositions developed for this purpose are opaque after strengthening. They are also relatively refractory, with softening points in excess of 900 °C, adding to the forming difficulties. Furthermore, the ion exchange temperatures, in excess of 850 °C (Appendix I), are extremely dangerous. However similar processes are in use in Japan with moderate

strength increase. For example, the Yamamura Glass Company has successfully developed and utilised a method of chemically strengthening returnable and non-returnable glass containers. In the US and the Europe, chemically strengthened glass has filled a niche market, particularly in the area of architectural glass products.

1.2 AIMS OF RESEARCH

The main aim of this project was to produce strengthening of container glasses and related compositions. The work is based on simple and on commercial silicate glass compositions including a range of soda lime silica glasses. Specific objectives were

- to establish viable compositional changes for container and related glasses
- to explore several routes for strengthening
- to investigate the general nature of the crystallisation behaviour of container and related glasses
- to assess and investigate the control parameters needed for strengthening by surface compression

1.3 LAYOUT OF THESIS

Chapter 1 is a brief introduction, with a historical perspective, of the work and outlines the overall aims of the research undertaken.

Chapter 2 describes the theory and background of this research. It also presents a survey of current knowledge and reviews and discusses the overall information covering

the principles of glass formation, general physical and chemical properties, crystallisation behaviour and strengthening of glasses.

Chapter 3 is a description of the techniques used in this work for the preparation of glasses and indicates the means by which specific glass compositions, with predetermined forms such as rods or plates, can be obtained. This is combined with a commentary on the principle and practice of the various characterisation methods used, in order to gain an understanding of the underlying physical and mechanical properties of the glasses.

Chapter 4 is a detailed account of the general experimental methods employed indicating various control parameters necessary to realise the objectives of the programme.

Chapter 5 presents the results and discussion of experiments relating to thermal, compositional and structural properties, along with the crystallisation behaviour of container and related glass compositions. This includes the study of the modes of surface crystallisation in these glasses relevant to their subsequent strengthening.

Chapter 6 presents and discusses the results of various strengthening methods employed to achieve strength enhancement. In particular, it discusses the relative merits and demerits of these processes in relation to their practical use.

Chapter 7 is a brief report of the limited field trials undertaken.

Chapter 8 summarises the conclusions drawn from the present investigation as a whole. Future work is suggested in order to achieve further understanding and to explore possible avenues to the additional strength enhancement of container and related glasses.

Chapter 2

THEORY AND BACKGROUND OF RESEARCH

2.1 INTRODUCTION

This Chapter gives a brief overview of those theories relevant to the scope of the present investigation. The aim is to provide some understanding of the processes employed in the present work although, generally, detailed analysis of the theories has been avoided.

2.2 THEORIES OF GLASS FORMATION

Amorphous solids are characterised by the existence of a state in which the atomic or molecular arrangement lacks the long range periodicity typical of crystals, and exhibits short range order only. The terms 'vitreous' and 'glassy', widely used in scientific research, are considered to be synonymous and are descriptive of a restricted class of amorphous materials. A qualitative understanding, as to why glasses are obtained on melting of only certain compositions, can be gained when the crystallisation processes occurring on cooling liquids are considered.

It is widely acknowledged that formation of a glass depends as much on its chemical composition as on the rate of cooling. In this regard, two general theories of

glass formation have been developed to describe the conditions under which the glassy state can be realised. The first deals with the kinetics of crystallisation below the melting point viz. the rate controlling processes of nucleation and crystal growth. The second type comprises structural theories which consider the geometrical (dimensional) arrangement of the constituent atoms. The former theory is relevant to the present work and although no structural work has been carried out here, a brief description of common structural theories of glass formation will also be presented.

2.2.1 KINETIC THEORY

The process of crystallisation occurs in all liquids or melts by structural rearrangement, where an atom or molecule becomes separated from the liquid structure and attaches itself to the surface of a crystal nucleus. The crystal nucleus can be generated either homogeneously (that is by random thermal fluctuation of the melt) or heterogeneously (as a result of foreign particle additions or at a liquid surface). Thus, when a liquid is cooled below its freezing point, crystallisation does not occur by an instantaneous or homogeneous transformation but by the growth of crystals, at a finite rate, from a number of centres or nuclei. In order for a material to remain glassy on cooling, the rate of formation of nuclei and/or the rate of crystal growth must be low. Although a decrease in free energy occurs when the volume of the material forming the nucleus transforms from the liquid to crystalline state, the formation of a crystal/liquid interface at the nucleus surface involves a free energy increase. If this is greater than the volume free energy decrease associated with crystallisation, the nucleus will be unstable. Thus, stable nuclei form at a detectable rate only when the liquid is supercooled to below the liquidus temperature, depending on the relative magnitudes of the free energies of both the interface and of crystallisation. Thus a kinetic theory of glass formation was developed

by considering the rates of nucleation and of crystal growth. Staveley[2] derived the following equation for the rate of nucleation

$$I = A.\exp(-W^* / RT)\exp(-\Delta G_b / RT) \qquad \text{....(2.1)}$$

I = the number of stable nuclei formed per cm^3 of liquid per second

T = temperature in K

R = gas constant

A = constant, characteristic of composition

ΔG_b = activation energy for the process controlling the liquid-crystal structural rearrangement

W^* = $16\pi\sigma^3 V_m^{\,2} / 3\Delta G^2$ where σ is the energy per unit of crystal-liquid interface (surface energy)

V_m = molar volume

ΔG = decrease in free energy per mole when the liquid crystallises

The first exponential term involving W^* gives the probability of forming a nucleus of the critical size at the temperature T, and W^* has been termed by Turnbull and Cohen[3] *the thermodynamic barrier* to nucleation where $16\pi/3$ (for a spherical nucleus) is a numerical factor depending on the shape of the nucleus. The second exponential term, ΔG_b, governs the rate at which the particles in the liquid transfer to the crystal nucleus. This free energy of activation was termed by Turnbull and Cohen *the kinetic barrier to nucleation.*

The rate of nucleation, I, shown in equation 2.1 is zero at the melting temperature, rises to a maximum at some temperature below the melting temperature and then drops to zero. Thus, sufficiently rapid cooling of the melt through the nucleation region can prevent crystal growth. With further cooling, the structure of the melt becomes unable to

relax rapidly enough to be in equilibrium with the decreasing temperature, eventually reaching the point where the viscosity of the liquid has increased to such an extent that the *liquid-like* structure may be described as *frozen-in*. The temperature at which the structure departs from its equilibrium is called the transition temperature, T_g. Consequently, the rate of cooling will determine the structure of the glass. Cooling below T_g, the supercooled liquid becomes a glass and, due to the greatly increased viscosity, behaves like a solid.

The formula for the rate of crystal growth is expressed by the Hillig-Turnbull equation[4]

$$u = a_o.\gamma \exp(-\Delta G^{'} / RT)(1-\exp\langle v\Delta G_v / RT\rangle) \qquad \text{....(2.2)}$$

a_o = interatomic distance

γ = vibrational frequency of atoms at the nucleus-liquid interface

$\Delta G^{'}$ = activation energy controlling the rate at which structural units detach themselves from the liquid structure and attach to the surface of the growing crystals (*kinetic barrier to growth*)

v = volume per formula unit

$\Delta G_v = \Delta G/V_m$

The equation 2.2 is commonly described as a *normal growth model* where $\Delta G^{'}$ acts as a kinetic barrier to growth.

As a result of high undercooling below the liquidus i.e. $\Delta G_v >> RT$, the growth rate becomes

$$u = a_o.\gamma \exp(-\Delta G^{'} / RT) \qquad \text{....(2.3)}$$

Although both $\Delta G'$ and ΔG will vary with temperature, it is assumed here that kinetic barriers to nucleation and growth for a given composition at a given temperature are equal (i.e. $\Delta G' = \Delta G$).

2.2.2 STRUCTURAL THEORIES

As far back as 1926, Goldschmidt[5] put forward, using the radius-ratio rule, an empirical formula suggesting that a tetrahedral arrangement of oxygen anions around a given cation is a pre-requisite for glass formation. However this theory is limited since it was based on the assumption that purely ionic bonds were involved. Obviously this is not strictly so, for many of the glass forming oxides are strongly covalent in nature. Later, Zachariasen[6] amplified Goldschimdt's views and developed the *random network hypothesis*. He postulated a set of rules for glass formation based on structural energy considerations and proposed the following four major conditions that an oxide M_2O_n must obey, if it is to be considered a glass former:

(i) no oxygen atoms may be linked to more than two atoms of M

(ii) the number of oxygen atoms surrounding M atoms must be three or four i.e. the structural unit must be MO_3 or MO_4

(iii) the metal-oxygen polyhedra share corners, not edges or sides with each other

(iv) at least three corners in each polyhedron must be shared

The structural implications of these rules are illustrated in Figures 2.1(a) and (b), which show the two-dimensional representation of the arrangement of atoms in both polycrystalline and glassy forms of a hypothetical compound M_2O_3. The author suggested

that the glassy and crystalline forms of an oxide should be similar in the type of structural group they contain and in the way the groups are joined together, the only difference between the two forms being that the arrangement of atomic groups in a crystalline material is regular whilst in the glassy form the arrangement is irregular.

Warren[7] determined the structure of simple silicate glasses (SiO_2 and Na_2O-SiO_2) using X-ray diffraction. The structural model he suggested was in agreement with that of Zachariasen and postulated that glass is a three dimensional network of atoms lacking symmetry and long range order. The model was based on a continuous network of SiO_4 tetrahedra with sodium ions filling the interstices within the network. In fused silica each oxygen atom is bonded to two silicon atoms, whereas in sodium silicate glasses extra oxygens are introduced as Na_2O. Thus certain oxygen atoms act as bridging oxygens whilst others are bonded only to one silicon atom and are termed non-bridging oxygens. The charge neutrality is preserved by the sodium atoms in the interstices of the network. This is illustrated in Figure 2.2.

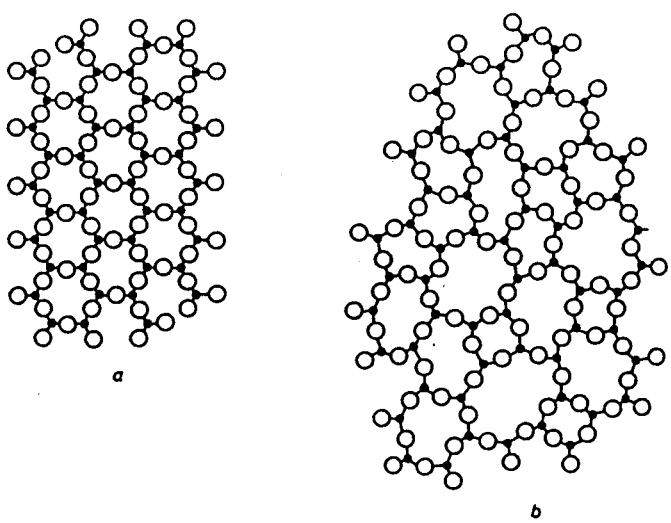

Figure 2.1 Structure of an hypothetical Compound M_2O_3 in
(a) Crystalline form
(b) Vitreous form

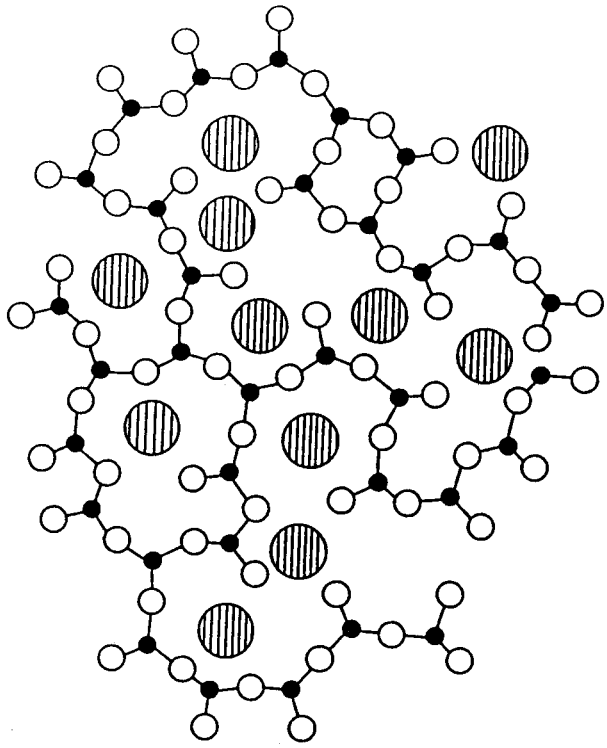

Figure 2.2 Structure of Na_2O-SiO_2 glass

• **silicon**
O **oxygen**
sodium

Goodman[8], has proposed a strained mixed cluster model for glass structure. The model develops a phase diagram approach and defines polymorphism as a prerequisite for glass formation. The theory postulates that, on cooling below the freezing point, clusters of atoms (quasi-crystallites) are formed. Goodman argued on thermodynamical grounds that, for the silica system, such quasicrystallites of cristobalite, tridymite and quartz would form on cooling just below the freezing point. Brownian motion would cause random collision between the quasi crystals. In the case where two dissimilar quasicrystals come together, the interface produced would be highly strained. As further collisions occur, the free energy of the assembly increases further. This decreases the driving force for nucleation. Consequently, crystallisation would not occur. Such progressive build up of

strained mixed cluster agglomerates would continue to impede nucleation as temperature decreases but the presence of an increasingly extended structure in the liquid would cause an increase in viscosity. At a given time, the overall structure would change from a liquid, containing discrete agglomerates to a continuous solid phase with liquid trapped at interstices. The conversion represents T_g. As cooling continues, the residual liquid is deposited onto the strained clusters; the very last material to freeze contains a concentration of vacancies and residual impurities. Goodman used these ideas to suggest the following rules of glass formation by a particular system:

(i) It must show at least two polymorphic forms in the solid state

(ii) It must be capable of being melted i.e. glass can only be formed from the liquid state

(iii) The polymorphic forms must not be capable of forming low strain interfaces with each other

(iv) Bond strength should be high but relative elastic constants small

The theory is able to explain T_g but still needs to be verified experimentally on a range of compositions. The model also fails to predict glass formation in the borate systems.

2.3 CRYSTALLISATION

Essentially, the process of crystallisation originates from the following types of phase transformations commonly observed in glass and is shown below in Figure 2.3.

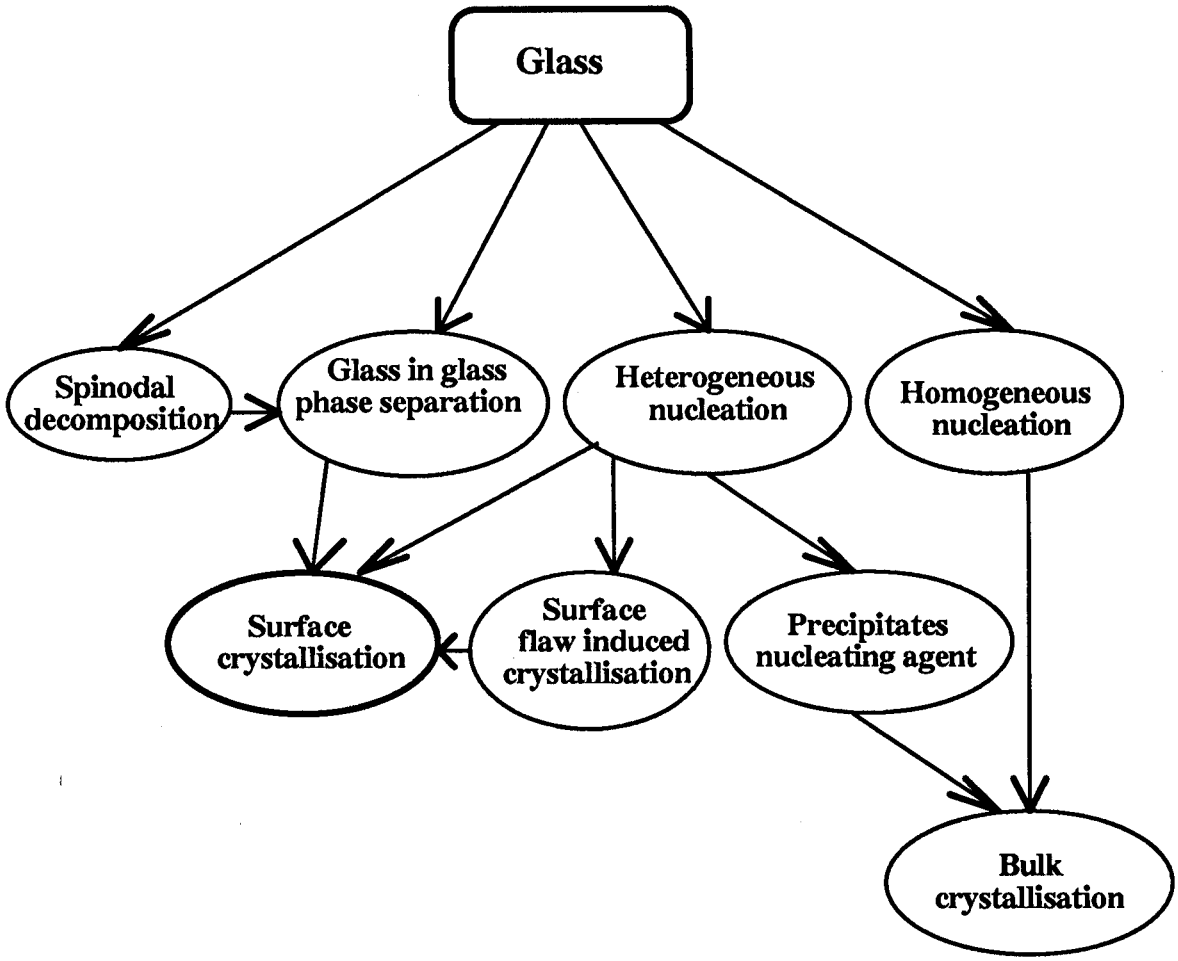

Figure 2.3 Flowchart for crystallisation process in glass

Crystallisation involves nucleation and growth of crystal phase(s) which may or may not conform to the same composition as the original liquid or melt. Both surface and volume crystallisation form the general scenarios of this process.

2.3.1 VOLUME CRYSTALLISATION

Crystal growth in volume crystallisation begins from preferred nucleation sites within the body of the glass. These sites may simply be material(s) foreign to the bulk of

the material and the process is known as heterogeneous nucleation, whereas if the nucleus is the same as the bulk material, the process is termed homogeneous nucleation.

2.3.2 LIQUID-LIQUID PHASE SEPARATION

This involves the growth of non crystalline phases having different composition from the original phase.

2.3.3 SPINODAL DECOMPOSITION

This type of decomposition occurs in a region which separates into two liquid phases where there is no energy barrier to nucleation and hence phase separation is limited only by diffusion.

2.3.4 SURFACE CRYSTALLISATION

Surface crystallisation is, as mentioned earlier, a type of phase transformation in glass where crystal growth begins or nucleates at the glass/atmosphere interface and usually grows perpendicular to this interface. This can be achieved by simple heat treatment in air. If this produces a surface crystallised layer which has a lower thermal expansion than that of the bulk glass, then on cooling the glass from the crystallisation temperature, the interior attempts to contract more than the surface and so places the surface in compression.

In the present work, the phenomenon of surface crystallisation has been investigated to demonstrate that surface crystallisable container glasses will show greatly improved mechanical strength (results and discussion in Chapter 5) and to develop routes by which such materials may be obtained. The three major routes are

(i) destabilisation of the bulk glass by a composition change

(ii) destabilisation by introduction of a low solubility component

(iii) alteration of the glass surface after fabrication to render it crystallisable

The routes, (i) and (ii) in particular, were aimed at selectively surface crystallising "desirable" crystal phases to give surface compression and also to determine the kinetics of the crystallisation processes, considered to be a very important factor in ultimately deriving a process suitable for insertion in a production line. The work has therefore been concentrated on modifying the existing container glass compositions and on examining some simple ternary Na_2O-CaO-SiO_2 (referred to hereafter as NCS) systems in an attempt to understand the phase development process. The results presented in Section 5.4.2 also examine the effect of nucleating agents on the NCS systems and will be shown to be important, in later Chapters, in developing the third route to surface crystallisation i.e. surface modification.

2.3.5 LITERATURE REVIEW OF SURFACE CRYSTALLISATION IN SODA LIME SILICA AND RELATED GLASSES

Early work on surface crystallisation was carried out by Tabata[9] for several glasses that included flint, borosilicate and soda lime silica. He concluded that the degree of crystallisation is related to defects such as cracks and craters on the surface of the glass.

Although Morey[10] studied a large number of soda lime silica glass compositions, he failed to observe crystallisation around internal bubble surfaces and assumed that surface crystallisation was due to compositional variations caused by selective volatilisation from the external surfaces.

Swift[11] demonstrated that the glass specimens with unclean or dirty surfaces in the soda lime silica system showed a considerably higher degree of crystallisation than clean specimens.

It was suggested by Scott and Pask[12] that the surface crystallisation of $Na_2O.2SiO_2$ glasses was due to NaOH crystals which developed by reaction with water vapour. Specimens which were heat treated in vacuum or dry air did not exhibit any crystallisation. Internal bubbles were also found to be free of crystals.

Klingsberg[13] studied crystallisation of $BaAl_2Si_2O_8$ (celsian) in a BaO-Al_2O_3-TiO_2-SiO_2 glass and concluded that bubbles act as preferred nucleating sites for the process of crystallisation. However, no evidence was presented for nucleation on all bubbles.

Neely and Ernsberger[14] observed that crystal nucleation occurred only on a few bubbles in soda lime silica glasses melted at low temperatures and that the internal crystallisation was increased in specimens doped with undissolved powdered garnet or alumina. Glasses melted at higher temperatures showed only surface crystallisation since the powders had dissolved. The authors suggested that selective evaporation and contamination with solid particles caused external surfaces to crystallise more readily.

Bergeronand and De Luca[15] detected crystallisation of $PbTiO_3$ on both the external surface and some internal bubbles in a PbO-B_2O_3-SiO_2-TiO_2 glass. Following a treatment at 400 °C for 4 hours, crystallisation appeared in bubbles that were previously crystal free. They concluded that crystals grew preferentially at bubble surfaces.

Mattox[16] reported preferential crystallisation, in a CaO-Al_2O_3-B_2O_3 glass, originating from bubbles containing graphite particles acquired from the mould. The author noted, however, that crystal growth, which hides the devitrification centres, made it difficult to detect precisely the contamination in the centres.

Burnett and Douglas[17] investigated the number of $BaO.2SiO_2$ spherulites initiating from the Rh/Pt container surface after the molten glass was quenched directly to the heat

treatment temperature. They also determined the nucleation rates of the spherulites in a Na_2O-BaO-SiO_2 glass.

Strnad and Douglas[18] studied the crystallisation kinetics of three glass compositions in the Na_2O-CaO-SiO_2 system with 55, 57.5 and 60 mole % SiO_2. The authors determined the surface and internal nucleation rates after a heat treatment at 850 °C as a function of rate of undercooling and concluded that smaller undercooling is required to induce surface nucleation than is required for internal nucleation.

Du et al[19] investigated the kinetics of phase separation of soda lime silica glasses with minor P_2O_5 addition (< 2 wt %) and described the growth kinetics of the second phase particles by a term involving the one sixth power of time for the initial growth. In addition, the authors also found that the time for the coalescence of discrete particles is prolonged with the P_2O_5 addition due to an increase in glass viscosity.

Bansal and Doremus[20] studied the crystallisation kinetics of a mechanically polished Sr-Ba-La-F glass heat treated at 322-390 °C when spherical crystals of up to 10 μ m developed and the number of crystals appeared to be time and temperature dependent.

Zanotto et al[21] determined the detailed kinetics of both crystal nucleation and liquid phase separation in a series of BaO-SiO_2 glasses. The authors concluded that the surfaces of amorphous droplets do not catalyse nucleation since crystal nucleation rate is affected only by compositional changes, having established lack of any relationship between the surface area of the amorphous droplets and the internal crystal nucleation rate.

Zanotto and Basso[22] studied an almost stoichiometric diopside glass heated to 820 °C from 1-4 hours and found that the nucleation rate of diopside crystals was too high to be detectable and originated from a fixed number of particular sites on the external glass surface.

Recently, surface crystallisation kinetics have been investigated by Zanotto[23] for soda lime silica glasses which showed the nucleation efficiency of foreign particles as a

function of both parent glass and crystallising phase viz. enhanced nucleation rates at the external surfaces being the result of the catalytic effect of solid impurity particles and faster diffusion rates.

Hishinuma[24] carried out an extensive investigation with the aim of detecting internal nucleation in $Na_2O.2SiO_2$ and $PbO.SiO_2$ glasses and observed that crystallisation was limited to the external surfaces only and none was detected at the internal bubble surfaces. He also found no evidence of surface crystallisation in $PbO.SiO_2$ glasses which were previously etched with HF.

Stookey et al[25] studied in detail the modes of surface crystallisation in some lithium aluminosilicate glasses and found that β-eucryptite can be successfully formed on the surface of these glasses with layer thickness in the range 80-100 μm at 800-900 °C.

McMillan and Partridge[26-28] investigated the process of surface crystallisation of a range of zinc aluminosilicate glasses and found that a variety of phases can be successfully formed at temperatures not exceeding 850 °C. The major precipitating phases were identified as willemite, albite and stuffed keatite.

In the crystallisation study of calcium zinc aluminosilicate glasses, Adams and McMillan[29] found evidence of willemite as the main crystallisable phase. The same authors also produced surface crystallisation in some binary calcium aluminate glasses.

In summary, the available literature data on surface crystallisation behaviour of the commercial container glass and related compositions is very scarce. This is particularly true in the case of viable methods of surface destabilisation or bulk compositional changes in order to promote surface crystallisation. For convenience, some representative data for surface crystallisable glasses is given in Table 2.1. The table includes the heat treatment protocol employed by the authors cited in the corresponding reference. Compositional details of these glasses can be found in an excellent review by Donald[30].

TABLE 2.1
SUMMARY OF SOME SURFACE CRYSTALLISABLE GLASSES

Glass	Heat Treatment Protocol (°C/h)	Major Crystalline Phase	Nominal Phase Composition	Surface Crystallised Layer Thickness (μm)	Modulus of Rupture (MPa)	Ref
Li_2O-Al_2O_3-SiO_2	890/18	β-eucryptite	$Li_2O.Al_2O_3.2SiO_2$	80	600-700	25
	860/48	β-eucryptite		80	600-700	25
	890/20	β-eucryptite		100	600-700	25
	860/60	β-eucryptite		100	600-700	25
ZnO-Al_2O_3-SiO_2	800-850/2	willemite	Zn_2SiO_4	-	366	26
ZnO-Al_2O_3-SiO_2	800-850/2	willemite		-	708	26
ZnO-Al_2O_3-SiO_2	800-850/2	willemite		-	372	26
MgO-ZnO-Al_2O_3-SiO_2	800-850/2	willemite		-	439	26
MgO-ZnO-Al_2O_3-SiO_2	800-850/2	willemite		-	524	26
MgO-ZnO-Al_2O_3-SiO_2	800-850/2	willemite		-	607-634	26
Li_2O-ZnO-Al_2O_3-SiO_2	750/0.5	-		-	493-551	26
Li_2O-ZnO-Al_2O_3-SiO_2	700/16.7	*stuffed* keatite	$ZnO(ZnO.SiO_2)$	100	670	27
Li_2O-ZnO-Al_2O_3-SiO_2	800/0.5	*stuffed* keatite		100	670	28
Li_2O-ZnO-Al_2O_3-SiO_2	850/0.1	*stuffed* keatite		100	670	28
Li_2O-CaO-ZnO-Al_2O_3-SiO_2	750/0.5	-		-	584	28
Na_2O-ZnO-Al_2O_3-SiO_2	750/50	albite	$Na_2O.Al_2O_3.6SiO_2$	60	300	28
Na_2O-ZnO-Al_2O_3-SiO_2	800/16.7	albite		60	300	28
BaO-ZnO-Al_2O_3-SiO_2	800/9.4	*stuffed* keatite	$ZnO(ZnO.SiO_2)$	90	620	28
BaO-ZnO-Al_2O_3-SiO_2	850/1.9	*stuffed* keatite		90	620	28
TiO_2-ZnO-Al_2O_3-SiO_2	800/9.9	*stuffed* keatite		160	830	28
TiO_2-ZnO-Al_2O_3-SiO_2	850/2.4	*stuffed* keatite		160	830	28
CaO-ZnO-Al_2O_3-SiO_2	800-850/2	willemite	Zn_2SiO_4	-	414-517	26
CaO-ZnO-Al_2O_3-SiO_2	820/1	willemite		11	145	29
CaO-ZnO-Al_2O_3-SiO_2	820/2.5	willemite		40	245	29
CaO-ZnO-Al_2O_3-SiO_2	820/4.3	willemite		49	275	29
CaO-ZnO-Al_2O_3-SiO_2	840/1	willemite		23	180	29
CaO-ZnO-Al_2O_3-SiO_2	840/2.5	willemite		54	283	29
CaO-Al_2O_3	850/3	-		20	510	29
Na_2O-CaO-SiO_2	600-1000/ 1-20	devitrite	$Na_2O.3CaO.6SiO_2$			this work
		cristobalite	SiO_2			
		tridymite	SiO_2			
		wallastonite	$CaO.SiO_2$			
	670/3	tenorite	CuO	30	300	
	500-600 /10*s*-2*min*	β-eucryptite/ β-spodumene	$Li_2O.Al_2O_3.2SiO_2$ / $Li_2O.Al_2O_3.4SiO_2$	20-70	530	

2.4 STRENGTHENING OF CONTAINER AND RELATED GLASS COMPOSITIONS

2.4.1 INTRODUCTION

The operational steps associated with the manufacturing of glass containers involve (a) preparation and charging of batch materials into the melting furnace (b) glass melting (c) forming (d) annealing and finally (e) finishing. The raw materials used are usually in the form of natural quartz sand (Angolan or other grades) for SiO_2, soda ash (Na_2CO_3) for Na_2O, calcined or hydrated potash (K_2CO_3 or $K_2CO_3.1.5\ H_2O$) for K_2O, limestone for CaO, dolomite for CaO and MgO, boric acid and borax or borax dehydrated to pentahydrate for B_2O_3, barium carbonate for BaO, aluminium oxide, hydroxide, feldspar and kaolin or phonolite for Al_2O_3. It is also now a common practice to make use of blast furnace slag containing CaO, SiO_2, Al_2O_3 and sulphides, which offer favourable conditions in melting and refining due to the reducing effect of sulphur. The batch is then fed continuously in one end of continuous tank furnaces and the melted glass is drawn out from the other for subsequent working by the automatic forming machines. In the forming operation, the glass flows from the furnace to a gob feeder which employs a plunger and a pair of mechanical shears to sever a glass gob of required size and weight. This is then conveyed into moulds of the forming machines where ~ 300 bottles per minute can be produced using either a *press and blow*, using a combination of pressing and blowing, or a *blow and blow* using compressed air for both preforming and final forming, the latter of which is universally used in the making of container glass. From this point onwards, two types of coating are applied to the container to protect the pristine surface from subsequent mechanical damage due to on-line handling. The *hot end coating* takes place between the forming machine and the annealing tunnel or lehr, through which all the containers pass in order to relieve them of thermally induced internal stress. The

atmosphere in the chamber contains vapourised metallic salts, usually chlorides, although organometallic compounds can be used. Titanium and tin compounds, capable of being readily volatilised, are most widely used although many industries nowadays use the vapour of anhydrous stannic chloride. At temperatures between 500 and 700 °C, a chemical reaction takes place between the vapour and the glass surface. It is believed that this results in an actual modification of the structure of the glass itself rather than just a superficial coating and thus confers a toughening action. The *cold end coating*, on the other hand, is carried out near the discharge end of the lehr and introduces lubricity to the glass container. Untreated glass surfaces, sliding in contact with one another, display a tendency, especially when wet, to bind together resulting in scratches. To counteract this, coating is usually carried out by spraying the container in the temperature range 60-130 °C with a dilute (up to 0.3 %) aqueous solution of a suitable material and for this purpose, a wide range of substances have been investigated and used. The preferred materials are polyoxyethylene stearates, polyethylene glycols, low molecular weight polythene waxes, silicones and long chain fatty acids. However, the basic problem with the surface coating treatment of glass containers by these methods lies in the difficulty of monitoring treatments so that a coating of the correct thickness can be applied to the whole surface of the containers and also the general cost of the whole process can be high.

2.4.2 MECHANICAL STRENGTH OF GLASS

At temperatures less than the transformation temperature, T_g, glass exhibits the typical brittle behaviour of solids where elastic response predominates upto the breaking point without any significant macroscopic ductility. The strength of glass can be considered from two aspects. The first is the theoretical strength which has been estimated by Kelly[31] to be of the order of a tenth of the Young's Modulus, E. The second is the

practical strength which is significantly lower than the theoretical value. This can be explained in terms of defects in the glass. In particular, flaws at the surface act as stress concentrators and thereby limit the theoretical strength in the event of local stress being applied. The weakening effect of flaws was originally described by Inglis[32] who showed that the maximum stress, σ_m, at the tip of an *elliptical critical flaw* can be described as

$$\sigma_m \approx 2\sigma (c/\varrho)^{1/2} \qquad \text{....(2.4)}$$

where σ is the applied stress, c the half length of elliptical flaw and ϱ the radius of curvature of the flaw tip. Griffith[33,34] further developed this idea into the now well known theory which gives the following relationship

$$\sigma = (2E\gamma / \pi c)^{1/2} \qquad \text{....(2.5)}$$

where σ is the applied stress, E the Young's Modulus and γ the fracture surface energy. For conditions of plain strain, the equation 2.5 becomes

$$\sigma = \left[2E\gamma / \pi (1-\nu^2) c\right]^{1/2} \qquad \text{....(2.6)}$$

where ν *is* the Poisson's ratio.

It can be deduced from these expressions that the smaller the value of ϱ or higher the value of c, the greater will be the effect of stress concentration at the *flaw tip* thus lowering the strength of glass. It follows therefore that the low practical/effective strength associated with most oxide glasses is a direct consequence of the presence of critical flaws or cracks acting as stress concentrators. This situation is further exacerbated by the absence of any stress relieving mechanism. As a result, catastrophic failure occurs, when

the critical load is applied, due to the rapid propagation of flaws or cracks which may have been initiated at any stage of glass making.

Normally, the effective strength of ordinary glass is low (70-100 MPa) although the theoretical strength may be as high as ~ 7000 MPa. In addition, under the usual ambient temperature and atmosphere, most glasses undergo static fatigue where the strength deteriorates, under sustained loading, due to stress-corrosion effects. An improvement in the means by which the low practical strength of glass might therefore be increased is highly desirable. Achievement of this objective would not only widen the possible uses for glass in building and engineering applications but would also allow the use of thinner sections of glass in current applications and thus lead to savings in energy and raw materials. One such area where substantial savings might be accomplished concerns the glass container industry. A large number of containers such as bottles are produced annually and even a small reduction in wall thickness would lead to significant overall savings in energy costs as well as substantial lowering of the total cost of manufacture. Designs and prototypes exist for machines capable of producing glass containers at much higher rates than present equipment but the new machines produce thin-walled containers where the strength of the glass in current production is still inadequate.

Only a small fraction of the theoretical strength of glass is realised under normal forming techniques. A minute flaw on the glass surface, under relatively low stress, can initiate a crack which can subsequently propagate to failure. Therefore, one of the main factors limiting the strength of containers is damage produced at the hot end, prior to application of cold end coatings. Current hot end coating of SnO_2 or TiO_2 forms a thin oxide layer and is not effective in preventing hot end damage. The other factor is damage during on-line handling of the containers.

There exist several approaches to reduce the influence of surface flaws that weaken and subsequently damage the surface of the glass in container manufacturing. Briefly, these are

(a) Etching and polishing to remove flaws, commonly known as flaw healing and acid polishing - however any subsequent minor damage to the glass surface reverses this
(b) Surface coating with polymers, silicones or metal films, known as glazing and cladding - protects glass surface only from those flaws resulting from scratches
(c) Introduction of compressive stress by thermal or chemical toughening
(d) Dispersion strengthening
(e) Fluorination
(f) Surface crystallisation

In the case of etching and associated techniques, a dilute aqueous solution of HF, or a mixture of HF and other acids or sometimes molten salts are used to etch away the surface damage. The resulting surfaces then exhibit very high strength. The related method of flame polishing causes the glass surface to be softened by heating, culminating in the removal or healing of flaws and it is commonly practised in the industry as a standard method of improving the mechanical properties of glasswares. Simple annealing can also be used very effectively to blunt the crack tips, thus increasing the strength, although heating at temperatures lower than the transformation temperatures can have the reverse effect of reducing the strength. However, the major drawback of these methods is the transient nature of the strength improvement, in that any increase can soon disappear following normal handling of glass articles unless the surface is protected by coatings.

Coating is widely used in the container industry, primarily to preserve the pristine strength. An additional benefit of such a coating would be to protect the glass surface against the production of strength limiting flaws through abrasion and indentation. Special cladding, on the other hand, involves coating the surface with a compatible lower expansion material such as glass which gives surface compression.

The present work is concerned with the technique of surface crystallisation where the article, after forming, is given simple heat treatments to enhance the practical strength of the glass. This is generally achieved in three ways as follows:

(i) Formation of an outer layer with a lower thermal expansion coefficient than the container glass. This results in a compressive stress which has to be overcome by an externally applied stress of a sufficient magnitude before fracture can occur

(ii) Presence of small crystals near the surface area acting to 'arrest' cracks, and

(iv) Increased surface hardness to resist further abrasion damage

Although it is difficult to predict, as a rough guide, the strength expected following the formation of a surface compressive layer is normally equal to the magnitude of the compressive stress plus the fracture strength of the untreated glass article. In order for the stress concentrating effect of surface defects to be overcome, a compressive layer in the order of 30-50 μm is desirable.

As is also the case with thermally or chemically strengthened glasses, a balancing tensile stress is created in the interior. In the case of a thermally treated glass, a state of surface compression is achieved by forced cooling of the glass surface more rapidly than the interior, from above the glass transition temperature, using air or liquid jets or gas fluidised particulates. A similar surface compressive layer is achieved by chemical

toughening, typified by ion exchange methods, to form a surface layer with a chemical composition different from that of the bulk. When a large ion from the molten salt is exchanged for a small ion in the host glass, at a temperature below its strain point, the large ion is said to yield a high density or *stuffed* surface, placing it into compression. The parabolic stress distribution profiles[35] for these cases are shown in Figure 2.4. However, the stress distribution obtained by surface crystallisation is usually very different in character. In particular, the transition from compression to tension may be very sharp leading to the degradation of strength due to spalling of the surface layer either during the surface crystallisation process or later due to the influence of static fatigue.

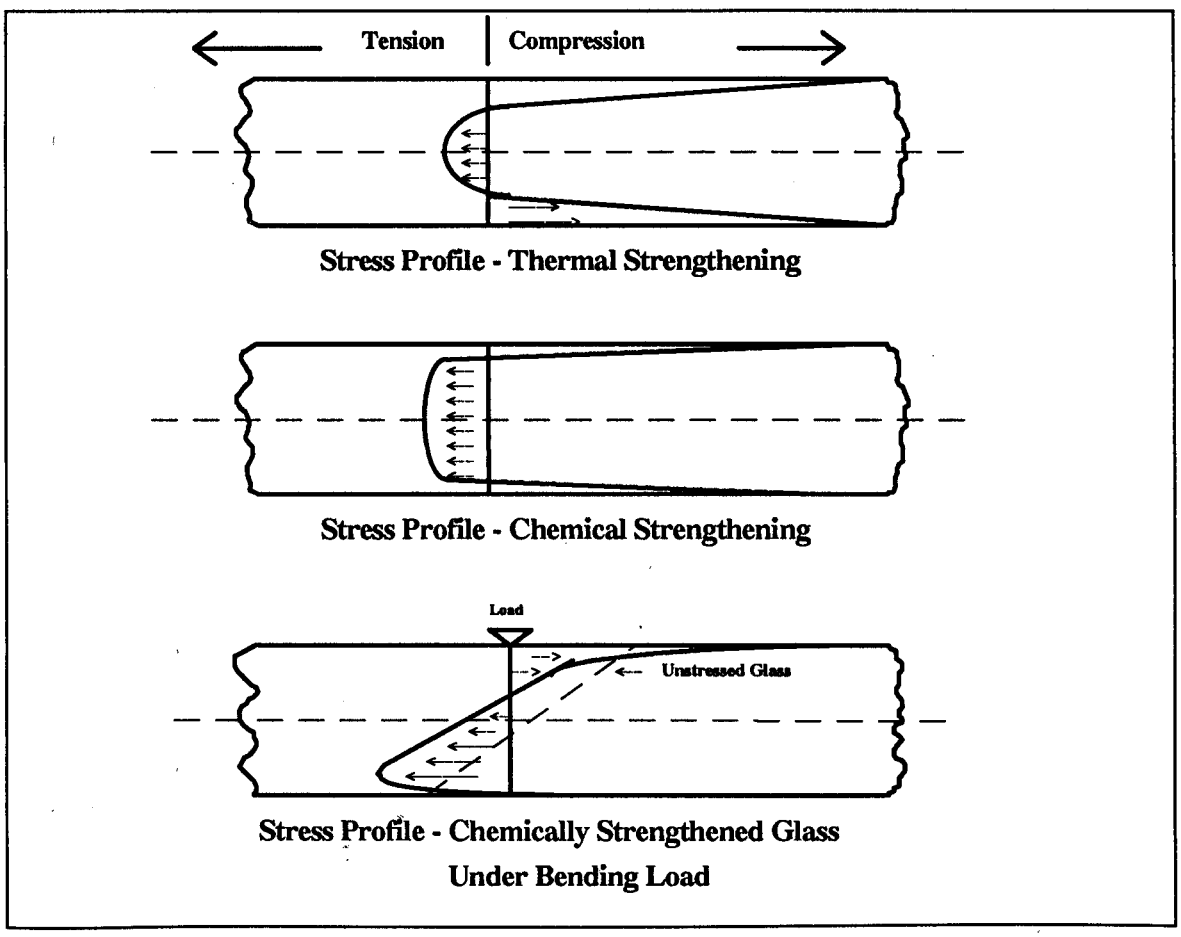

Figure 2.4 Stress profiles developed in thermally and chemically strengthened glass

The main aim of the present work is therefore to utilise the method of surface crystallisation to enhance strength using the following routes

- Destabilisation by introduction and subsequent precipitation of a low solubility component at the surface
- Destabilisation of the bulk composition
- Modification and/or alteration of the surface composition of the glass to improve nucleation/crystallisation

2.4.3 LITERATURE REVIEW OF STRENGTHENING OF CONTAINER AND RELATED GLASSES

2.4.3.1 ETCHING, POLISHING AND THERMAL TOUGHENING

As early as 1962, acid etching had been successfully used to produce very high mechanical strength in excess of 1000 MPa, by Symmers et al[36] and others[37,38] and more recently by Saha and Cooper[39] for bulk glasses. Mould[40] has reported increase in strength by reaction with other liquid agents including water. Etching with anhydrous molten salts such as $NaBF_4$ in $NaNO_3$ and KBF_4 in KNO_3 can also lead to higher strength, as reported by Ray and Stacey[41].

Strengthening of soda lime glass tubes and containers by flame-sprayed glazing has been reported by Sozanski and Varshneya[42] to show a strength increase of 2.75 times the unglazed tubes with a 40-50 μm coating. The authors also found that selective glazing of the base of the containers showed a strength enhancement of 16 % over those that were unglazed. Related finite element analysis of stress in glaze-coated glass containers has also been conducted by Longobardo et al[43,44] in order assess the possibility of the introduction of the cladding method in the production line.

Thermal methods were first employed as early as 1870 and later in 1920 practical methods were developed and a discourse is provided in an excellent review by Gardon[45]. Similarly, flame polishing or flaw healing to improve strength is widely used as reported by Hirao and Tomozawa[46]and Sugarman[47].

2.4.3.2 COATING

As mentioned earlier, container glasses are usually given some form of surface coating to prevent strength degradation during handling and, as a result, numerous studies have been made. The effect of metal oxide coating on the strength of soda lime silica glasses has been investigated by Davis et al[48]. The authors showed that the SnO_2 coatings had no effect on the strength or static fatigue characteristics of the substrates. However, subsequent investigation by Smay[49] has shown that more covalent SnO_2 coating increased the bond strength of organic coatings to soda lime silica glass. This resulted in significant improvement of the friction damage resistance of glass surfaces coated with metal oxides and organics compared with glass surfaces coated with organics only. Jackson et al[50] studied the interaction of stearic acid and octadecylamine protective coatings with container glass surfaces and concluded that the dual SnO_2/octadecylamine film was superior and highly effective in wear resistance to all other coatings.

Cunningham et al[51] have recently used UV curable coatings for glass containers of carbonated beverage bottles to improve moisture driven degradation of the burst strength. The coating comprised reactive film formers having silanes, alkyl monoacrylates, other (meth)acryloyl groups and photoinitiators.

Toughening and strengthening of soda lime silica glass by an applied reinforced coating has been reported by McCarthy and Rossell[52]. The authors have shown that an enhancement of strength and toughness by factors of 2 and 40 are attainable by a 0.1 mm coating of polyurethane containing 6-9 % SiC whiskers. In another work the effect of polymer coating (epoxy, acrylate and polyamide) on strength and fatigue behaviour of

indented soda lime glasses has been investigated by Ritter and Lin[53]. It was shown that ageing limits the access of water to the surface thus improving the fatigue strength and that the epoxy coating appeared to be the most resistant.

A study by Daly and Byers[54] showed that heat treatment alone increased the strength of soda lime silica rods from 124-276 MPa and to an additional 30% when dipped into diethyldichlorosilane or exposed to silane vapour prior to heat treatment.

Significantly, in the area of coating, Chen et al[55] recently studied strengthening of gel coated soda lime silica glasses by dipping glass rods and slides in solutions containing metal alkoxides and salts of zinc borosilicate and sodium aluminoborosilicate glass compositions. On firing at 600 °C, the authors reported strength increases of 39-87 % with a largest strength of 545 MPa over that of uncoated rods. The authors concluded that the strength increase is due to flaw filling and compressive stresses produced by the coating having low thermal expansion. The effect of varying the thermal expansion co-efficients of the sol gel coating using lead silicate and borosilicate compositions has been investigated by James et al[56] and the authors reported a strength increase upto 148 % for soda lime silica glass rods. Marked improvement of strength upto 548 MPa for soda lime glasses has also been reported by Wang and James[57] when a low expansion zinc borate glass coating was applied by a melt dipping method.

In another study, Green[58] has demonstrated a method of strengthening by cladding with a lower expansion glass, This is known as the 'Corelle' process.

2.4.3.3 SURFACE CRYSTALLISATION

Glasses most suitable for strengthening by surface crystallisation include lithium aluminosilicates where a crystalline surface layer of low expansion β-spodumene or β-eucryptite can be produced as reported by Stookey et al[25], Petticrew et al[59], Kiefer et al[60], Fine and Danielson[61] and also in lithium silicates by McMillan et al[62]. Other compositions

include zinc aluminosilicates where low expansion willemite or stuffed keatite can be formed, reported by McMillan[63] and McMillan and Partridge[26,27].

Previous work[28] has shown that surface crystallisable $ZnO\text{-}Al_2O_3\text{-}SiO_2$ glasses can be produced where the average bending strength is increased from 80 MPa to 400-600 MPa. Similarly, the strength of $CaO\text{-}ZnO\text{-}Al_2O_3$ glass and that of a calcium aluminate glass composition could be increased from 100 to 240 MPa and from 120 to 500 MPa, respectively[29]. Further research[35] also showed that the glasses, basically of the soda lime silica composition can be surface crystallised and strength can be improved compared to conventional soda lime silica glass under the same conditions.

Using chemical methods, Stookey et al[25] have demonstrated that lithium aluminosilicate glasses can be successfully crystallised with a β-eucryptite surface layer to strength values of 600-700 MPa. Reports by Corning[64] and Philips[65] have also shown similar strength enhancement due to the crystallisation of an ion exchanged layer.

In order to promote surface crystallisation and subsequent strengthening, it is also necessary to provide crystal nucleation sites on the glass surface. This has been achieved by various techniques aimed at providing an even distribution of fine scratches in the surface from which crystals can nucleate and grow as reported by McMillan and Partridge[63] and McMillan et al[62]. These authors also successfully used polishing followed by vibration in a bed of sand and SiC grit to produce a homogeneous distribution of surface crystals.

2.4.3.4 ION EXCHANGE STRENGTHENING

The successful use of chemical ion exchange strengthening for soda lime silica glasses treated in KNO_3 melt was first reported by Kistler[66]. Bartholomew and Garfinkel[67] studied the role of diffusivity of chemical species and found that aluminosilicate and to a lesser extent alkali zirconium silicate glasses showed the highest strength.

In recent years a large volume of research on ion exchange strengthening has been carried out, particularly for lithium, sodium and magnesium aluminosilicate glass compositions, based on the exchange of larger alkali ions for lithium or sodium using nitrate salt baths. Notable work includes replacement of Li in lithium aluminosilicate glasses by Na from sodium salt baths[68-79]. Similarly Na ions have been replaced in sodium aluminosilicate glasses by larger K ions from potassium salt baths[80-87].

Ion exchange strengthening of specific soda lime silica glass compositions has been reported, by Rinehart[88], which showed a maximum flexural strength value of 350 MPa for a compression layer between 70 and 99 μm thick.

Various other ion exchange treatments have been investigated, including mixed multi-ion exchange[74] and also exchange[77,80,89-92] of Na/K ion for Rb, Cs, Ag, Cd, Zn and Cu ions. Stookey[93] has reported that very high compressive stresses are theoretically possible by ion exchange in the absence of any stress relaxation and related processes.

Strengthening effects on glass of anions from a molten KNO_3 salt bath was first reported first by Jijiian and Zhi[94]. Later, Youmei and Linge[95] investigated the effects of anion group additions of OH^-, Cl^-, NO_3^{2-}, SO_4^{2-} and PO_4^{3-} to the salt bath on the strengthening of an aluminosilicate glass. The authors determined the order of strengthening effect to be $OH^- > PO_4^{3-} > SO_4^{2-} > Cl^- > NO_3^{2-}$ where the glass, after treatment with the salt bath containing OH^- additive showed an average bending strength of 851 MPa with a maximum thickness of a stress layer of 18 μm. Similar work on the effect of impurity ions in a molten KNO_3 bath on ion exchange and strengthening of glass has been carried out by Zhang Xiangchen et al[96]. The authors showed that the impurity ions Ca, Sr, Ba and Na caused a restraining effect on $K^+ \rightarrow Na^+$ exchange, thus reducing strength.

Relatively few ion exchange investigations have been carried out in salt baths other than nitrates. Stookey[25] used Li_2SO_4-Na_2SO_4 to strengthen lithium aluminosilicate glass compositions. The investigation by Manitz et al[97] used lithium nitrate, sulphate and

phosphate baths to chemically strengthen various glasses including those with high alkali content to >500 MPa. Fine and Danielson[61] re-examined the chemical strengthening of certain sodium aluminosilicate glasses by immersion in molten sulphate and found that the replacement of Na ions by Li ions results in surface crystallisation of β-quartz and a strength of nearly 600 MPa with layer thickness of 100-200 μm. The authors attributed part of the strength improvement to the inadvertent thermal tempering. Chemical strengthening of sodium aluminosilicate glasses by controlled crystallisation has been reported by Jiijian et al[98] to demonstrate the effectiveness of a ternary sulphate bath of Li, K and Na compared with a binary Li-Na sulphate, giving a strength of 700 MPa for a compressive layer of 156-165 μm.

It is reported[99] that moderate increase in strength can be achieved by exposing the glass surface to lithium vapours. In this way the lithium ions migrate into the glass surface and partially replace the alkali ions present. On cooling, the lithium rich shell is set in compression about the glass samples thus improving the strength.

In order to enhance the process of ion exchange, a DC electric field has been applied by a number of investigators[100-105] to produce strong glasses which appear to be less affected by chemical corrosion which would otherwise degrade the glass surface.

There are only a limited number of reported results which show a significantly higher mechanical strength improvement when chemical ion-exchange is used. A flexural strength near or above 800 MPa has been cited by Bartholomew[67], Hill and Donald[78], Saha and Cooper[103] and Abou-el-Leil[104].

Since it is the diffusion that controls the ion exchange process, the effect of time and temperature of diffusion on the subsequent flexural strength has been studied by several investigators[76-86,106]. They observed that, for a range of glass compositions and treatments, a characteristic $t^{1/2}$ dependence of strength is normally observed. A maximum

strength resulted for the shorter treatment times as the temperature is increased but overall strength is decreased with increased temperature due to stress relaxation effects[82,86].

Although chemical strengthening is highly effective in imparting high strength to a number of glasses, it should be borne in mind that the effectiveness of the surface compression layer and/or coating depends critically on the thickness of the coating relative to the surface flaws already present before the coating is applied. Therefore, to extract the maximum benefit in strength, the severest flaw must be coated. Green[58] presented a quantitative treatment of this problem using fracture mechanics and showed the strength to be a function of the surface compressive stress (S_c) and the ratio of the thickness (d) of coating to the depth of strength controlling flaw (a_o) as well as to the strength (S_f) in the absence of residual stress. To affect high strength, d/a_o should be greater than unity.

Some results reported for the strengthening of glass containers have been re-examined by Rawson[107] and Green[58]. The authors have determined that a surface compressive stress of ~ 100 MPa would correspond to a layer thickness of ~ 15 μm and most containers showed an increase of bursting strength by a factor 1.5 to 2 but the initially weak containers with severe flaws showed no increase. Therefore it is imperative that the containers are carefully handled prior to chemical strengthening.

Further information on chemical strengthening is given in the publication by Bartholomew and Garfinkel[67]. Some representative data for chemically strengthened glasses are given in Table 2.2.

TABLE 2.2
SUMMARY OF SOME CHEMICALLY STRENGTHENED ION-EXCHANGED GLASSES

Glass/ Salt Bath	Exchange Protocol (°C/h)	Exchange Mechanism	Modulus of Rupture (MPa)		Reference
			Pre-treatment	Post-treatment	
Li_2O-Al_2O_3-SiO_2					
$NaNO_3$	400/4	$Na^+ \rightleftarrows Li^+$	-	731	69
$NaNO_3$	400/4		-	681	69
$NaNO_3$	400/4		-	669	69
$NaNO_3$	400/4		-	703	69
$NaNO_3$	400/4		-	572	69
$NaNO_3$	385/6		74	470	76
$NaNO_3$	385/49		74	383	76
$NaNO_3$	385/97.5		74	336	76
$NaNO_3$	385/49		-	309	76
$NaNO_3$	404/4		-	669	73
$45Na_2SO_4$-$55ZnSO_4$	585/0.25		69	400	75
Na_2O-Al_2O_3-SiO_2					
KNO_3	350/0.17	$K^+ \rightleftarrows Na^+$	234	579	81
KNO_3	350/17		234	497	81
KNO_3	400/0.17		234	607	81
KNO_3	400/16		-	598	81
KNO_3	400/16		-	476	82
KNO_3	400/16		-	338	82
KNO_3	400/16		-	200	82
KNO_3	400/16		-	600	82
KNO_3	500/24		-	469	83
KNO_3	500/24		-	498	83
KNO_3	482/4		-	650	85
KNO_3	482/4		-	700	85
KNO_3	400/24		-	690	77
KNO_3	430/1		-	552	77
KNO_3	430/16		-	483	77
KNO_3	550/1.5		140	490	95
Li_2O-Na_2O-Al_2O_3-SiO_2					
$NaNO_3$	385/49	$Na^+ \rightleftarrows Li^+$	80-100	503	76
$NaNO_3$	385/49		80-100	516	76
$NaNO_3$	385/49		80-100	574	76
$NaNO_3$	385/49		80-100	858	76
$NaNO_3$	454/0.5		-	414	74
$NaNO_3$	496/0.5		-	666	74
$80Li_2SO_4$-$20Na_2SO_4$	700-800/0.5		150-200	600	63
$90Li_2SO_4$-$10Na_2SO_4$	800/0.25		240	700	98

TABLE 2.2 (contd)
SUMMARY OF SOME CHEMICALLY STRENGTHENED ION-EXCHANGED GLASSES

Glass/ Salt Bath	Exchange Protocol ($^{O}C/h$)	Exchange Mechanism	Modulus of Rupture (MPa)		Reference
			Pre-treatment	Post-treatment	
$80Li_2SO_4$-$20Na_2SO_4$	650/16	$Na^+ \rightleftarrows Li^+$	-	600	97
KNO_3	454/1.5		-	772	74
KNO_3	427/1.5	$K^+ \rightleftarrows Na^+$	-	786	74
Li_2O-SiO_2					
					69
$NaNO_3$	400/4	$Na^+ \rightleftarrows Li^+$	62	228	77
$NaNO_3$	400/4		55-83	441	77
$NaNO_3$	400/4		-	366	
					81
KNO_3	400/16	$K^+ \rightleftarrows Na^+$	-	235	
Li_2O-Na_2O-Al_2O_3-SiO_2		$Li^+ \rightleftarrows Na^+$			
			-	638	25
$95Li_2SO_4$-$5Na_2SO_4$	860/0.08	β-eucryptite/	-	700	25
$95Li_2SO_4$-$5Na_2SO_4$	800/0.25	β-spodumene			
Na_2O-CaO-SiO_2	480/16	-	-	350	88
KNO_3					
		$Li^+ \rightleftarrows Na^+$			
100LiCl					Present Work
$90Li_2SO_4$-$10Na_2SO_4$		β-eucryptite/	100	300-500	
$90Li_2SO_4$-$5Na_2SO_4$-$5K_2SO_4$		β-spodumene			

2.5 VISCOSITY OF GLASS

Viscosity (η) is considered to be the most important criterion in glass making and the way the viscosity of a melt varies with temperature forms the only determining step for shaping of glass articles. Consequently, numerous treatments of glass viscosity as a function of temperature and composition have been made[108]. The relationship between viscosity and other physical properties can also lead to a better understanding of the glass structure. For the forming machines used in the container glass making industry, it is essential that a constant viscosity regime is maintained throughout in order to avoid or minimise any dimensional variation and also to avoid defect formation. A typical viscosity-temperature profile of a soda lime silica container glass is shown in Figure 2.5. The plot includes certain very well defined and internationally recognised reference points. The points refer to specific viscosity values corresponding to important stages of glass forming. They are considered extremely useful, being employed throughout the glass industry to optimise composition, glass property and overall operational efficiency. These are

1. Glass melting temperature at $\log \eta = 2$
2. Gob temperature at $\log \eta = 3$
3. Working temperature or sink point at $\log \eta = 4$
4. Flow point at $\log \eta = 5$
5. Littleton softening point at $\log \eta = 7.65$
6. Upper annealing point (annealing point) at $\log \eta = 13$
7. Lower annealing point (strain point) at $\log \eta = 14.5$
8. Transformation temperature (T_g) at $\log \eta = 13.3$

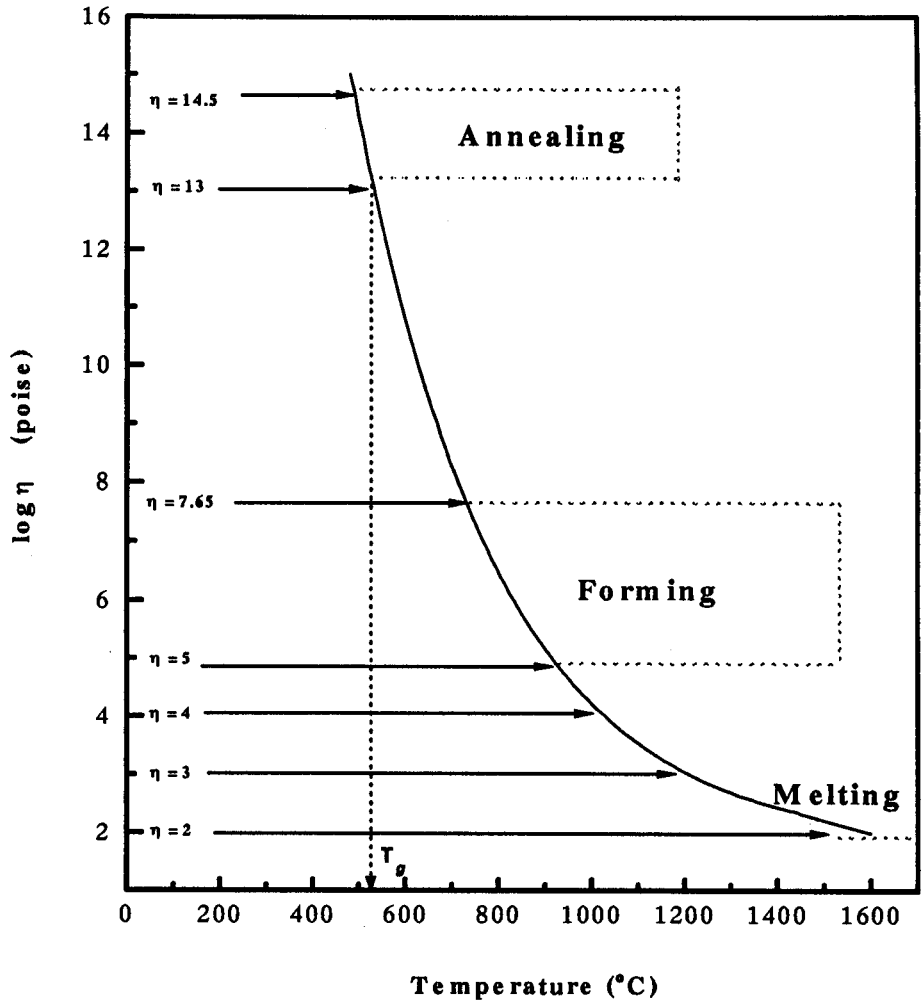

Figure 2.5 A typical viscosity-temperature profile of a soda lime silica glass

These reference points for viscosity have been set internationally and are described elsewhere[109-111]. They are defined according to the standard measuring methods and relevant information can be found in the published literature[112-117]. Of practical importance is the working range which covers several orders of magnitude of viscosity. For example, $10^{3.5}$ poise is appropriate for fast working such as glass bulbs, and 10^{7} poise

for drawing operations. At the temperature corresponding to the annealing point, the atoms can move significantly so that residual thermal stresses can be relieved within a 15 minute period, an internal timescale that is compatible with production schedule. The strain point is also regarded as an important marker since below this point the glass is sufficiently rigid that it may be handled without the generation of additional residual stresses.

For industrial glasses, the value of η required by current technological practices lies in the range 10^2-$10^{14.5}$ poise. Melting and refining of glass requires 10^2 poise and must not exceed 300 poise, forming requires 10^3-10^7 poise, the annealing of the glass takes place at 10^{13}-$10^{14.5}$ poise, whilst working with a flame requires a viscosity of 10^6-10^9 poise.

2.5.1 TEMPERATURE DEPENDENCE OF VISCOSITY

The viscosity-temperature relation of a glass is, in the main, based on conceptions commonly employed to describe transport phenomena in solids and liquids where ionic species have to overcome a potential barrier to affect conduction or diffusion under the influence of an electrical field. In the present case, however, the viscous flow of atoms or molecules has to overcome the energy barrier, using the thermal energy available at a given temperature. The exponential equation of viscosity versus temperature is given by

$$\eta = A \exp(E_n / RT) \qquad \text{....(2.7)}$$

Where A is constant, E_n is activation energy for viscous flow, R is the gas constant and T is the temperature in K. This exponential expression, however, does not adequately describe viscosity variation over a wide temperature range since, with glass forming melts, the activation energy is not a constant over the entire viscosity range.

The Fulcher equation

Due to the limitations described above, various empirical equations have been put forward to deal with practical production situations. Notably, Vogel, Fulcher and Tammann and Hesse found independently that the following general equation[118] provides a very good representation of the viscosity-temperature relationship which is satisfactory, for most practical purpose, for a wide temperature interval

$$\eta = A\exp\left[B/(T-T_0)\right] \qquad \text{....(2.8)}$$

or

$$\log\eta = \log A + \left[\frac{B}{T-T_0}\right] \qquad \text{....(2.9)}$$

where A, B and T_0 are three constants for a given glass melt and can be calculated from three viscosity points of interest. It is then possible to interpolate satisfactorily and even to extrapolate the entire viscosity curve for desired glasses. The plot of log η versus $1/(T-T_0)$ yields a straight line. The relation predicts that, as T approaches T_0, viscosity will rise rapidly to an infinite value and the activation energy, E_n in the transformation range approaches a constant thus complying with equation 2.7.

Doremus[119] provided a further theoretical explanation of the Fulcher equation based on either free volume or temperature dependence of the size of the structural units actively participating in the viscous flow.

Another simple Arrhenius equation, without T_0 as is the case in the Fulcher equation, has also been used by Geiss and Knickerbocker[120] to obtain viscosity data using an APL algorithm[121] for magnesium aluminosilicate cordierite glasses over short temperature ranges.

2.5.2 VARIATION OF VISCOSITY WITH COMPOSITION

As viscosity of glass depends very sharply on composition, it is difficult to describe the relation between viscosity and composition since individual components may increase the viscosity in one type and may decrease it in another. Of course, it also depends on how much of each individual component is present in the glass. Additivity of the contributions arising from individual constituents to viscosity has been demonstrated for silicate glasses[122,123]. In silicate glasses, oxides such as SiO_2 and Al_2O_3 will increase the viscosity while oxides in Group I of the periodic table, PbO and other modifiers will reduce it. B_2O_3 decreases viscosity at the melting temperature while increasing it at lower temperature (up to 15 wt % B_2O_3). High alkaline earth content such as CaO and MgO usually results in a steep viscosity curve whereas introduction of high alkali content, R_2O (where R = Na, K or Li) produces a more gently sloping curve. These effects of individual components have been studied exhaustively by Gehlhoff et al[109,110], Shartsis et al[124], Scholze[125], Morey[126] and a book by Mazurin[127] offers a collection of very useful data on binary and ternary oxide glasses. A guide to the relative effects of various oxides on viscosity is given in Table 2.3.

The effect of cations on viscosity has been variously investigated. Winter[128,129] has shown that addition of cations affects viscosity in a different way at low temperatures in the transformation range, than they do in the high temperatures associated with melting, thus requiring two separate relationships in the two regions. Later, Dingwall and Moore[130] proposed the spatial arrangement of ions as being the main factor in the transformation range such that individual oxides contribute mainly via their ionic radius which, in turn is proportional to the number of coordinated oxygen atoms. The major findings by these authors are that the smaller ions produce higher viscosities, the increased deformability of larger ions results in considerable decrease in viscosity and a combination

TABLE 2.3
EFFECT OF VARIOUS OXIDES ON VISCOSITY

Increase in Viscosity	Decrease in Viscosity	No effect on Viscosity
substituting	substituting	substituting
P_2O_5 for CaO.MgO		P_2O_5 for SiO_2
BaO for Na_2O	Na_2O for SiO_2	
ZnO for CaO.MgO	K_2O for SiO_2	
ZnO for Na_2O	F_2 for SiO_2	
K_2O for Na_2O	BaO for SiO_2	
MgO for CaO	BaO for CaO.MgO	
CaO for Na_2O	ZnO for SiO_2	
CaO for SiO_2	Li_2O for Na_2O	B_2O_3 for SiO_2 (at low temperatures)
CaO for $SiO_2.Na_2O$	B_2O_3 for SiO_2 (at high temperatures proportionally decreases)	
MgO for Na_2O		B_2O_3 for CaO.MgO (at low temperatures)
MgO for SiO_2 (very slight)	B_2O_3 for CaO.MgO (at high temperatures proportionally decreases)	SrO for SiO_2 (at low temperatures)
MgO for $SiO_2.Na_2O$		
Al_2O_3 for Na_2O	SrO for SiO_2 (at high temperatures proportionally increases)	
Al_2O_3 for SiO_2		
Al_2O_3 for CaO	BaO for $SiO_2.Na_2O$	
SrO for $SiO_2.Na_2O$		

of various ions with the same charge decreases viscosity significantly. More recently, Stryjak[131] has shown that the substitution of oxides of divalent and trivalent cations for SiO_2 causes a change in the viscosity depending on their field strength so that viscosity, at a given temperature, is increased with increasing field strength (smaller radius). The author also found increase in viscosity due to small scale (2 mole %) substitution of oxides of the larger quadrivalent or transition metal ions of Zr^{4+}, Ti^{4+}, Sn^{4+} and Ce^{4+} for SiO_2. In this case, the change in viscosity due to 'structure' building oxides of a quadrivalent ion depends on the stability of the structure. Larger ions would form structural units larger than the SiO_4 units and reduce the extent to which the oxygen bonds must be strained in order to accommodate other modifying divalent (or even monovalent) ions.

It is commonly recognised that the additive effects of constituents on viscosity, in multicomponent systems with compositions covering a wide range of commercial container, sheet or architectural glasses, is particularly difficult to assess. However, recent work by Lakatos et al[123] has greatly simplified this task by the introduction of a method of multiple regression analysis. The three constants in the Fulcher equation are calculated using factors depending on the molar ratio of the major oxides in the glass composition. It was generally found that the agreement between the calculated and measured values of viscosity for a given glass composition can be extremely accurate.

Chapter 3

TECHNIQUES FOR PREPARATION AND CHARACTERISATION OF GLASSES

3.1 INTRODUCTION

The details of the methods used for synthesis and an overview of the compositions of glasses used are covered in Part 1 of this Chapter, whilst Part II is concerned with various experimental methods employed for the characterisation of these glasses. Such characterisation includes more general physico-chemical properties to evaluate the material property requirements of the glasses, in particular crystallisation behaviour and/or extent of surface destabilisation. An understanding of these properties is essential if the glasses are to be exploited for any technological applications.

PART I

3.2 METHODS FOR THE PREPARATION OF GLASSES

3.2.1 COMPOSITIONS

A global list of all glass compositions melted in the present investigation is given in Table 3.1. This includes simple as well as commercial soda lime silica and Float glasses with or without nucleating agents, Rockware container glasses modified with alumina and Emhart and related soda lime glasses with added P_2O_5 content.

TABLE 3.1
COMPOSITIONS OF EXPERIMENTAL GLASSES

wt %	SiO_2	Na_2O	CaO	MgO	Al_2O_3	K_2O	CuO	Sb_2O_3	R_2O_3	P_2O_5	BaO	Others
NBS 710	64.97	8.27	9.98	-	-	11.13	-	4.92	0.49	-	-	0.25
Glass 1	60.11	11.00	18.10	-	8.23	-	2.57	-	-	-	-	-
Glass 2	61.60	11.27	9.74	6.33	8.43	-	2.63	-	-	-	-	-
Glass 3	61.50	11.08	19.13	-	3.25	-	-	-	-	-	-	-
R4795	73.00	11.60	11.34	2.12	1.17	0.47	-	-	-	-	-	-
R4795/3	70.87	11.26	11.01	2.06	4.05	0.46	-	-	-	-	-	-
R4795/5	69.51	11.05	10.80	2.02	5.88	0.45	-	-	-	-	-	-
R4795/10	66.35	10.54	10.31	1.93	10.15	0.43	-	-	-	-	-	-
NLS 1	73.00	17.00	10.00	-	-	-	-	-	-	-	-	-
NLS 2	69.50	16.50	14.00	-	-	-	-	-	-	-	-	-
NLS 3	67.00	17.00	16.00	-	-	-	-	-	-	-	-	-
NLS 4	63.00	22.50	14.50	-	-	-	-	-	-	-	-	-
NLS 5	74.00	15.00	11.00	-	-	-	-	-	-	-	-	-
NLS 6	72.50	15.00	12.50	-	-	-	-	-	-	-	-	-
NLS 7	70.00	15.00	15.00	-	-	-	-	-	-	-	-	-
NLS 8	66.50	16.00	17.50	-	-	-	-	-	-	-	-	-
NLS 9	65.00	18.00	17.00	-	-	-	-	-	-	-	-	-
NLS 10	63.00	20.50	16.50	-	-	-	-	-	-	-	-	
NLS 11	66.00	14.00	20.00	-	-	-	-	-	-	-	-	-
NLS 12	73.00	21.00	6.00	-	-	-	-	-	-	-	-	-
NLS 1P	72.00	16.00	10.00	-	-	-	-	-	-	2.00	-	-
NLS 8P	66.00	15.00	17.00	-	-	-	-	-	-	2.00	-	-
Float F1	70.00	15.00	6.00	6.00	2.50	-	-	-	-	-	0.50	-
EMH 7	73.00	12.16	9.97	2.39	1.31	0.6	-	-	-	-	0.07	0.5
NCS 1	79.00	15.50	5.50	-	-	-	-	-	-	-	-	-
NCS 2	80.00	10.00	10.00	-	-	-	-	-	-	-	-	-
NCS 3	80.00	7.00	13.00	-	-	-	-	-	-	-	-	-
NCS 4	66.25	16.75	17.00	-	-	-	-	-	-	-	-	-
NCS 5	71.25	14.25	14.50	-	-	-	-	-	-	-	-	-
NCS 6	67.50	23.25	9.5	-	-	-	-	-	-	-	-	-
NCS 7	64.00	22.00	14.00	-	-	-	-	-	-	-	-	-
NCS 8	60.50	20.25	19.25	-	-	-	-	-	-	-	-	-
NCS 9	57.00	19.50	23.50	-	-	-	-	-	-	-	-	-
NCS 10	53.25	18.25	28.50	-	-	-	-	-	-	-	-	-
Emhart 1	71.80	10.57	10.60	3.43	1.62	0.76	-	-	-	-	-	1.22
Emhart 2	72.20	11.61	10.89	2.52	1.59	0.75	-	-	-	-	-	0.44
Emhart 3	73.10	12.62	9.89	1.23	1.95	0.78	-	-	-	-	-	1.25
Emhart 4	72.50	12.37	10.40	1.67	1.87	0.79	-	-	-	-	-	0.40
Emhart 5	73.00	11.26	11.15	2.52	1.17	0.60	-	-	-	-	-	0.30
Emhart 6	73.20	12.27	10.03	1.71	1.36	0.67	-	-	-	-	-	0.76
Emhart 7	73.30	12.16	9.97	2.39	1.31	0.60	-	-	-	-	-	0.57

3.2.2 GLASS MELTING TECHNIQUES

In this section, a detailed summary of the procedures employed for glass melting and drawing of glass rods will be given.

3.2.2.1 TYPES OF GLASSES PREPARED

Numerous compositions in the soda lime silica based glass system were melted. These melts were usually on a 100 *g* scale for the purposes outlined below:

(i) to determine crystallisation behaviour and extent of surface crystallisation

(ii) to study the effect of nucleating agents

(iii) for use in DTA i.e. the determination of the glass transition temperature, crystallisation and melting temperatures

(iv) to draw glass rods from the melt for subsequent use in the surface destabilisation treatments

(v) to measure modulus of rupture (MOR) using drawn rods

3.2.2.2 BATCH MATERIALS

For all 100 *g* batch compositions melted, the batch materials used, where available, were AnalaR grade high purity reagents of less than 1 *ppm* impurity level; otherwise SLR laboratory grade reagents were employed. In many cases, glass bottles, without protective tin oxide coating, supplied by Rockware were melted to duplicate the actual glass composition used by the industry.

3.2.2.3 BATCH PREPARATION

The batch preparation was identical for the majority of the melts. The raw materials, in stoichiometric proportion, were thoroughly dried, carefully weighed on an "Oertling GC 32" top load balance to an accuracy of ± 0.001 *g* and mixed in a rotary ball

mill for 2 hours. The batch compositions had previously been computed to provide mass after melting 100-1000 *g* glass depending on the intended use.

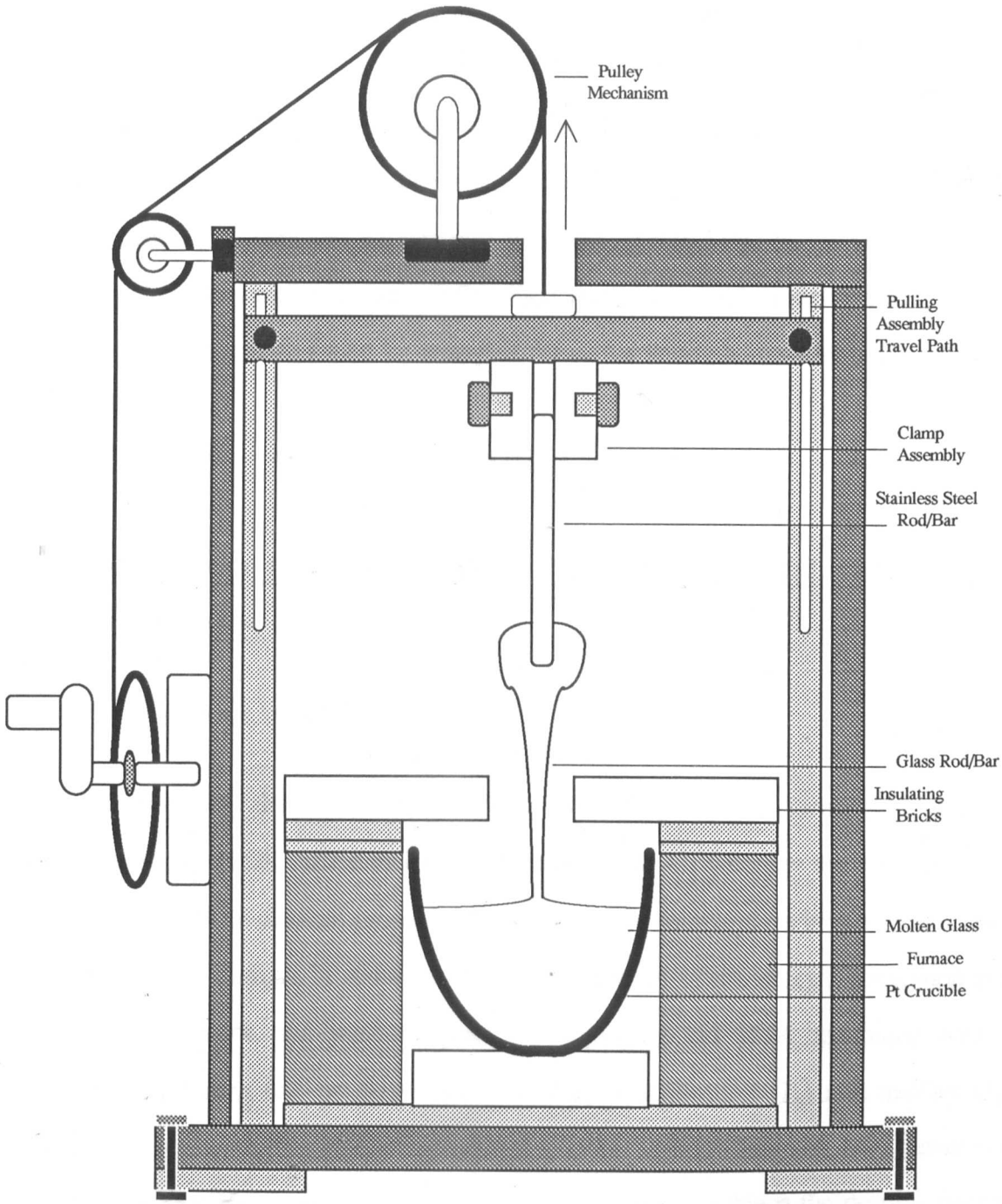

Figure 3.1 Schematic diagram of apparatus for drawing glass rods and bars

3.2.2.4 GLASS MELTING AND DRAWING OF RODS

The batch compositions were melted until seed free in a Pt-10%Rh crucible (to avoid contamination by crucible dissolution) at temperatures from 1400-1500 °C for periods up to 3 hours in an electrically heated furnace with hydraulic loading lift. Rods of varying diameters (1-4 *mm*) were hand drawn using a "Rod-Pulling" rig designed and built in the Department of Physics. A schematic diagram is shown in Figure 3.1. The technique employed, involved transferring the melt at 1400-1500 °C to another low temperature furnace in the rig, where the temperature was held at 950-1000 °C during the pulling operation. In some cases cylinders or flat discs were cast. These rods or flat specimens were used, in either unannealed or annealed form, for strength measurements following various treatments.

PART II

3.3 PROCEDURES FOR THE CHARACTERISATION OF GLASSES

3.3.1 THERMAL ANALYSIS

Methods of thermal analysis are a related group of techniques such as thermogravimetry (TG), differential thermal analysis (DTA), whereby the dependence of the parameters of any physical property of a substance on temperature is measured. These techniques follow changes in some property of the system (mass, energy, dimension etc). In the present work, the main purpose of employing the DTA technique was to characterise softening (T_s) or glass transition (T_g), crystallisation (T_c) and melting (T_m) temperatures of the various glass compositions studied. A knowledge of these parameters is essential to develop appropriate heat treatment protocol to achieve the desired material property objectives. Briefly, the theory of the method is given below:

The basic parameter important for the methods of thermal analysis, is the change in heat content (ΔH) found in the usual free energy expression $\Delta G = \Delta H - T\Delta S$. This change in heat content arises from either the evolution or absorption of energy that accompanies chemical reactions and structural changes within materials. It is manifested as an increase or decrease in temperature depending on whether a particular reaction is exothermic or endothermic. In DTA, graphical record is made of the temperature difference, between the test sample and an inert reference material, against time or temperature as both specimens

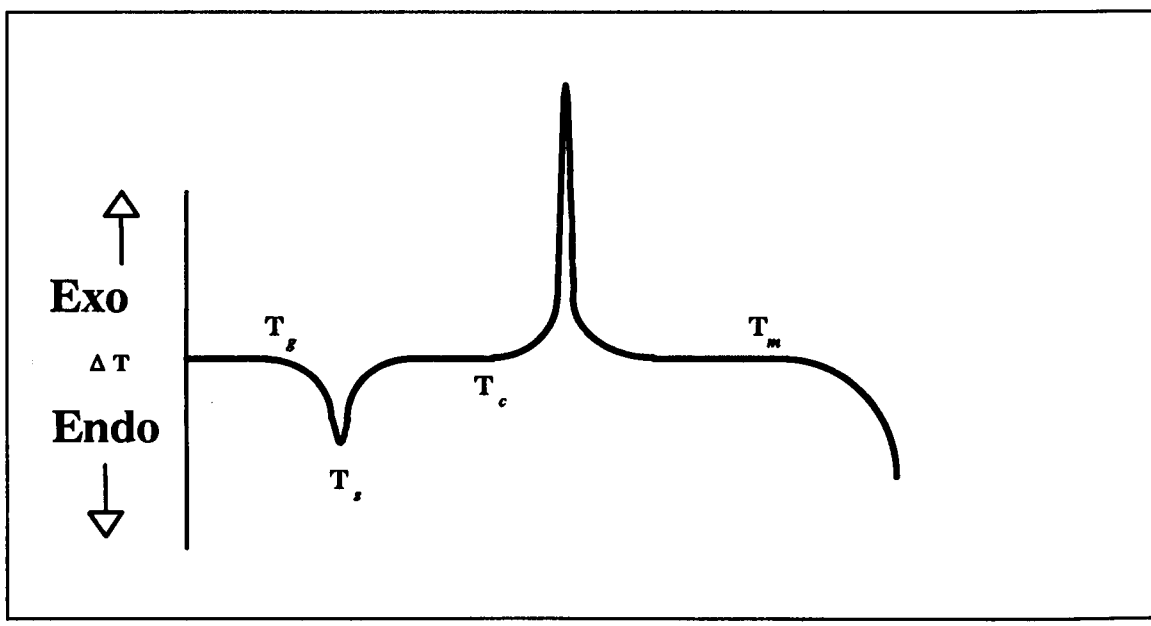

Figure 3.2 A typical DTA thermogram

are subjected to identical temperature regimes in an environment heated or cooled at a controlled rate. The DTA curve shows sharp decreases or increases in the temperature difference depending on whether a change in the sample causes absorption or liberation of heat characterising the phase transformation and chemical reactions occurring within the test sample. In practice, the weights, particle sizes and packing density of both the test and reference material are matched to maintain parity between sample and reference thus avoiding any asymmetries in the apparatus and/or experimental procedure associated with

signal collection. Various practical aspects of the technique related to the study of glass are further reviewed by McMillan[132] and George and Veasey[133]. A full guide to DTA can also be found in Pope and Judd[134]. A typical graphical representation of the DTA analysis of an hypothetical compound is shown in Figure 3.2.

Generally, three distinct effects are observed when powdered glass is subjected to DTA:

(i) an endothermic peak at low temperatures characterising the glass transition temperature (T_g)

(ii) one or more exothermic responses at higher temperatures as a consequence of crystallisation or devitrification corresponding to the precipitation of crystal phases, and

(iii) one or more endothermic peaks due to melting of the crystalline phases

The relationship between the glass property and temperature during slow cooling, normal cooling and fast cooling is illustrated in Figure 3.3 for volume. Curve I refers to slow cooling which allows more time for the glass to approach the equilibrium structural "configuration", depicted in dashed-dotted line, than does the faster cooling rate, where consequential higher viscosities hinder configurational changes. If a well annealed glass is subsequently reheated at a rate greater than the cooling rate used for annealing, the change in the glass property (volume, in this case) will follow the plain dashed curve shown. Such a glass will have greater resistance to configurational changes since the structure of the glass approaches closer to the equilibrium "configuration". As a result, on heating, the structural changes will fall behind the rising temperature until a temperature higher than the normal T_g is reached. Increased specific heat will then be absorbed by the glass in order to allow the glassy network structure to acquire equilibrium configurational motion with this elevated temperature, thus yielding the endothermic dip at T_g.

All DTA parameters were determined by using either a 'Stanton' Model 673-4 or a P L Thermal Sciences STA1500 simultaneous DTA-TG instrument with a high temperature head upto 1500 ^{o}C. The instruments employed a linear temperature variable rate programmer. Glass samples were ground and sieved into a particle size range of 150-200 μm and runs were carried out normally with a heating rate of 10 ^{o}C/min in static air using platinum crucibles. Alumina or quartz was used as an inert reference material having the same particle size as the test specimen. When quartz, usually Limoges quartz, was used as a reference it acted as an internal standard for temperature since at 573 ^{o}C there appears a well documented and characterised $\alpha \rightarrow \beta$ transition. This transition is endothermic but since quartz is the reference it appears as an exothermic peak on the trace.

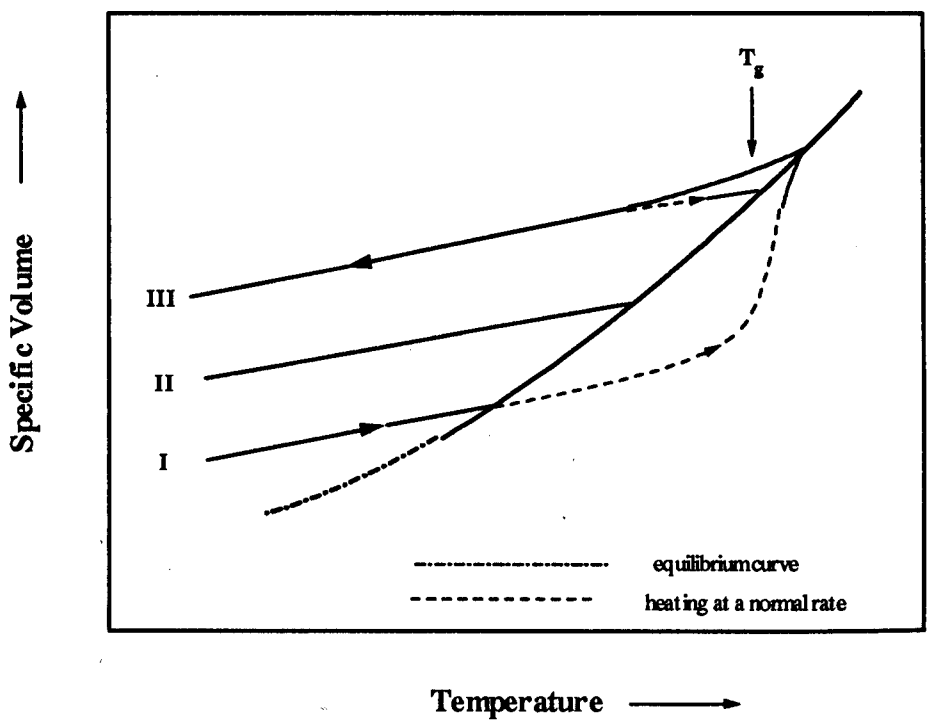

Figure 3.3 Relationship between the glass property and temperature during slow cooling (I), normal cooling (II) and fast cooling (III)

3.3.2 X-RAY DIFFRACTION ANALYSIS

X-ray diffraction (XRD) is widely used for the determination of phases in devitrified materials. In the present work, the presence of any crystalline phase in the glasses studied was routinely checked by this method to confirm glass formation and identification of crystalline phases present in the devitrified specimens. Briefly the salient features of the method are as follows:

In perfect crystals the three dimensional long range atomic periodicity produces sharp diffraction peaks. In amorphous materials, such as glasses, only a small degree of local or short range order exits; and absence of long range order gives rise to broad, diffuse 'haloes' or 'humps' as they are commonly known, on the X-ray diffraction pattern. This is because of the long range atomic environment generally not being the same for any two atoms in the assemblage. Thus, on devitrification or crystallisation of the glass the diffraction peaks will be those corresponding to the crystalline phases. The technique of X-ray diffraction analysis is very well established and is well documented in detail by Klug and Alexander[135].

XRD was carried out on selected glass compositions in the form of either flat pieces or samples ground and pulverised to about 150-200 μm particle size. A Philips diffractometer (Model PW 1965/60 and Model PW 1830) with CuK_α radiation of λ = 1.5405 Å was used. The setting was 40 kV and 30/40 mA. The 2θ range of 5 to 80° with a scan rate of 1-¼ °/min was employed. The scan rate and time constant were kept constant for the majority of samples. Identification of phases was made by way of comparing the experimental trace with standard JCPDS database patterns accessible via the fully automated APD 1700 software package. The software was also used to carry out cell parameter calculation and structural determinations.

3.3.3 MECHANICAL STRENGTH

Bend test

Modulus of rupture was determined on an Instron Universal Testing machine. Mostly four-point bend testing was employed on all samples using a jig with a 20 mm span. The diameter of rods for testing was 2 mm in most cases, although 1 mm rods were also used. Three-point bend testing was also performed on a few samples for the purpose of comparing the strength values obtained by four-point bending test. In all cases, a crosshead speed of 0.05 mm/min was used. On average 8 specimens were used for each strength determination. Values of modulus of rupture (MOR), σ_F of rod samples was determined from the following equation:

Three-point bend $$\frac{P_F L}{\pi r^3} \quad \text{....(3.1)}$$

Four-point bend $$\frac{2P_F d'}{\pi r^3} \quad \text{....(3.2)}$$

where P_F = load to fracture

L = distance between the outer knife edges

d' = distance between inner and outer knife edges

r = radius of the sample

Hertzian indentation fracture

The method involves pressing a spherical sapphire indenter into a glass surface under controlled conditions until a ring crack is initiated. The interpretation of the results relies upon the calculation of the radial tensile stress field required to open a microcrack at

a given distance from the centre of initiation. A detailed explanation for the formation of the characteristic ring cracks has been discussed by Frank and Lawson[136]. The mechanism involves two separate steps, one being the growth of a shallow ring crack originating from a pre-existing surface flaw and the other consisting of deepening of this into a core crack under increased indenter force. However, if the original flaw is sufficiently small the force necessary for the first stage can cause the second spontaneously. This process is illustrated in Figure 3.4.

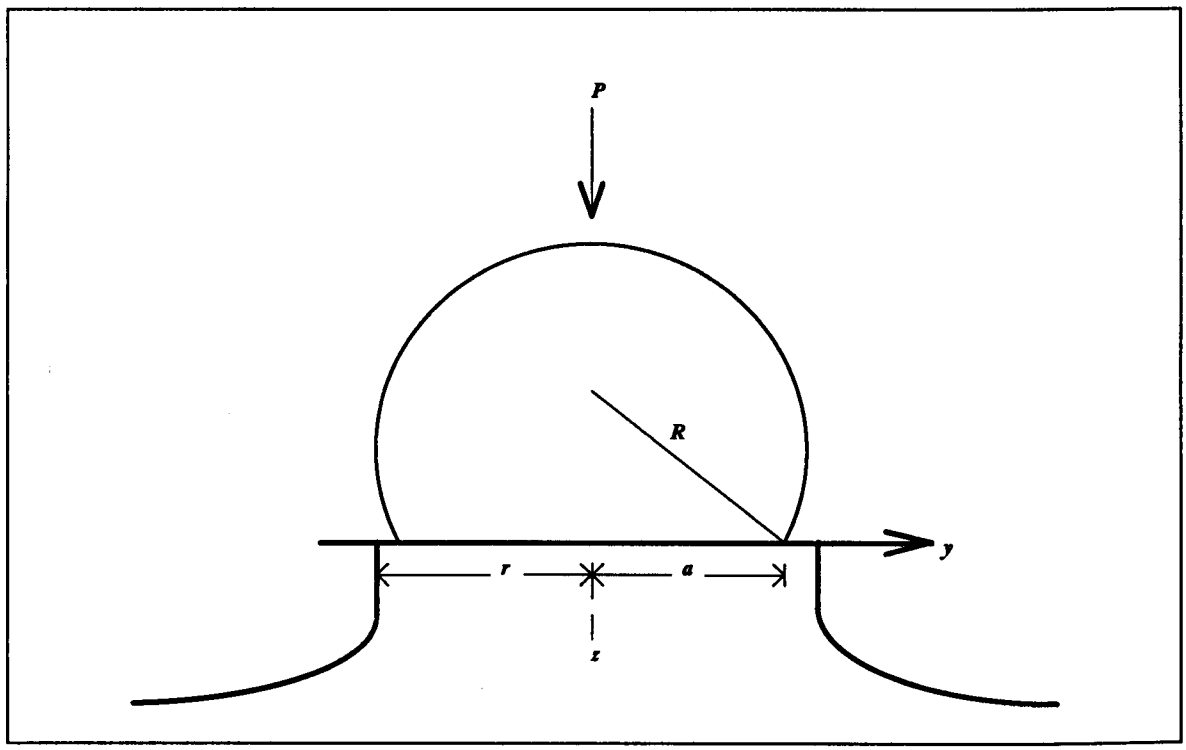

To form crack c at critical load P_{TC}, usually $r > a$

Figure 3.4 Illustration of Hertzian indentation loading geometry

When the spherical indenter is loaded against the flat glass surface, a symmetrical stress distribution is set up in which the principal stresses are compressive in a tear-drop

shaped hemispherical region immediately beneath the indenter to a depth of the order of the contact diameter. Outside the contact region, the greatest stress component is tensile and reaches its maximum value on the surface of the glass on the circle of contact. The tensile stress decreases according to an inverse law from the edge of contact area and does so rapidly in magnitude with both distance z from the surface and the distance y along the surface. Along the surface the tensile stress is radial at any crack initiating flaw and can be written as

$$\sigma_{TC} = \frac{(1-2\gamma)}{2\pi a^2} P_{TC} \left(\frac{a}{y}\right)^2 \quad ; \text{y = r at crack} \qquad \text{....(3.3)}$$

where σ_{TC} is the surface radial tensile stress. γ is the Poisson's ratio of the glass specimen and y is the distance from the centre of the circle of contact radius a. The force applied to the indenter is P_{TC}.

The Hertzian load was calibrated using accurate measurements from the Instron and the following relation obtained

$$P = \left[\left(lb_{gauge}\, 1.75\right) - 7\right] 9.812\, Newtons$$

where lb_{gauge} refers to the gauge pressure reading on the gas supply used to provide the piston load. The micrometer with the Hertzian rig using an eyepiece magnification of x 10, was calibrated as 1 div of micrometer = 0.466 μm. The crack was observed as dark field and the bright field corresponded to the area of contact as Newtonian rings. The following equation was used to calculate the Hertzian stress and is given by

$$\sigma_{TC} = \frac{(1-2\gamma)\, 9.812\, ([lb\ 1.75] - 7)}{\pi \left(micometer\ div\, [300/644] 10^{-6}\right)^2} \qquad \text{....(3.4)}$$

The apparatus used for the Hertzian fracture measurement was constructed in this Department and is shown in Figure 3.5.

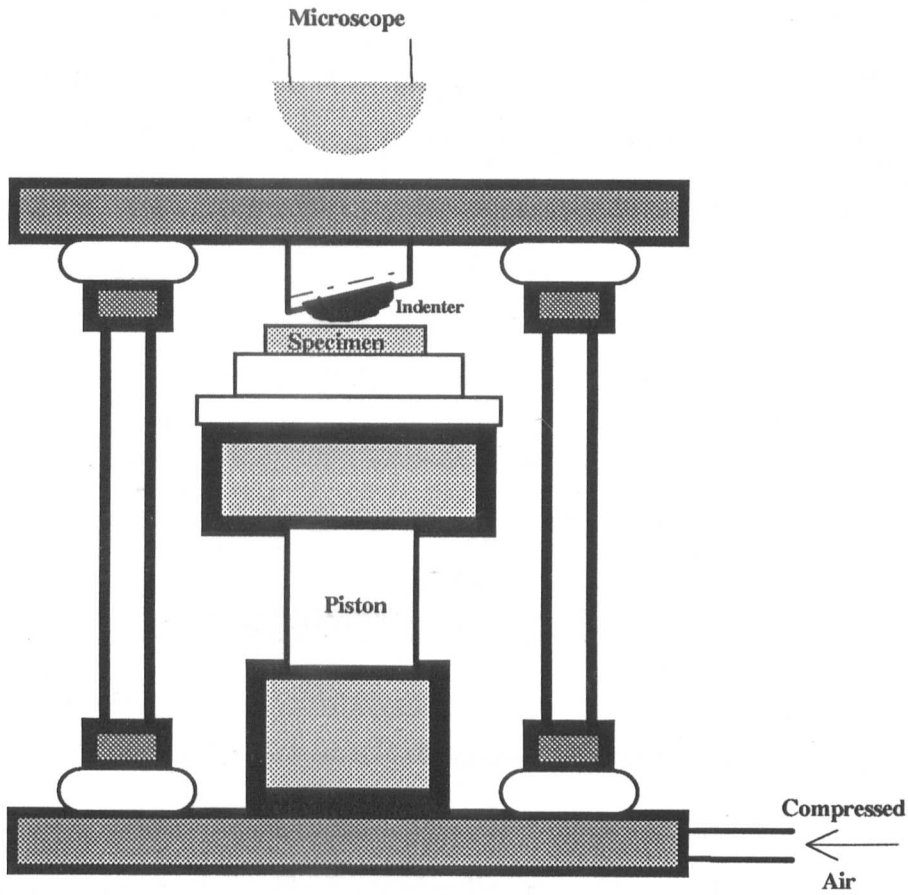

Figure 3.5 Schematic diagram of Hertzian indentation fracture apparatus

The rig comprises a hemispherical sapphire (4 mm diameter) and specimen support block connected to a a compressed air supply. The applied load is controlled by a pressure regulator geared to a constant load rate of 13 kg/sec. The appearance of Newton's rings at the indenter/specimen interface allows the variation of contact area with applied load to be measured. The fracture diameter is determined using a calibrated eye piece.

3.3.4 HIGH TEMPERATURE VISCOSITY MEASUREMENT

Viscosity is considered to be the most important criterion in glass making and the way the viscosity of a melt varies with temperature forms the only determining step for shaping of glass articles. The relationship between viscosity and other physical properties can also lead to a better understanding of the glass structure.

If a liquid is contained between two parallel plates the upper of which is moving at a velocity v_o and the lower plate stationary the distance y between the plates remains constant as shown in Figure 3.6 .

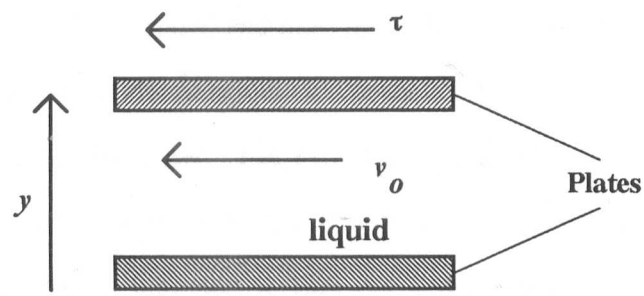

Figure 3.6 Schematic diagram of viscous flow

For a large number of liquids, v_o varies linearly with y and a force has to be applied, in order to maintain this motion. The force is applied to the upper plate, in the direction of its motion, to overcome the frictional force within the liquid. The shear stress τ in force per unit area is given by

$$\tau = \eta \frac{dv}{dy} \qquad \text{....(3.5)}$$

where η is the proportionality constant or viscosity in poise and dv/dy is the velocity gradient. The equation is only valid when v_o is below a certain value and if v_o is high enough, turbulent flow may develop. However, this flow is never encountered in a glass

melt due to its high viscosity. The equation is also only valid for Newtonian fluids and is normally true for glasses above the transformation range.

The particular method of measuring viscosity is generally dependent on the range of interest to the manufacturers and it is not possible to measure the entire range using only one method. As a result a variety of methods are used. However the common and most important factor is the measurement of temperature. The thermocouples should lie in as close proximity as possible to the glass being measured and the design of furnace must include facilities to equilibrate the temperature and to maintain constancy of temperature. In the present work, viscosities in the range 10^2-10^7 poise were measured, using a rotating concentric cylinder viscometer designed and built in the Department of Physics.

The geometry of the apparatus is shown schematically in Figure 3.7 and Figure 3.8 shows a photograph of the viscometer. The Pt-2%Rh crucible measured 5 cm of internal diameter and was 8 cm high. The spindle, each end of which terminated in a 45° cone, was made of the same alloy, had a diameter of 1.25 cm and an overall length of 4 cm; the cylinder part was 3 cm long. The spindle was attached to an alumina tube by means of a platinum tube connected to the spindle. The alumina tube served as a support for the spindle and acted as an insulator for the main temperature measuring thermocouple. The alumina tube terminated in a small chuck by which it was attached to a torsion wire. The crucible was mounted on an alumina tube pedestal which was rotated by means of a 1/75 HP synchronous motor. This motor was coupled to a pedestal (which rotated on a ball race) through a gear box with interchangeable gears giving speeds of revolution, in both directions, whose periods were 30, 64 and 120 seconds.

The torsion wires from which the spindle was suspended were made from 7.62 cm lengths of steel piano wire of different gauges. Two wires were used of torsional constant 4.405×10^4 and 9.827×10^4 dyne cm/radian of twist. These wires were connected to a brass disc which could be clamped when only the lower suspension wire was used. A

mirror was attached to the lower chuck holding the suspension wire and an optical system was used to measure the deflections of the spindle.

The furnace was designed using 12 'Crystolon' hot rods connected in series in three parallel branches of four. The elements were connected in a circle around a large alumina tube surrounding the crucible and spindle. The crucible and pedestal were raised into the furnace by a pneumatic lift. Two more thermocouples were employed, one just below the crucible in the pedestal and the other on the inside of the large alumina tube which was used as the sensor for the temperature controller and thyristor unit.

The initial procedures were firstly to melt the glass in the crucible in another furnace and, when the desired depth of glass (approximately 6.5 cm) was achieved, the crucible was transferred (when cold) to the pedestal where it was held in place using "Saffil" high temperature wool. The pedestal was raised to a height just below the spindle and the furnace was switched on. When the melting temperature had been reached, the pedestal was slowly raised so that the spindle was immersed in the glass.

There are two methods in use by which the viscosity at high temperatures can be calculated. The first of these consists of rotating the outer crucible at a constant speed and measuring the angular deflection of the inner spindle using the mirror and scale arrangement. This method is used when the viscosity is less than 10^4 poise and is called the periodic method. The equation used for this method is

$$\eta = \frac{KDt}{4\pi CdLE} \qquad \text{.... (3.6)}$$

where η = viscosity (poise)

D = scale of deflection (cm)

t = time of revolution of the outer crucible (sec)

$$C = \frac{4\pi (R_1)^2 (R_2)^2}{(R_2)^2 - (R_1)^2} \qquad \text{.... (3.7)}$$

R_1 = crucible radius (cm)

R_2 = spindle radius (cm)

d = scale distance from the torsion wire (cm); a circular scale at a radius of one mitre has been used

K = torque constant of the wire(s) dyne cm/radian of twist

E = volume temperature expansion factor (approx. 1.04 between 1200 and 1300 °C)

L = effective spindle length determined by calibration to be 4.23 cm

For higher viscosities the aperiodic method is used. In this method, the outer crucible is turned slowly until the deflection shown is at one extreme of the scale. Due to the extreme viscosity of the liquid glass, the spindle returns to its zero position very slowly. The time taken for the beam to cross two points on the scale is measured. The deflection is made in both directions and it is important that the rest position of the spindle be such that the position of the light beam registers accurately on zero under no torque. It is the extension of the viscosity range by this aperiodic method which makes an apparatus of this type so valuable in measuring viscosities of glasses. In the aperiodic method, the viscosity can be calculated from the following equation:

$$\eta = \frac{0.4343\, K\, (T_2 - T_1)}{ECL \log (\theta_1/\theta_2)} \qquad \text{....(3.8)}$$

where K, E, C and L are defined in equation and $(T_2 - T_1)$ is the time in seconds required for the spindle to return from angle θ_1 to angle θ_2.

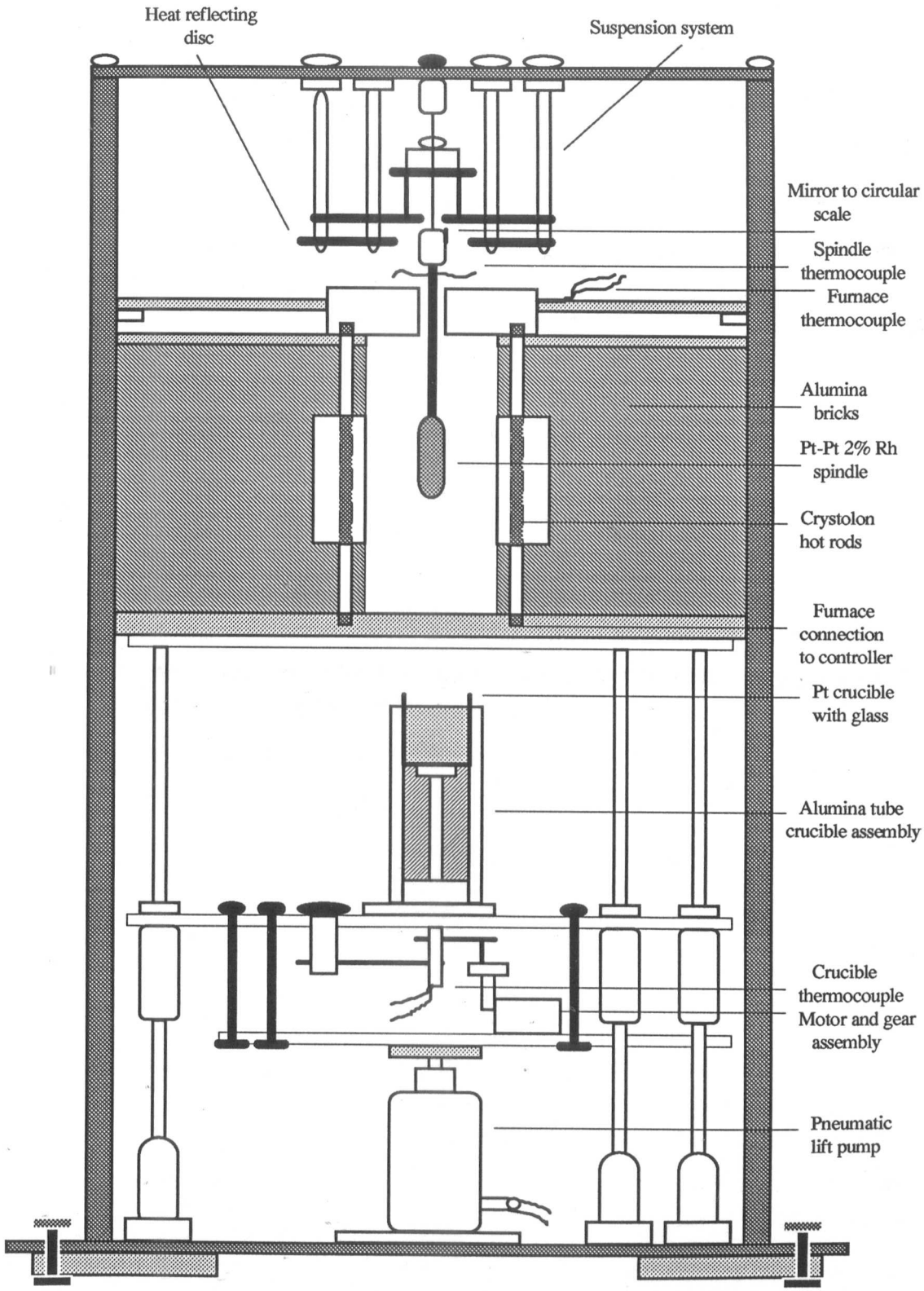

Figure 3.7 Schematic diagram of high temperature viscometer

Figure 3.8 Photograph showing (a) high temperature viscometer apparatus and (b) torsion wire assembly

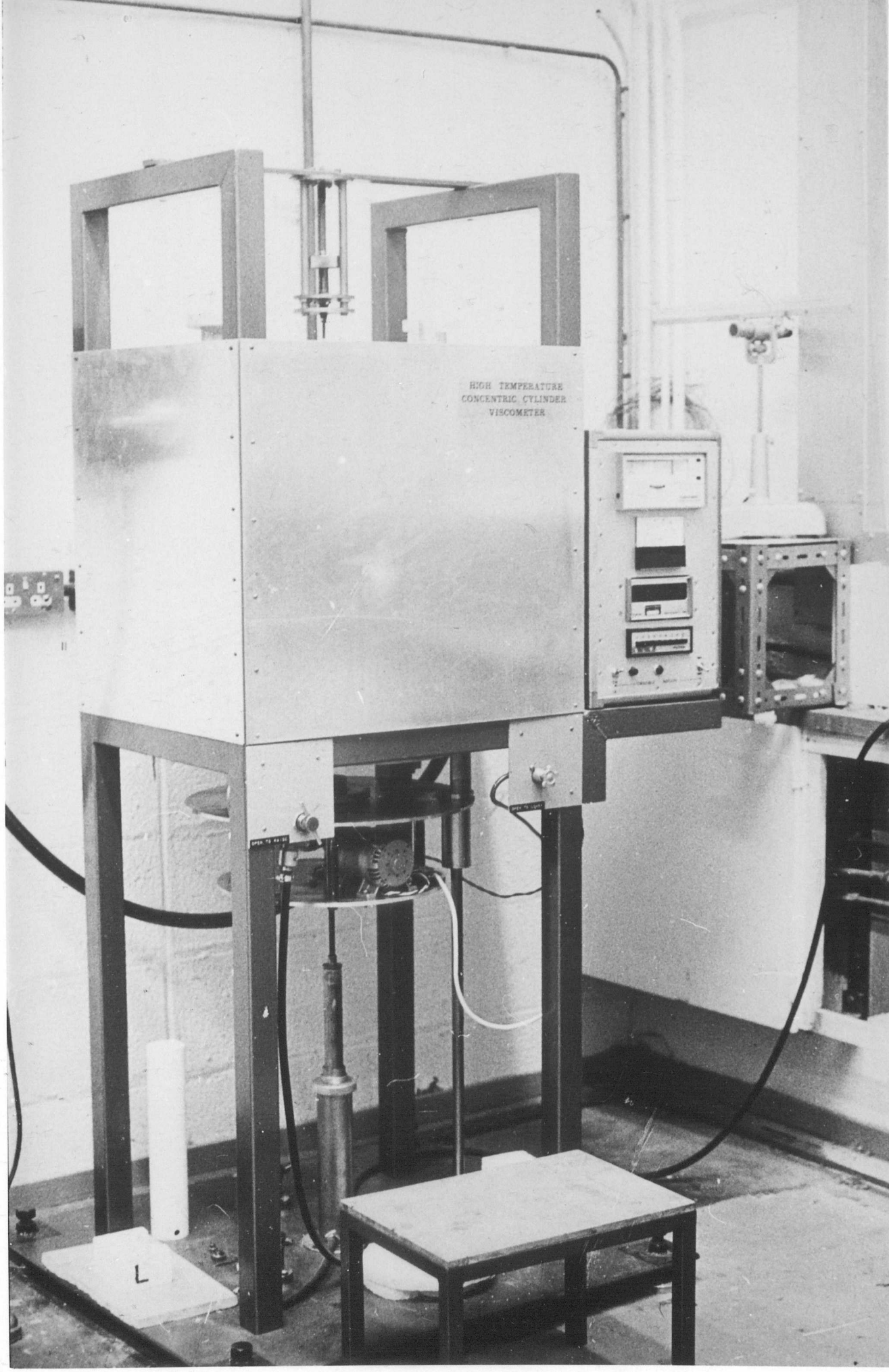
HIGH TEMPERATURE
CONCENTRIC CYLINDER
VISCOMETER

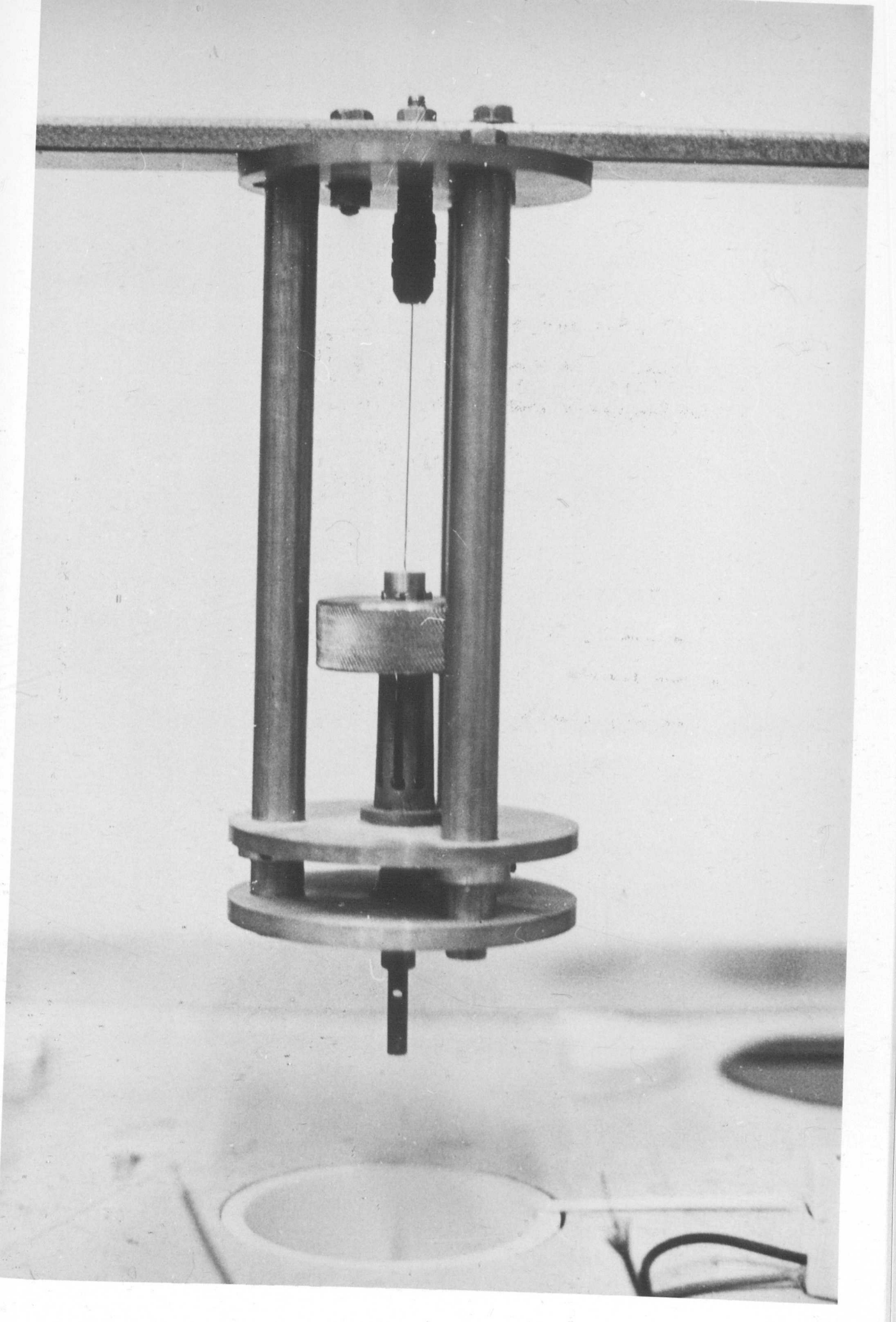

3.3.5 SCANNING ELECTRON MICROSCOPY

Scanning Electron Microscopy (SEM) was used to study the topological surface characteristics and crystal morphology using a Cambridge S250 MkIII Stereoscan based at the Department of Physics. The instrument was equipped with an EDAX analysis system and LINK AN10000 software package. The specimens were coated with either a thin layer of carbon by an evaporation technique or sputtered with gold. The problem of sample charging was solved by trial and error to establish an optimum coating thickness. Normally, an accelerating voltage of 10-20 kV was used wherever possible.

3.3.6 SECONDARY ION MASS SPECTROSCOPY

In the technique of secondary ion mass spectroscopy (SIMS) the sample being analysed is continuously bombarded with a beam of ions. Material is sputtered from the sample surface and some of this material is in the form of ions; these secondary ions are then mass analysed using a mas spectrometer. Electropositive elements predominantly produce positive ions whilst electronegative elements give negative ions. The yield of these ions is enhanced by using primary ions of oxygen and caesium respectively. The technique has the ability to cover the entire periodic table and can resolve isotopes. For inhomogeneous systems the method produces qualitative information, but for uniform matrices quantitative analyses can be performed.

Depth profiling is concerned with determining the distribution of material below the surface of the sample. The depth distribution of interest can extend from a few atomic layers to several microns or more. There are several approaches that can be used to obtain depth information; (a) non-destructive depth profiling (b) sputter depth profiling and (c) taper sectioning. In the present work, sputter depth profiling which involves the erosion of the sample surface with a beam of ions has been used. As material is removed from the

sample surface by the ion beam the composition of the surface is monitored by one of the electron spectroscopic techniques or the sputtered flux is analysed with a mass spectrometer.

The secondary Ion Mass spectroscopy (SIMS) facility of Loughborough Consultants at the University of Loughborough was used to carry out the depth profiling of a few representative ion-exchanged samples to ascertain the degree of lithium penetration in the treated glass rods.

The instrument used was a CAMECA 1ms 3f dynamic SIMS system equipped with a duoplasmatron ion source (for O^{2+} and O^{2-} ions) and a Cs^{+} ion source together with a mass filter to ensure beam purity. The instrument employed a double focussing magnetic sector mass spectrometer with variable mass resolution (250-10000) and a mass range of 0-250 amu. Analysis can be performed on areas from 2 to 400 μm in diameter and is capable of submicron resolution in the ion imaging mode. The instrument was computer controlled and offered the following modes of operation: (i) bargraph mass spectra over the entire mass range (ii) continuous mass spectra over a limited mass range (iii) high resolution mass spectra of individual mass peaks (iv) ion energy distribution measurements (v) step scanning across the sample in any direction to determine lateral variations in composition (vi) depth profiling to determine the variations in compositions with depth (v) isotope ratio measurements. The experimental conditions used are given in Table 3.2

Five samples, treated with LiBr and $AlBr_3$, with polished cross sections were used to determine the diffusion profiles of ion exchanged surface regions. The same analytical procedure was used for all five samples. The cross sections of the samples were first sputter coated with a thin gold coating to prevent excessive charge build-up on the sample surface. The O^{-} primary ion beam was used to minimise the sample charging problems normally associated with glass analysis and positive ions were detected to maximise the sensitivity to the alkali metals.

TABLE 3.2
EXPERIMENTAL CONDITIONS FOR SIMS

Conditions	
Primary ion species	O^-
Primary ion energy	12.5 keV
Primary ion current	0.1 and 0.5 μA
Raster size	250 μm
Secondary ions	Positive
Transfer ions	150 μm
Analysed area	60 μm and 10 μm
Contrast aperture	No. 4
Mass resolution	250

Mass spectra were recorded from two areas 60 μm in diameter on each sample, one in the central region of the cross section and one close to the outer edge of the sample. Step scans were then recorded from a position outside the sample, across the edge of the sample and into the central region. The scan was then repeated in the opposite direction from the centre to the outside. The analysed area was nominally 10 μm in diameter, the step size was 5 μm and 50 steps were performed from each analysis. The elements monitored in the step scans were Si, Li, Na, K and Ca.

Chapter 4

GENERAL EXPERIMENTAL METHODS

4.1 INTRODUCTION

Various experimental procedures employed, to treat and strengthen glasses, are covered in this Chapter. Some of the methods included the construction of apparatus to meet special requirements demanded by the aims of the project. Materials used for this purpose were silica, PTFE or platinum to avoid contamination, hazards due to toxicity or influence of any other external factors that might have an effect on the results obtained.

4.2 ABRASION OR VIBRASION METHOD

The rod specimens were given vibrasion for a period of 90 minutes in a container, with ~ 30 mesh SiC powder, on a vibrating bed. After vibrasion the grit was removed by first gently brushing the samples and then by ultrasonically cleaning in a genklene bath. This produced a standard vibraded surface of uniformly dispersed small flaws.

In order to produce a more uniformly abraded surface, an alternative method termed "vapour blasting" or "airabrasion" was developed for this programme. The technique utilised specimens in the form of glass rods or flat pieces which were air abraded with Al_2O_3 powder of 9 μm particle size. Examination by optical microscopy showed a more homogeneous flaw distribution.

4.3 HEAT TREATMENT

'Pristine' as well as 'vibraded' glass samples were heat treated at temperatures ranging from 675-800 °C for times between 10 minutes and 3 hours. The samples were always cooled, where possible, in the furnace to eliminate any significant thermal stressing of the samples. The heat treatments were carried out, where appropriate, either in an inert atmosphere of oxygen free N_2 or in static air. The temperatures of the mufffle furnaces were controlled within ± 5 °C.

4.4 DESCRIPTION OF THE APPARATUS USED FOR VAPOUR TREATMENT

A schematic diagram of the apparatus used for vapour treatment experiments is shown in Figure 4.1. The vapour treatment involved the use of two vertical furnaces, one directly above the other, connected by a silica tube. The first furnace (Furnace 1), through which ran a closed end silica tube, was maintained at temperatures of 700- 900 °C to generate lithium or aluminium vapours from LiBr or $AlBr_3$ powders in an alumina crucible, placed at the bottom of the tube. The temperature at which LiBr vapour was generated was kept generally at 880 °C. In the case of $AlBr_3$ it was lower at 300-700 °C and generally a temperature of 700 °C was employed. Although this temperature was considerably higher than the melting point of $AlBr_3$ (90 °C), it was found to be necessary in order to generate a high enough vapour pressure and also to avoid the possible formation of an alumina crust which could occur at lower temperatures. The glass rods or flat plates were placed in the second furnace (Furnace 2) supported upright in a recessed silica disc platform. The platform was specially designed so as to allow the rods to hang freely and thereby separating them from each other. The furnace temperature was

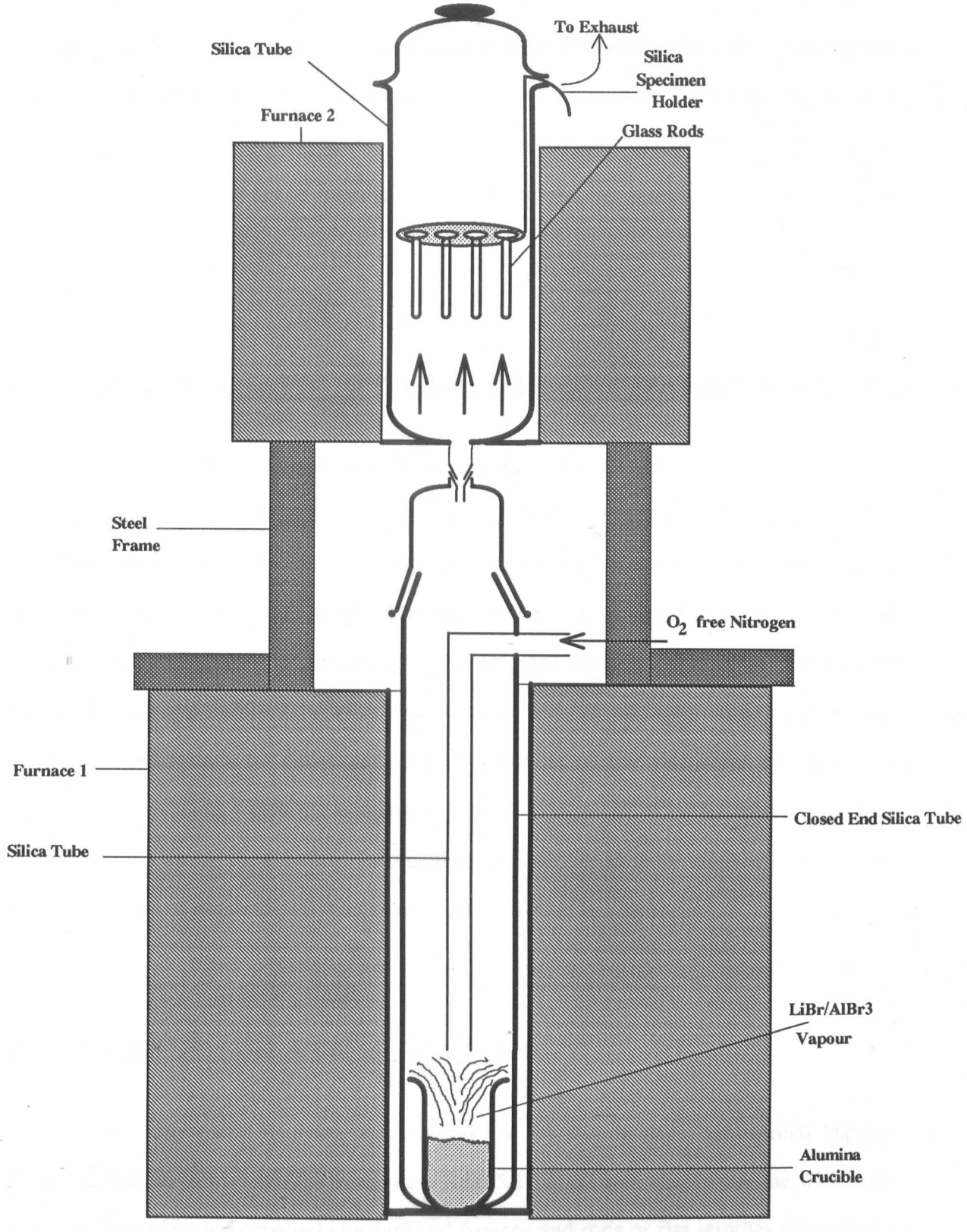

Figure 4.1 Schematic diagram of vapour treatment apparatus

maintained above the annealing temperature of container glasses (550-580 °C) during the exposure. A set of runs were carried out in an inert atmosphere where the vapour was then carried by oxygen free N_2 to the second furnace for exposure times ranging from 10-40 minutes. In another set of runs, the annealed rod and bar samples were treated in an enclosed environment of air.

4.5 MOLTEN SALT LITHIUM ION-EXCHANGE METHOD

For the Li-base exchange experiments, halide baths of LiCl and LiBr were used, as well as sulphate baths including Li_2SO_4, binary Li_2SO_4-Na_2SO_4 and ternary Li_2SO_4-Na_2SO_4-K_2SO_4. Mostly the ternary composition $90Li_2SO_4$-$5Na_2SO_4$-$5K_2SO_4$ which has a melting point of 750 °C was used. The technique involved was to simply dip the flat samples in the salt bath for periods up to 15 minutes at a temperature of 620-650 °C followed by an appropriate heat treatment, in some cases at the same temperature. Some samples were dipped in the bath from 'as cold' condition; others were given a temperature equalisation treatment where the samples were preheated to 500 °C prior to dipping either in LiCl or LiBr or sulphate baths. Information collected on toxicity, thermal stability and other properties of some lithium compounds are presented in Appendix I.

4.6 ELECTROSTATIC SPRAYING

The electrostatic spraying was carried out by means of a commercial sprayer loaned to the project by IPGR. Rockware R4795/10 glass was chosen for the trial runs. 1000 g of this glass were melted in a gas fired furnace and rods or flat samples were drawn from a fireclay crucible. The *as-drawn* rods were then sprayed with the powdered salt

mixture of $90Li_2SO_4$-$5Na_2SO_4$-$5K_2SO_4$ as they emerged from the hot zone of the furnace. The other samples used were *already drawn* flat pieces which were then reheated at the mouth of the furnace (temperature being in excess of 1000 °C) and salt was sprayed onto the samples.

4.7 CHEMICAL VAPOUR DEPOSITION

A chemical vapour deposition (CVD) rig has been designed and constructed in-house at the Department of Physics. Diagrams of the apparatus and the design of the gas feed system are shown in Figures 4.2 and 4.3.

The CVD apparatus comprised a reaction chamber, a rotating sample stage and a gas feed system. The deposition chamber used a specially designed open ended silica tube, 900 mm long and 200 mm diameter, with top and bottom ends made of pyrex, secured by means of a buttress joint assembly. This assembly was necessary to permit loading and unloading of samples by manipulating the clamps. The reaction area of the tube was positioned to be in the hot zone (~ 10 cm) of a Kanthal wound vertical furnace which maintained temperature within ± 4 °C. The bottom of the reaction tube was joined to a PTFE cone of a stirrer gland assembly which was in turn attached to a motor and pulley system so that a silica rod running through could be rotated freely at a desired speed. A silica specimen stage was placed at the top end of the silica rod.

Special emphasis was placed on the accurate control of reacting gases so that the required doping/deposited film level could be readily assessed by controlling the deposition rate. The uniformity of deposition was enhanced by the construction of a specially designed rotating specimen stage enclosed in the gas-tight silica glass liner tube. This stage was so designed as to accommodate both flat specimens on a platinum dish and rods

that were allowed to hang freely from specially designed sample holder. The gas mixture was fed via the inlet at the top of the assembly from a gas feed system. The arrangement included a series of PTFE flowmeters and bubblers containing metal sources such as $POCl_3$ and $TiCl_4$. Nitrogen was used as a carrier gas and a flow as high as 2*l*/min could be adequately controlled.

The chamber was purged with nitrogen before the runs and in all cases, the sample stage was rotated (~ 60 rev/min) both prior to and during the deposition to ensure, as far as possible. an even deposition on the substrate.

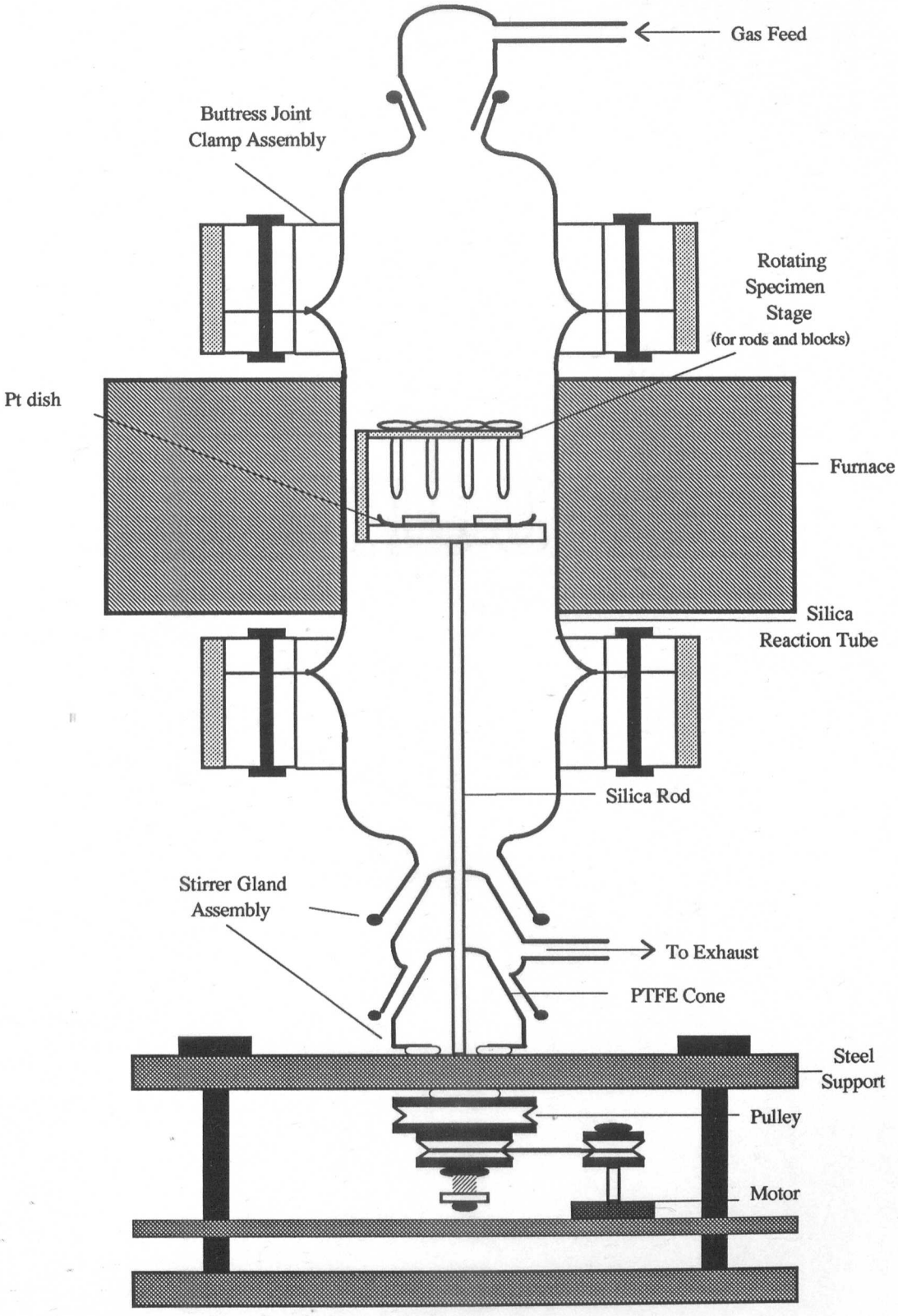

Figure 4.2(a) Schematic diagram of CVD reaction chamber

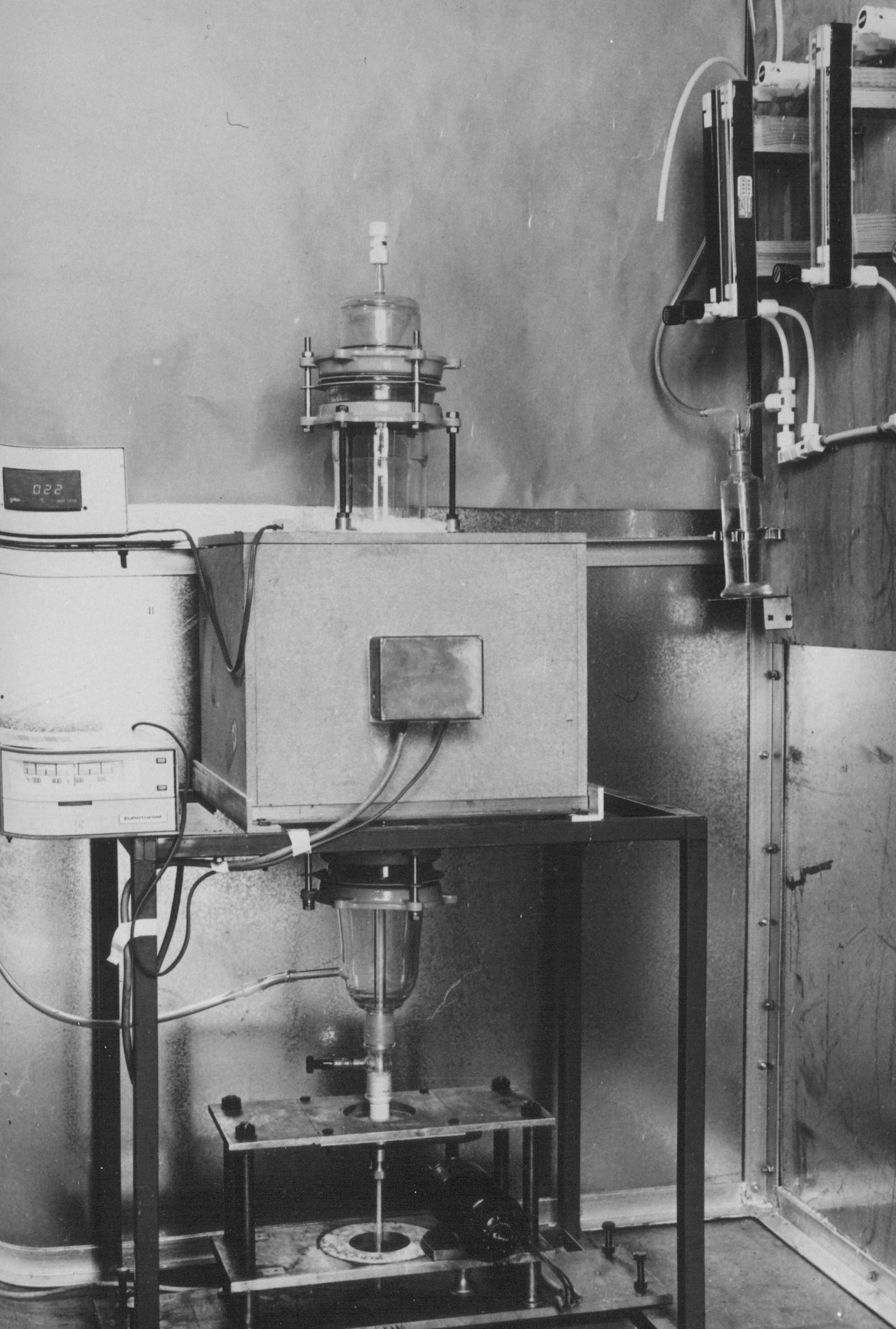
022
EUROTHERM

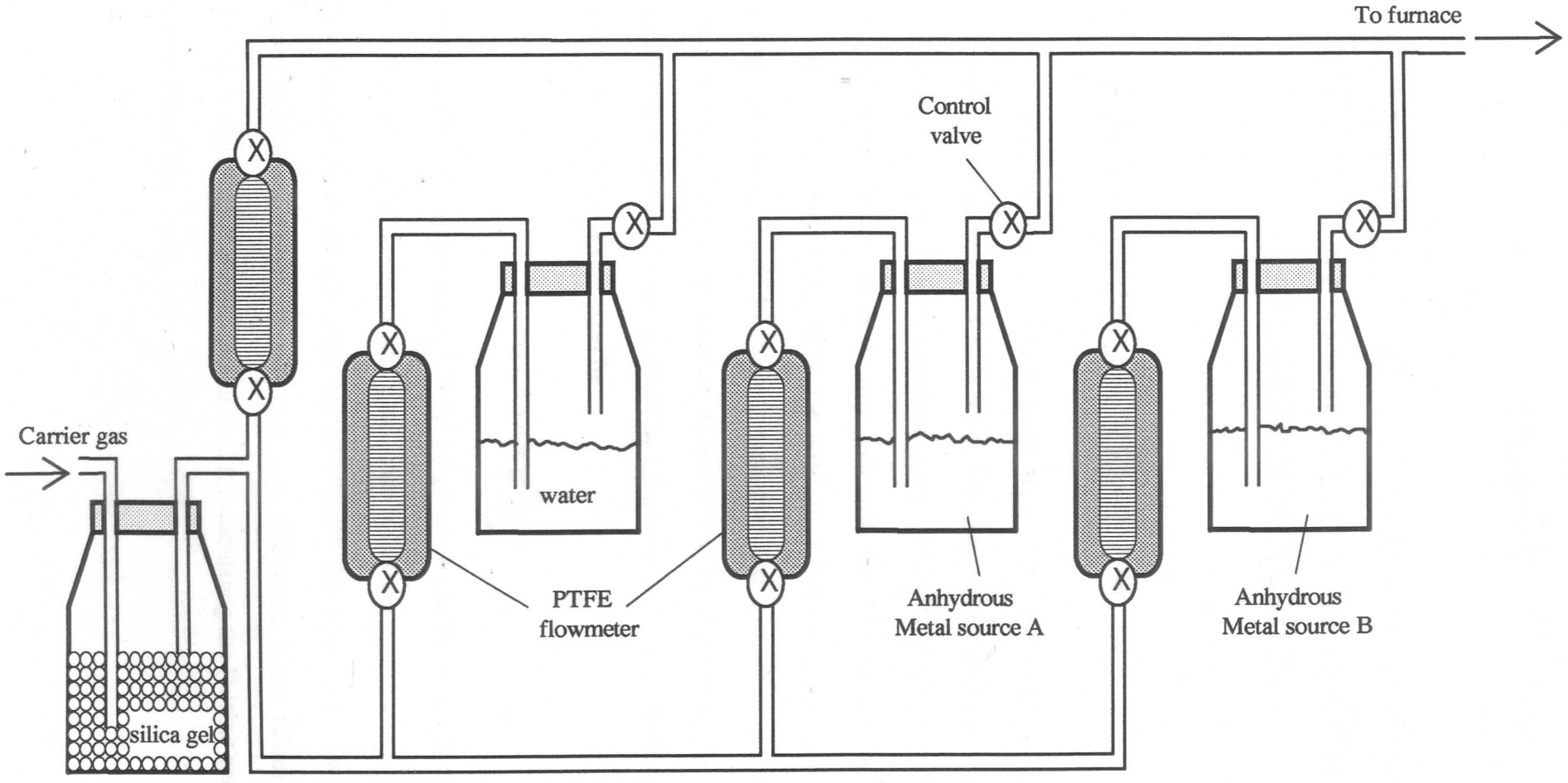

Figure 4.3 Gas feed system for CVD

Chapter 5

RESULTS AND DISCUSSION OF VISCOSITY AND CRYSTALLISATION BEHAVIOUR OF GLASSES STUDIED

5.1 VISCOSITY MEASUREMENTS

Calibration tests were performed using Tate and Lyle's Golden Syrup and a National Bureau of Standards' soda lime silica glass (National Bureau of Standards USA, Standard Sample No 710 soda lime silica glass). At 24 °C, the measured viscosity, $\log_{10}\eta$ of 2.33 for the Syrup compares very well with the 2.34, quoted by Stott, Irvine and Turner[137]. The curves relating to the NBS glass 710 are shown in Figure 5.1. These include the curves for NBS quoted, measured and one which is predicted from the composition of the glass substituting constants into the Fulcher equation which had been derived from chemical factors as given by Lakatos et al[123]. This equation of the viscosity-temperature relation is expressed by

$$\log\eta = -A + \frac{B}{T - T_0} \qquad \text{....(5.1)}$$

where $\log\eta = \log_{10}\eta$ in poise, T is the temperature and T_0, B and A are constants. This equation with three constants was used since it has the special characteristics that quite large differences in the constants can give nearly the same final values while the small errors in measured values can give very large differences in the values of the constants. The three equations given by Lakatos et al for calculating the Fulcher constants from glass compositions are

$$B = -6039.7Na_2O-1439.6K_2O-3919.3CaO+6285.3MgO+2253.4Al_2O_3+5736.4$$

$$A = -1.4788Na_2O+0.8350K_2O+1.6030CaO+5.4936MgO-1.5183Al_2O_3+1.4550$$

$$T_0 = -25.07Na_2O-321.0K_2O+544.3CaO-384.0MgO+294.4Al_2O_3+198.1$$

where the concentrations of the components are expressed as mole per mole of SiO_2.

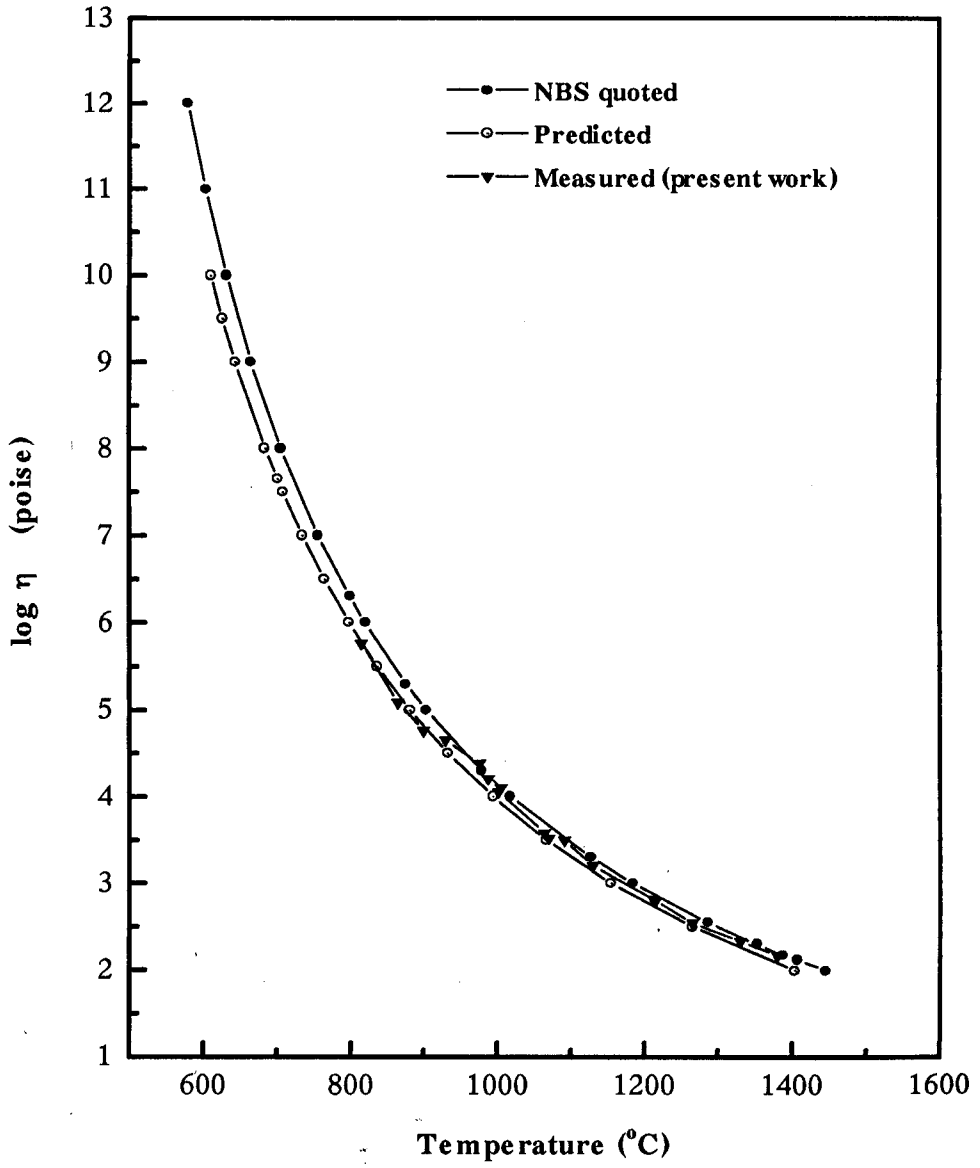

Figure 5.1 Calibration curves for National Bureau of Standards Glass 710

The temperature-viscosity relation obtained from the equation for the NBS soda lime silica glass composition given in Table 5.1 is

$$\log \eta = -1.626 + \frac{4236.118}{T - 266} (\pm 0.02) \qquad \text{....(5.2)}$$

TABLE 5.1
COMPOSITIONS OF GLASSES FOR VISCOSITY MEASUREMENT

Mole %	Composition		
	Glass 1	Glass 2	NBS
SiO_2	62	62	70.5
Na_2O	11	11	8.7
K_2O	-	-	7.7
CaO	20	10.5	11.6
MgO	-	9.5	-
Al_2O_3	5	5	-
Sb_2O_3	-	-	1.1
CuO	2	2	-
SO_3	-	-	0.2
R_2O_3	-	-	0.2

The figure shows an excellent correlation between measured viscosities and values quoted by NBS and those predicted from the composition for this glass. This also agrees extremely well with the measured and calculated values obtained by Napolitano and Hawkins[138,139].

Table 5.1 also shows the compositions of glasses investigated for viscosity measurements. The two glasses, Glass 1 and Glass 2, were chosen to approximate the

container glasses but Glass 2 was doped with a low solubility component CuO, to induce surface crystallisation and with nearly half the CaO of Glass 1, substituted by MgO.

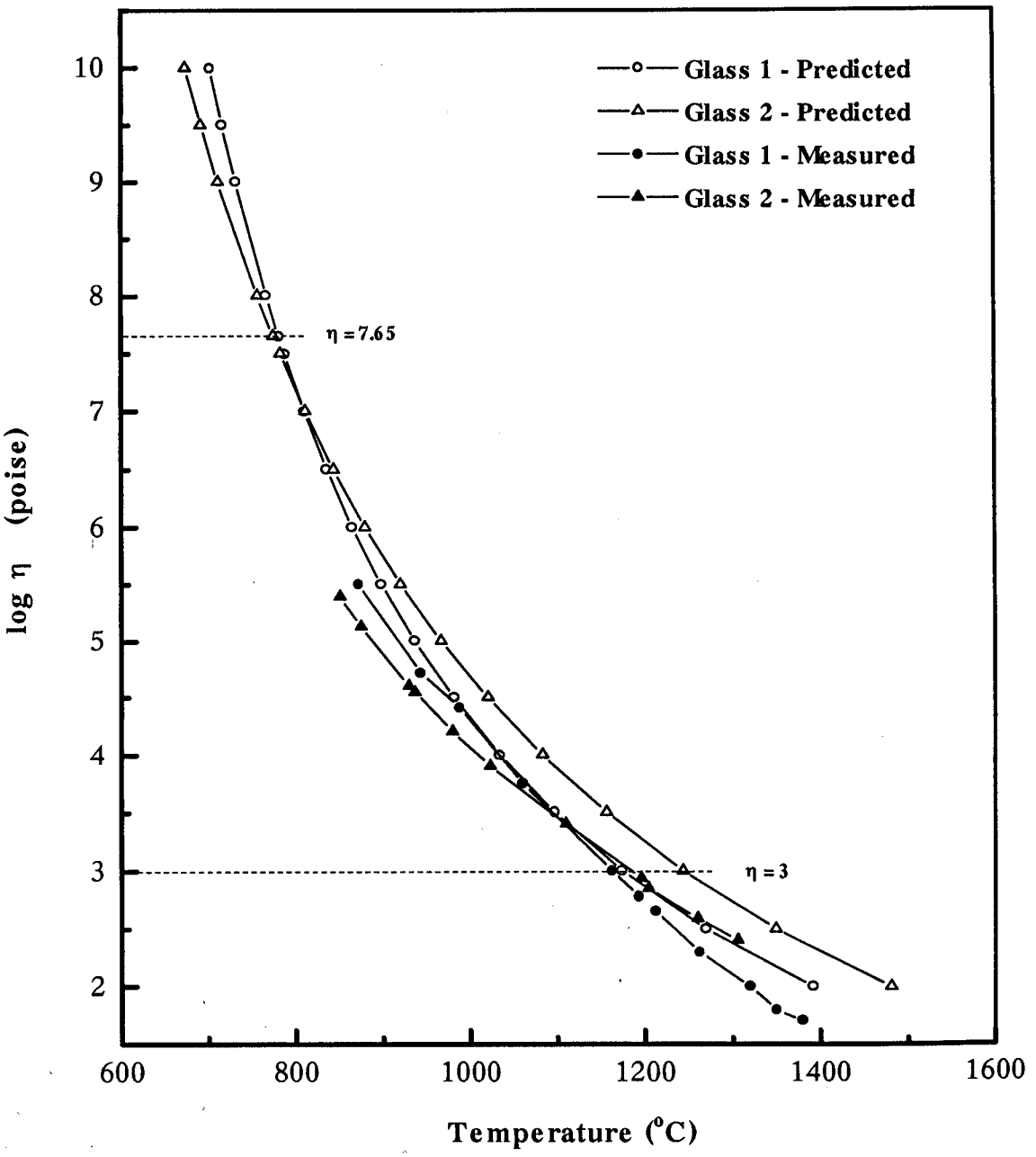

Figure 5.2 Measured and calculated viscosity showing the effect of CuO and MgO in container grade silicate glasses

Figure 5.2 shows the measured and calculated viscosity-temperature relationship for these glasses. It can be seen that there is greater agreement between the measured and predicted viscosity values for Glass 2 than for Glass 1 which shows some departure from parallelity especially at high temperatures. Another feature of the relation is indicated by the appearance of a point of intersection for each set of predicted and measured plots for both glass compositions. In case of the predicted set of data, the intersection corresponds approximately to the softening temperature at log η = 7.65, whereas measured data intersects at $\log_{10} \eta = 3$, the sink point or working temperature; i.e. the glass without the MgO substitution for CaO exhibits a steeper viscosity beyond the intersection points. Although it is expected[111] that replacement of CaO by MgO reduces crystallisation and the liquidus temperature, no such evidence is found in the present case. However, the results are consistent with a previous observation in the literature[140,141] that the liquidus temperature is lowered by no more than 4 wt % MgO, but then increases very steeply to ~ 12 wt % MgO addition. This will result in an increase in viscosity as seen in the present case.

The usefulness of Lakatos constants, in conjunction with the Fulcher equation, has also been demonstrated by Napolitano et al[139] who found an extremely good agreement between the calculated and measured viscosity of a sheet glass[142] as well as for the NBS glass. Consequently, in the present work, the equations for the Fulcher constants have been used to calculate viscosity-temperature profiles for all the experimental glasses investigated. Table 5.2 summarises the calculated molar compositions of the glasses in relation to one mole of SiO_2.

The viscosity curves of various glasses are shown in Figures 5.3-5.8. The reference points at specific viscosity values are also indicated in the plots that provide a comparative view of general nature of the relationship. Details of the predicted values of viscosities and corresponding temperatures at $\log_{10} \eta = 3$, 7.5, 13 and 14.5 are given in Table 5.3.

TABLE 5.2
COMPOSITIONS OF EXPERIMENTAL GLASSES PER MOLE OF SiO_2 FOR VISCOSITY CALCULATION OF FULCHER CONSTANTS

Glass code	Oxide contents (mole/mole SiO_2)				
	Na_2O	K_2O	CaO	MgO	Al_2O_3
NBS 710	0.12340	0.10922	0.16454	0	0
Glass 1	0.17742	0	0.32258	0	0.08065
Glass 2	0.17742	0	0.16935	0.15323	0.08065
Glass 3	0.17460	0	0.33333	0	0.07937
Float F1	0.22107	0	0.08006	0.05750	0.06066
EMH 7	0.16027	0.00548	0.14521	0.04795	0.01096
NLS 1P	0.22920	0	0.12963	0	0
NLS 8P	0.23445	0	0.23943	0	0
R4795	0.15397	0.00413	0.16637	0.04324	0.00950
R4795/3	0.15403	0.00420	0.16636	0.04331	0.03364
R4795/5	0.15412	0.00411	0.16645	0.04339	0.04991
R4795/10	0.15398	0.00408	0.16652	0.04331	0.09011
NLS 1	0.22578	0	0.14672	0	0
NLS 2	0.23019	0	0.21588	0	0
NLS 3	0.24598	0	0.25589	0	0
NLS 4	0.34629	0	0.24658	0	0
NLS 5	0.19916	0	0.15930	0	0
NLS 6	0.20335	0	0.18465	0	0
NLS 7	0.21055	0	0.22952	0	0
NLS 8	0.23318	0	0.28197	0	0
NLS 9	0.26839	0	0.28016	0	0
NLS 10	0.31535	0	0.28056	0	0
NLS 11	0.20566	0	0.32456	0	0
NLS12	0.27884	0	0.08803	0	0

TABLE 5.2 (contd)
COMPOSITIONS OF EXPERIMENTAL GLASSES PER MOLE OF SiO_2 FOR VISCOSITY CALCULATION OF FULCHER CONSTANTS

Glass code	Oxide contents (mole/mole SiO_2)				
	Na_2O	K_2O	CaO	MgO	Al_2O_3
Emhart 1	0.14732	0.01115	0.14832	0.04802	0.02321
Emhart 2	0.16115	0.01002	0.15124	0.03503	0.02212
Emhart 3	0.17321	0.01113	0.13563	0.01730	0.02752
Emhart 4	0.17136	0.01115	0.14314	0.02351	0.02623
Emhart 5	0.15420	0.00852	0.15321	0.03507	0.01631
Emhart 6	0.16806	0.00938	0.13713	0.02313	0.01922
Emhart 7	0.16621	0.00811	0.13631	0.03321	0.01842
NCS 1	0.02241	0	0.06502	0	0
NCS 2	0.12892	0	0.11672	0	0
NCS 3	0.09029	0	0.15164	0	0
NCS 4	0.24906	0	0.23946	0	0
NCS 5	0.20637	0	0.18989	0	0
NCS 6	0.35538	0	0.12786	0	0
NCS 7	0.35464	0	0.20592	0	0
NCS 8	0.34521	0	0.29693	0	0
NCS 9	0.35291	0	0.38471	0	0
NCS 10	0.35353	0	0.49954	0	0

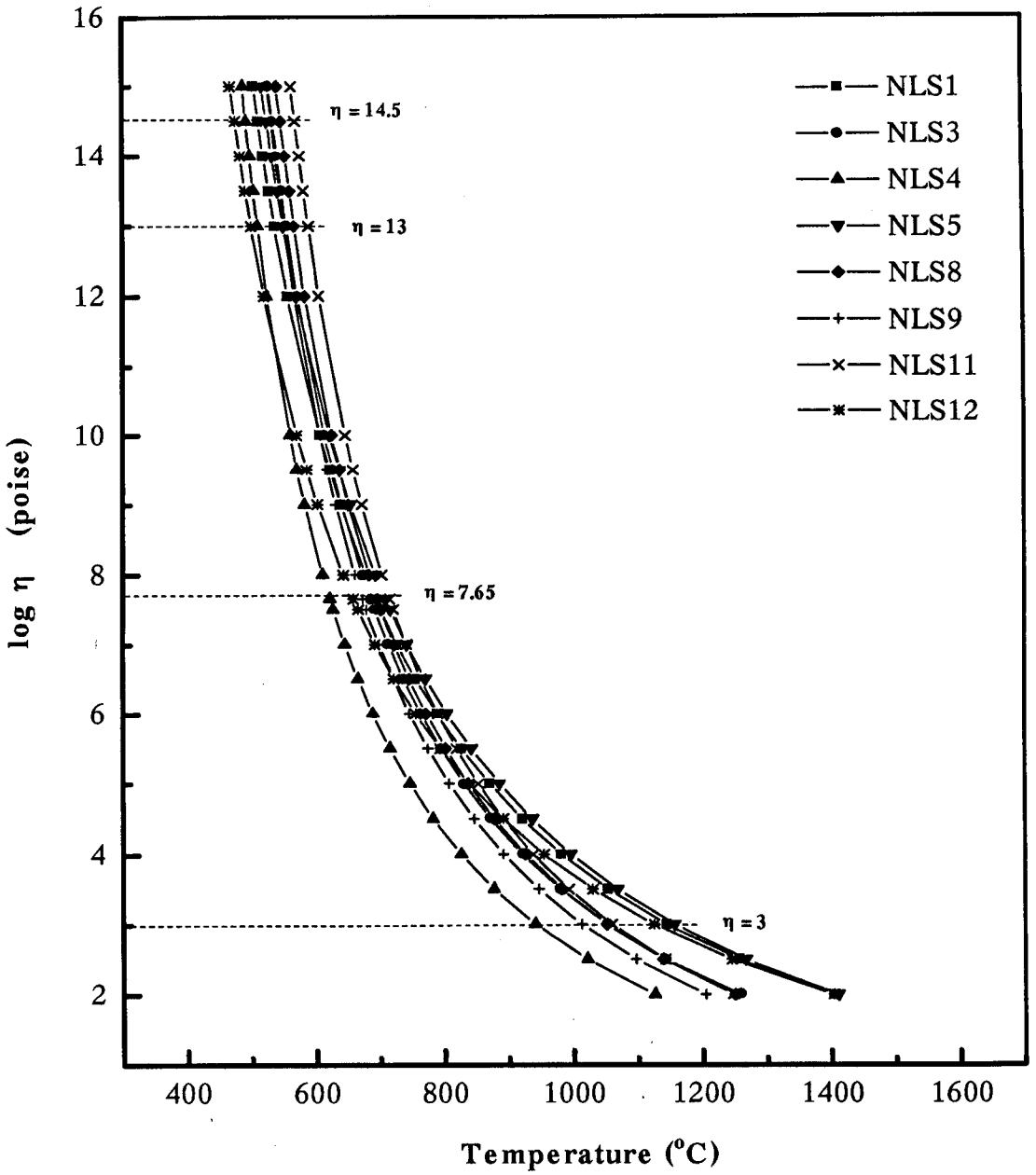

Figure 5.3 Variation of calculated viscosity with temperature for NLS series glasses

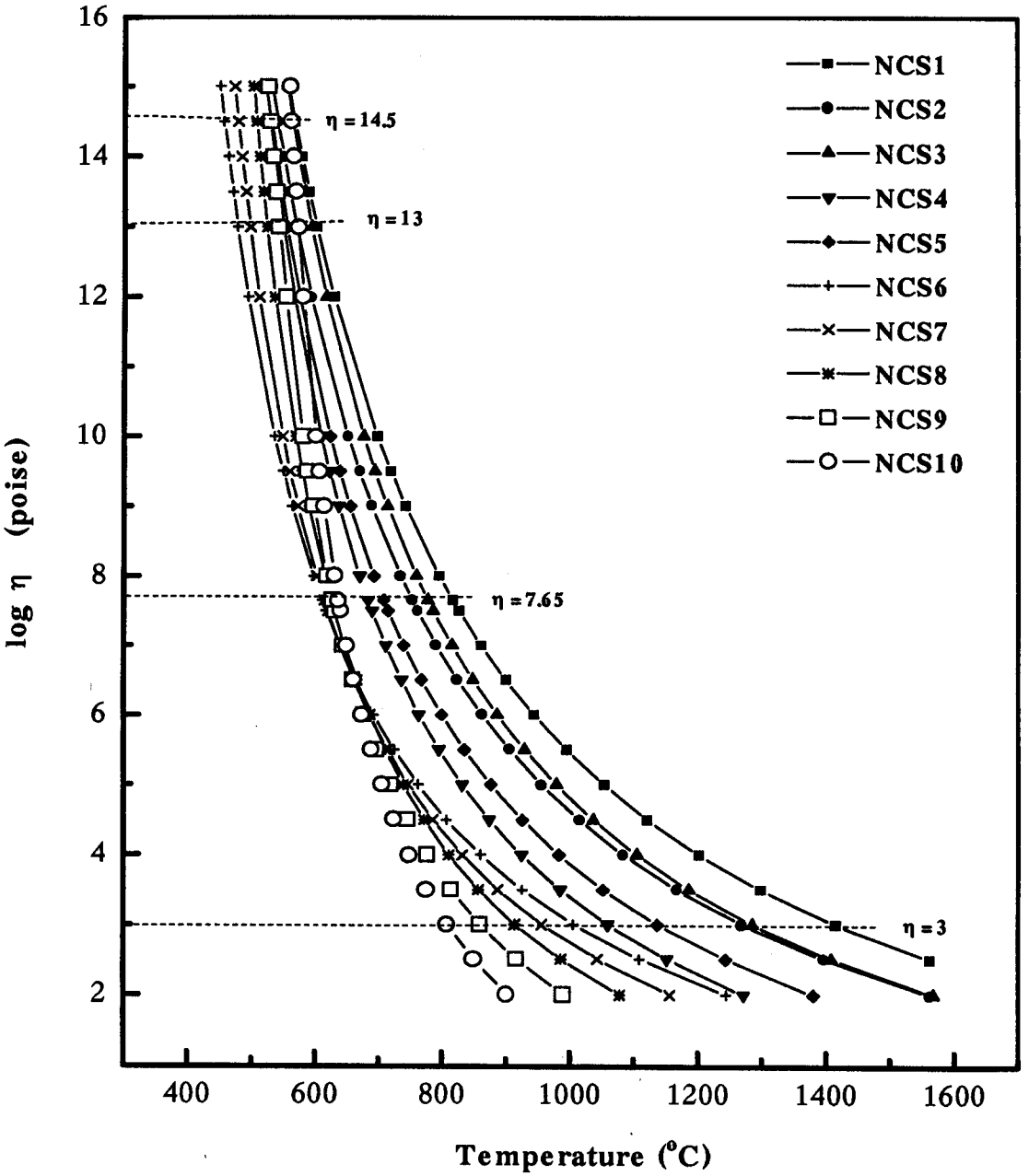

Figure 5.4 Variation of calculated viscosity with temperature for NCS series glasses

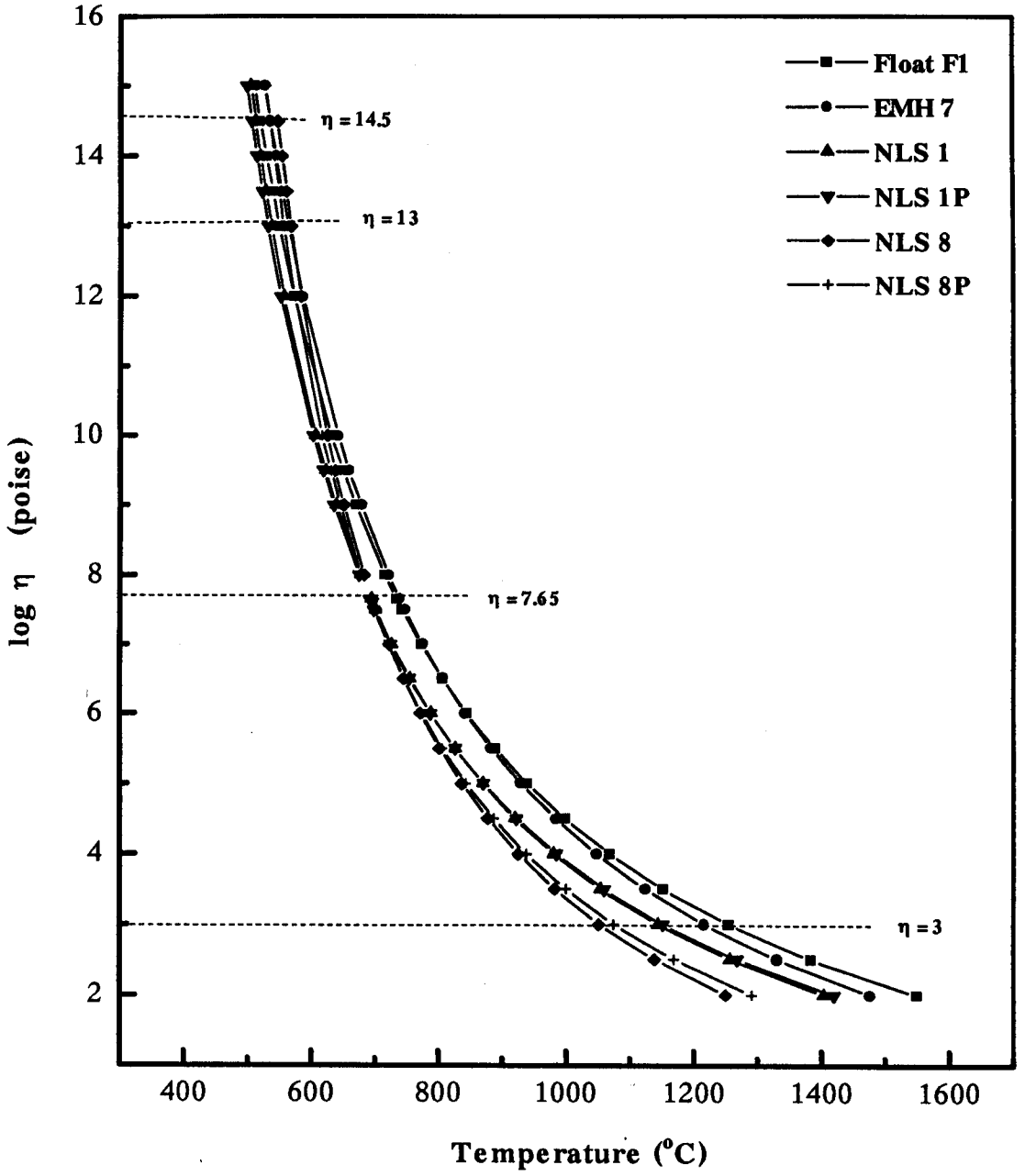

Figure 5.5 Variation of calculated viscosity with temperature for the Float, NLS 1, NLS 8 and EMH 7 and P_2O_5 modified soda lime silica glasses

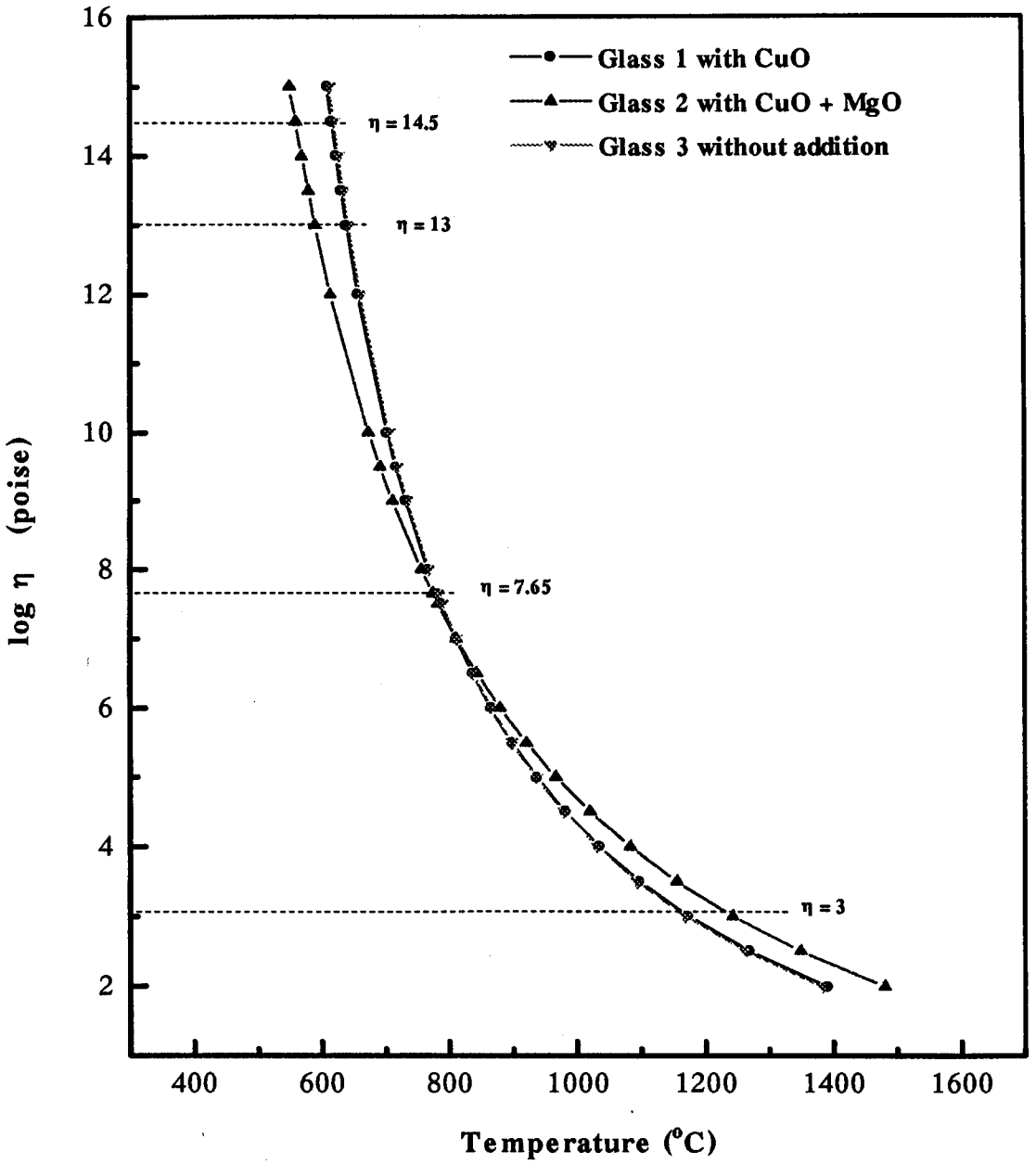

Figure 5.6 Effect of CuO and MgO on calculated viscosity in simple container grade silicate glasses

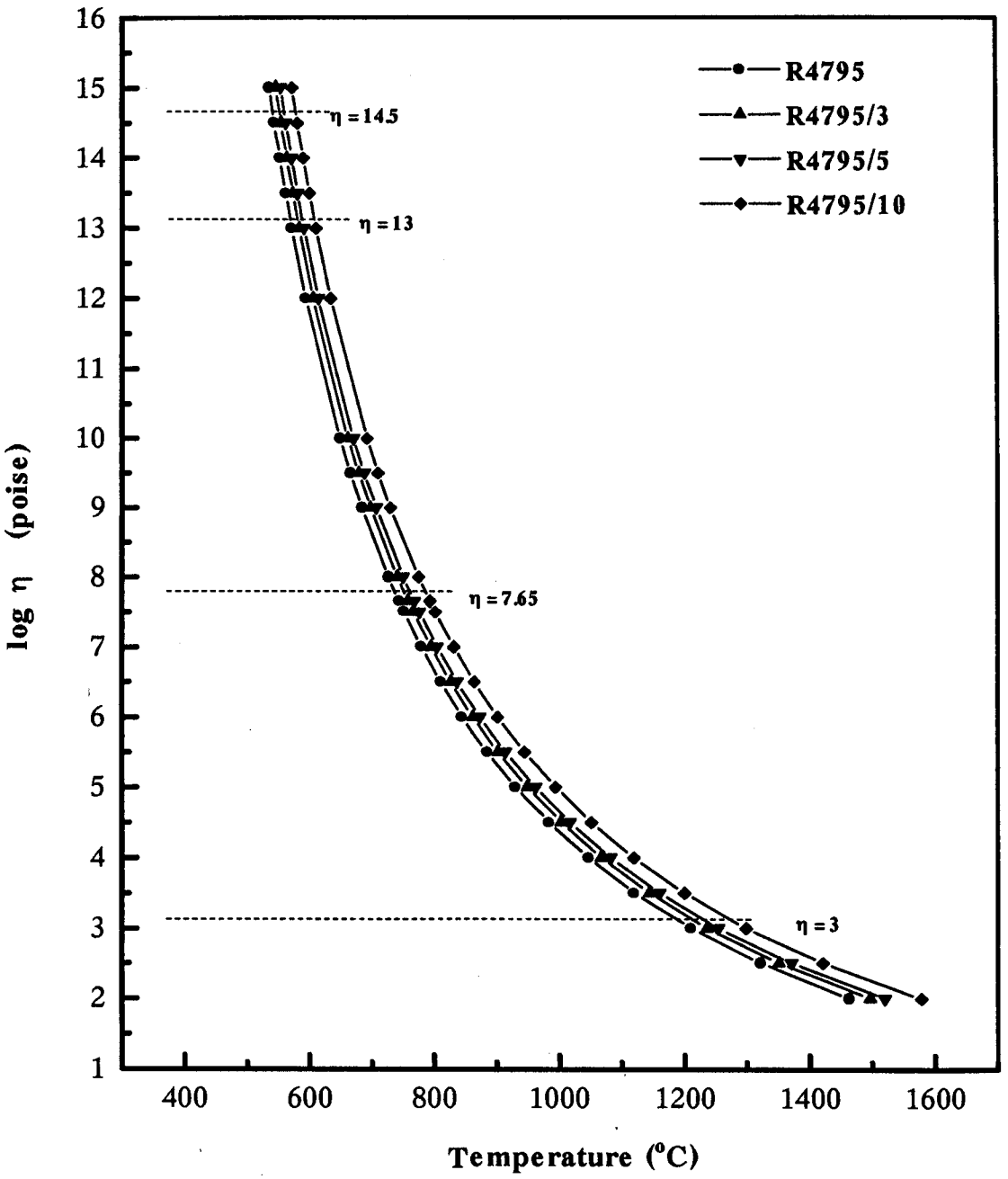

Figure 5.7 Variation of calculated viscosity with temperature for alumina modified Rockware glasses

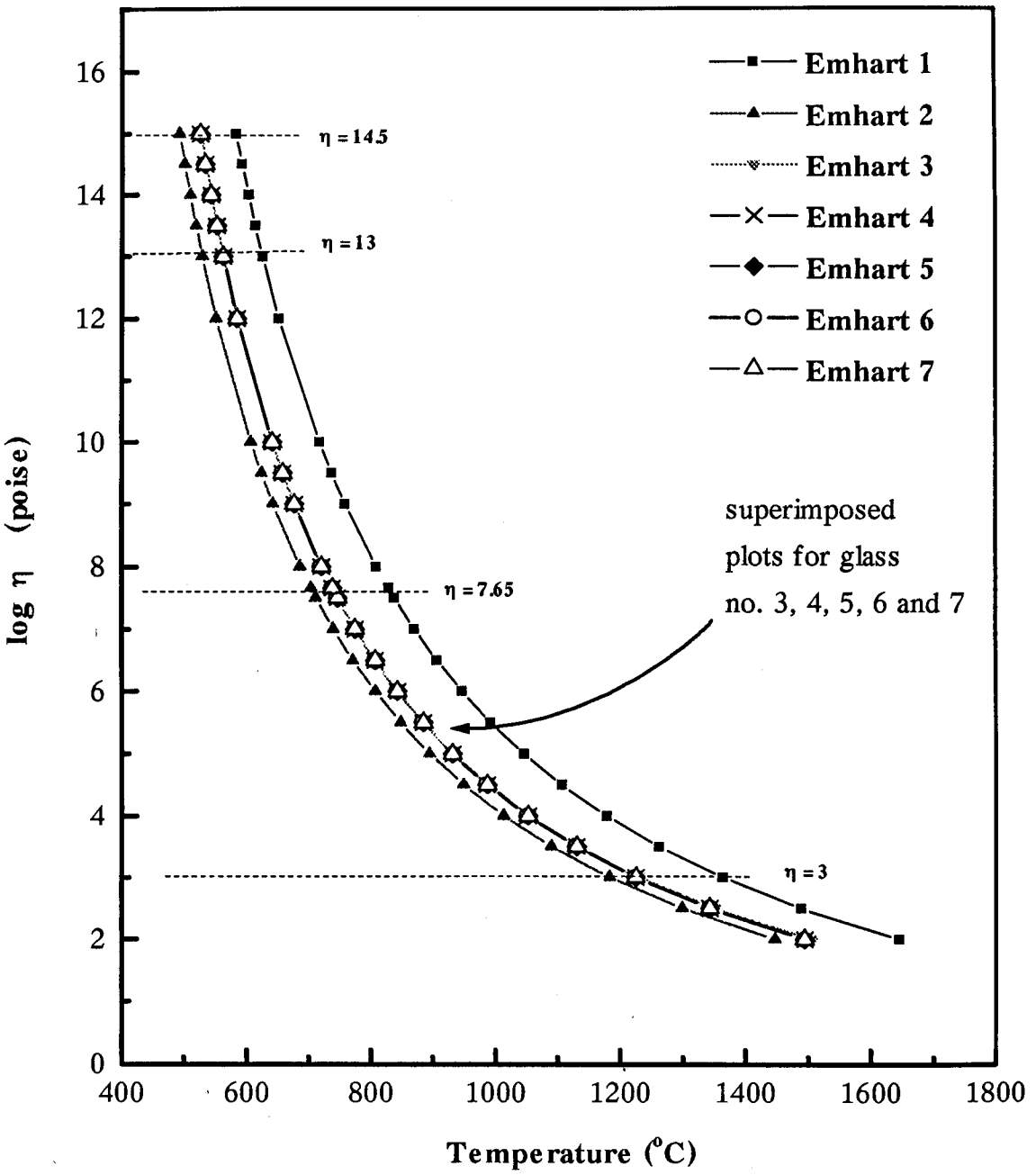

Figure 5.8 Variation of calculated viscosity with temperature for Emhart glasses

TABLE 5.3
SUMMARY OF CALCULATED TEMPERATURES FOR SPECIFIC VISCOSITY VALUES

Glass code	Glass Property (°C)					
	Gob temperature	Softening point S	Annealing point A	Strain point	WRI S-A	RMS (S-450) x 100/ (S-A+80)
	log η = 3	log η = 7.65	log η = 13	log η = 14.5		
NBS 710	1154	701	552	531	149	110
Glass 1	1174	781	639	616	142	149
Glass 2	1244	774	590	560	184	123
Glass 3	1169	782	642	619	140	151
Float F1	1255	734	549	519	185	107
EMH 7	1217	739	563	535	176	113
R4795	1211	743	571	543	172	116
R4795/3	1237	758	583	555	175	121
R4795/5	1254	768	591	562	177	124
R4795/10	1299	793	610	581	183	130
NLS 1	1144	694	536	511	158	103
NLS 2	1094	694	552	529	142	110
NLS 3	1052	686	555	534	131	112
NLS 4	941	622	510	493	112	90
NLS 5	1157	709	550	525	159	108
NLS 6	1144	709	555	531	154	111
NLS 7	1108	707	563	540	144	115
NLS 8	1052	696	567	546	129	118
NLS 9	1013	673	552	532	121	111
NLS 10	958	644	532	514	112	101
NLS 11	1059	715	589	569	126	129
NLS 12	1125	659	500	475	159	87
NLS 1P	1152	691	531	506	160	101
NLS 8P	1075	692	556	536	136	112

TABLE 5.3 (contd)
SUMMARY OF CALCULATED TEMPERATURES FOR SPECIFIC VISCOSITY VALUES

Glass code	Glass Property (°C)					
	Gob temperature	Softening point S	Annealing point A	Strain point	WRI S-A	RMS (S-450) x 100/ (S-A+80)
	log η = 3	log η = 7.65	log η = 13	log η = 14.5		
Emhart 1	1489	828	626	593	202	134
Emhart 2	1299	703	529	501	174	100
Emhart 3	1350	738	563	535	175	113
Emhart 4	1342	739	565	537	174	114
Emhart 5	1340	745	570	542	175	116
Emhart 6	1344	737	562	534	175	113
Emhart 7	1343	738	561	533	177	112
NCS 1	1416	817	602	567	215	124
NCS 2	1269	753	570	541	183	115
NCS 3	1285	777	594	565	183	124
NCS 4	1059	683	550	528	133	109
NCS 5	1137	708	555	531	153	111
NCS 6	1006	610	477	456	133	75
NCS 7	956	614	497	478	117	83
NCS 8	914	625	524	507	101	97
NCS 9	860	627	543	529	84	108
NCS 10	808	636	573	562	63	130

WRI = Working Range Index

RMS = Relative Machine Speed

Figures 5.3 and 5.4 represent calculated viscosity data for two series of soda lime silica glasses (see Table 3.1). For most glass compositions in the NLS series the calculated values for temperatures corresponding to the selected viscosity points varied only slightly, especially the softening, annealing and strain points (93, 89 and 94 °C, respectively) whereas at $\eta = 3$, the melting temperature variation is approximately 220 °C. This reflects the small range of compositional variation in these glasses. On the other hand, the variation is large for the NCS series glasses at all selected viscosities. In particular, the liquidus temperature shifted by as much as 600 °C, and progressively to lower temperatures, due to increasing alkali content. The corresponding range for the softening temperature was estimated to be ~ 200 °C with variation in annealing point and strain points being 130 and 111 °C, respectively.

Figure 5.5 shows the influence of P_2O_5 on the viscosity of the selected soda lime silica glasses, including commercial Float F1 and EMH 7, subsequently investigated for the crystallisation studies. Comparing Float F1 and EMH 7, both show similar profiles, except for a slight increase in η in the Float glass at higher temperatures, attributed to the additional MgO content. NLS 1, NLS 8 and their P_2O_5 modified versions exhibited corresponding lower viscosities due to the absence of alumina in these glasses. The effect of P_2O_5 on NLS glasses is apparent only in the shift of the melting temperatures.

The effect of alumina additions (3, 5 and 10 wt %) on viscosity in commercial Rockware container glasses is shown in Figure 5.7. It is interesting to observe that the variation of the reference viscosities is extremely narrow. This suggests the possibility of using high alumina container glasses without incurring adverse working properties. The increase in viscosity at any given temperature is evidently due to the additive effect of alumina on η.

The viscosity temperature profiles for all Emhart series of commercial container glasses are shown in Figure 5.8. Of these, glasses 4, 6 and 7 are fairly typical of present

European practice. The viscosity relations for all these glasses are very similar except Emhart 1 which shows a significant temperature shift to the high side at all reference points. This is due to its compositional difference from other glasses, since it contains 11.33 wt % R_2O, 14.10 wt % RO and 1.88 wt % R_2O_3 i.e. reduced alkali content.

The working range index (WRI) and RMS, given in Table 5.3, are two parameters commonly used in the industry to assess the ease and extent of forming operations. of these, RMS is considered more important since it provides a criterion as to the overall suitability of a given glass for forming. It can be seen that most commercial container glasses such as Rockware R4795 and Emhart series give values ranging between 100 and 116. It is important to note that the ternary glasses NLS 1 - NLS 10, NCS 2, NCS 4, NCS 5 and NCS 9 fall within this range. Moreover, some of these glasses have also been successfully surface crystallised and can therefore be considered as suitable base compositions for further modification into full specifications of container glass.

5.2 THERMAL PROPERTIES

The DTA spectra of some of the experimental glasses are shown in Figures 5.9-5.11 and Table 5.4 summarises the results. In this work the extrapolated point with the baseline was taken as relaxation temperature, T_g, the peak of the first endotherm as a general value for T_s and the peak of the exotherms as crystallisation point T_c.

Figures 5.9 and 5.10 show the DTA curves for a container grade soda lime silica glass with or without the addition of CuO. Although T_g and melting point, T_m remain essentially unchanged for both glasses, the T_s of Glass 1 at 660 °C with added CuO was found to be slightly higher than Glass 3, without the addition of nucleating agent. It is well known that the shape of the crystallisation peak is related to the devitrification mechanism.

A broad crystallisation peak indicates surface crystallisation whereas a very sharp peak signifies a bulk/volume crystallisation process. For Glass 1, the appearance of a poorly resolved, broad crystallisation peak at ~ 700 °C has been masked by the T_s at 660 °C and is thought to be due to the precipitation of tenorite. This crystallisation is confirmed by the X-ray diffraction analysis (see section 5.3) of this glass at 670 °C, without evidence of any surface deformation. This indicates that the bulk glass in the XRD study is more resistant to softening and amenable to surface crystallisation than the powdered material as used in the DTA, where softening occurred more readily from the particle surface. The other broad exothermic peak at ~ 860 °C corresponds to the crystallisation of parawollastonite ($CaSiO_3$) as confirmed by XRD analysis.

TABLE 5.4
SUMMARY OF THERMAL ANALYSIS RESULTS

Glass	T_g	T_s	T_c	T_m
	(°C)			
Glass 3	590	636	-	900
Glass 1	594	660	700, 860	998
R4795	650	693	-	1005
R4795/3	659	700	-	1020
R4795/5	689	736	-	1081
R4795/10	725	770	-	1103

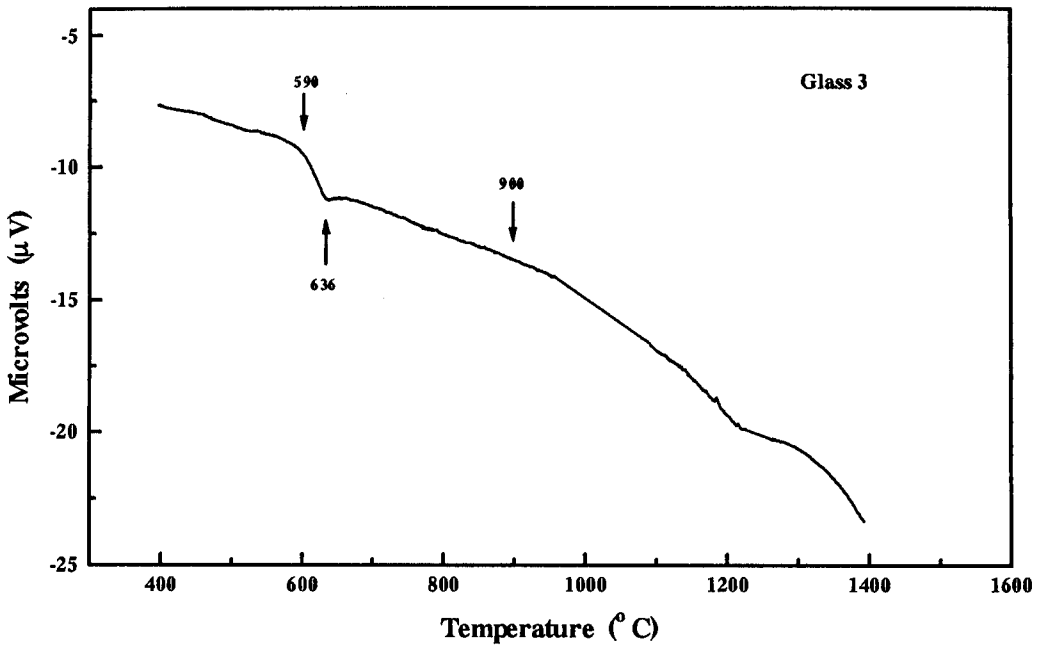

Figure 5.9 DTA thermogram of Glass 3 without added CuO

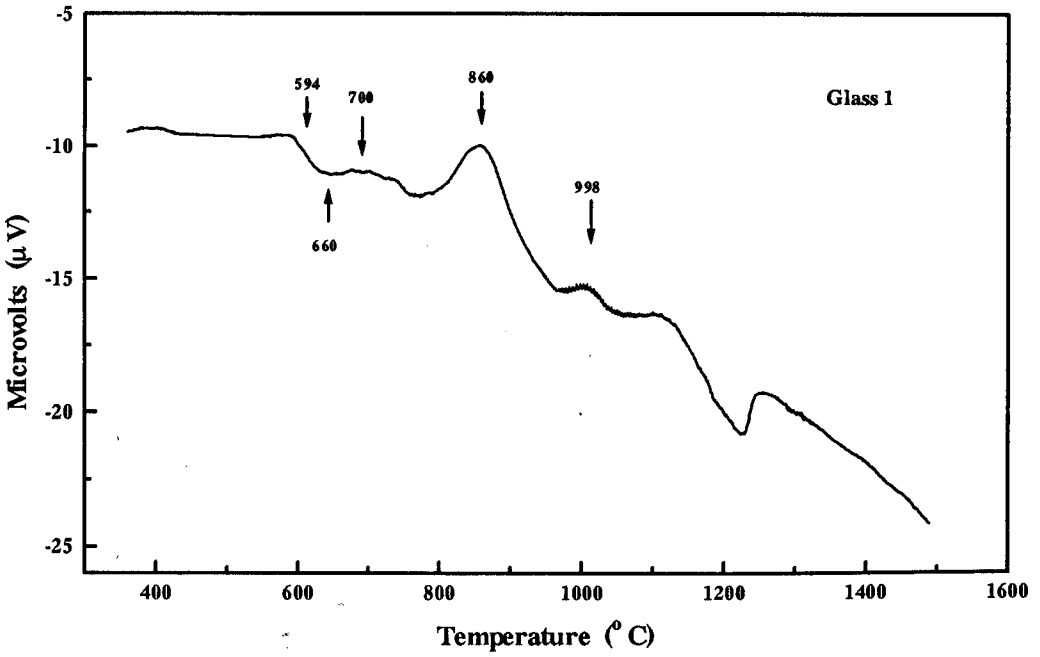

Figure 5.10 DTA thermogram of Glass 1 with added CuO

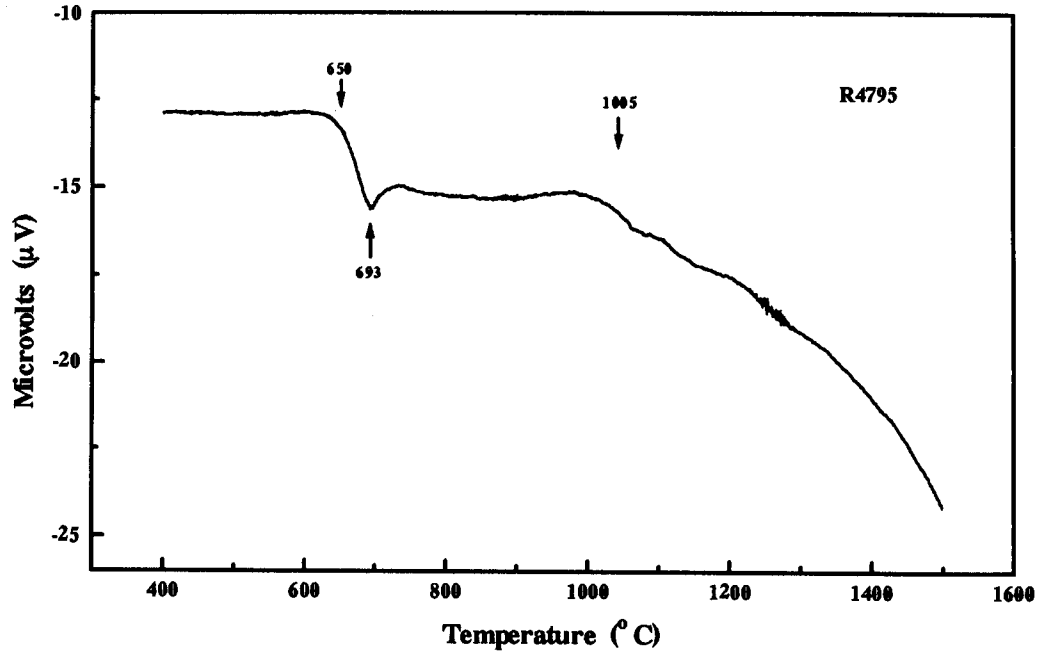

Figure 5.11(a) DTA thermogram of Rockware R4795 base glass

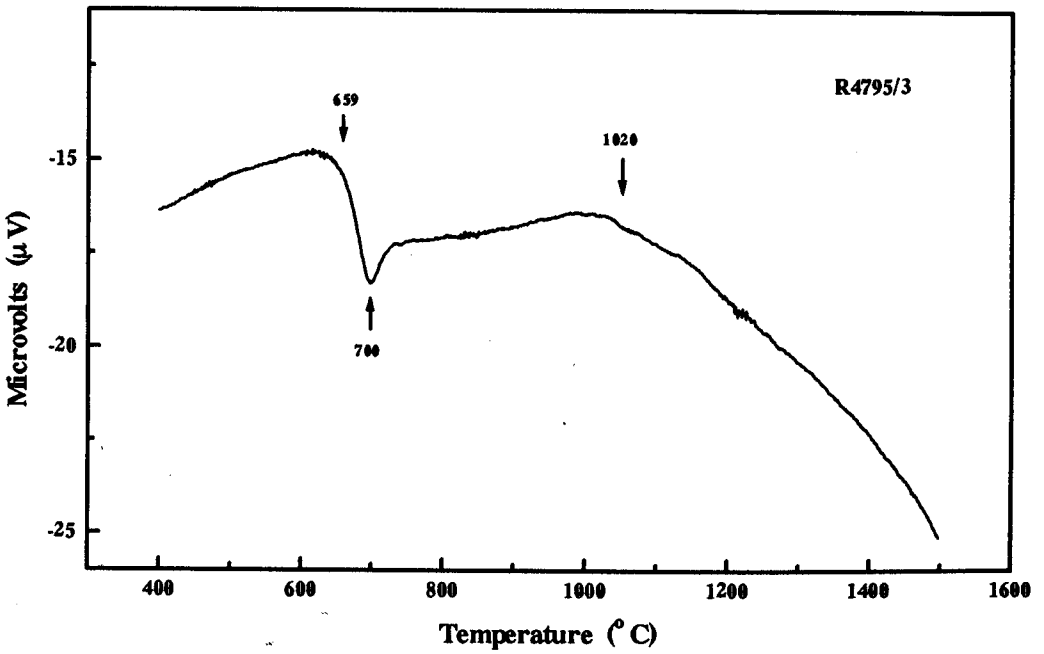

Figure 5.11(b) DTA thermogram of Rockware glass modified with 3 wt % alumina

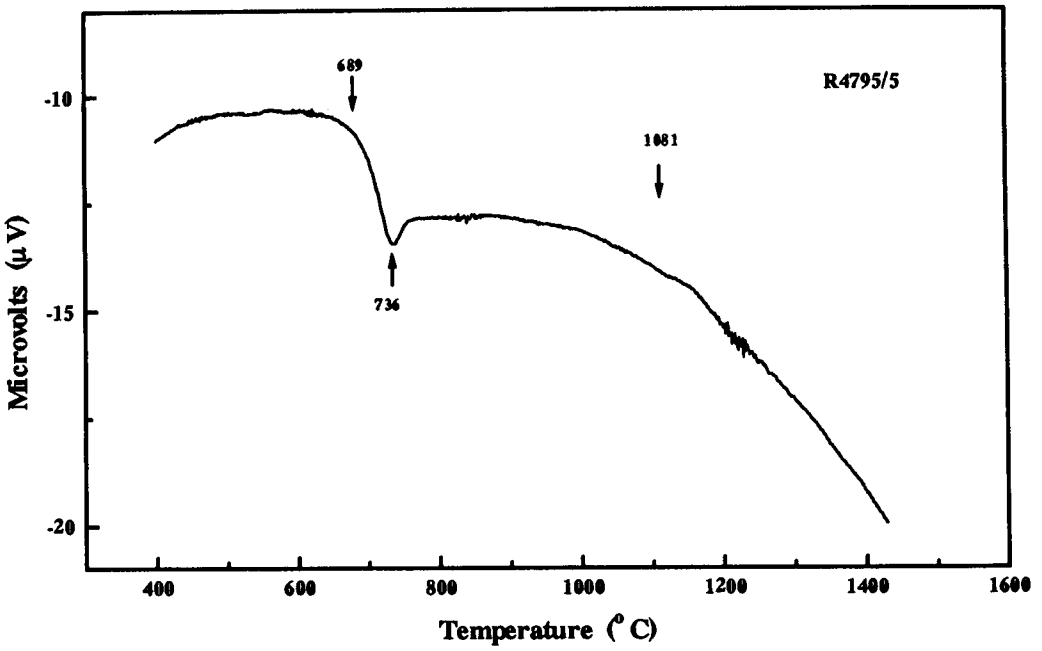

Figure 5.11(c) DTA thermogram of Rockware glass modified with 5 wt % alumina

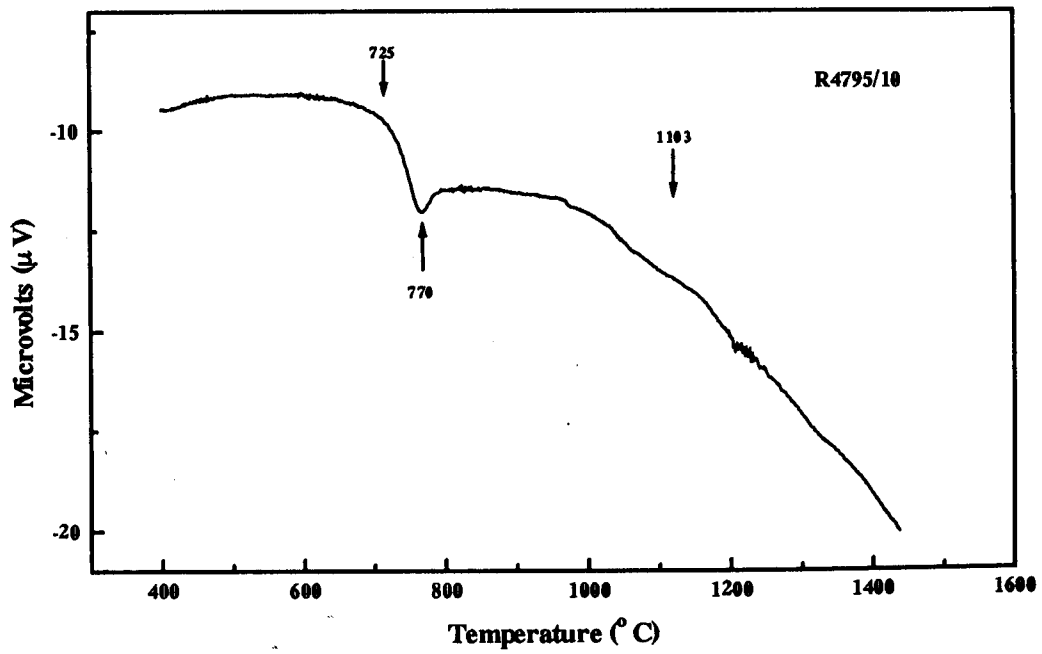

Figure 5.11(d) DTA thermogram of Rockware glass modified with 10 wt % alumina

DTA curves for Rockware R4795 base glass and those modified with alumina of varying amount are shown in Figures 5.11(a)-(d). The shift of the endotherms in these glasses i.e. increased T_s with higher Al_2O_3 content suggests that it is raising the glass viscosity and may be strengthening the glass network.

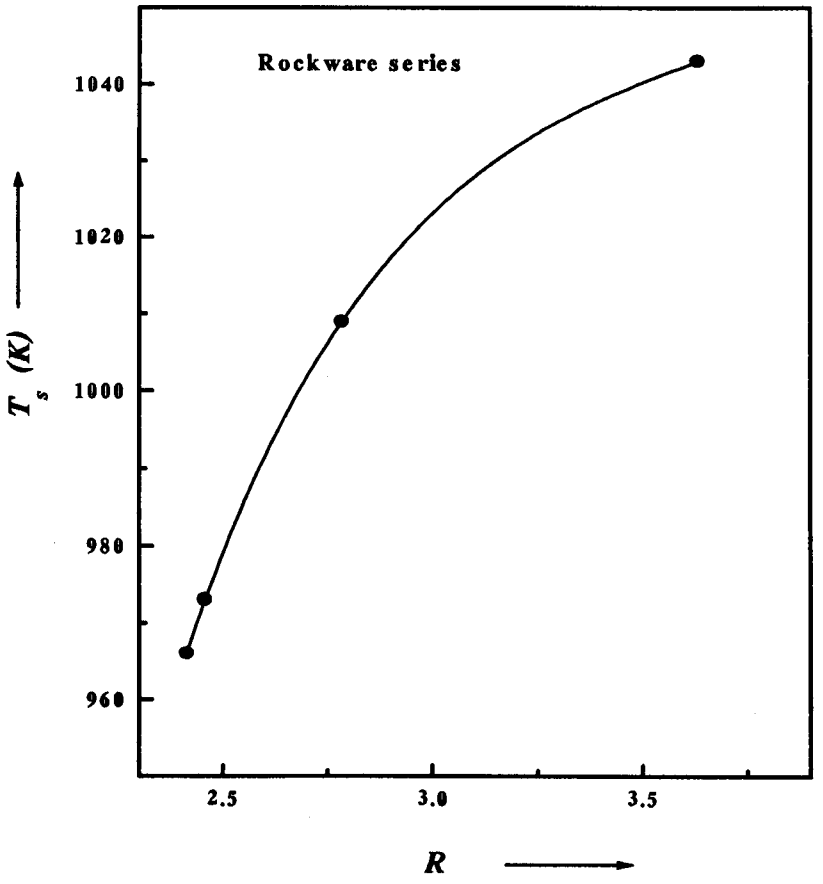

Figure 5.11(e) Variation of T_s values as a function of R = O/Si molar ratio for Rockware series glasses

The values of the T_s for the four Rockware series glasses are also plotted as a function of oxygen/silicon molar ratio R in Figure 5.11(e). Normally, the relation is found to be linear but only when a given glass is a mixture of oxides each proportionally contributing to the whole property of the glass[143]. However, when the glass consists of

constituents such as Al_2O_3 or MgO, other than SiO_2 as a network former, the deviation from linearity is observed, particularly if the Na_2O/CaO ratio is constant. In the series of glasses investigated, this ratio is between 0.925 and 0.926. It can be seen therefore that the slightly bent or non-linear increase of T_s values with respect to the progressive increase of R is consistent with the increase of the average number of non bridging oxygen atoms in a SiO_4 group because network bonds involving bridging oxygen atoms are thermally less labile than those involving non bridging oxygen atoms.

5.3 PHASE ANALYSIS

The XRD spectra of the two surface crystallised glasses, namely, Glass 1 and a Rockware R4795/10 glass, are shown in Figures 5.12 and 5.13. The results are also summarised in Table 5.5

Figure 5.12 shows the development of the surface crystallisation of tenorite crystals in a container grade glass with CuO. The pristine glass shows the diffuse spectrum, characteristic of the amorphous form. With further heat treatment of the pristine glass (with or without the aid of abrasion), it could be seen that tenorite crystals had formed on the surface. Line broadening analysis of both the $(\bar{1}11)$ and (111) peaks yields an estimate of the average crystallite size of approximately 400 and 435 Å for heat treated samples with and without abrasion, respectively. It is clear that abrasion produced a narrower distribution of considerably smaller crystallite size due to the presence of uniform density of flaws. The refined parameters for a monoclinic cell (space group *C2/c*), listed in Table 5.5, agree well with the published data for tenorite. Variation in the relative intensity of the peaks was not significant and the effect of preferred orientation was minimal.

Development of surface crystallisation on Li^+ ion-exchange in a Rockware glass R4795/10 is shown in Figure 5.13. It can be seen that the untreated glass shows the expected amorphous trace. With increasing duration of exchange, a surface layer of solid solution of β-eucryptite/β-spodumene forms and the corresponding spectra are shown.

TABLE 5.5
SUMMARY OF XRD PHASE ANALYSIS

Glass	History	Phase	2θ (degrees)	FWHM	Crystallite Size (Å)	Lattice Parameter (Å)	c/a
Glass 1	Unabraded + Heat Treated	Tenorite	35.5146	0.1920	435	a = 4.687(0) b = 3.423(7) c = 5.123(6)	
	Airabraded + Heat Treated		35.5077	0.2081	400	a = 4.688(7) b = 3.471(3) c = 5.093(1)	
R4795/10	Ion-exchanged for 10 seconds	β-eucryptite	25.6418	0.3479	235	a = 5.218(4) c = 11.200(0)	2.146
	Ion-exchanged for 20 seconds		25.4856	0.2378	343	a = 5.228(4) c = 10.938(4)	2.092
	Ion-exchanged for 30 seconds		25.1066	0.2328	380	a = 5.245(1) c = 10.925(5)	2.083

The cell parameters for the hexagonal phase agrees well with the JCPDS data for β -eucryptite and the *c/a* ratio decreases with the time of ion-exchange. The measured crystallite size using the (102) peak of the solid solution phase is shown to increase slowly with the exchange time. The sizes are remarkably small and in the nanometer scale and indicative of a low TCE phase with both *c* and *a* parameters changing with exchange time.

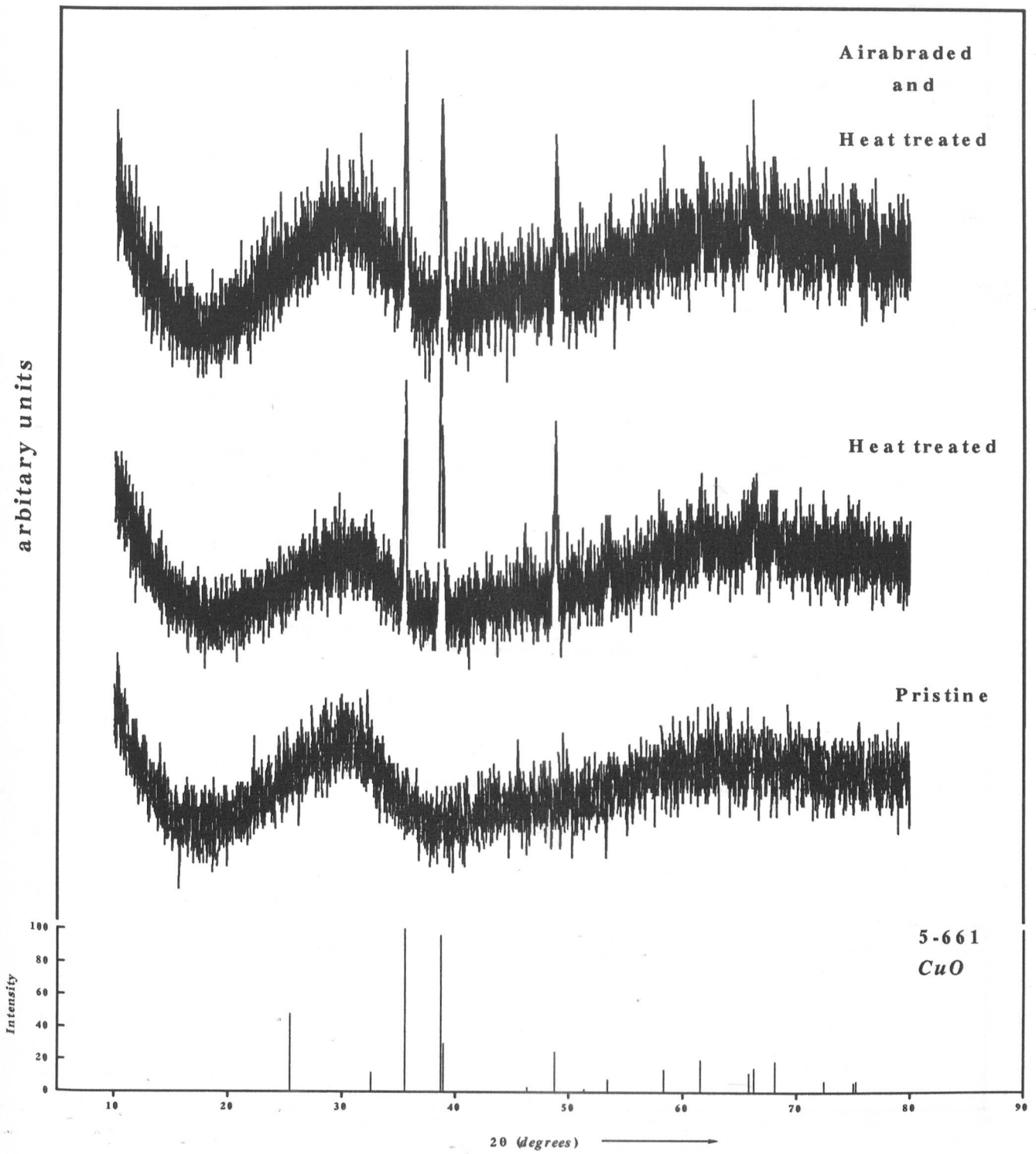

Figure 5.12 XRD diffractogram of Glass 1 showing surface crystallisation of tenorite

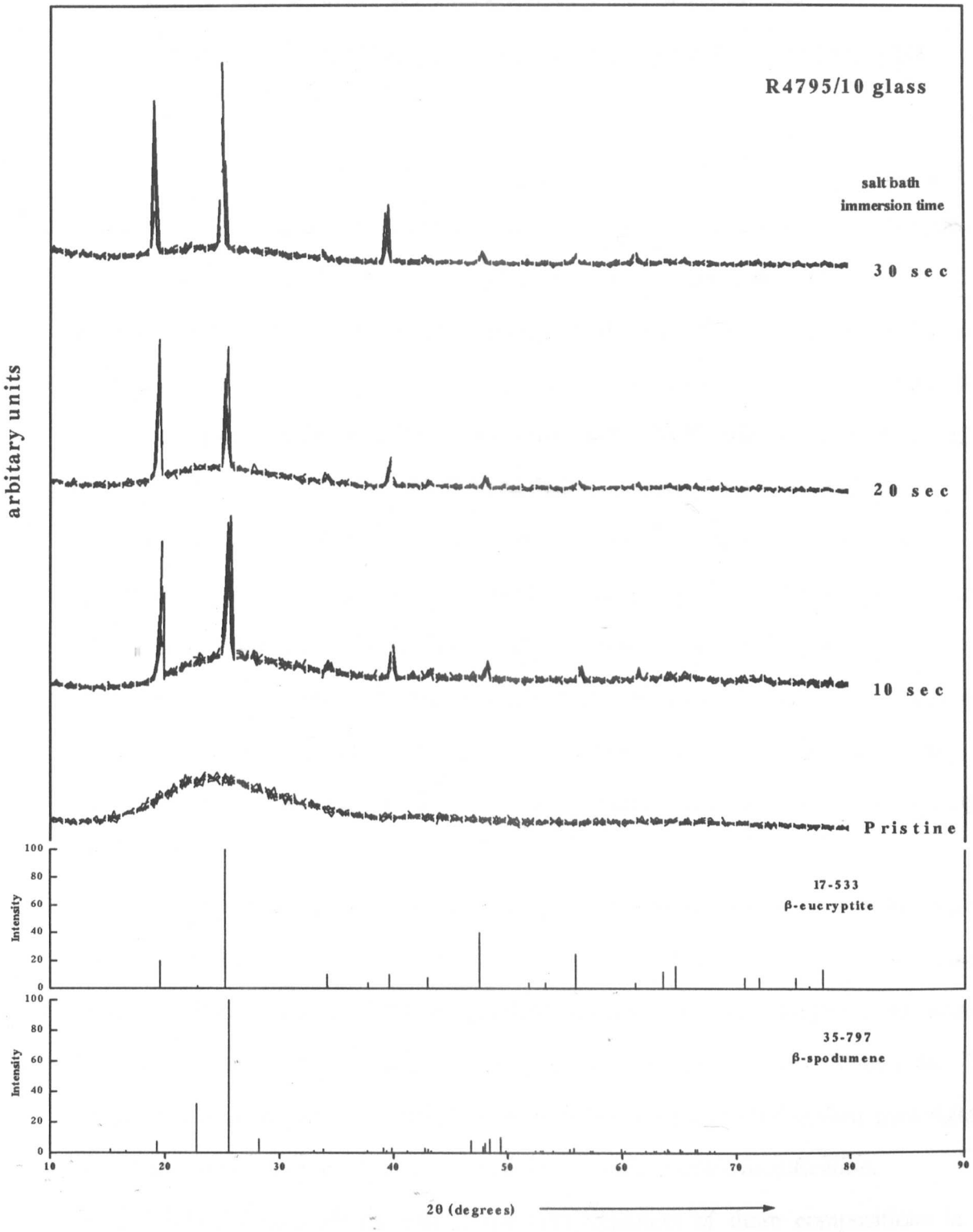

Figure 5.13 XRD diffractogram of alumina modified Rockware R4795/10 showing development of lithium containing phases with ion exchange time

5.4 SURFACE CRYSTALLISATION STUDIES

5.4.1 CRYSTALLISATION BEHAVIOUR OF GLASSES IN THE Na_2O-CaO-SiO_2 SYSTEM

The results presented in this section refer to a systematic investigation carried out on selected glass compositions from the soda lime silica ternary Na_2O-CaO-SiO_2 system in order to establish phase development and crystallisation kinetics of these glasses. These are coded as NLS and NCS glasses. Although both series belong to the soda lime silica system, for the purpose of convenience, the NLS series refer to those compositions designed to give specific viscosity regimes whereas the NCS series were not so designed. The compositions are given in Table 5.6 and their respective phase fields indicated.

Figure 5.14 indicates the positions of the NLS series compositions in the equilibrium NLS phase diagram with respect to three constant viscosity curves (isokoms) where log η = 5.1 and 5.5 and 6.0 at 900 °C (Data from the Properties of Glass by Morey[126]). These isokoms are chosen since they include the characteristic behaviour of container glass and approximate to industrial practice in terms of choice of forming and heat treatment temperatures to induce crystallisation. The isokoms are presented in Appendix II.

The aim was to produce basic compositions which are capable of fairly rapid surface crystallisation at temperatures low enough to avoid deformation of a container. Once identified, samples of the appropriate glasses were later subjected to strength determination to see if the surface layer does enhance strength (see Chapter 6). The glasses may then be further modified to produce container materials in their own right or the compositions may provide an indication for container surface modification.

Table 5.7 presents the results for heat treatment of these compositions in the temperature range 750-800 °C for periods of 1-2 hours. Phase development was followed using XRD and the extent of crystallisation, deformation and reduction in transparency

TABLE 5.6
NLS SERIES GLASS COMPOSITIONS FROM THE Na_2O-CaO-SiO_2 TERNARY WITH VISCOSITY BEHAVIOUR SIMILAR TO CONTAINER GLASS

Glass	Log η at 900 °C (poise)	Composition (wt %)			Thermodynamic Phase Fields
		SiO_2	CaO	Na_2O	
NLS 1	*5.1*	73	10	17	NC_3S_6
NLS 2		69.5	14	16.5	NC_3S_6
NLS 3		67	16	17	β-CS + NC_3S_6
NLS 4		63	14.5	22.5	NC_2S_3
NLS 5	*5.5*	74	11	15	NC_3S_6
NLS 6		72.5	12.5	15	NC_3S_6
NLS 7		70	15	15	β-CS + NC_3S_6
NLS 8		66.5	17.5	16	β-CS
NLS 9		65	17	18	β-CS + NC_2S_3
NLS 10		63	16.5	20.5	NC_2S_3
NLS 11	*6*	66	20	14	α-CS

NC_3S_6 = devirtite NC_2S_3 = $Na_2O.2CaO.3SiO_2$ α-CS and β-CS = wollastonite

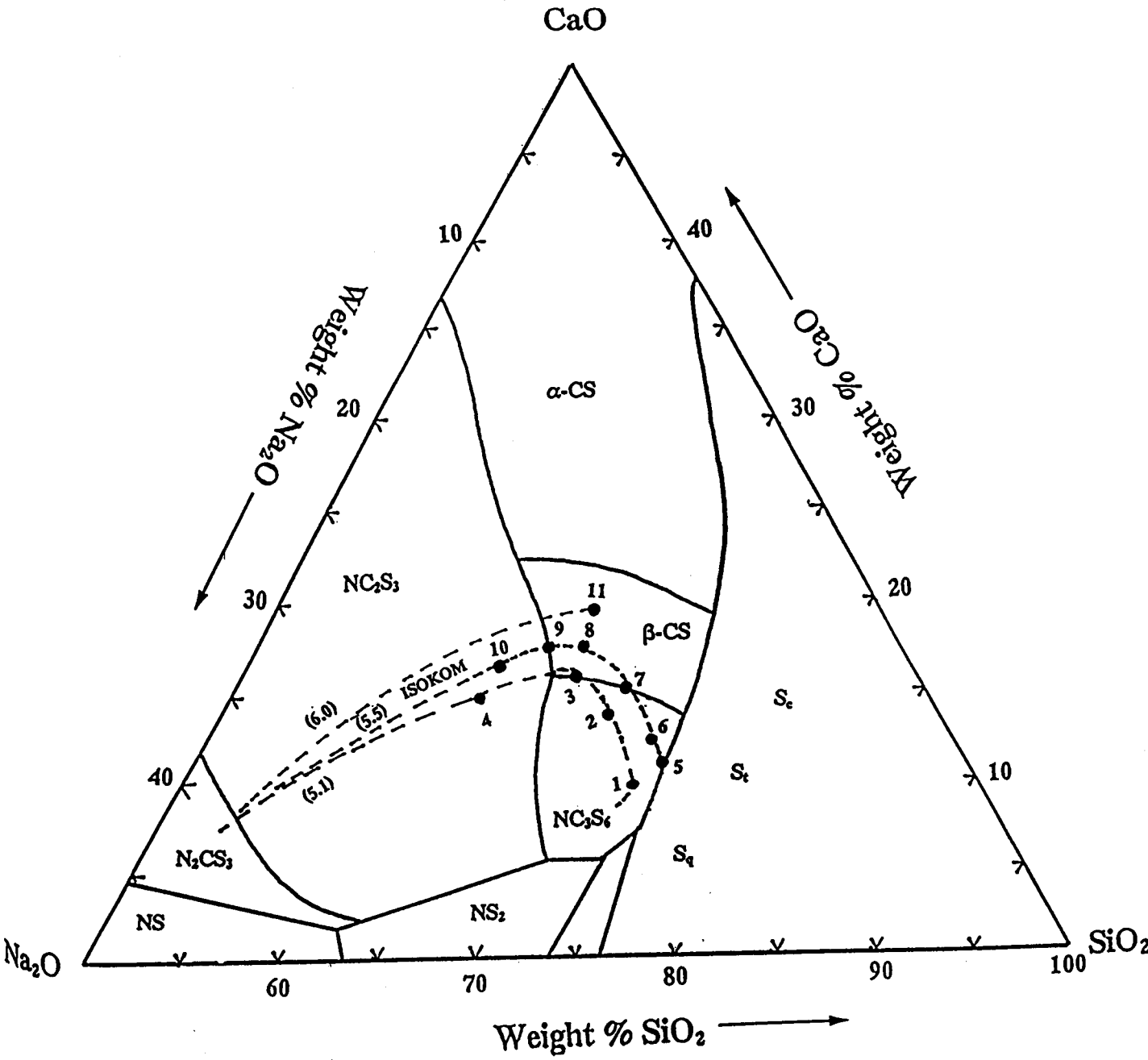

Figure 5.14 NLS Phase diagram

TABLE 5.7
RESULTS OF CRYSTALLISATION STUDIES FOR NLS SERIES GLASSES

Glass	Heat Treatment (°C/h)	Surface crystallisation	Deformation	Transparency	Thickness of surface layer	Crystal phase
NLS 1	750/1	*yes*	none/slight	transparent	thin	NC_3S_6
NLS 1	800/1	*yes*	slight	slightly opaque	thick	NC_3S_6
NLS 2	750/1	*yes*	none	transparent	thin	NC_3S_6
NLS 3	750/1	*yes*	none/slight	transparent	thin	NC_3S_6
NLS 4	750/1	*yes*	slight/significant	opaque	thick	NC_2S_3+ ?
NLS 6	750/1	*yes*	none	transparent	thin	NC_3S_6
NLS 7	750/1	*yes*	none	transparent	thin	NC_3S_6+ βCS
NLS 8	750/1	*yes*	none/slight	lightly opaque	thin	NC_3S_6+ βCS
NLS 8	800/1	*yes*	slight	opaque	thick	NC_3S_6+ βCS

thin = upto ~50 μm thick = upto ~500 μm NC_3S_6 = devitrite β-CS = wollastonite

TABLE 5.8
DEVITRIFICATION BEHAVIOUR OF SOME NCS SERIES Na_2O-CaO-SiO_2 GLASSES

Heat Treatment (°C/h)	NCS 1	NCS 2	NCS 3	NCS 4	NCS 5	NCS 6	NCS 7	NCS 8	NCS 9	NCS 10
600/20	phase separated	glass	phase separated							
675/20	ditto + surface αC	phase separated	ditto							
750/4				surface NC_3S_6 (deformed)	surface NC_3S_6 (deformed)	negligible surface crystallisn	surface NC_2S_3 + NC_3S_6 (deformed)	surface NC_2S_3 + NC_3S_6	bulk NC_2S_3	bulk NC_2S_3 (deformed)
750/15		ditto + surface αC	ditto + surface αC							
1000/15	ditto + t, NC_3S_6	ditto + t, NC_3S_6	ditto + t							

NC_3S_6 = devitrite αC = α-cristobalite t = tridymite

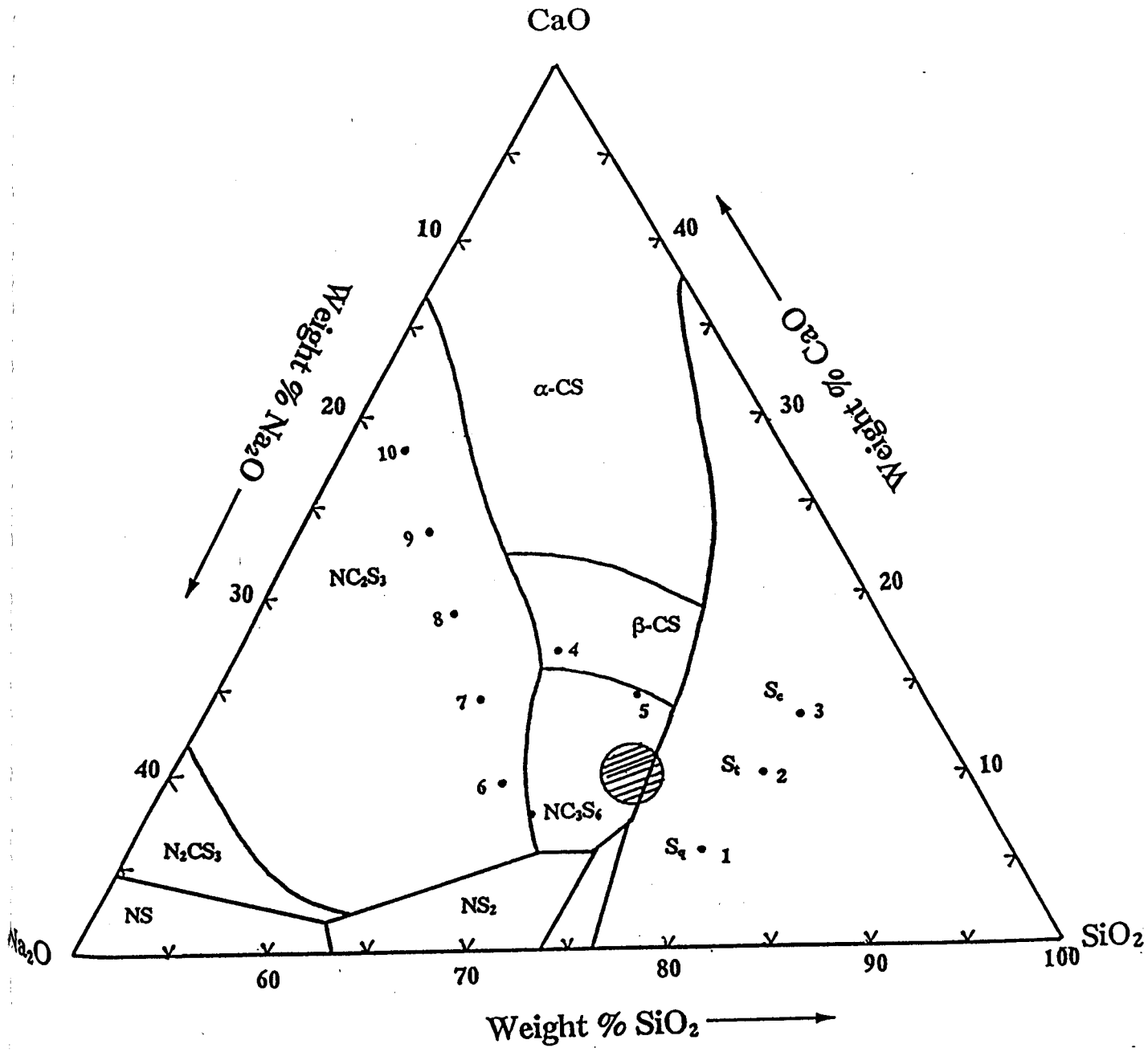

Figure 5.15 NCS Phase diagram (shaded area = container glass compositions)

estimated roughly by eye. All glasses showed varying degrees of surface crystallisation to produce layers from 50-500 μm thick. Several compositions, namely, NLS 1, NLS 2, NLS 6, NLS7 and NLS8 were found to offer reasonable control parameters in that they exhibited significant crystallisation without deformation or loss of transparency. The observed crystal phases mostly correspond with the appropriate phase field although β-wollastonite was not formed as readily as devitrite probably due to its higher liquidus temperature.

The devitrification behaviour of some NCS series glasses (NCS 1 - NCS 10) is shown in Table 5.8 and Figure 5.15. Deformation was observed for all NCS series of samples at a heat treatment temperature of 800 °C or above. Where crystallisation was observed, this was restricted to the surface except for NCS 9 and NCS 10 glasses and was found to consist of approximately equal amounts of α-cristobalite and devitrite.

5.4.2 EFFECT OF NUCLEATING AGENTS ON DEVITRIFICATION

The compositions of two previously identified glasses, namely, NLS 1 and NLS 8, showed promising crystallisation properties such as minimum deformation and excellent transparency. These compositions and a float glass composition were further modified by the addition of a nucleating agent and are given in Tables 5.9 and 5.10. The approximate position of the float glass F1 in the NCS phase diagram is indicated in Figure 5.15. The CaO and MgO contents have been summed and plotted as CaO for this purpose. The influence of various types of nucleating agent on the devitrification behaviour of both the NLS and float glass compositions was studied.

The selected nucleating agents were added, initially in low concentrations, to crushed float glass and NLS glasses, ball-milled and re-melted. The resulting annealed

glasses were heat treated to achieve crystallisation. A summary of compositions and heat treatment protocol is given in Table 5.10.

Float glass with no additions (F1) showed no crystallisation under these conditions. This was true for both as-received and remelted float glass. Surface crystallisation was observed in all the other float glass compositions containing various nucleating agents and to the greatest extent in those containing P_2O_5. Significantly, P_2O_5 addition of as little as 0.1 mole % was found to be highly effective in enhancing surface crystallisation behaviour.

TABLE 5.9
COMPOSITION OF A FLOAT GLASS AND NLS GLASSES

Code	Composition (wt %)		
	F1	NLS 1P	NLS 8P
SiO_2	70	72	66
Na_2O	15	16	15
CaO	6.5	10	17
MgO	6	-	-
BaO	0.5	-	-
Al_2O_3	2.5	-	-
P_2O_5	-	2	2

TABLE 5.10
NUCLEATING AGENT AND HEAT TREATMENT

Code	Glass/ Nucleating Agent	Temperature (°C)	Time (h)
F1	Commercial Float Glass	800	72
F2	F1 + 0.1 m/o P_2O_5	800	2, 4, 8, 16, 24, 84
F3	F1 + 0.1 m/o SnO_2	800	50
F4	F1 + 0.1 m/o TiO_2	800	72
NLS 1P	NLS 1 + 2 w/o P_2O_5	654	12, 24, 48, 72
		710	2, 4, 6, 12, 22
		800	1, 2, 4, 6, 22
NLS 8P	NLS 8 + 2 w/o P_2O_5	654	12, 24, 48, 72
		710	2, 4, 6, 12, 22
		800	1, 2, 4, 6, 22

SEM micrographs in Figure 5.16 show a typical example of the crystallised layer developing on the surface of a float glass at 800 °C. The dendritic morphology of the crystals is evident and is seen to grow into the bulk. In terms of growth rate, a surface layer of ~ 1.3 mm thickness was obtained for glass F2 after 84 h (Figure 5.16a) and ~ 0.1 mm after 24 h (figure 5.16b).

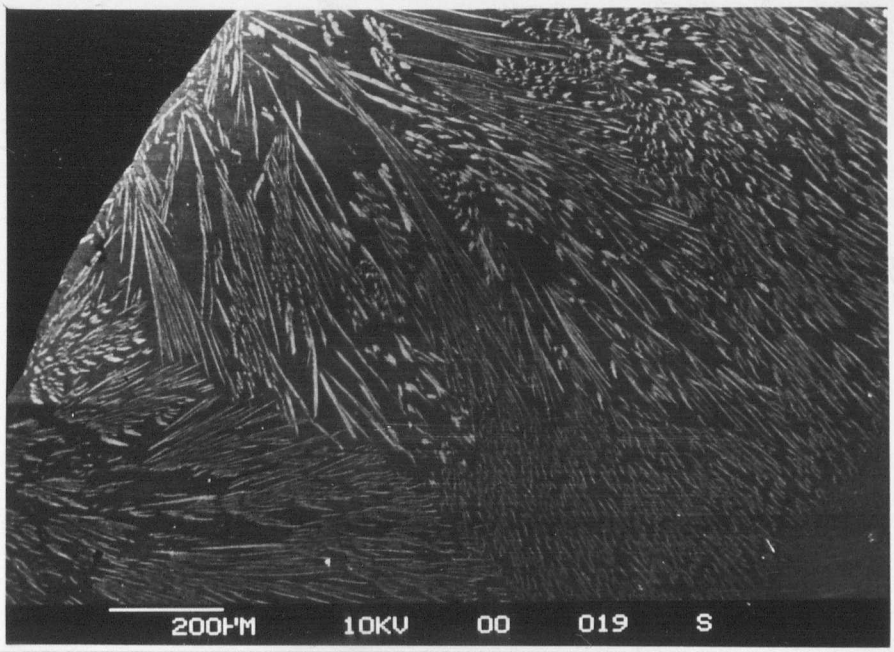

Figure 5.16 (a) Surface crystallised layer developed on float glass F2 after 84 hours at 800 °C

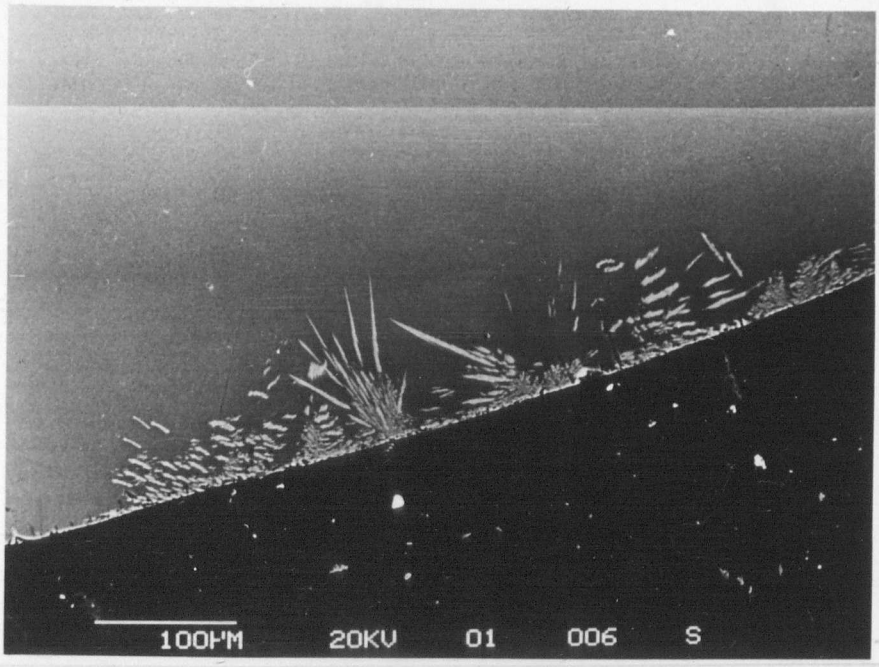

Figure 5.16 (b) Surface crystallised layer developed on float glass F2 after 24 hours at 800 °C

5.4.3 EFFECT OF TIME AND TEMPERATURE

The effect of 0.1 mole % P_2O_5 doping on the development of layer thickness with time in float glass is shown in Figure 5.17. The growth rate was calculated from the slope of the plot and was determined to be 0.29 μm/min.

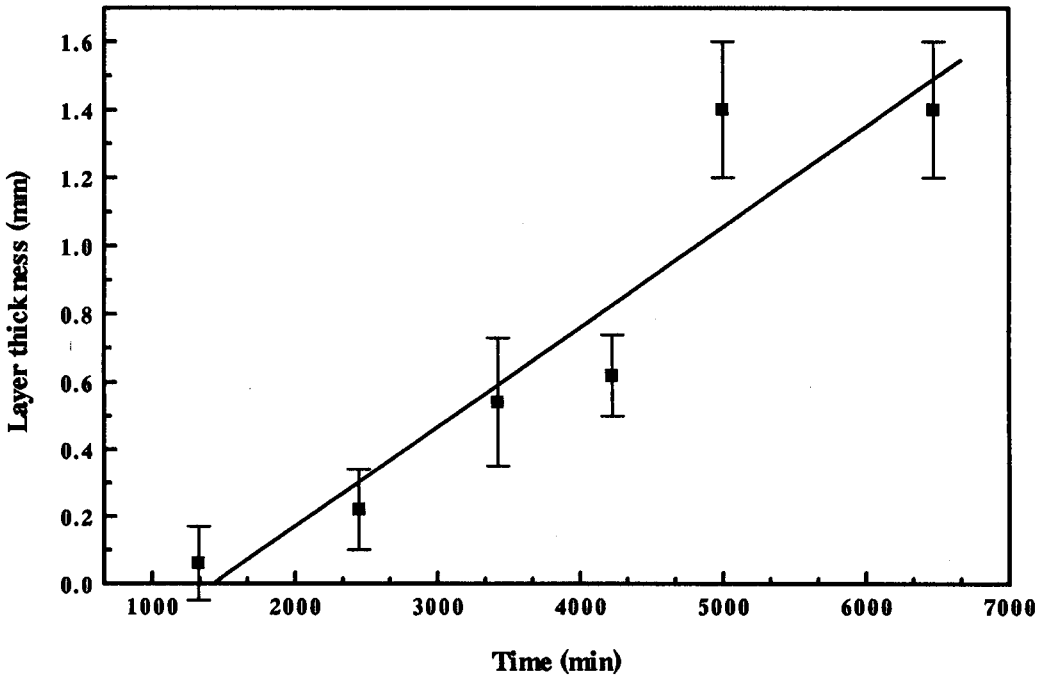

Figure 5.17 Variation of layer thickness with time at 800 °C of float glass with 0.1 m/o P_2O_5 doping

For the glasses NLS 1P and NLS 8P, the development of layer thickness on heat treatment at 654, 710 and 800 °C for varying times between 0.5-72 hours is shown in Figures 5.18-5.20.

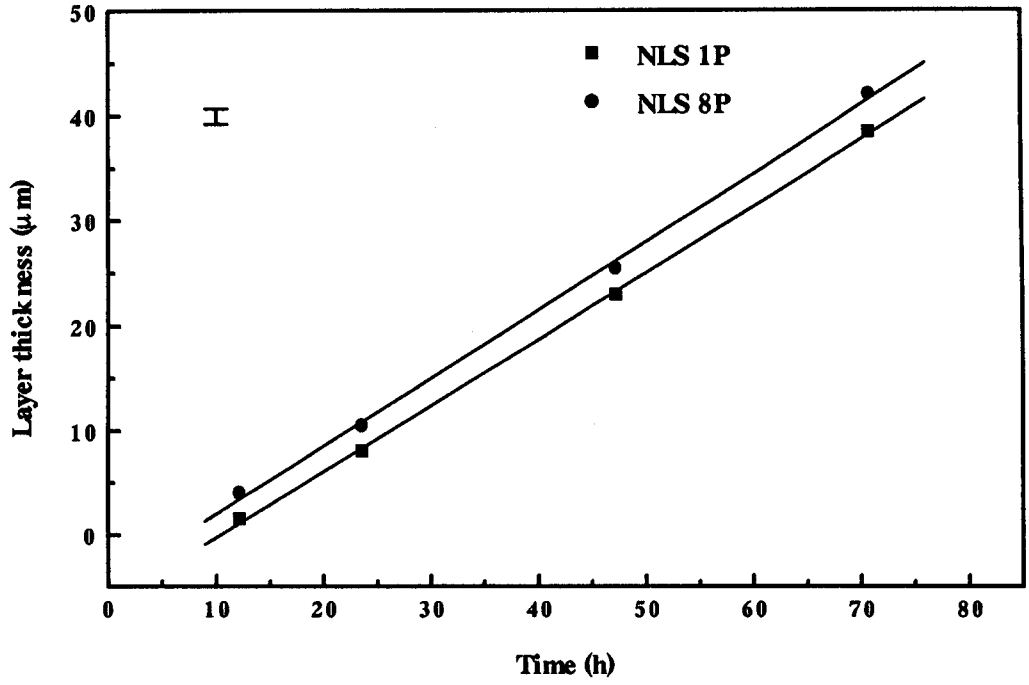

Figure 5.18 Variation of layer thickness at 654 °C with time

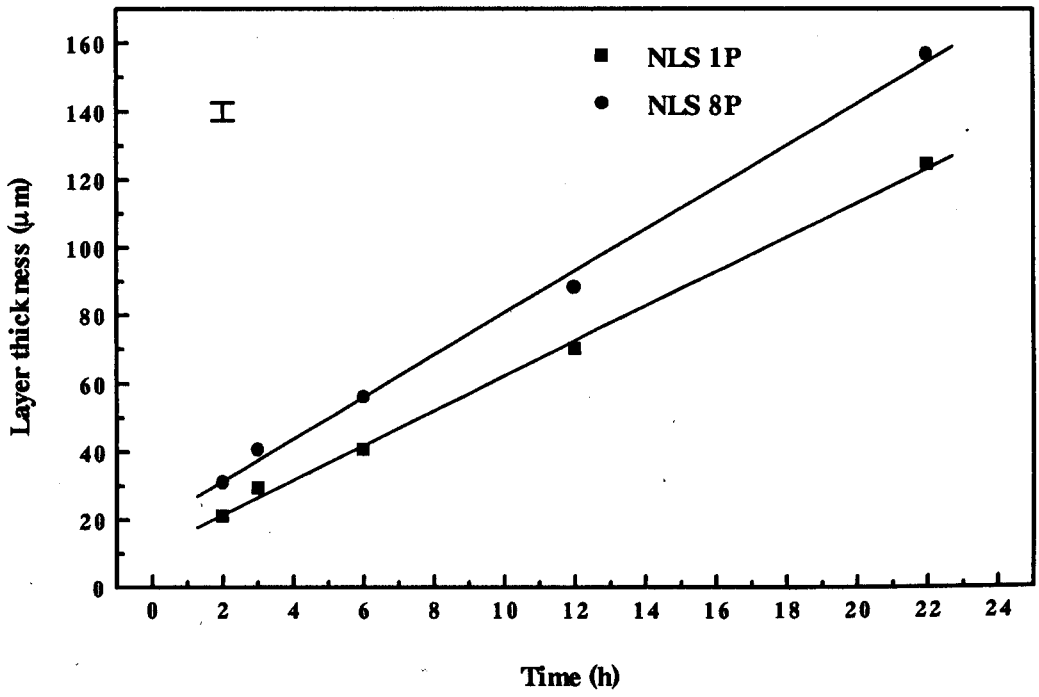

Figure 5.19 Variation of layer thickness at 710 °C with time

Deformation was found to be least (very little surface flow) at 654 °C and greatest at 800 °C. At 710 °C the deformation is still very slight. The level of transparency was found to be satisfactory up to a layer thickness of 80 μm.

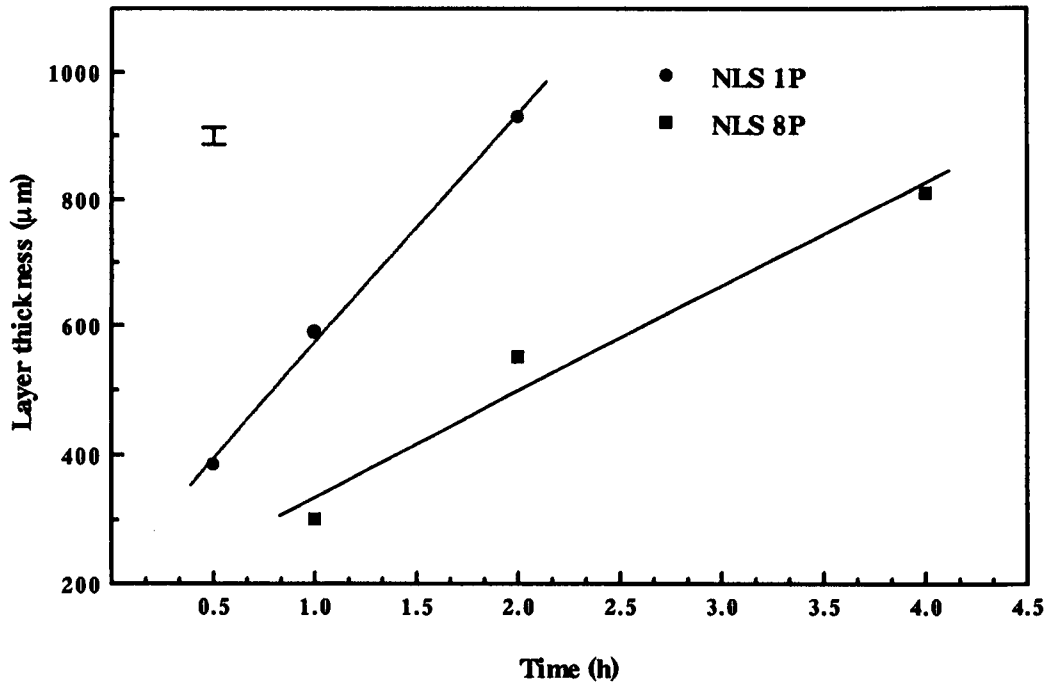

Figure 5.20 Variation of layer thickness at 800 °C with time

It can be seen from the figures that, in general, for a given temperature and time of treatment, glass NLS 8P showed a higher rate of crystallisation than glass NLS 1P. Deformation was also observed for both glasses, in varying degrees, at all temperatures.

A least square linear regression analysis has been performed to fit the best straight line through the growth data. The intercept on the x-axis was regarded as a growth induction time for these glasses. The growth rate and induction times are listed in Table 5.11.

Figure 5.18 shows variation of crystallisation layer with time at 654 °C for these glasses for times between 12-72 hours. Extrapolation of the growth rates indicate an induction period of ~ 7 hours at this temperature which is undesirable. The rate of crystal growth is marginally higher for NLS 8P than NLS 1P, and this difference is noticeably increased at higher temperatures and times, as shown in Figures 5.19 and 5.20. At 710 °C, the crystallisation layer in NLS 1P increased from 20 μm after 2 hours to 125 μm after 22 hours. For NLS 8P, the layer thickness increased from 32 μm after 2 hours to 158 μm after 22 hours. No induction period was required for nucleation at this temperature. The crystallisation at 800 °C was, as expected, found to be substantial and for glass NLS 1P, resulted in a layer of ≅ 1000 μm after 2 hours. Bulk crystallisation also occurred at this temperature when the glasses were heat treated for longer times.

TABLE 5.11
GROWTH RATE DATA FOR P_2O_5 DOPED GLASSES

Temperature (K)	Growth Rate, u μm/min			Induction Time, t (h)		
	NLS 1P	NLS 8P	Float F2	NLS 1P	NLS 8P	Float F2
927	0.0106	0.0108	-	6.6	4.5	-
983	0.085	0.103	-	-	-	-
1073	2.738	6.002	0.29	-	-	23.8

The activation energies for growth in NLS1P and NLS 8P were calculated from the slopes of the Arrhenius plots of $\log_{10}$ u versus reciprocal of temperature, shown in Figure 5.21. These were found to be 316 and 361 kJ/mole, respectively with NLS 8P having the higher value and higher CaO content.

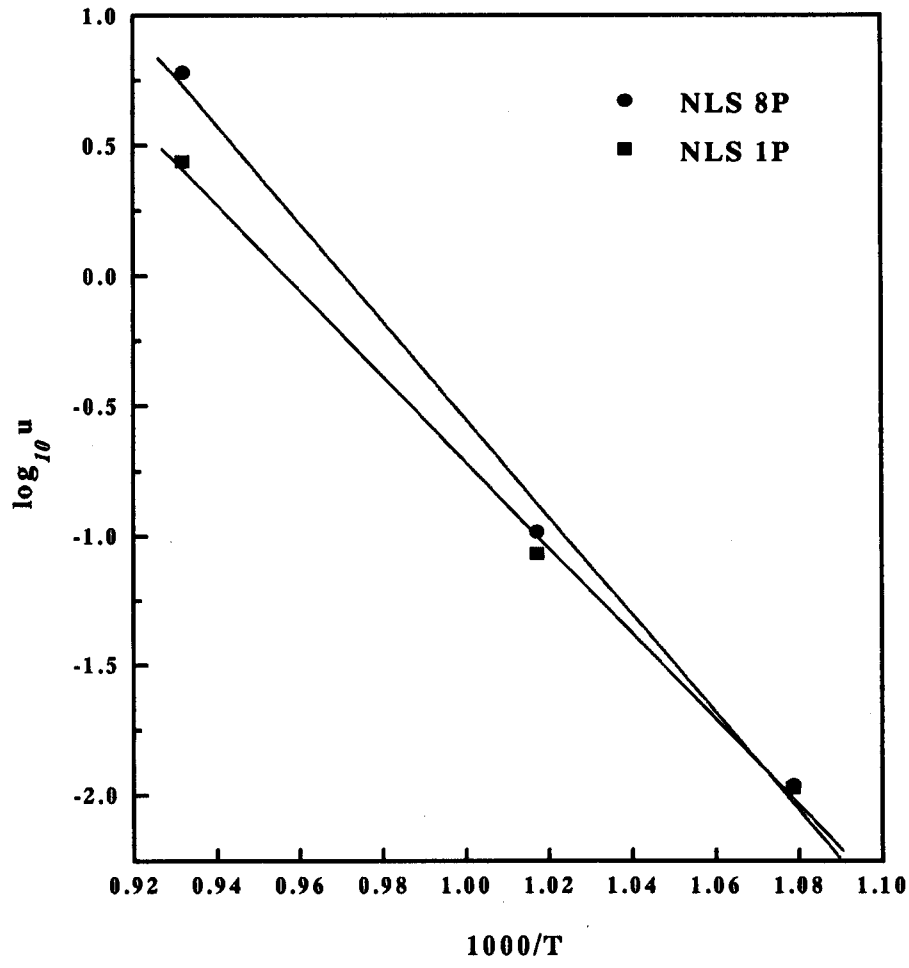

Figure 5.21 Arrhenius plot for growth rate in NLS glasses

5.4.4 EFFECT OF P_2O_5 CONTENT

A more detailed investigation of the effect of P_2O_5 content was carried out on two glass compositions, NLS 1 and EMH 7, given in Table 5.12. Of these, EMH 7 is a

simplified Emhart series glass (see Table 3.1 for the Emhart series of container glass compositions).

TABLE 5.12
COMPOSITION OF NLS 1 AND EMH 7

Composition (wt %)		
Code	**NLS 1**	**EMH 7**
SiO_2	73	73
Na_2O	16	12.16
CaO	11	9.97
MgO	-	2.39
BaO	-	0.07
Al_2O_3	-	1.31
K_2O	0.5	0.6
Others	-	0.5

The viscosity-temperature characteristics of both these glasses are expected to be similar. P_2O_5 was added to these glasses in amounts of 0.1. 0.5, 1.0, 1.5 and 2 w/o. All compositions were heat treated at a single temperature of 700 °C for times ranging from 4 to 48 hours. The effect of P_2O_5 addition at this temperature on the development of the crystallisation layer is shown in Figures 5.22 and 5.23 for NLS 1 and EMH 7, respectively.

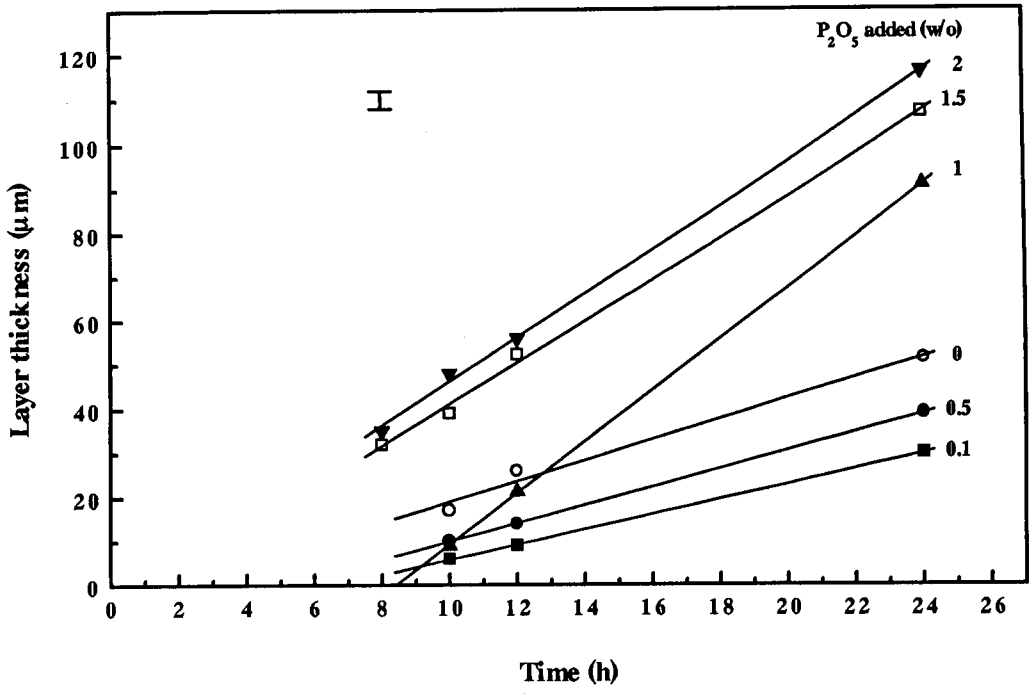

Figure 5.22 Effect of P_2O_5 doping on layer thickness at 700 °C for glass NLS 1

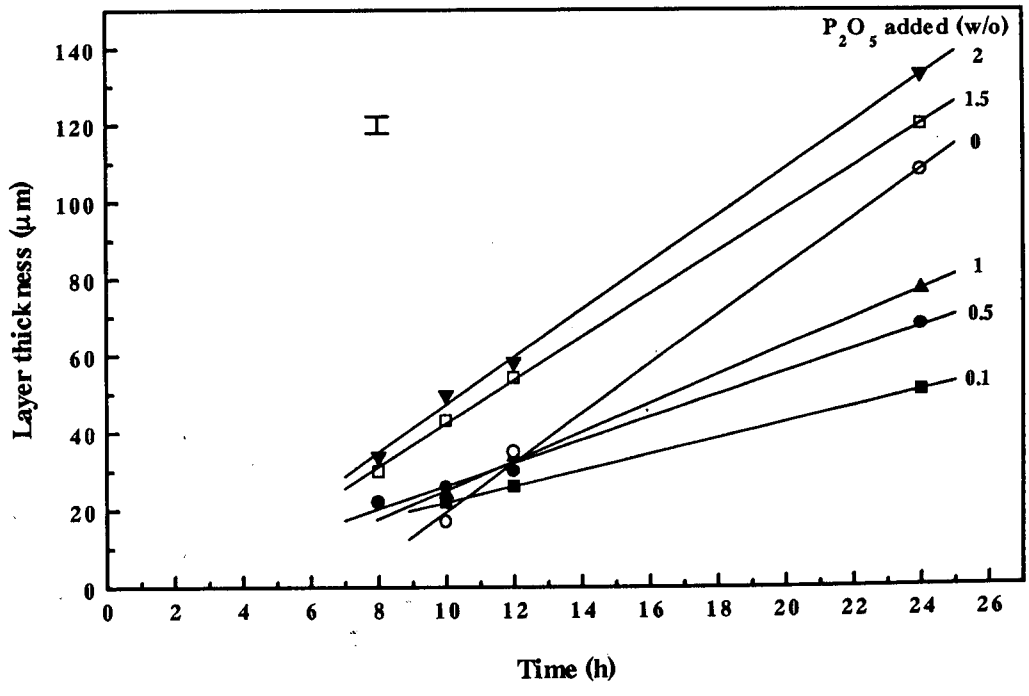

Figure 5.23 Effect of P_2O_5 doping on layer thickness at 700 °C for glass EMH 7

It can be seen from these figures that, in general for both glasses, addition of P_2O_5 shows similar crystallisation trends. When no P_2O_5 was added, back extrapolation of the growth rate showed an induction period of 7-8 hours for these glasses. However when P_2O_5 was added in varying amounts two separate regimes of growth rate were identified:

(a) for up to 1 wt % P_2O_5 added, back extrapolation of the growth rate curve showed the induction period for nucleation to be reduced considerably, extending to almost zero time, but there was a considerable reduction in actual growth rate compared with 0 wt % P_2O_5

(b) when the amount exceeds 1 wt %, it is clear that an induction period again becomes necessary for nucleation either glass composition

This suggests that at this concentration phase separation may be occurring due to its field strength (2.16 $Å^{-2}$) being closer to silicon (1.57 $Å^{-2}$) and also due to the competitive nature of network forming ability of these ions. This means that P is probably less able to participate in the glass network with silica, inducing amorphous phase separation. Therefore it can be concluded that the temperature of crystallisation can indeed be lowered by adding suitable amounts of P_2O_5. Thus adding P_2O_5 up to 1 wt %, a reduced growth rate has to be accommodated but the nucleation period is significantly reduced. In contrast, above 1 wt % P_2O_5 an induction period for nucleation will have to be tolerated in order to obtain increased growth rate. It is suggested that addition of P_2O_5 in excess of 0.5 wt % would significantly alter the viscosity-temperature relations for these glasses. This will entail an increased probability of phase separation where the energy barrier for the merging of new phase separated particles is expected to increase with P_2O_5 addition due to increase in glass viscosity restraining the motion of second phase particles.

5.5 GENERAL DISCUSSION AND CONCLUSIONS

In so far as container glass compositions are concerned, the need for reliable methods of predicting and measuring viscosity is of considerable importance. In the present work, although a high degree of parity between the measured and calculated viscosity has been found there still remains certain difficulty associated with the Fulcher equation and Lakatos constants. For example, addition of small amounts of P_2O_5, B_2O_3 or Li_2O are expected to alter the viscosity-temperature profile of the glass by increasing/decreasing the number of bridging or non-bridging oxygen moieties surrounding the network forming atom. The constants do not take the effect of such oxides into account. Referring to Figure 5.5, the profiles for NLS 1, NLS 8 and their P_2O_5 versions, NLS 1P and NLS 8P show very little variations especially at $\eta = 7.65$ with values at other viscosities being slightly modified. In this case, the Fulcher equation with constants for P_2O_5, if available, would have provided a plot, more realistically to predict the parameters for forming processes. This is particularly relevant where either composition is being changed either in the bulk or the surface to induce surface crystallisation in order to enhance strength.

In general, the measured values for T_g, T_s and T_m obtained from the DTA study of the glasses were found to be systematically higher than those calculated for certain viscosity regimes viz. η = 13.3, 7.65, 3 and 2. The difference lies in the way these reference points were defined in the literature; for example, $\eta = 13.3$ corresponds to T_g determined by dilatometry measurement as distinct from Littleton softening point and not by DTA methods as used in the present work. Also, T_m does not refer to a particular η and T_s (DTA) is lower than the temperature corresponding to $\log \eta = 7.65$.

It is evident from crystallisation studies that the change in the bulk composition can be utilised successfully to induce surface crystallisation. In particular, of all the glasses

investigated for this purpose, NLS 1, NLS 2, NLS 3, NLS 6, NLS 7 and NLS 8 were found to be most promising. Using any of these compositions, it is possible to produce a satisfactorily transparent yet thin (upto 50 μm) layer without any deformation. This layer, in turn, may be adequate to act as a crack-stopper by exerting compression on the surface. Where surface crystallisation occurred, for example in the Float F2 glass, the possible mechanism is dictated by the heterogeneous nucleation at the surface since the coordination of certain ions is incomplete and deviation from the bulk structure is locally large. The oriented dendritic crystal morphology observed on the glass surface is typical of this form of heterogeneous nucleation proceeding generally to give a coarse surface crystallised layer that is normally expected to result in a weak glass. To achieve this however, it is apparent that a specific isokom contour should be adhered to, preferably at log η = 5.1 or 5.5 in order to conform to the IPGR requirement for container glass compositions. Although, as explained, some of the crystals produced at the surface are not low TCE phases essential for producing a surface compressive glass skin in order to enhance strength, the compositions nevertheless should provide a basis to further modify the bulk by incorporating other constituents such as P_2O_5, TiO_2, CeO_2 or ZrO_2 acting as nucleating agents or by proportional substitution of MgO, Al_2O_3, B_2O_3 or Li_2O for SiO_2 and/or CaO without deviating from the preferred isokom field. As discussed earlier, P_2O_5 was found to be the most effective nucleating agent. Although not investigated in the present work, it was not clear whether similar results could be obtained for TiO_2 or SnO_2 doping at comparable levels i.e. higher than those employed in the present study to induce surface crystallisation. Indeed, other advantages can be derived from using TiO_2 or SnO_2, for these are expected to avoid the possible phase separation associated with P_2O_5 doping at amounts higher than 1 wt %, as discussed in the preceding section. Unfortunately, no kinetic data for these additives are available. However, the reported literature data indicate that ions such as Ti, Sn or Ce would act as intermediates, although Sn can also be

a modifier. The substitutional effect of Sn, on a small scale addition (~ 2 mole %), is thought to be curious because it raises the viscosity quite dramatically whilst the related activation energy is lowered marginally. It would therefore be very difficult to predict any viscosity change because not only should the ionic radius be considered but also the structural role of the ion (see section 2.5.2). Also, the other factors such as the coordination number (as considered by Dingwall and Moore[130] for divalent ions and their effect on viscosity) and the oxidation state of the ion that affects the glass structure, particularly the low temperature viscosity, should be analysed in any viscosity calculations.

Chapter 6

RESULTS AND DISCUSSION OF STRENGTHENING OF CONTAINER GLASSES

6.1 ABRASION OR VIBRASION AND HEAT TREATMENT

Table 6.1 shows the strength results from measurements performed on abraded or vibraded Glass 1 which had been treated at temperatures in the range of 675 °C to 800 °C for up to 4 hours (see section 4.2). The results show that vibrasion alone results in significant lowering of the 'pristine' strength by approximately 26%. However, on follow-up heat treatment of the vibraded glasses at 675 °C for 3 h, the strength recovered its original value (~ 175 MPa) but no increase of rupture strength could be observed. The two stage heat treatment showed a similar trend. The mean breaking strength of these vibraded and heat treated glasses was expected to be higher than the 'pristine' glass strength since there was some evidence of detectable surface crystallisation, small crystals near the surface acting as 'crack-stoppers'. However any change in the modulus of rupture (MOR), σ_F is related to surface conditions, i.e. flaw severity (mean critical stress to failure) produced by abrasion and nucleation density. One explanation for nearly constant strength values of 'pristine' and vibraded and heat treated glasses is that the abrasion technique using SiC has produced larger flaw sizes thus requiring the same critical stress for failure in the vibraded and heat treated samples i.e. there are a few severe flaws which are deeper than the crystalline surface layer. It is also likely that some flaw healing due to viscous flow had occurred, especially during the two stage heat treatment process. However, when airabrasion was used (see the following section), it was found that this type of

abrasion markedly influenced the crystal growth and strength. Optical microscopy confirmed a surface of dense nucleation sites that induced surface crystallisation and consequent increase in cross breaking strength. A similar observation has been previously made by Partridge et al[28].

TABLE 6.1
STRENGTH VALUES FROM FOUR-POINT AND THREE-POINT BENDING TESTS FOR GLASS 1

Condition	Temperature (°C)	Time (h)	Type of Test	Modulus of Rupture (MPa)
Unvibraded 'Pristine'	room	-	four-point	174.4 ± 20
Vibraded (before test)	room	-	four-point	118.2 ± 18
Vibraded and Heat Treated	675	3	four-point	174.9 ± 33
Vibraded and Heat Treated	675 + 800	3 + 1	four-point	157.2 ± 15
Unvibraded 'Pristine'	room	-	three-point	236 ± 17
Vibraded and Heat Treated	675	3	three-point	243 ± 17

The table also highlights the comparison of four-point and three-point bending test results of the unvibraded 'Pristine' glass rods. The latter gave a significantly higher value of 236 MPa compared to the four-point test. However, as the results show, no apparent increase in strength could be observed when compared with the corresponding three-point bend test result of the same glass in the 'as-drawn' condition. It is therefore important to be aware of the difficulty when comparing strength results reported in the literature since four-point bend testing is considered to be more reliable than the three-point test.

6.2 PRECIPITATION OF A LOW SOLUBILITY COMPONENT

The composition of the soda lime silica glasses to which a low solubility component CuO has been introduced is given in Table 6.2. It can be seen from the table that 2 mole % CuO is added to both Glass 1 and Glass 2 which has half the CaO content of Glass 1 replaced by MgO. Glass 3 and Glass 4 were without CuO added.

These glasses were air abraded to provide a uniform distribution of nucleating sites and were heat treated to produce the desired phase. It is seen from the summary of XRD results (Table 6.3) that tenorite was the only precipitating phase identified in both Glass 1 and Glass 2, with no crystallisation occurring in the other glasses, although Glass 3 is similar to Glass 1. It is therefore the presence of CuO that resulted in surface crystallisation.

Subsequent strength measurements summarised in Table 6.4 show that a MOR of ~ 300 MPa is achieved compared with ~ 175 MPa for pristine container glass but this required abrasion to produce the required nucleation density.

SEM analysis showed the major component in the composition of surface crystals to be Cu and typical examples of surface crystallisation are shown in Figure 6.1(a) and (b).

(a)

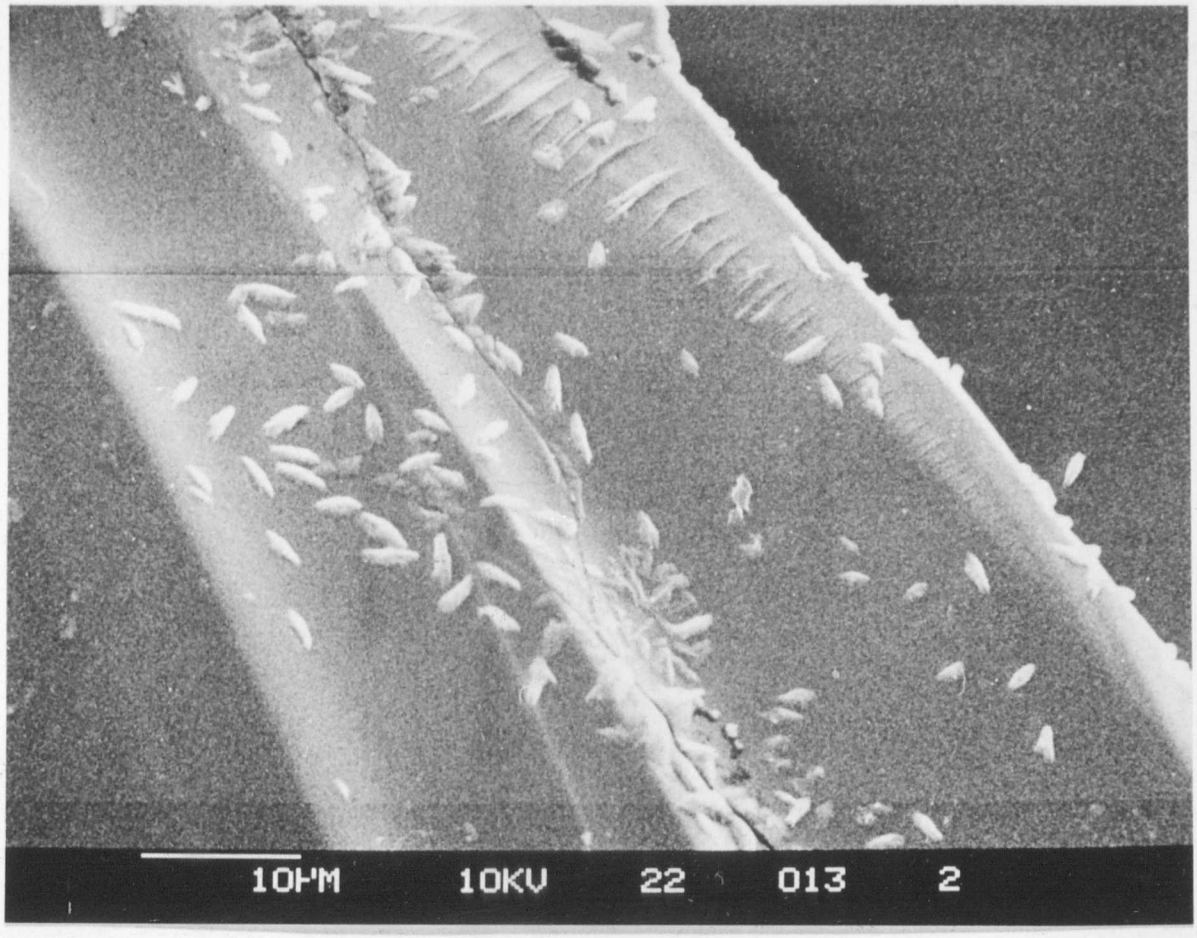

(b)

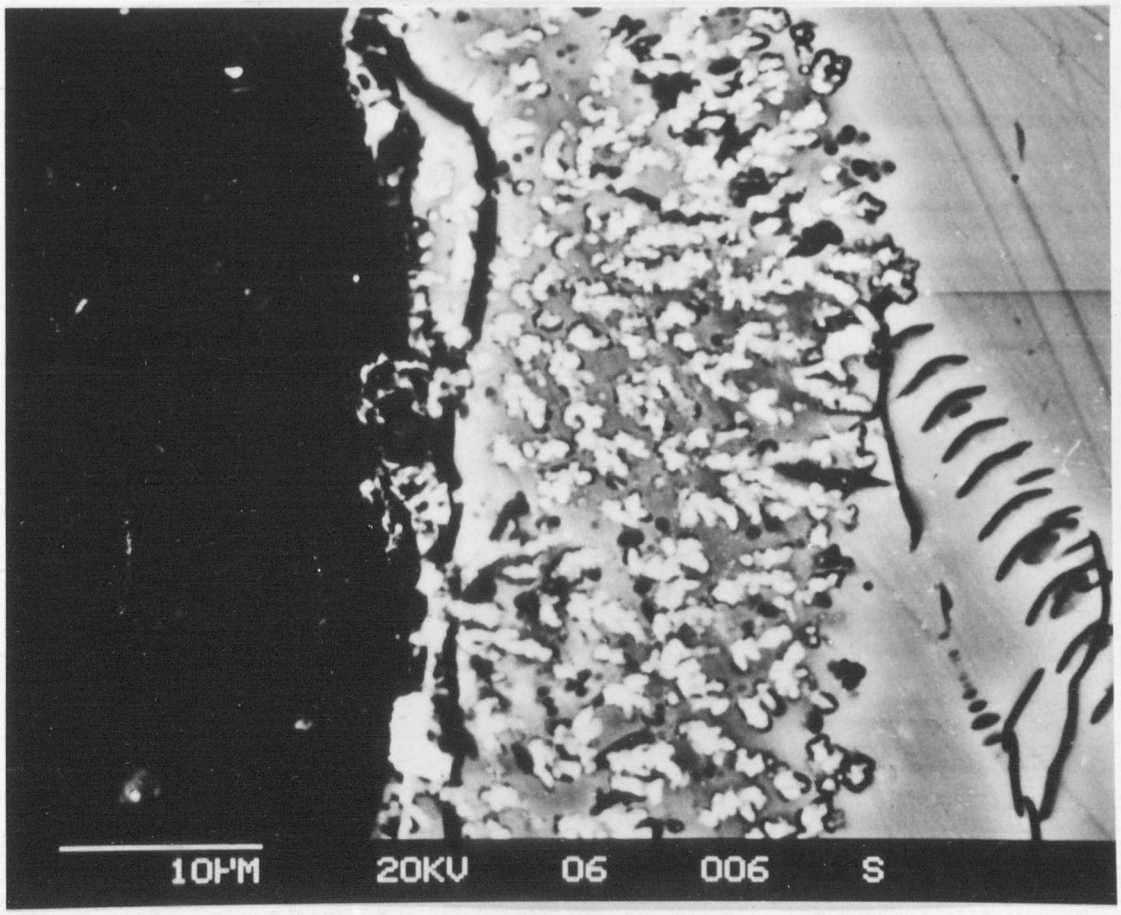

Figure 6.1 SEM micrographs showing tenorite surface crystals

TABLE 6.2
COMPOSITION OF SODA LIME SILICA GLASSES

Mole %	Composition			
	Glass 1	Glass 2	Glass 3	Glass 4
SiO_2	62	62	63	Milk Bottle Glass @ Northern Dairies Ltd
Na_2O	11	11	11	
K_2O	-	-	-	
CaO	20	10.5	21	
MgO	-	9.5	-	
Al_2O_3	5	5	5	
CuO	2	2	-	

The morphology of the tenorite crystals was cone shaped, as shown in Figure 6.1(a), for a fractured surface edge of a sample and the precipitates are approximately a micron in size although the average primary crystallite size was estimated to be in the nanometer scale, as determined by XRD line broadening analysis. The surface crystalline layer is shown in Figure 6.1(b). The layer developed following a heat treatment at 670 °C for 3 h was approximately 20 μm thick and found to be uniform particularly in samples where airabrasion has been used.

SEM microscopy of several samples showed that the observed layer exists on the surface of the material and seems to grow into the bulk glass. Growth did not appear to favour any particular orientation.

TABLE 6.3
IDENTIFICATION OF CRYSTAL PHASES BY XRD

Code	Surface Condition	Heat Treatment		Phase
		Temperature (°C)	Time (h)	
Glass 1	Pristine	670	3	Tenorite
	Abraded	670	3	Tenorite
Glass 2	Pristine	670	3	Tenorite
	Abraded	670	3	Tenorite
Glass 3	Pristine	650	3	none
	Abraded	650	3	none
Milk Bottle Glass	Pristine (Titanised side)	615	2	none
	Pristine (Inside)	615	2	none
	Abraded	615	2	none

TABLE 6.4
STRENGTH VALUES OF AIRABRADED AND HEAT TREATED RODS OF SODA LIME SILICA GLASSES

Code	Pristine	Abraded	Heat Treatment		Modulus of Rupture	
			Temperature (°C)	Time (h)	Heat Treated	Abraded & Heat Treated (MPa)
Glass 1	174.4 ± 20	100.2 ± 16	670 670	3 3	221.5 ± 19	287.7 ± 20 (2 mm) 309.0 ± 25 (1mm)
Glass 2	200.9 ± 18	97.3 ± 10	670	3	215.6 ± 15	240.8 ± 19
Glass 3	178.6 ± 21	99.6 ± 10	650	3	205.0 ± 12	230.5 ± 25
Milk Bottle Glass	192.6 ± 15	100.8 ± 10	650	3	200.2 ± 12	215.6 ± 15

6.3 VAPOUR TREATMENT

This section primarily deals with strengthening of container glass compositions by exposing them to lithium and/or aluminium containing vapours. The possibility that the resulting modification to surface composition may facilitate devitrification, and the consequent strength enhancement, has been investigated. Also, the effect of LiBr or $AlBr_3$ treatments, either on their own or consecutively, on the strength enhancement of commercial container glass compositions has been evaluated. These results are presented and discussed below.

In the present work, a vapour pressure of 10 mm at 887 °C has been estimated from the literature data. Table 6.5 shows melting points and comparative vapour pressures for a range of halides including LiBr. Handling of $AlBr_3$ and establishing the conditions in terms of vapour pressure and temperature of vapour generation proved to be difficult due to its very low melting temperature of approximately 90 °C. A temperature range of 550-580 °C was employed as this was below the transition temperature (T_g) of the glasses studied and was considered to be 'safe' (i.e. no surface flow occurred during the exposure).

TABLE 6.5
MELTING POINTS AND VAPOUR PRESSURE OF Li-HALIDES

Substance	Melting Point (°C)	1 *mm* Pressure (°C)	10 *mm* Pressure (°C)
LiI	446	772	841
LiBr	547	747	887
LiCl	613	782	932
LiF	841	1087	1211

6.3.1 GENERAL OBSERVATIONS

Visual observation of the glass rods indicated no surface clouding, common in molten bath treatment, when exposed to vapour treatment. The degree of transparency was found to be same as the pristine glass rods prior to their exposure to vapours. Immediately following the vapour treatment, the surfaces of the treated samples were covered by a white layer but they were quickly returned to the original pristine transparency when washed in water. XRD of these surfaces showed the soluble compound to be NaBr, formed by the replacement of Na by Li and/or Al on the surface. This is consistent with the prediction as outlined below:

6.3.1.1 CALCULATION OF THE STABILITY OF NaBr IN OXYGEN

Thermodynamic calculations regarding the stability of NaBr formed under the conditions employed in LiBr vapour treatment in the presence of oxygen were carried out assuming a reaction

$$4\,NaBr\,(g) + O_2 \rightarrow 2\,Na_2O\,(C) + 2\,Br_2\,(g) \qquad ....(6.1)$$

The data used in the present case (in kJ/mole) is given in Table 6.6 and is taken from the JANAF electrochemical Tables (see also Appendix III).

Thus for the reaction of interest, Table 6.7 gives the calculated values for the parameters indicated. At 883 K therefore:

$$K_p = \exp(-\Delta G_f/RT)$$

$$K_p = \exp(-248860/8.31441 \times 883)$$

$$= 1.89 \times 10^{-15}$$

where ΔG_f = Free energy of formation

TABLE 6.6
CORRECTED DATA FROM THE JANAF THERMOCHEMICAL TABLES

Temperature/K	ΔG_f /kJ mole^{-1}			
	Na_2O (C)	Br_2 (g)	O_2 (g)	NaBr (g)
600 K	-336.44	0	0	-196.58
800 K	-308.11	0	0	-206.61
883 K *	-296.69	0	0	-210.56
1000 K	-280.59	0	0	-216.12

* linearly interpolated values at 883 K

TABLE 6.7
CALCULATED THERMODYNAMIC PARAMETERS FOR REACTION 6.1

Temperature /K	$2\Delta G_f$ (Na_2O (C)	-	$4\Delta G_f$ (NaBr) (g)	$\Delta G_{forward}$/ kJ mole^{-1}
600 K	-672.88	+	786.32	+113.44
800 K	-616.22	+	826.44	+210.22
883 K	-593.38	+	842.24	+248.86
1000 K	-561.18	+	864.48	+303.30

The tendency for oxidation of the vaporised alkali metal bromide is therefore much reduced when the alkali metal is Na rather than Li. At 1000 K, $K_p = 1.14 \times 10^{-18}$ for the above reaction, thus increased temperature favours the establishment of the left hand side of the equilibrium, as before.

6.3.2 FLEXURAL STRENGTH

Table 6.8 shows the strength values obtained after the rods of float F1 and NLS 1 glasses were treated with Li and Al bromide vapours.

TABLE 6.8
STRENGTH VALUES OF FLOAT F1 AND NLS 1 GLASS RODS TREATED WITH LITHIUM AND ALUMINIUM VAPOURS

Glass	Temperature (°C)	Time (min)	Treatment	Modulus of Rupture (MPa)	% Strength Increase
Float F1	-	-	Pristine	178 ± 10	-
	550	10	LiBr vapour	240 ± 13	*38*
	550	20	LiBr vapour	310 ± 12	*74*
NLS 1	-	-	Pristine	174 ± 12	-
	550	10	LiBr vapour	260 ± 11	*49*
	550	20	LiBr vapour	330 ± 10	*89*
Float F1	-	-	Pristine	178 ± 10	-
	550	12	$AlBr_3$ vapour	273 ± 15	*53*

6.3.2.1 LiBr VAPOUR TREATMENT

On exposure to LiBr vapours, an appreciable level of strength enhancement was achieved, with the strength being increased by 38-89 % of pristine strength for varying times of treatment of 10-20 minutes. It can be seen from the table that the glass NLS 1 showed slightly higher improvement in strength values compared to float glass F1 when treated with Li vapours for 20 minutes. This may be due to some effect of Ca on Na replaceability or possibly a combined replaceability of both Na and Ca in NLS 1. The CaO content in this glass is 11 wt % compared to 6.5 wt % in float, with the Na_2O content being nearly the same in both glasses.

Table 6.9 summarises the results of four point bend tests of the rods of Rockware glasses R4795, R4795/3 and R4795/10 with increasing alumina content (see Tables 3.1 and 6.19 for compositions) following exposure to LiBr vapour for a set of times i.e. 20, 40 and 60 minutes. All samples presented in this table were annealed and then exposed to LiBr vapour in static air except for those marked with an asterisk, which were unannealed, *as drawn* rods exposed to LiBr vapour in a flowing, oxygen free, inert atmosphere.

The *annealed* glasses exhibited a significant improvement in strength over their original pristine values. For the base glass R4795, a maximum increase in strength of 353 MPa (93 %) over its pristine strength of 183 MPa was achieved for a 60 minute treatment. A slightly higher value was recorded for the corresponding alumina modified glass R4795/3 treated under identical conditions. The tests show an improvement, from its pristine value of about 200 MPa, to 387 MPa (94 %). The strength values obtained for other treatment times showed a similar trend. For the base glass, the strength improved from 183 MPa to 242 (33 %) and 291 MPa (60 %) after treatment for 20 and 40 minutes respectively. For the modified R4795/3, treated for identical times, this corresponded to an improvement in its strength values to 253 MPa (27 %) and 296 MPa (48 %),

respectively. The relationship of the enhancement of strength to the duration of treatment is, within experimental error, one of linearity as illustrated in Figure 6.2.

TABLE 6.9
STRENGTH VALUES OF LiBr VAPOUR TREATED ROCKWARE R4795 AND ALUMINA MODIFIED GLASS RODS

Glass	Temperature (°C)	Time (min)	LiBr Vapour Treatment		Modulus of Rupture (MPa)	% Strength Increase
			Prior Treatment	Atm		
R4795	Pristine	0	Annealed	Air	183 ± 11	*0*
	585	20	Annealed	Air	242 ± 16	*33*
		40	Annealed	Air	291 ± 14	*60*
		60	Annealed	Air	353 ± 9	*93*
		40	Unannealed	Air	302 ± 12	*66**
		40	Unannealed	N_2	341 ± 9	*86**
R4795/3	Pristine	0	Annealed	Air	200 ± 11	*0*
	585	20	Annealed	Air	253 ± 10	*27*
		40	Annealed	Air	296 ± 12	*48*
		40	Unannealed	Air	310 ± 9	*56**
		40	Unannealed	N_2	390 ± 10	*95**
		60	Annealed	Air	387 ± 10	*94*
R4795/10	Pristine	0	Annealed	Air	192 ± 12	*0*
	585	40	Unannealed	N_2	392 ± 13	*104**

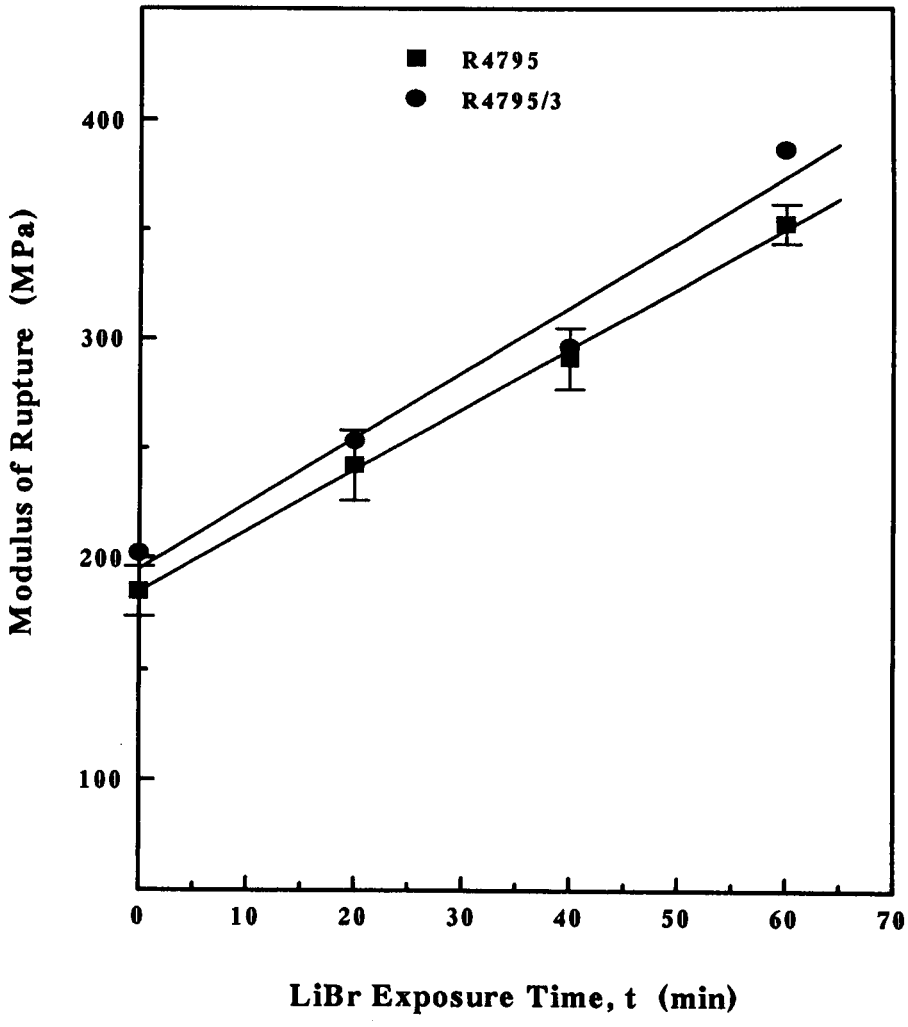

Figure 6.2 Variation of MOR strength with LiBr exposure time for annealed Rockware base R4795 and alumina modified R4795/3

The results from the *unannealed* rods treated in inert N_2 atmosphere show that the strength improved, following an exposure of 40 minutes in inert N_2 atmosphere, to 341 MPa (86 %), 390 MPa (95 %) and 392 MPa (104 %) for both the unmodified and alumina modified glasses, respectively. Comparing the results obtained under these two different conditions (i.e. annealed and unannealed states), it can be seen that the same level of

strength improvement of approximately 86-104 % is achievable for either the base glass or both modified glass compositions. However, for the modified R4795/3 glass, the treatment time would have to be extended to 60 minutes in an environment of static air whereas the same improvement is recorded for the same glass for only a 40 minutes treatment but in an inert atmosphere. It is suggested that the following reasons may, either singly or in combination, explain the above observation: (a) the rate of Li diffusion into the glass surfaces is significantly retarded in static air due to depletion of diffusing species which would be readily replenished in the case of a flowing carrier gas or (b) unfavourable conversion of some diffusing species occurs in the presence of air before reaching the glass surface or (c) part of the conversion actually occurs on the glass surface during treatment thus retarding the rate of Li diffusion or (d) the diffusion rate is faster for unannealed samples. The activity of lithium is thought unlikely to be affected since LiBr would generate sufficient vapour pressure at 890 °C.

TABLE 6.10
STRENGTH VALUES FOR LiBr VAPOUR TREATED ROCKWARE GLASSES, WITH A FOLLOW UP HEAT TREATMENT

Glass	Duration of LiBr Exposure (min)	Atm	Modulus of Rupture	Modulus of Rupture on Follow-up Heat treatment		Overall % Strength Increase
				610 °C/2h	610 °C/24h	
R4795	Pristine	N_2	183 ± 10	190 ± 12	-	*0*
	40		341 ± 9	338 ± 11	-	*86*
R4795/3	Pristine	N_2	200 ± 10	190 ± 11	195 ± 6	*0*
	40		390 ± 10	385 ± 8	392 ± 11	*95*

Overall, the results obtained for *unannealed as drawn* glass rods and LiBr treated in air showed an improvement in strength of 302 ± 12 MPa (66 %) and 310 ± 9 MPa (56 %) for R4795 and R4795/3, respectively. These values, when compared to the values obtained for the same glasses treated in an inert atmosphere (marked asterisk) show 20-40 % less increase in strength. The trend is also similar when these values are compared with the corresponding data for annealed samples treated in air. It was anticipated that the strength values of unannealed samples, although in air, would at least match the values obtained in experiments using an inert environment.

Subsequent heat treatment still in inert atmosphere at 585-610 °C for 2 and 24 h, of unmodified glass rods which had been exposed to LiBr for 40 and 60 minutes, respectively showed a small reduction in strength improvement Table 6.10). For example, a value of 335 ± 12 MPa (about 12 % reduction) was recorded for R4795/3 glass which was given a follow-up heat treatment for 2 h.

6.3.2.2 $AlBr_3$ VAPOUR TREATMENT

Table 6.11 summarises the strength results of Rockware RB1 glass, similar in composition to R4795, which had been subjected to $AlBr_3$ vapour treatment at 550 °C for a duration of 10, 20 and 30 minutes and given a follow-up heat treatment at the same temperature for 1 h.

It is clear from the Table 6.11 that, in general the strength showed a linear increase with time of exposure as indicated in Figure 6.3. The MOR values achieved were 271, 301 and 355 MPa after 10, 20 and 30 minutes, respectively. This corresponded to a strength improvement of 49, 65 and 95 %. Referring to the results described earlier in Table 4.5, it was found that approximately 53 % increase in strength was achieved for a float glass when $AlBr_3$ treated for 12 minutes. The results are very comparable although the glass composition is different in each case. Furthermore, it noteworthy that the trend in the strength enhancement on exposure to Al vapour is similar to that observed for the LiBr

treatment. It is therefore reasonable to anticipate the use of Al diffusion, if another source, preferably organometallic, could be used since it was the experience of the author that the handling of $AlBr_3$ is probably more difficult than LiBr, as the substance is corrosive.

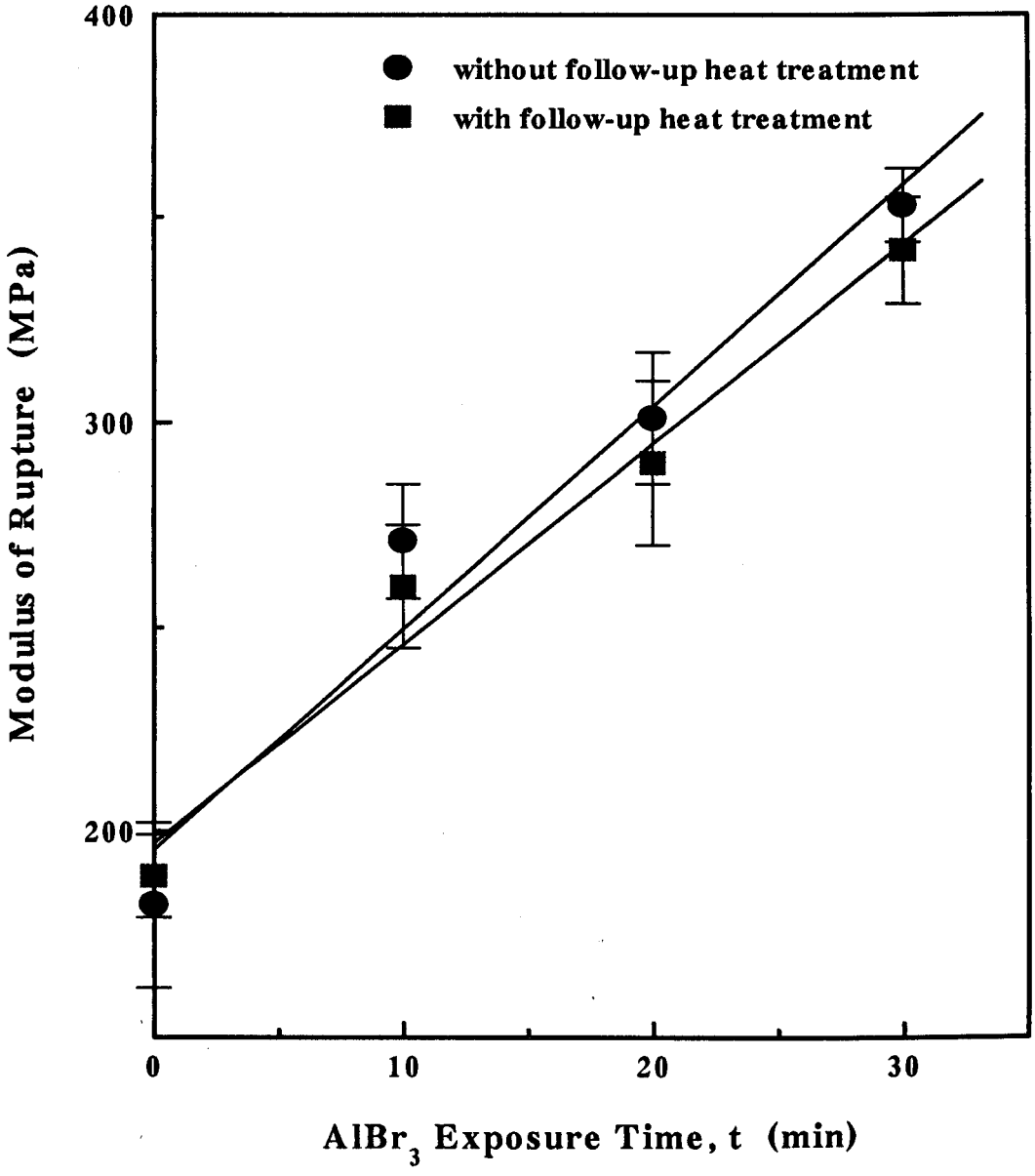

Figure 6.3 Variation of MOR with $AlBr_3$ exposure time (t) For Rockware RB 1 glass

Subsequent heat treatment at 550 °C for 1 h of the RB 1 glass rods showed no appreciable change in the strength improvement already achieved. These values are given in Table 6.11.

TABLE 6.11
STRENGTH RESULTS FOR $AlBr_3$ VAPOUR TREATED ROCKWARE RB 1 GLASS

Glass	Temperature (°C)	Time (min)	Modulus of Rupture (MPa)	Modulus of Rupture on Follow-up Heat treatment at 550 °C/1h (MPa)	Overall % Strength Increase
RB 1	550	Pristine	182 ± 20	189 ± 10	*0*
		10	271 ± 14	260 ± 15	*49*
		20	301 ± 16	290 ± 20	*65*
		30	355 ± 9	342 ± 13	*93*

6.3.2.3 COMBINED $AlBr_3$ AND LiBr VAPOUR TREATMENT

Table 6.12 summarises the results for the RB 1 rods which were treated with $AlBr_3$ for various times and then followed by LiBr treatment for a fixed period of 10 minutes. The data also include the strength value obtained after the rods were treated for 10 minutes in LiBr vapour only.

In this case, the pristine strength of 182 MPa improved by 32 % to 241 MPa. This value is similar to that obtained for float glass F1 as well as R4795 glass vapour treated for a similar duration. The follow-up LiBr treatment resulted in further enhancement of the strength values already achieved by $AlBr_3$ vapour exposure for varying times. The general

trend of the strength improvement, as shown in Figure 6.4 is linear, when the value, obtained for LiBr treatment only, is included. The dotted curve indicates the trend in the increase in strength over its pristine value. The values recorded were 328, 376 and 401 MPa for the glass rods which were given a follow-up LiBr treatment for 10, 20 and 30 minutes only. This corresponds to a percentile increase in the additional strength of 21, 25 and 19 for these times of treatment. The increase in strength over the pristine strength of the glass corresponded to 80, 106 and 119 %, respectively.

TABLE 6.12
RESULTS FOR $AlBr_3$ VAPOUR TREATED ROCKWARE RB 1 GLASS WITH A FOLLOW-UP LiBr TREATMENT

Glass	Temperature (°C)	Time (min)	Modulus of Rupture $AlBr_3$ Treated (MPa)	Modulus of Rupture on Follow-up LiBr treatment at 550 °C/10 min (MPa)	Overall % Strength Increase	Modulus of Rupture on Follow-up heat treatment at 550 °C/1h (MPa)
RB 1	550	Pristine	182 ± 20	241 ± 9	*32*	229 ± 9
		10	271 ± 14	328 ± 9	*80*	305 ± 11
		20	301 ± 16	376 ± 12	*106*	346 ± 13
		30	353 ± 9	401 ± 11	*119*	385 ± 10

It is also to be noted that no appreciable loss of strength was discernible when the rods were further heat treated at 550 °C for 1 h. The values are given in Table 6.12. Clearly, it can be concluded from these results that significant strength improvement is achievable from a follow-up 10 minute LiBr treatment. Furthermore, it is suggested that

the overall strength increase is due to combined diffusion of both Al and Li. It is suggested that the presence of Al is important, as its introduction into the surface provides $[AlO_4]^-$ ionic groups necessary for Na^+ or Li^+ ions to maintain charge neutrality. Also the presence of Al reduces the number of non-bridging oxygens and as a result, lowers the thermal expansion coefficient of the glass skin.

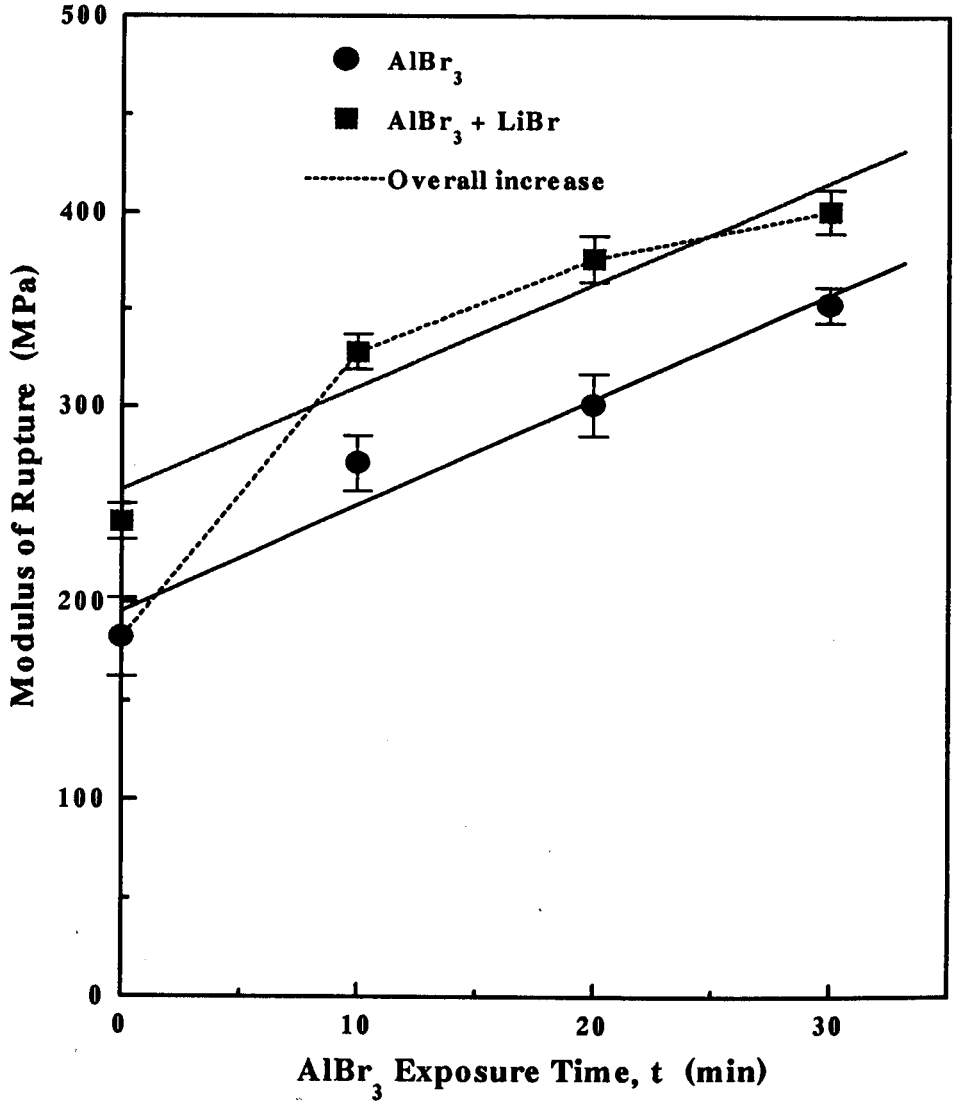

Figure 6.4 Strength enhancement For Rockware RB1 glass shown as MOR versus duration of vapour treatment

It will be clear from the results presented in section 6.5 that the use of vapour treatment forms an integral part of the processes used in the present investigation in strengthening commercial container glass compositions.

6.4 CHEMICAL VAPOUR DEPOSITION

6.4.1 DETERMINATION OF DEPOSITION CONDITIONS

Table 6.13 shows results of various runs to establish the optimum deposition rate. The flow rate of the metal source vapour and the nitrogen dilution were identified as the principal control parameters to obtain a satisfactory deposition. The influence of water was found to be less important but if the flow rate was lowered below 50 cc/min, unreacted source vapour deposited on the surface of the glass. The single most important factor in obtaining a high quality coating was found to be the proper control of nitrogen dilution of the metal source. A combination of 1.2-1.4 *l*/min of N_2 and a flow rate of metal source vapour of 50 cc/min for 20 minutes produced a coating of high quality. A high flow rate of metal source, for example, 100 cc/min with 1.2 *l*/min by N_2 dilution produced a surface containing traces of unreacted source material although increasing the dilution to 1.41 *l*/min marginally improved this problem. It was found that a fast deposition is, nevertheless, possible provided the dilution is high i.e. 1.7 *l*/min dilution for a shorter deposition time of 10 minutes with 100 *cc*/min of source. The quality of the coating still did not match that obtained with slow deposition conditions. Visual observation of the coating achieved after slow deposition revealed a surface with an appearance comparable to that of the pristine glass and, on crystallisation, the surface still largely maintained a high degree of transparency. A fast deposition, on the other hand, exhibited a surface with bubbles in some areas. A summary of the deposition conditions is given in Table 6.13.

TABLE 6.13
SUMMARY OF DEPOSITION CONDITIONS FOR FLOAT GLASS

Run	Flow Rate (cc/min)				Time	Temperature	Presence of Unreacted Vapour Particles	Coating Quality
	N_2	$POCl_3$	$TiCl_4$	H_2O	(min)	(°C)		
1	1000	100	-	100	20	600	yes	poor
2	1000	100	-	200	20	600	yes	poor
3	1200	50	-	200	20	600	none	excellent
4	1200	100	-	100	20	600	yes	poor
5	1400	100	-	200	20	600	yes	poor/medium
6	1400	50	-	200	20	600	none	excellent
7	1400	100	-	200	20	600	trace	medium/poor
8	1400	50	50	200	20	600	none	excellent
9	1700	100	-	200	10	600	none/trace	good

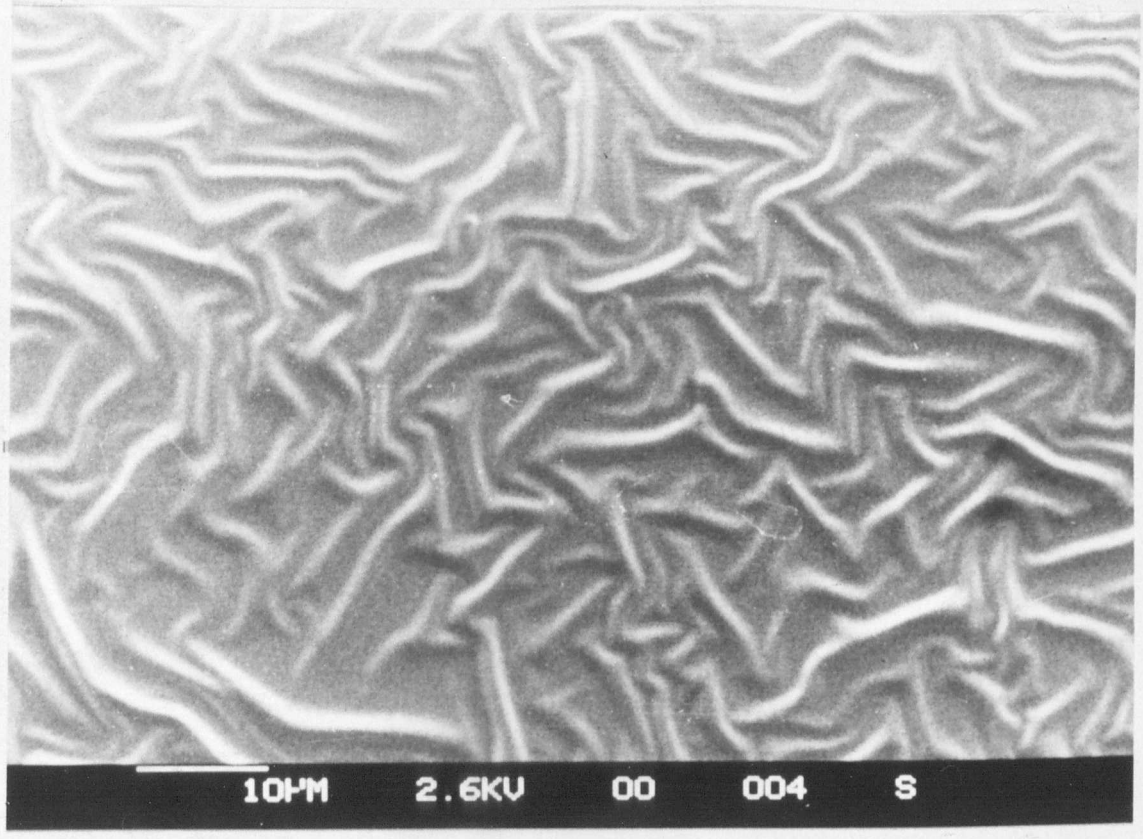

Figure 6.5 (a) SEM micrograph showing CVD coating of P_2O_5

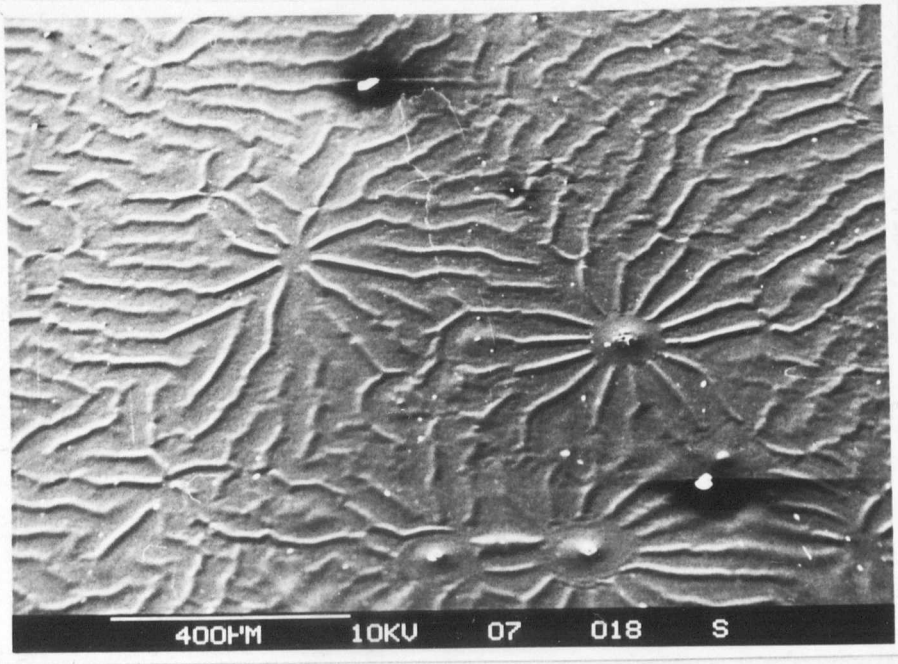

Figure 6.5 (b) Large area view of float glass surface doped with P_2O_5 and heat treated at 600 °C for 4 hours

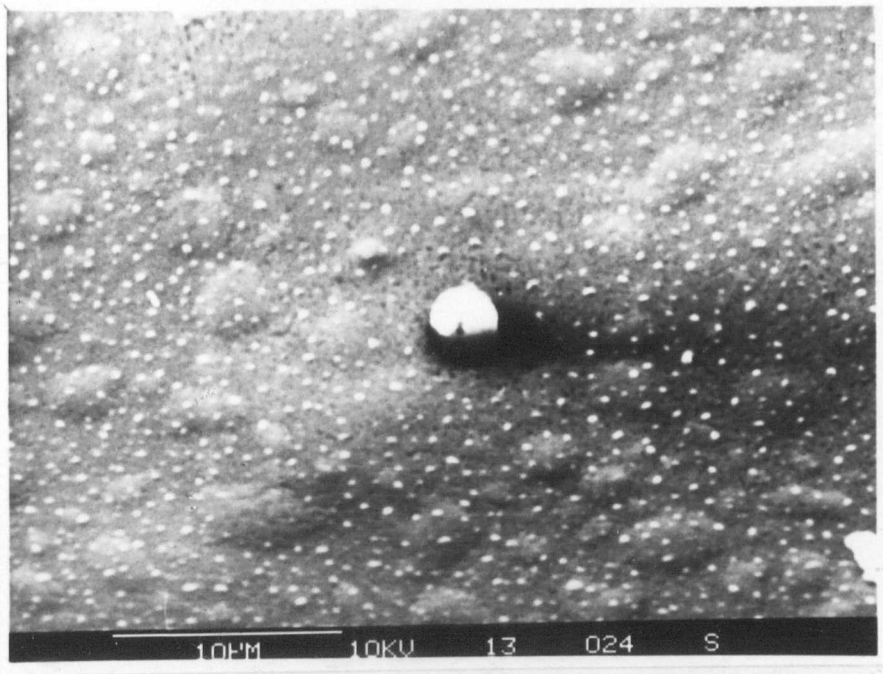

Figure 6.5 (c) Enlarged view of the above sample

It was found from the trial runs that further improvement in the coating quality could be achieved following a purging for an hour, prior to actual deposition, with inert gas at the heat treatment temperature. In this way, a much smoother and relatively bubble-free coating could be produced in addition to the optimised deposition rate described earlier.

Figure 6.5 (a) shows a SEM micrograph of the P_2O_5 doped but uncrystallised surface of the float glass. The surface coating consists of two regions, namely, planar areas and ridges. Elemental analysis showed that both regions are very rich in phosphorus with the concentration of *P* being almost identical in both areas (approx. 68 %). The formation of such elevated areas is attributed to the thermal expansion mismatch of the coating and the host glass surface. The depth of *P* diffusion into the glass was estimated to be ~ 2 μm after the glass was heat treated at 600 °C for 1 h. The concentration interface of the diffused layer and the glass was found to be very sharp. It is clear from the results that, whilst deposition of phosphorus can be readily achieved, there remains a problem in producing sufficient diffusion into the substrate. Where surface crystallisation was achieved with greater control of deposition, the type of the surfaces produced are illustrated in Figures 6.5 (b) and (c). Surface crystallisation consists largely of phosphates and phosphosilicates as a result of excessively high P_2O_5 doping.

6.4.2 MECHANICAL STRENGTH

The results of mechanical strength testing of CVD treated float glass (F1) and NLS 1 (see Tables 5.5 and 5.8 for nominal compositions) rods, measured by four point bending are given in Table 6.14. It can be seen from the table that the pristine strengths of as-drawn float glass and NLS 1 are very similar and lie, within experimental error, in the region of 174-178 MPa. The P_2O_5 doping and subsequent 'drive-in' heat treatment at 600 °C for 1 h did not produce surface crystallisation in either glasses and the strength of both

TABLE 6.14
STRENGTH VALUES OF FLOAT F1 AND NLS 1 GLASS RODS AFTER CVD TREATMENT

Glass	Treatment	Heat Treatment	Surface Crystallisation	Modulus of Rupture (MPa)	% Strength Increase
Float F1	Pristine	-	-	178 ± 10	-
	CVD of P_2O_5	600 °C/1h	no	190 ± 12	*6*
	CVD of TiO_2	600 °C/1h	yes	281 ± 10	*58*
NLS 1	Pristine	-	-	174 ± 12	-
	CVD of P_2O_5	600 °C/1h	no	205 ± 13	*17*
	CVD of TiO_2	600 °C/1h	yes	215 ± 10	*23*

glasses remained close to their original pristine strength, except a marginal increase in strength for float glass was observed. However, when the float glass was doped with P_2O_5 and TiO_2 followed by heat treatment at 600 °C for 1 h, both glasses crystallised. The strength of the float glass increased by 58%, over the pristine value, whilst NLS 1 showed a less marked improvement in strength. It therefore appears that TiO_2, in conjunction with P_2O_5, is more effective in promoting nucleation and surface crystallisation than P_2O_5 alone. It is thought that even higher strength may be achieved if the heat treatment temperature can be extended to promote faster growth rate. However, as reported earlier in Chapter 5 (section 5.4.1) during surface crystallisation, there is a problem of surface flow of the specimens. Heat treatment at high enough temperatures produced samples unsuitable for cross-breaking strength measurements. However, attempts have been made to overcome this problem by the use of the Hertzian indentation technique, as described earlier (see Chapter 3, section 3.3.3). Although it was found that this technique tolerated limited surface flow, there exist other problems as described below. A comparison of the strength values obtained by four-point and Hertzian fracture methods is given in Table 6.15. It is seen that the critical stress for Hertzian fracture is, generally, 30-40 % higher than that obtained by four-point bending. It was found that initiation of cracks in smooth surfaces such as pristine glass or uncrystallised doped surface was less difficult to observe than rough surfaces such as crystallised glass where the crack initiation is difficult to detect due to a reduction in clarity of the field of view caused by the loss of transparency during crystallisation. In addition, the measurement of crack radius was also complicated by the variable area of contact, resulting from the uneven crystallised surface. Attempts were made to lessen these problems by the use of illumination at near grazing incidence, on one side of the area of contact, so that the crack initiation can easily be detected, especially for the glass specimens which crystallised or exhibited limited surface flow, thus permitting the use of higher crystallisation temperatures. Using optical fibre and other forms of

illumination did not completely resolve this problem and, as result, strength testing using this method was limited to pristine or near clear surfaces. However, a limited number of strength measurements on surfaces of the glass specimens which crystallised was undertaken successfully and the results have been reported.

TABLE 6.15
COMPARISON OF STRENGTH VALUES MEASURED BY HERTZIAN FRACTURE AND FOUR POINT BENDING

Glass	Treatment	Surface Crystallisation	Hertzian Critical Stress σ_{TC} (MPa)	Modulus of Rupture (MPa)	% Strength Difference
Float F1	Pristine	-	243 ± 15	178 ± 10	*37*
	CVD of P_2O_5 & TiO_2 + Heat treated @ 600 °C/1h	yes	368 ± 15	281 ± 10	*31*
NLS 1	Pristine	-	239 ± 12	174 ± 12	*38*
	CVD of P_2O_5 & TiO_2 + Heat treated @ 600 °C/1h	yes	320 ± 18	215 ± 10	*48*

6.5 SURFACE MODIFICATION AND STRENGTHENING BY COMBINED VAPOUR AND CVD TREATMENT

In this section, the possibility for the glass surface to be ion exchanged via vapour treatment prior to the CVD process has been extended, and thus doping of known and effective nucleating agents such as P_2O_5 or TiO_2 or a combination of both to induce surface crystallisation has been fully investigated. The results presented and discussed, in which the techniques outlined in sections 6.3 and 6.4 have been expanded, include a commercial glass supplied by Rockware Glass Limited, UK and also a modified version of this base glass with added Al_2O_3. The intention here was to investigate the following:

(a) the strengthening effect of LiBr and $AlBr_3$ exposure on these glasses

(b) the influence of TiO_2 and P_2O_5 doping and/or heat treatment prior to/following LiBr exposure

(c) whether or not additional Al_2O_3 added to the base glass could result in surface crystallisation of low expansion phases such as β-spodumene or β-eucryptite thus enhancing the strength further than what can be achieved by LiBr treatment only

The composition of base glass R4795 and RAM 4795, modified with 3 wt % Al_2O_3, are given in Table 6.16. Some of the physical properties are included in Table 6.17.

6.5.1 GENERAL OBSERVATIONS

Although the softening point of the base glass R4795 was reported to be 716 °C, it was found that, in practice, the rods would deform at only 720 °C. Consequently a 'safe' temperature of 610 °C was chosen. It is, however, desirable that a temperature of ≈ 700 °C or higher at the point of exit for containers (hot end coating) be used. Such a

temperature regime, if employed, for all the treatments described below could further reduce the timescale of vapour treatments used.

TABLE 6.16
NORMALISED NOMINAL COMPOSITIONS OF ROCKWARE R4795 AND ALUMINA MODIFIED RAM 4795 GLASSES

Composition (wt %)		
Code	**R4795**	**RAM 4795**
SiO_2	73	70.87
Na_2O	11.60	11.26
K_2O	0.47	0.46
CaO	11.34	11.01
MgO	2.12	2.06
Al_2O_3	1.17	4.05

Although the temperature-viscosity relationship of the base glass R4795 is expected to be slightly modified by the addition of 3 wt % Al_2O_3, in practice none of the control parameters had to be altered at all to ease the drawing operation which remained essentially the same as for the base glass. No evidence of surface crystallisation could be detected at any stage of the investigation by XRD or DTA/DSC.

TABLE 6.17
PHYSICAL PROPERTIES OF R4795 AND RAM 4795

Property	R4795	RAM 4795
Softening point	716	795
Annealing point	573.1	610
Gob temperature	1220	1300
Strain point	543	581

NaBr was detected at the surface by XRD after LiBr and $AlBr_3$ treatment suggesting the replacement of Na by Li on the surface. The clouded layer following the treatment could be removed by simply washing in water to return the rods to their original transparency.

6.5.2 MECHANICAL STRENGTH OF PRISTINE AND HEAT TREATED RODS

The strength values of pristine rods of base glass R4795 and of the modified version RAM 4795 are given in Table 6.18. It can be seen that the pristine strengths of both glass compositions lie, within experimental error, in the region of 183-200 MPa. The addition of 3 wt % Al_2O_3 had no effect on the pristine strength value. On further heat treatment at 610 °C for 2 h and also over a longer period of 24 h at the same temperature, the MOR of pristine rods of both glasses remained unchanged.

6.5.3 LiBr TREATED RODS

The MOR values of rods of both glasses, on exposure to LiBr vapour for 40 minutes are shown in Table 6.18. The glasses showed a significant increase in their respective strength values i.e. 86 % for R4795 and 95 % for RAM 4795 over their pristine values.

TABLE 6.18
FLEXURAL STRENGTH OF ROCKWARE R4795 AND RAM4795 GLASS RODS USING CVD AND LiBr VAPOUR TREATMENTS

Glass	Treatment	Modulus of Rupture σ_F (MPa)			
		Vapour treated without follow-up heat treatment	% strength increase	Heat Treatment	
				610 °C/2h	610 °C/24h
R4795	Pristine	183 ± 15	*0*	190 ± 12	-
	LiBr	341 ± 9	*86*	338 ± 11	-
	TiO_2 doped	190 ± 10	*0*	200 ± 9	-
	TiO_2 + LiBr	335 ± 11	*83*	330 ± 15	-
RAM 4795	Pristine	200 ± 10	*0*	190 ± 11	195 ± 6
	LiBr	390 ± 10	*95*	385 ± 15	392 ± 11
	TiO_2 doped	205 ± 8	*2.5*	210 ± 10	212 ± 8
	TiO_2 + LiBr	442 ± 12	*121*	413 ± 15	441 ± 16

The slightly higher values obtained for the modified glass must be directly attributable to Al_2O_3 addition. On further heat treatments at 610 °C for 2 and 24 h (for R4795) the improvement in strength (341-390 MPa) for both glasses remained unchanged at a level of 338 and 392 MPa for R4795 and RAM 4795, respectively.

6.5.4 RODS DOPED WITH TiO_2 BY CVD AND EXPOSED TO LiBr VAPOUR

It was found that neither glass showed any improvement in their strength value when the rods were doped with TiO_2 alone. Heat treating the rods, the strength values remained unaltered (i.e. no improvement). However, exposure of the TiO_2 doped rods to LiBr vapours exhibited, particularly for the modified glass RAM 4795 with added Al_2O_3, a marked enhancement of strength approaching 442 MPa compared with its pristine value of 200 MPa. On the other hand, the base glass with no added Al_2O_3, when doped with TiO_2 followed by LiBr exposure, showed no additional improvement in strength (335 MPa) over the value already achieved (341 MPa) by LiBr treatment alone. It is therefore reasonable to conclude that, at least for the base glass, prior doping with TiO_2 seems to be ineffective in acting as a nucleating agent for surface crystallisation. However, for the Al_2O_3 modified glass RAM 4795 it appears that it is the TiO_2 doping, in combination with LiBr treatment, which resulted in the observed strength improvement. The role of TiO_2 in the presence of extra Al on the surface is not clear. This is particularly relevant when one considers that XRD or DTA showed no evidence of crystallisation for any of the glasses investigated under all treatment conditions. However the possibility of surface crystallisation at a level undetected by XRD can not be ruled out. If, indeed, such a crystalline layer is present, the role of TiO_2 may simple be that of nucleating catalyst for the precipitating phase. Further heat treatment showed the strength level essentially remaining unchanged.

6.5.5 RODS DOPED WITH TiO_2 AND P_2O_5 BY CVD AND EXPOSED TO LiBr VAPOUR

The results are shown in Table 6.19. When rods of both glass compositions were doped simultaneously with TiO_2 and P_2O_5, neither glass showed any strength increase nor

TABLE 6.19
STRENGTH VALUES OF ROCKWARE R4795 AND RAM 4795 GLASS RODS USING CVD, $AlBr_3$ AND LiBr TREATMENTS

Glass	Treatment	Modulus of Rupture σ_F (MPa)			
		Vapour treated without follow-up heat treatment	% Increase	Heat Treatment	
				610 °C/2h	610 °C/24h
R4795	Pristine	183 ± 15	*0*	190 ± 12	-
	LiBr	341 ± 9	*86*	338 ± 11	-
	$TiO_2 + P_2O_5$	200 ± 10	*9*	210 ± 6	-
	$TiO_2 + P_2O_5$ + LiBr	343 ± 15	*87*	350 ± 12	-
	$TiO_2 + P_2O_5 + AlBr_3$	250 ± 10	*36*	240 ± 15	-
	$TiO_2 + P_2O_5 + AlBr_3$ +LiBr	402 ± 12	*120*	390 ± 10	-
RAM 4795	Pristine	200 ± 10	*0*	190 ± 11	195 ± 6
	LiBr	390 ± 10	*104*	385 ± 8	392 ± 11
	$TiO_2 + P_2O_5$	211 ± 7	*9*	195 ± 10	199 ± 12
	$TiO_2 + P_2O_5$ + LiBr	370 ± 11	*93*	311 ± 9	302 ± 12

did they exhibit any increase in strength on further heat treatment. However, further LiBr treatment of the doped rods of both glasses improved the strength to a level similar to that observed when undoped rods of these glasses were exposed to only LiBr vapour.

On further heat treatment at 610 °C/2h the improvement in strength for the doped and LiBr treated rods of R4795 glass remained unchanged (350 MPa), although for the modified glass the improved strength of 370 MPa, lower than the 390 MPa obtained by LiBr treatment only, actually dropped to 302 MPa. It appears therefore, that for a glass containing high Al_2O_3, P_2O_5 may actually inhibit Li diffusion in the glass (since phosphorus is a very effective scavenger of lithium in glass), thus rendering the lower strength improvement observed. This detrimental effect of a combination of TiO_2 and P_2O_5 on LiBr doped glass is increased on further heat treatment.

6.5.6 GLASS R4795 DOPED WITH TiO_2 AND P_2O_5 BY CVD AND EXPOSED TO $AlBr_3$ VAPOUR FOLLOWED BY LiBr VAPOURS

The difficulty in handling extremely corrosive $AlBr_3$ has already been mentioned. Despite this problem, a few runs were carried out and the results are given in Table 6.19. It was found that the pristine strength of the base glass improved from 183 MPa to about 250 MPa after the rods, doped with TiO_2 and P_2O_5, were exposed for a very short time of 10 minutes. It is clear from the results that when these doped rods, treated with $AlBr_3$ vapours, were further exposed to LiBr vapour the strength improved very markedly from its pristine strength of 183 MPa by about 119 % to 402 MPa. This compares favourably with the value of 343 MPa achieved for the doped rods with LiBr treatment only. On further heat treatment this value of 402 MPa remained essentially unchanged at 390 MPa. Clearly, the additional improvement observed is related to the $AlBr_3$ treatment and the role of Al in the surface modification requires further investigation, although experiments using

liquid aluminium isopropoxide in butanol as a source of Al presented containment problem and was not pursued.

6.6 STRENGTHENING BY ION EXCHANGE DIP COATING

The compositions of base Rockware base glass R4795, alumina modified R4795/3, R4795/5 and R4795/10 with 3, 5 and 10 wt % Al_2O_3, respectively are given in Table 6.20.

TABLE 6.20
NOMINAL NORMALISED COMPOSITION OF ROCKWARE BASE R4795 AND MODIFIED R4795/3, R4795/5 AND R4795/10 GLASSES

Code	Composition (wt %)			
	R4795	R4795/3	R4795/5	R4795/10
SiO_2	73	70.87	69.51	66.35
Na_2O	11.60	11.26	11.05	10.54
K_2O	0.47	0.46	0.45	0.43
CaO	11.34	11.01	10.80	10.31
MgO	2.12	2.06	2.02	1.93
Al_2O_3	1.17	4.05	5.88	10.15

6.6.1 GENERAL OBSERVATIONS

DTA traces of the base glass indicated that T_g of the base glass R4795 lies in the region of 650 °C whereas the modified R4795/3, R4795/5 and R4795/10 glasses, as expected, exhibited higher transformation temperatures i.e. 659, 689 and 725 °C, respectively. Clearly this is due to the increased Al_2O_3 content in the modified compositions.

6.6.2 LITHIUM BASE ION EXCHANGE USING MOLTEN HALIDE SALT BATHS

Table 6.21 summarises the results of lithium base exchange in a LiCl salt bath for all the glasses investigated. The level of transparency achieved following ion exchange is represented in Figure 6.6.

In general, the primary crystalline phase formed was β-spodumene solid solution, at the surfaces of the alumina modified glasses, after ion exchange and further heat treatment. This phase has a low thermal expansion coefficient (α = 0.08 x 10^6/K) and is known to produce high compressive stress. It will be shown later to render substantial strength enhancement.

Unmodified R4795

The surface of the glass samples of unmodified base glass R4795, following dipping in the LiCl salt bath at 620 °C for 5, 10 and 15 minutes, became translucent with a sputtering of white substance on the surface which could not be washed away in water. A similar observation was made when these samples were dipped in the LiBr salt bath for the same periods of time at the same temperature. XRD traces of the samples showed no

evidence of known crystalline phases viz. β-spodumene, β-eucryptite or devitrite being precipitated on the surface.

TABLE 6.21
SUMMARY OF ION EXCHANGE RESULTS

Glass	LiCl or LiBr Salt Bath Treatment		Heat Treatment		XRD Observation	
	Temp (°C)	Time (min)	Temperature (°C)	Time (h)	β-spodumene	others
R4795	620	5, 10,15	-	-	no	yes
R4795/3	625	5	-	-	no	not detectable
	625	10	-	-	no	not detectable
	625	15	-	-	yes	yes
	640	15	-	-	yes	yes
	625	15	625	2	yes	yes
R4795/10	630	5	-		yes	yes
	630	10	-		yes	yes
	630	15	-		yes	yes
	630	15	630	2	yes	yes
	760	2-3sec	620	15min	yes	yes

Figure 6.6 Photograph showing level of transparency achieved on lithium ion base exchange for the modified Rockware container glasses

ROCKWARE R4795/3 (plus 3 wt% Al_2O_3)

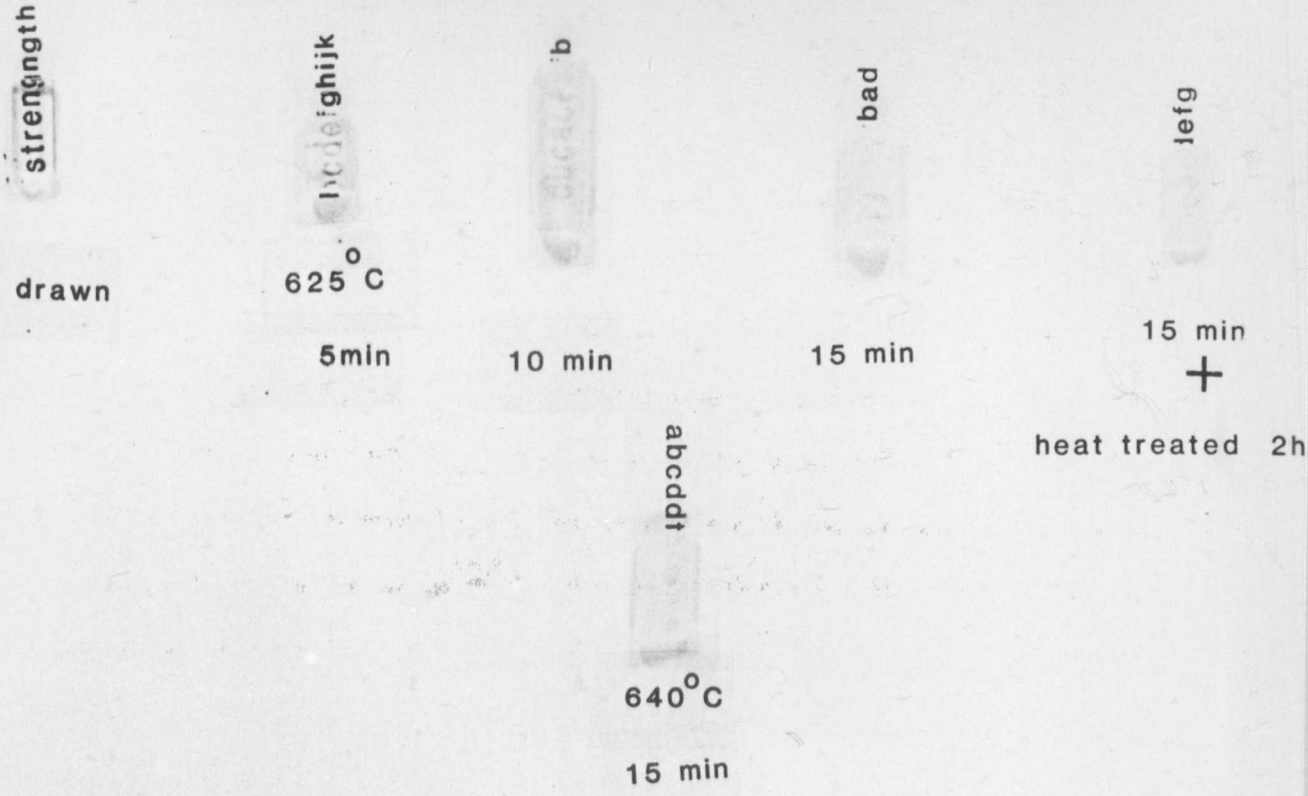

ROCKWARE R4795/10 (plus 10 wt% Al_2O_3)

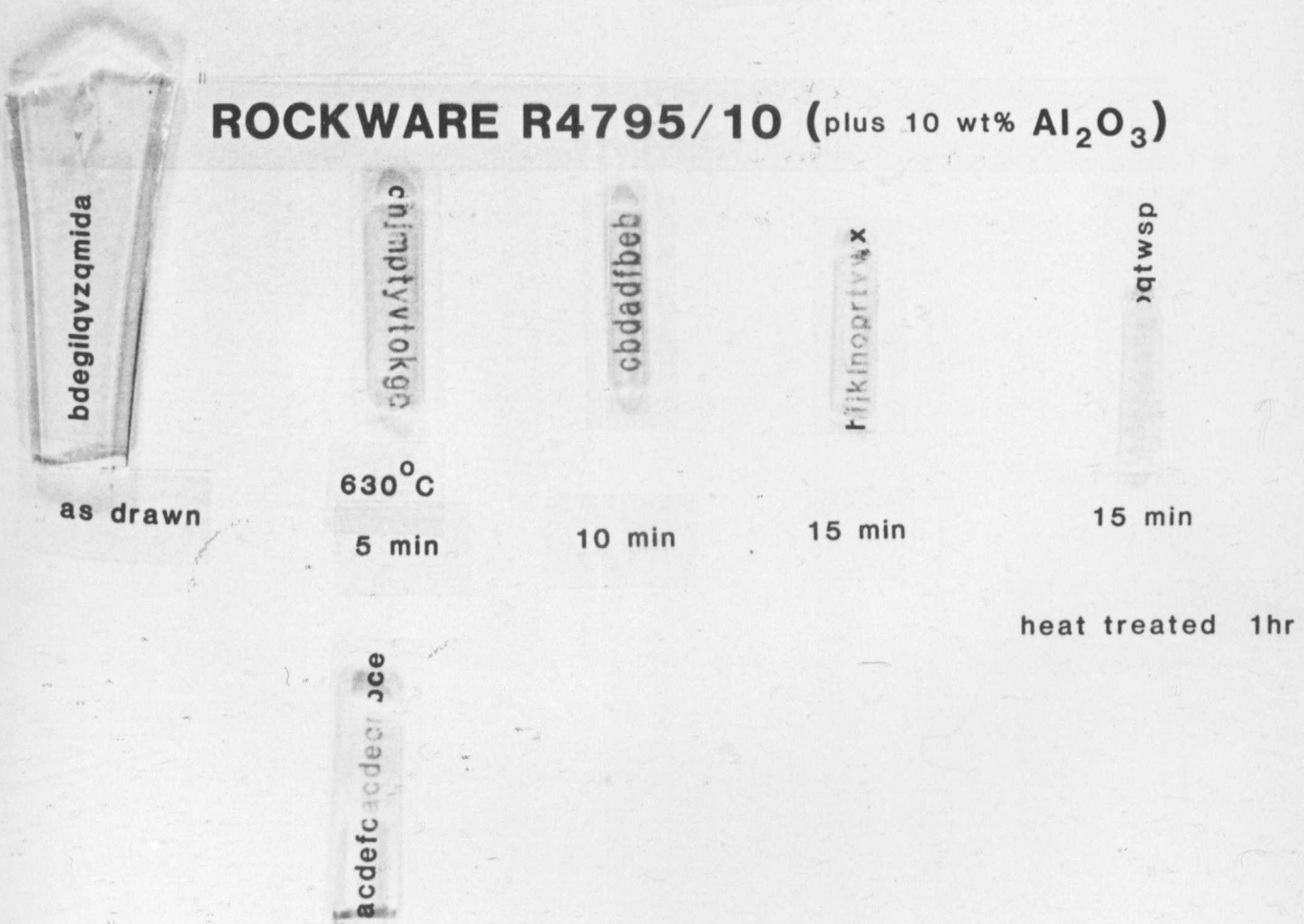

Modified R4795/3

Generally the surface of the glass samples of unmodified base glass R4795/3 following ion exchange at 625 °C appeared almost transparent but became slightly translucent when treated for longer times, e.g. for 15 minutes. In some cases, the same patchy white spots as mentioned before appeared, rendering the samples treated for longer times somewhat non-uniformly translucent in places. No β-spodumene could be detected by XRD for the samples treated for 5 and 10 minutes. However, ion exchange for 15 minutes in either of the salt baths produced crystallisation, primarily of the β-spodumene phase, on the surface as detected by XRD. The other unidentified phase is believed to be due to a reaction product appearing as a patchy white substance that could not be washed away in water. It is to be noted here that these additional peaks, attributed to the unidentified phase, were different for identical samples when treated separately in LiCl and LiBr salt bath. This probably indicates the presence of a surface film which appears to have been induced during the ion exchange reaction and which depends on the nature of the salt bath employed. Further heat treatment at the same temperature for 2 hours showed the growth of β-spodumene.

When the samples were ion exchanged at higher temperature i.e. substantially above the T_g of the glass, the surface became translucent, possibly either as a result of a surface film from the salt that became embedded in the glass by surface flow or because of faster growth of β-spodumene. The predominant phase in this case was therefore β-spodumene.

It should be emphasised that the thermal condition of the samples prior to dipping is considered important, in that the preheated samples appear to produce a better surface finish and improved transparency than those dipped 'as-cold'.

Modified R4795/10

In the case of this base glass, modified with 10 wt % alumina, the results of the Li-base exchange in either LiCl or LiBr salt bath were found to be most encouraging. All samples of this modified composition surface crystallised when ion exchanged for 5, 10 and 15 minutes at 630 °C. Significantly, even the preheated samples, produced surface crystallisation when dipped in LiCl bath for a couple of seconds at a relatively high temperature of 760 °C followed by heat treatment at 620 °C for 15 minutes . The phases identified were predominantly β-spodumene along with the same unidentified phase mentioned earlier.

The surface layer appeared to be relatively uniform and the degree of transparency obviously varied from slightly translucent to translucent depending on the duration of the ion exchange process. This is indicated in Figure 4.10. The decreased translucency was attributed to the reaction product during ion exchange originating from the salt bath.

Further heat treatment, at the same temperature for longer times (2 h), resulted in continued growth of β-spodumene crystals with the samples becoming, as expected, progressively opaque.

6.6.3 LITHIUM BASE ION EXCHANGE USING SULPHATE SALT BATHS

In the light of the results and discussions presented above which described the ease with which surface crystallisation of desirable phases can be produced, especially when the glass contains higher alumina content (3-10 wt %) relative to its base composition (~ 1.16 wt %), further investigation regarding the choice of baths has been carried out in order to eliminate possible etching problems (white patchy appearance) associated with LiCl and LiBr salt baths. In this investigation, baths of sulphate formulations were chosen. They

include Li_2SO_4, binary Li_2SO_4-Na_2SO_4 and ternary Li_2SO_4-Na_2SO_4-K_2SO_4 salt baths. The results presented below include an additional glass composition (R4795/5) with an 'optimum' alumina content of 5 wt % (see Table 6.20).

For the glass with 3 wt % added alumina, XRD traces showed no evidence of surface crystallisation up to a dipping time of 2 minutes when traces of a surface-crystallised, phase mixture of β-spodumene/β-eucryptite type solid solution were detected. The level of transparency for this sample was found to be excellent. For R4795/10 glass, XRD traces showed that the primary crystalline phase formed on the surface, following ion exchange at 800 °C for times from 10 second to 2 minutes, was β-spodumene and/or β-eucryptite type solid solution. The level of transparency for R4795/10 was found to be excellent in all cases except for the samples treated for 2 minutes, which showed a slight loss but were still very satisfactory. Unlike the white patchy areas associated with the LiCl or LiBr bath, all samples showed a uniform crystalline layer. This is attributed to the SO_4^{2-} ions being less likely to diffuse in the glass surface due to their relatively larger size than both Cl^- or Br^- ions and therefore the sulphate bath is more effective in maintaining transparency.

Table 6.22 summarises the strength results of Li-base exchange in the ternary sulphate salt bath for all three alumina modified glasses treated at 800 °C for times from 10 seconds to 2 minutes. The relationship between the glass strength and the time of ion exchange is shown in Figure 6.7.

The pristine strength of the high alumina R4795/10 glass rods gave a value of 192 ± 12 MPa, although this did not reflect the increased alumina content in the base glass, for a slightly higher value was anticipated. It is clear from the figure that the strength of this glass improved steadily with the duration of ion exchange and a value of approximately 500 MPa was achieved for the rod treated for 2 minutes. The plot does not show any

TABLE 6.22
SUMMARY OF STRENGTH RESULTS FOR ION EXCHANGED SAMPLES

Glass	Duration of Exchange t	$\sqrt{\tau}$ (min)	Temperature (°C)	Modulus of Rupture (MPa)	% Strength Increase
R4795/10	Pristine	-	800	192 ± 12	*0*
	10 sec	0.41		224 ± 6	*16*
	20 sec	0.58		253 ± 19	*32*
	30 sec	0.71		295 ± 7	*54*
	1 min	1.00		400 ± 18	*108*
	1.5 min	1.23		448 ± 7	*133*
	2 min	1.41		506 ± 11	*163*
R4795/5	Pristine	-	800	186 ± 10	*0*
	10 sec	0.41		184 ± 9	-
	20 sec	0.58		180 ± 13	-
	30 sec	0.71		185 ± 12	-
	1 min	1.00		188 ± 10	*18*
	1.5 min	1.23		220 ± 15	*41*
	2 min	1.41		263 ± 20	*0*
R4795/3	Pristine	-	800	177 ± 11	-
	10 sec	0.41		182 ± 10	-
	20 sec	0.58		187 ± 12	-
	30 sec	0.71		184 ± 15	*4*
	1 min	1.00		185 ± 12	*5*
	1.5 min	1.23		191 ± 16	*8*
	2 min	1.41		193 ± 22	*9*

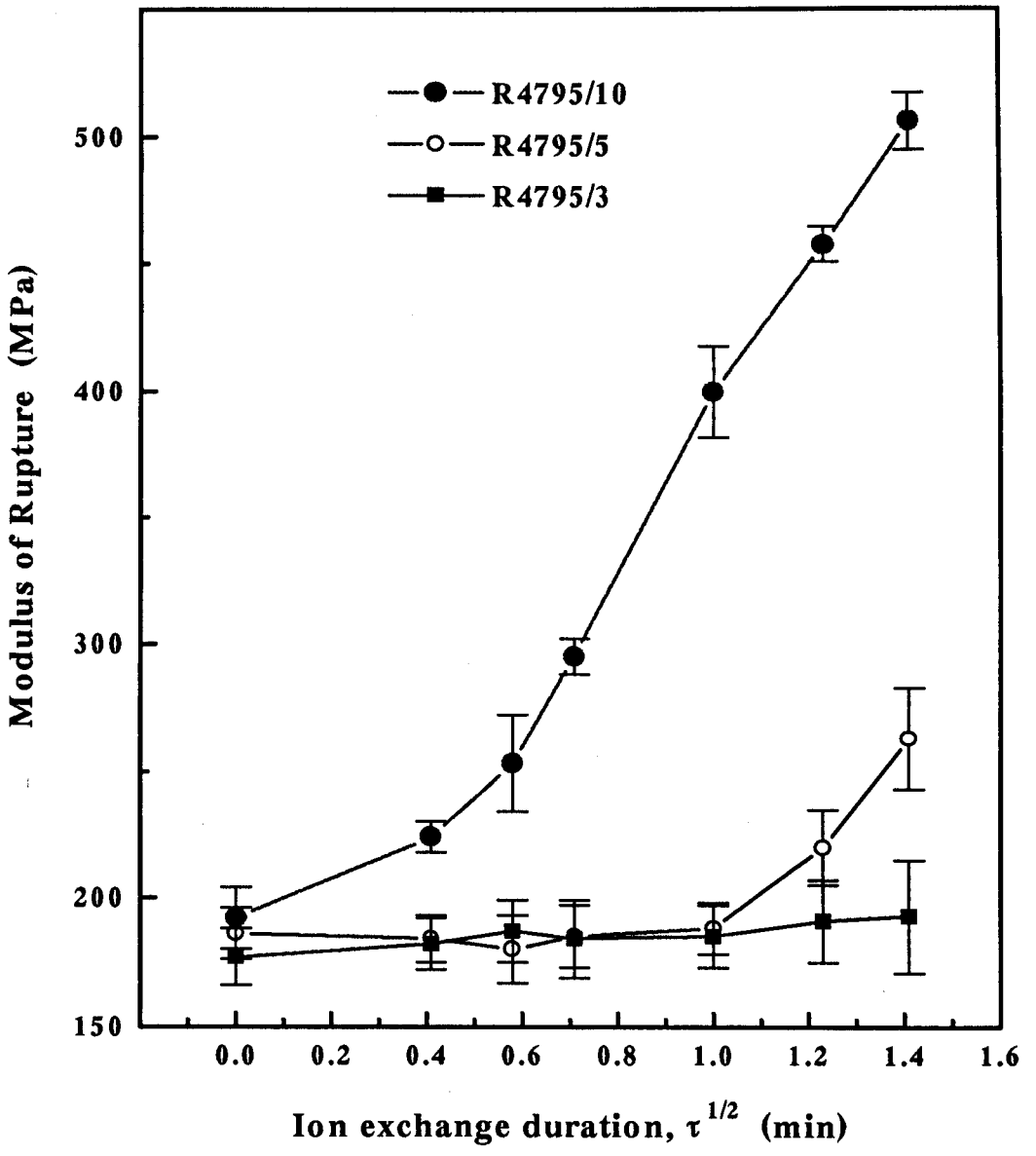

Figure 6.7 Variation of MOR with the duration of ion exchange

maximum and thus it is reasonable to expect even further enhancement of strength for longer times. However longer exchange times resulted in difficulty of obtaining undeformed rods for strength tests. Taking the values altogether, an improvement in strength of 16-163 % was achieved for treatment duration of 10 seconds to 2 minutes. It is to be borne in mind here that the rods were dipped 'as-cold' and the times quoted should

not be regarded as absolute values since a preheat treatment would reduce the "effective" time required to produce a given depth of crystalline layer. This has not been attempted since the rods would further deform and present even greater difficulty in achieving meaningful strength data.

As for glasses R4795/3 and R4795/5 with low and medium alumina added, there was no noticeable strength increase on ion exchange, unlike R4795/10. This is due to the absence of any crystallisable layer on the surface of the glasses except for the single sample of R4795/5 which exhibited slight improvement in strength, from a pristine value of 186 ± 10 MPa to 263 ± 20 MPa reflecting the increase due to the surface crystallised layer observed.

Also it is suggested, based on some evidence of recent soviet work[144] on Na-K exchange in glass, that the concentration of Li^+ ions in the surface layer of unannealed aluminosilicate glass is expected to be significantly greater than the concentration of Li^+ ions in the surface layer of a glass which has been ion strengthened after annealing. This in turn should result in increased strength as the diffusion of Li^+ ions also increases. Such acceleration of the diffusion process would be possible for glass rods strengthened immediately after drawing as the structure would be relatively 'open' as a result of lower activation energy in such a structure than the rods strengthened after being cooled or annealed thus having a more 'compact' structure. Also, equilibrium in glassy property is more rapid from the high temperature side than the low temperature side, thus treatment time in the production line would be expected to be shorter.

6.6.4 ELECTROSTATIC SPRAYING TRIALS

Generally, it proved to be difficult to carry out trials successfully on a laboratory scale. The outstanding problem was to maintain a furnace temperature that would allow

successful drawing of bubble-free rods that could be used for subsequent strength measurement. Coupled with this, maintaining a high enough temperature immediately after drawing to allow adequate diffusion of lithium into the glass also proved very difficult. The sprayed salt melted non-uniformly and also cooled too quickly as the rods were drawn. This produced a somewhat patchy surface with some of the areas of the salt layer being peeled off. Some of the rods or flat samples produced this way were heat treated at 700 °C for 1 h but exhibited no surface crystallisation. It was clear that a thick coating of molten salt (for example, 1 mm) together with a high diffusion temperature for a longer time (for example, 10 seconds compared to couple of seconds available during drawing) would be necessary for crystallisation. This was confirmed by a set of runs where *already drawn* flat pieces were held at the furnace mouth at temperatures exceeding 1000 °C. This was followed by continuously spraying the salt onto the samples, allowing it to melt properly and then holding at temperature for about 20 seconds. This resulted in surface crystallisation. The other problem was to maintain a continuous flow of the salt whose particle size was unavoidably greater than the recommended 54 μm. Also an efficient spray could not be achieved because of the lack of a sufficiently large amount of batch feed needed (for example, a minimum of a few kilograms).

None of the rods produced in the trial were found to be bubble free and as a result, it was not possible to obtain any strength data from these rods.

6.6.5 CHARACTERISATION OF SURFACE CRYSTALLISED LAYER

(a) Ion-exchange in molten salt bath

The general surface features following ion exchange in the molten salt bath are shown in Figure 6.8 (a) and (b). The same area magnified reveals the points of contact of the surface of the glass with the salt and is shown in figure 6.9. It is suggested that these

(a)

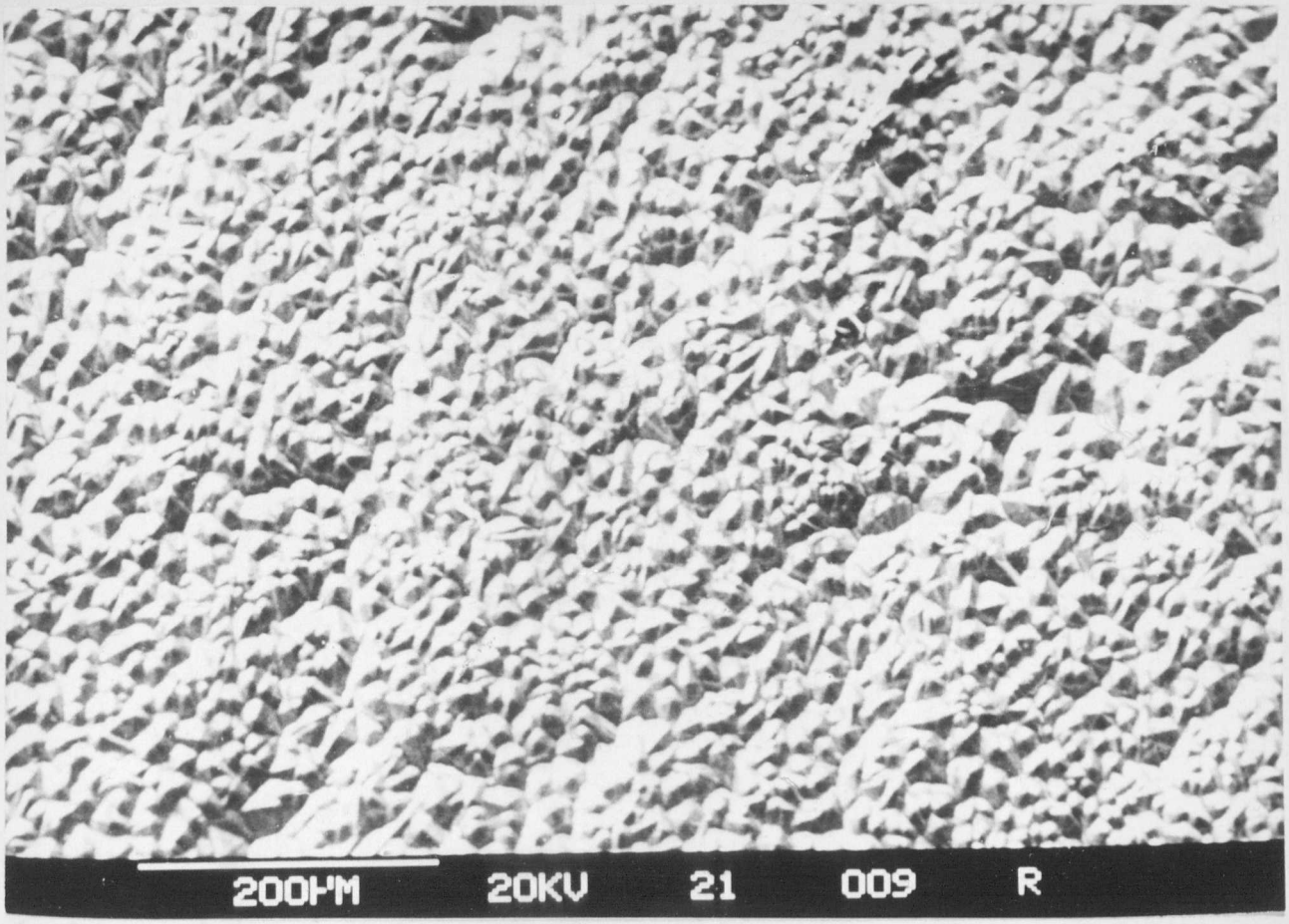

Figure 6.8 SEM micrographs showing the general feature of the surface crystallisation of a Rockware container glass (R4795/10)

(b)

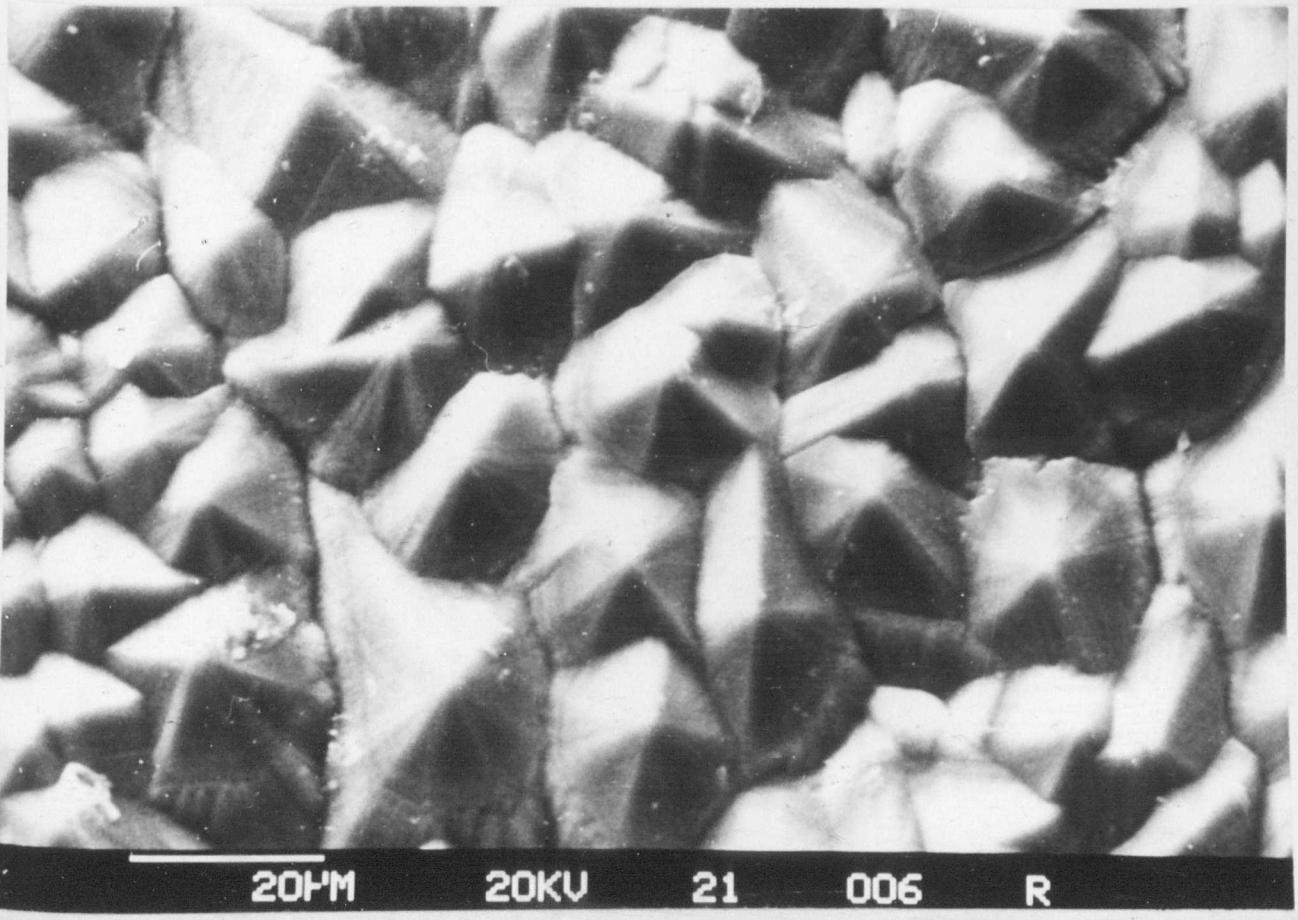

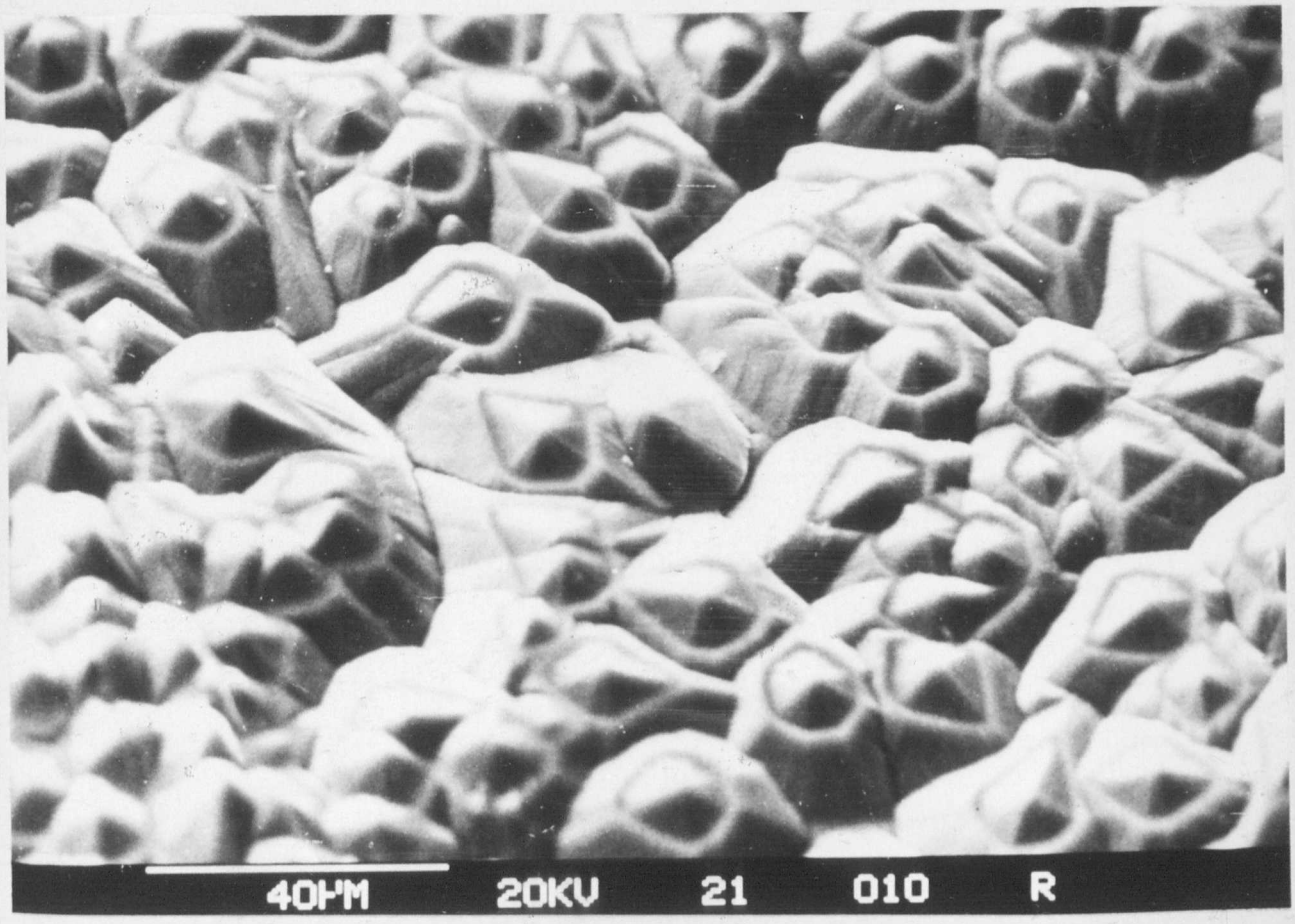

Figure 6.9 SEM micrograph showing the areas of contact between the molten salt and the glass surface resulting in surface crystallisation

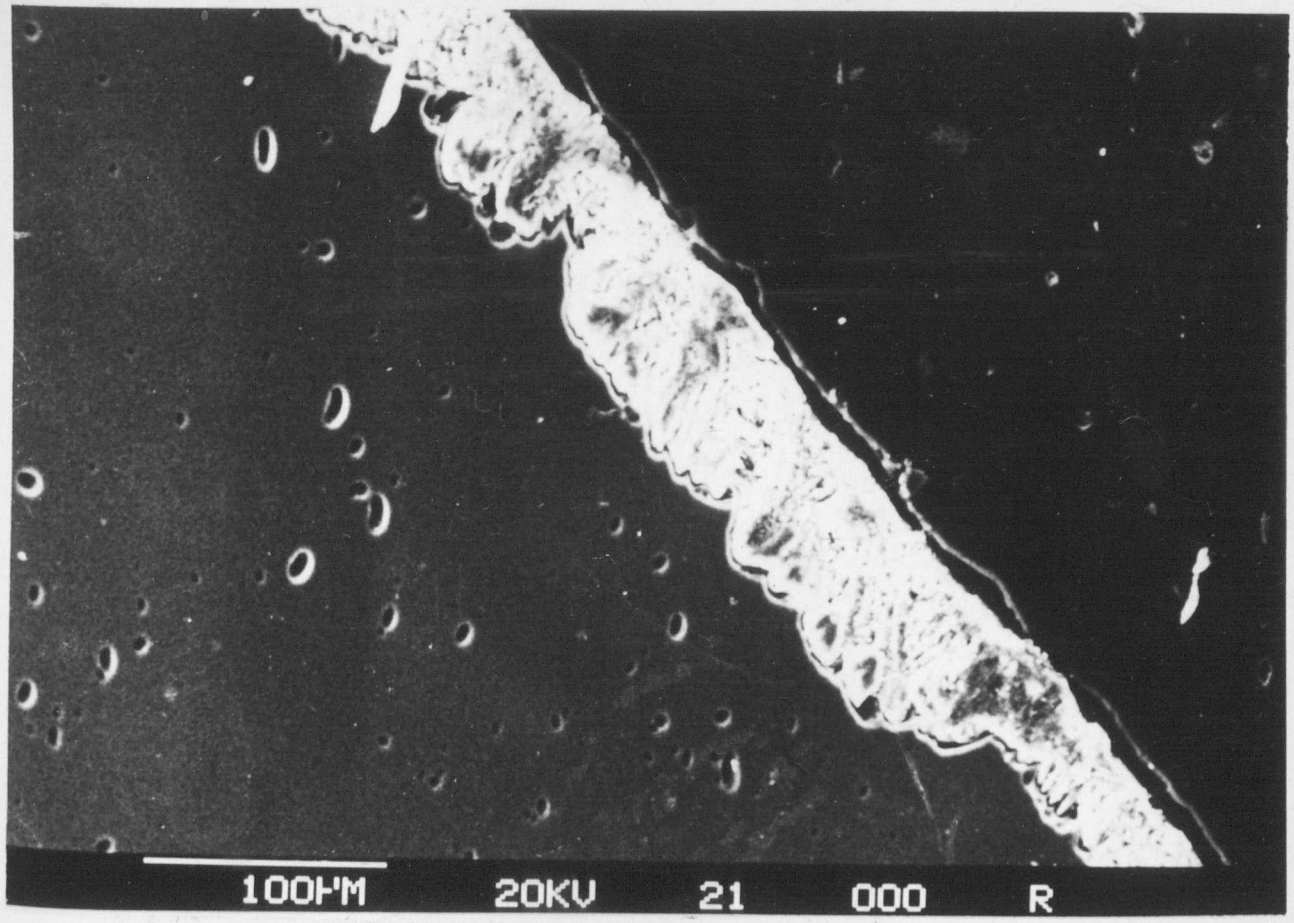

Figure 6.10 SEM micrographs showing the surface crystallised layer developed after an exposure of 120 seconds in a molten salt bath

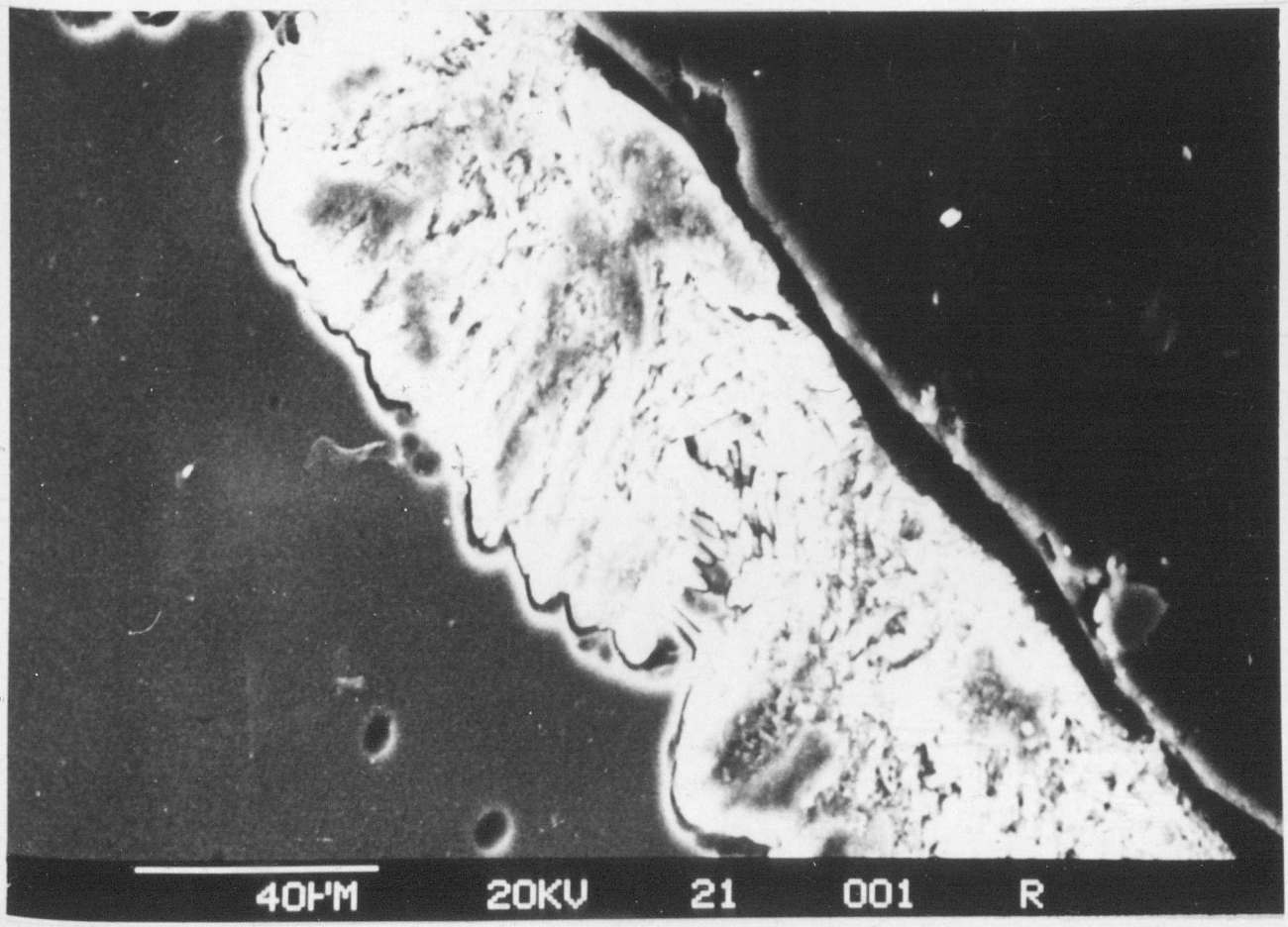

contact points act as stress concentrators and surface crystallisation commenced at these nucleating sites. The other possible explanation may be that these are simply nucleating sites and in some way related to crystallisation morphology. Elemental analysis concluded that these areas are rich in primarily Si and Al. Since the concentration of Li and O could not be determined, the calculated Si/Al ratio closely corresponds to that of β-spodumene phase, although it is likely that a mixture of β-eucryptite and β-spodumene solid solution types is the prevailing surface structure.

TABLE 6.23
SUMMARY OF ION EXCHANGE RESULTS FOR ALUMINA MODIFIED R4795/10

Glass	Duration of Exchange t	$\sqrt{\tau}$ (min)	Average Layer Thickness (μm)	Modulus of Rupture (MPa)
	Pristine	-	-	192 ± 12
	10	0.41	20	224 ± 6
	20	0.58	27	253 ± 19
R4795/10	30	0.71	39	295 ± 7
	1 min	1.00	54	400 ± 18
	1.5 min	1.23	61	448 ± 7
	2 min	1.41	70	506 ± 11

The depth of the surface crystallised layer formed following salt treatment for varying times is summarised in Table 6.23. The layer grew uniformly from 20 μm when

treated for 10 seconds to 70 μm after an exposure of 2 minutes. An example of the development of the surface crystallised layer is shown in Figure 6.10. The crystallisation was observed to start at the surface of the glass and then proceeds towards the interior of the glassy matrix. The original sample was transparent and remained so upto 30 second treatment; thereafter gradually became more opaque with the exchange duration. Figure 6.11 shows that the relationship between the layer thickness and the square root of the duration of ion exchange, within experimental error, is one of linearity.

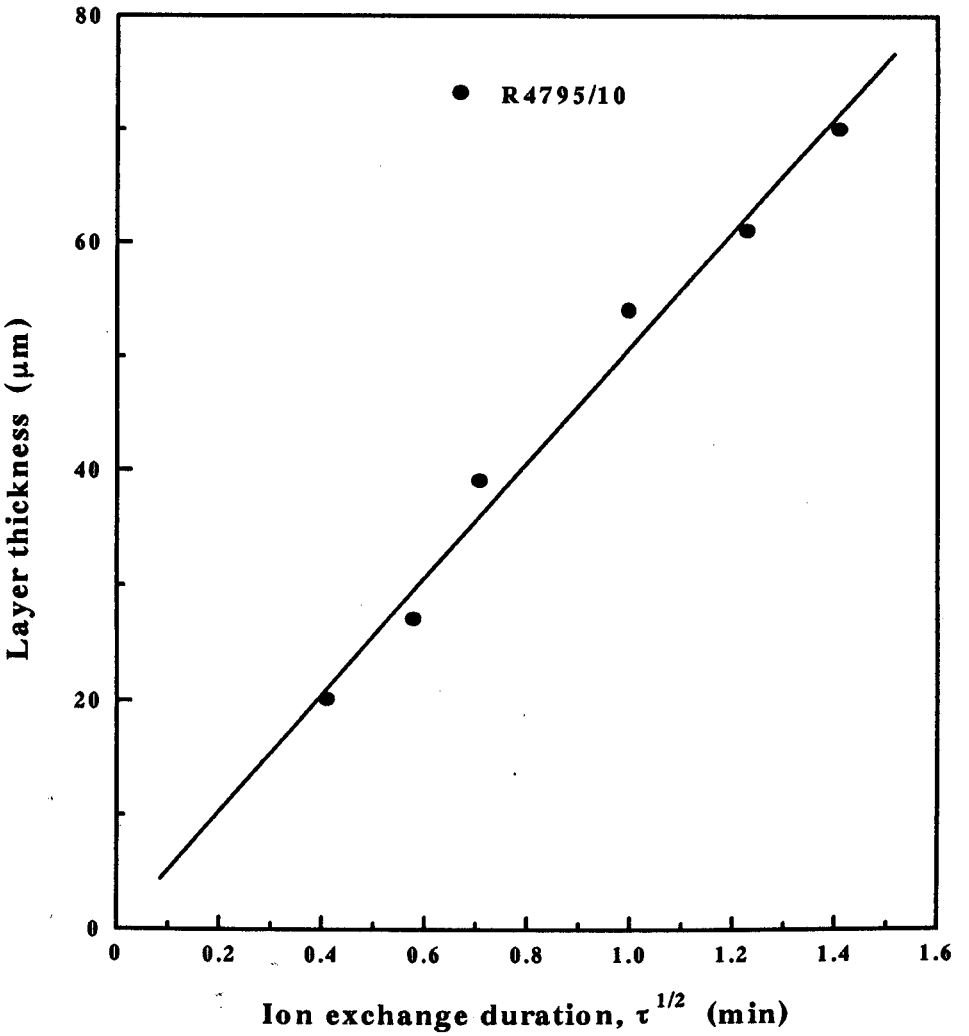

Figure 6.11 Variation of crystallised layer thickness with exchange duration

It can be seen from the table that the high strength of 506 MPa obtained corresponds to a layer of approximately 70 μm. For the glass R4795/5 with optimum alumina content, the layer thickness developed after surface crystallisation, following a 2 minute salt bath treatment, was measured to be only about 10 μm corresponding to a strength increase of 263 MPa. It is suggested that still further enhancement in strength greater than 506 MPa is possible, if the layer thickness can be improved by optimising the control parameters such as pre-treatment and/or exchange conditions.

(b) Ion-exchange by electrostatic spraying

Figure 6.12 shows a typical example of the general surface structure which is characterised by areas where surface crystallisation occurred, separated by regions that remained uncrystallised. As explained earlier, this is associated with the difficulty of controlling the spray and maintaining a high enough temperature for the diffusion to take place. As indicated in section 6.6.4, the flat specimens crystallised when held for a longer time following the spray. In this case, a layer thickness of 20 μm was measured and the surface structure was found to be similar to those observed in the case of straightforward dipping (for example, as shown in Figure 6.8)

6.7 DEPTH PROFILE ANALYSIS

Figure 6.13 summarises the data, collected from the paper by Sendt[145,146], on the lithium ion penetration in salt bath experiments. The temperature versus time curve is plotted for given n_x/n_o ratios (n_o = initial and n_x = final ion concentration) and a penetration depth of 50 μm. It is however suggested that there may be more than one rate constant involved, i.e. diffusion slows down as ion concentration in the glass increases.

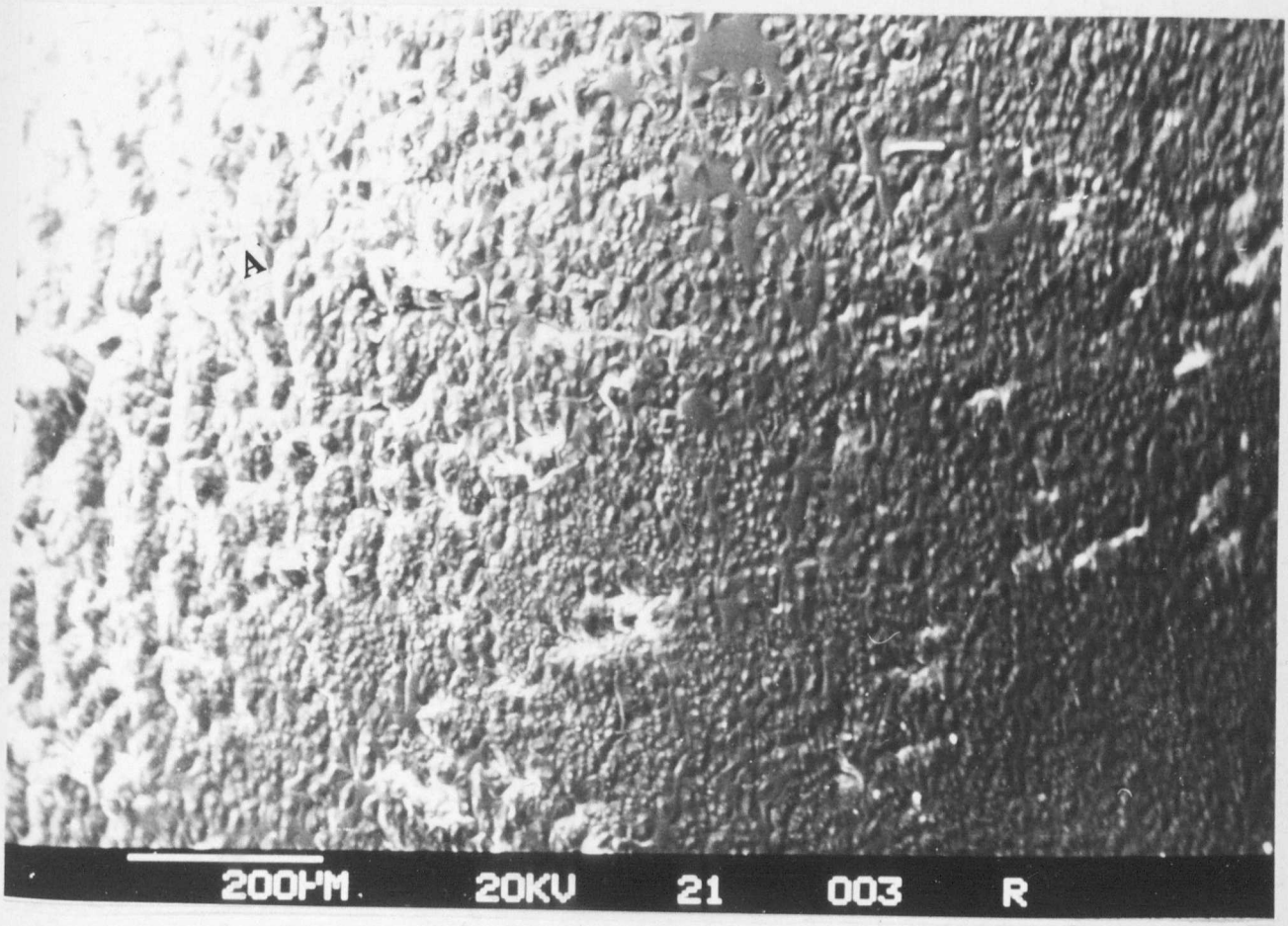

Figure 6.12 SEM micrographs showing surface features of an electrostatically sprayed sample with partial surface crystallisation (area A)

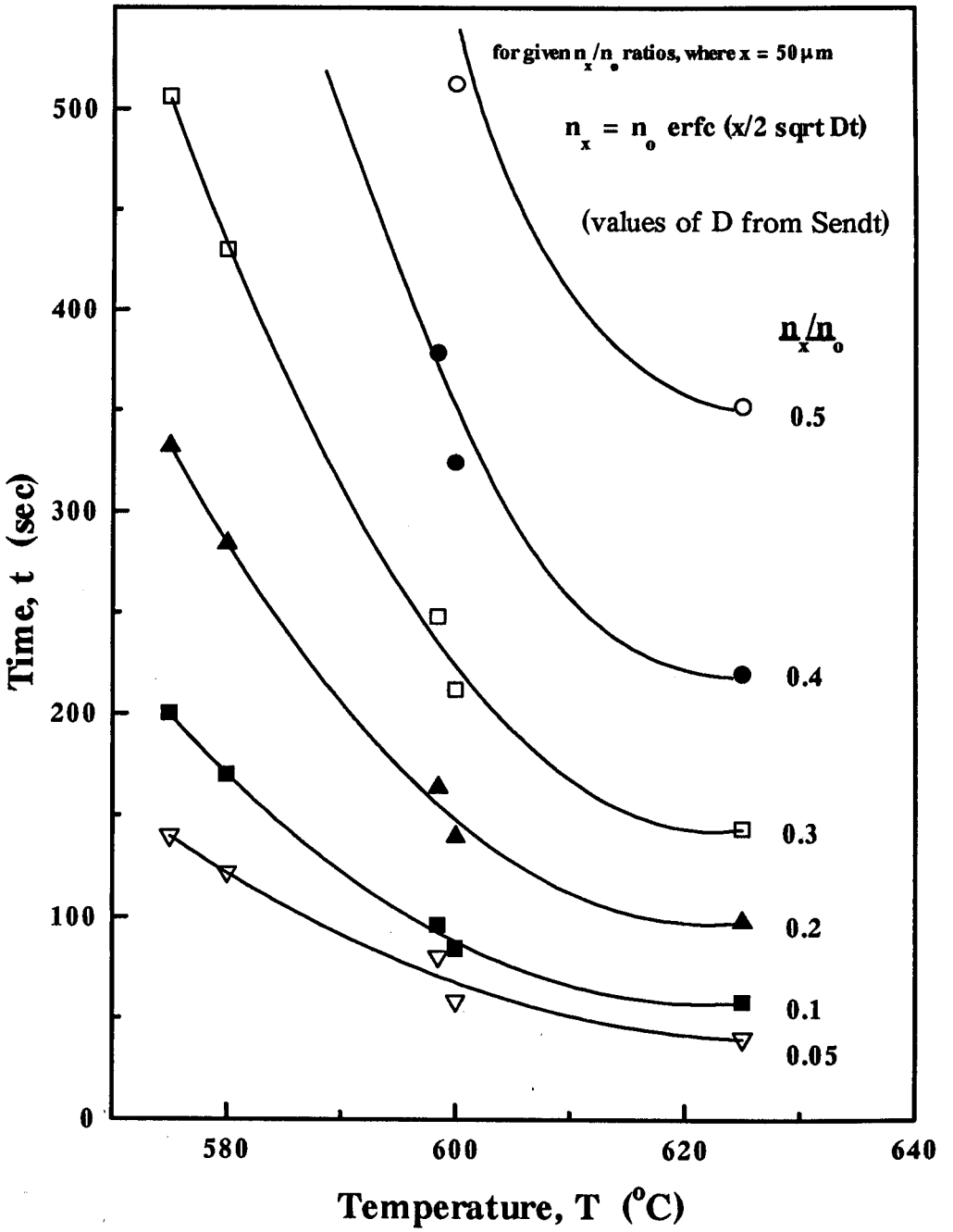

Figure 6.13 Time-temperature plot for a 50 μm layer (after Sendt[145])

A selected number of samples have been analysed by dynamic SIMS to establish the Li profile and the results are presented in Figure 6.14(a)-(h). Each plot shows the raw data and the same data set normalised to the Si signal plotted against depth.

TABLE 6.24
SUMMARY OF SIMS DEPTH PROFILE ANALYSIS

Sample no	Rockware glass R4795/10	Relative Li content at the surface	Decay rate of signal (μm/decade)
1	**As drawn rod**	< 0.0004	-
2	**LiBr vapour treated for 40 min**	0.06	51
3	**LiBr vapour treated for 60 min**	0.60	54
4	**$AlBr_3$ vapour treated for 20 min**	0.02	79
5	**$AlBr_3$ vapour treated for 20 min + LiBr vapour treated for 60 min**	~ 0.10	87

In interpreting the data there is a problem in defining the edge of the sample, especially in the normalised data set. This problem is caused by the fact that the samples were insulating and so the analysed area is not as well defined as would be the case if the samples were metallic. The best definition of the edge (as indicated in the relevant Figures) was established to be the point where the Si signal reaches 50 % of its maximum

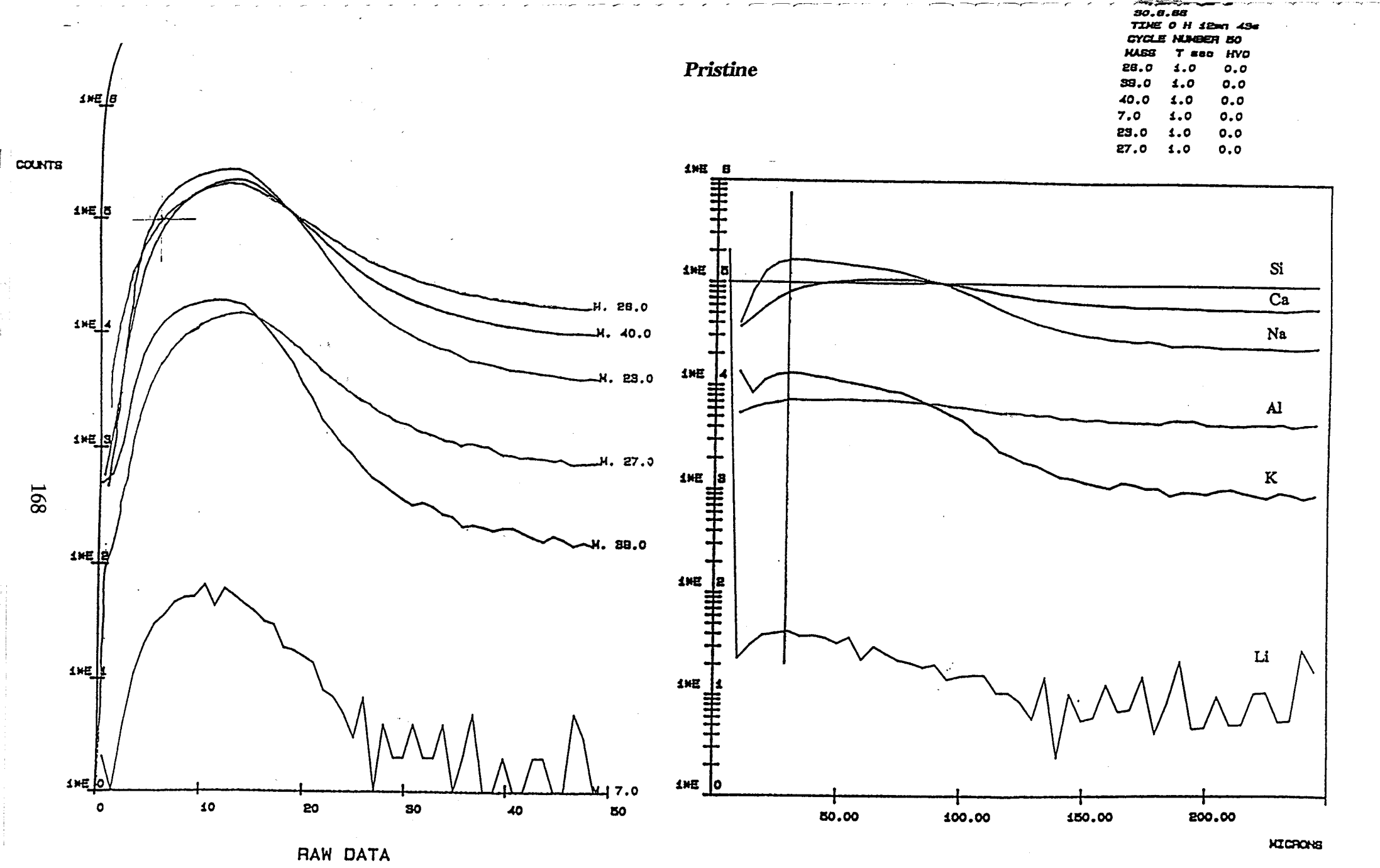

Figure 6.14(a) SIMS depth profile for as drawn Rockware R4795/10 glass (Sample 1)

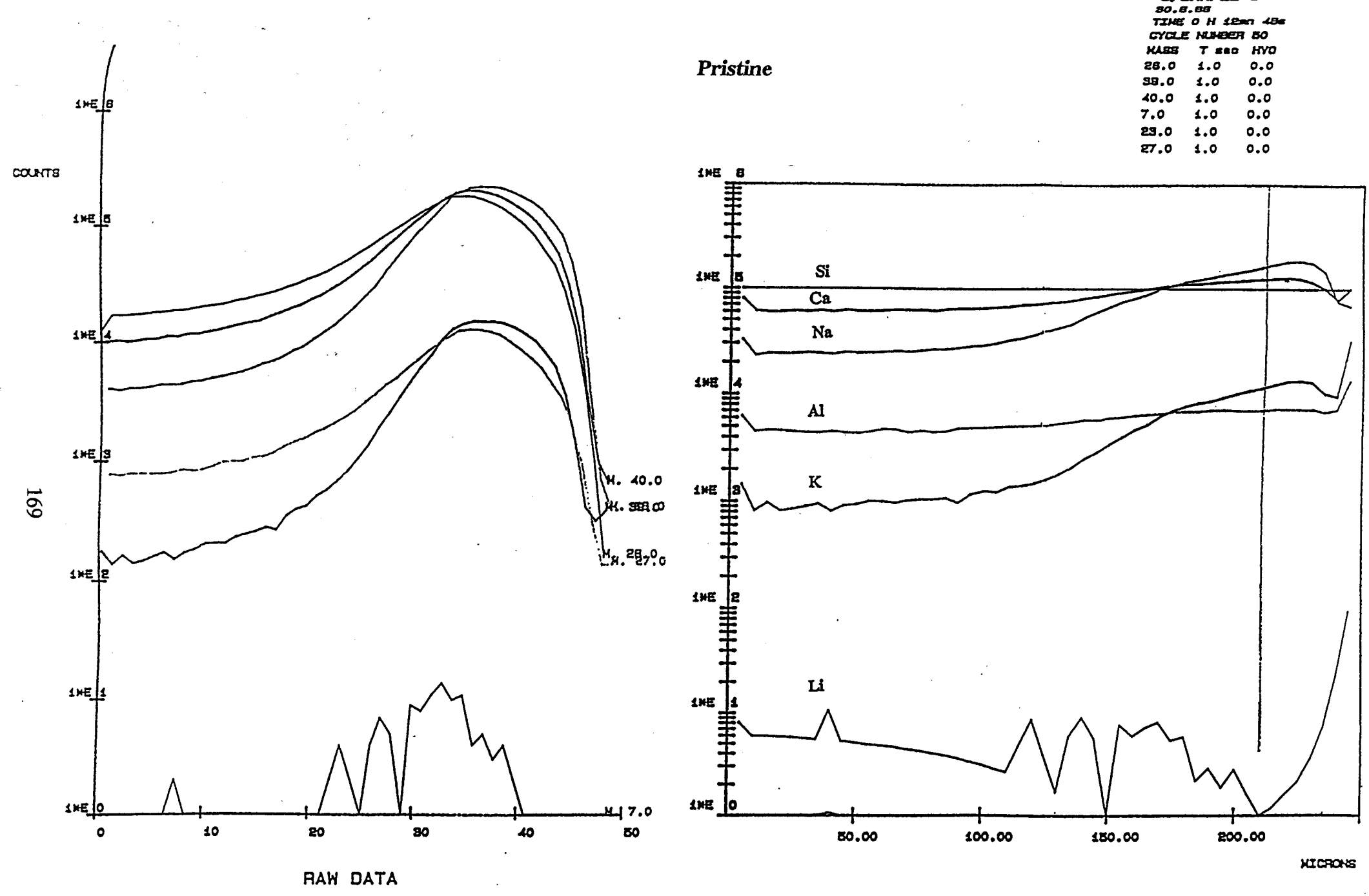

Figure 6.14(b) SIMS depth profile for as drawn Rockware R4795/10 glass (Sample 1)

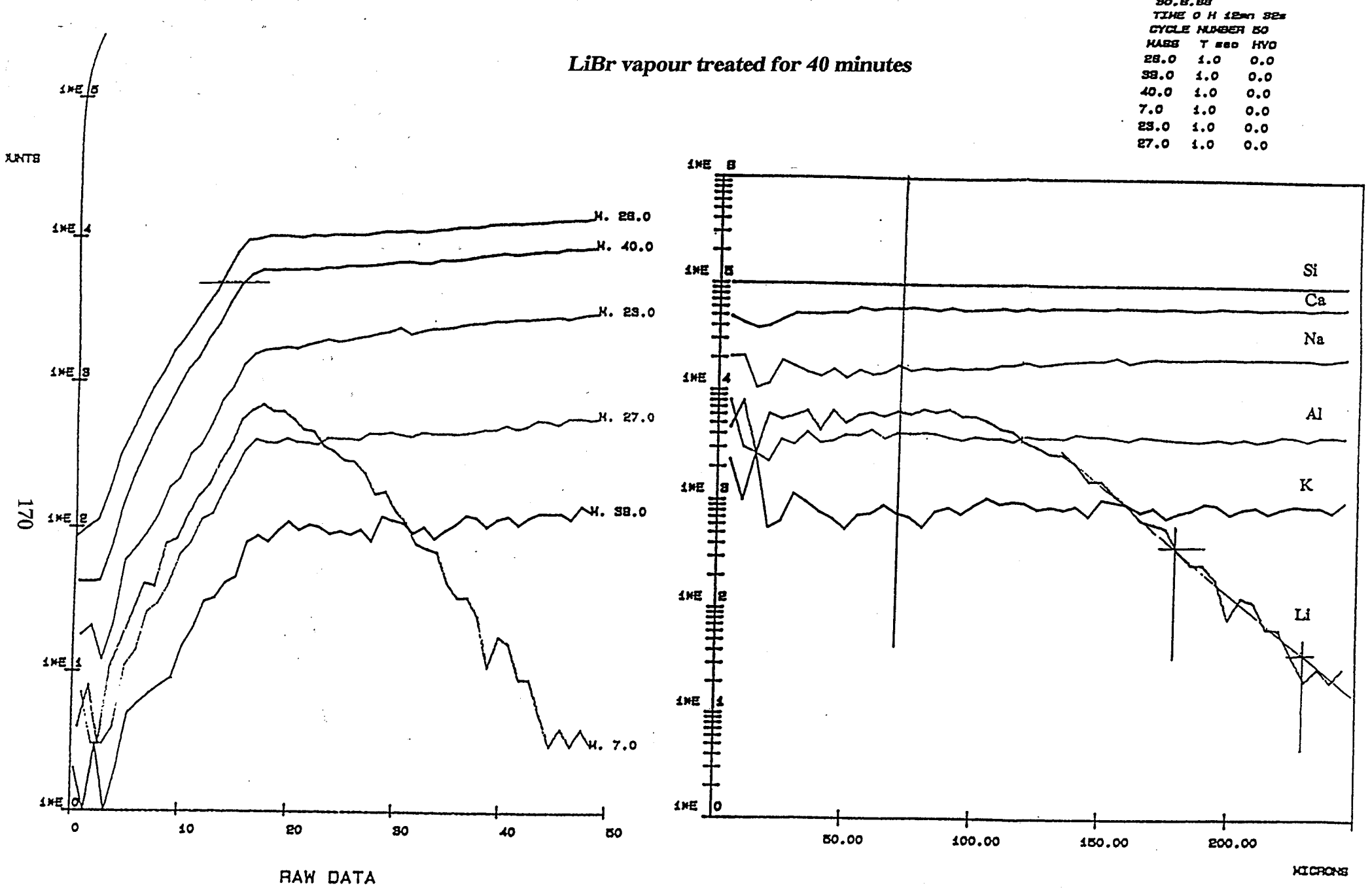

Figure 6.14(c) SIMS depth profile for Rockware R4795/10 glass treated by LiBr vapour for 40 minutes (Sample 2)

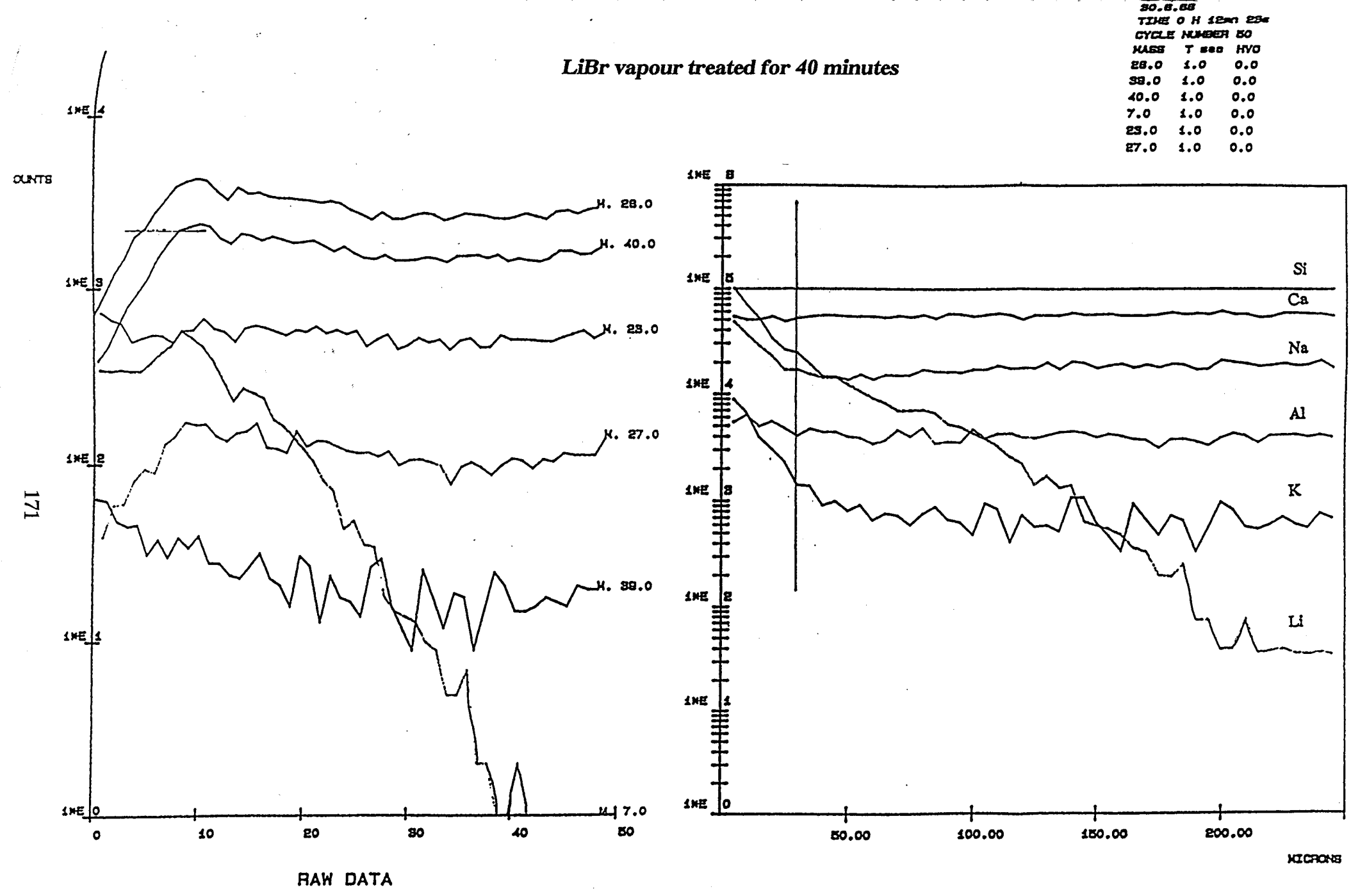

171

Figure 6.14(d) SIMS depth profile for Rockware R4795/10 glass treated by LiBr vapour for 40 minutes (Sample 2)

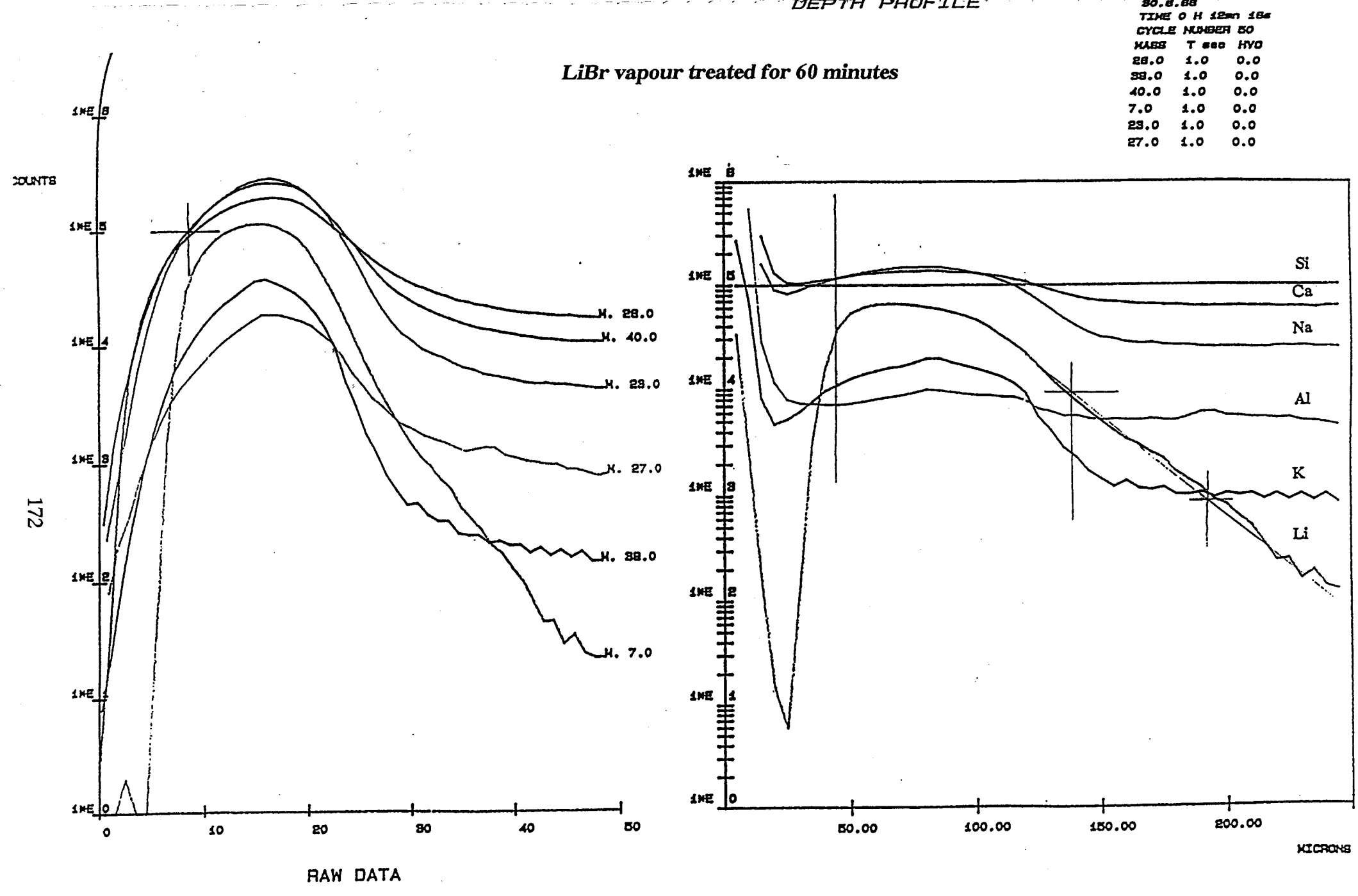

Figure 6.14(e) SIMS depth profile for Rockware R4795/10 glass treated by LiBr vapour for 60 minutes (Sample 3)

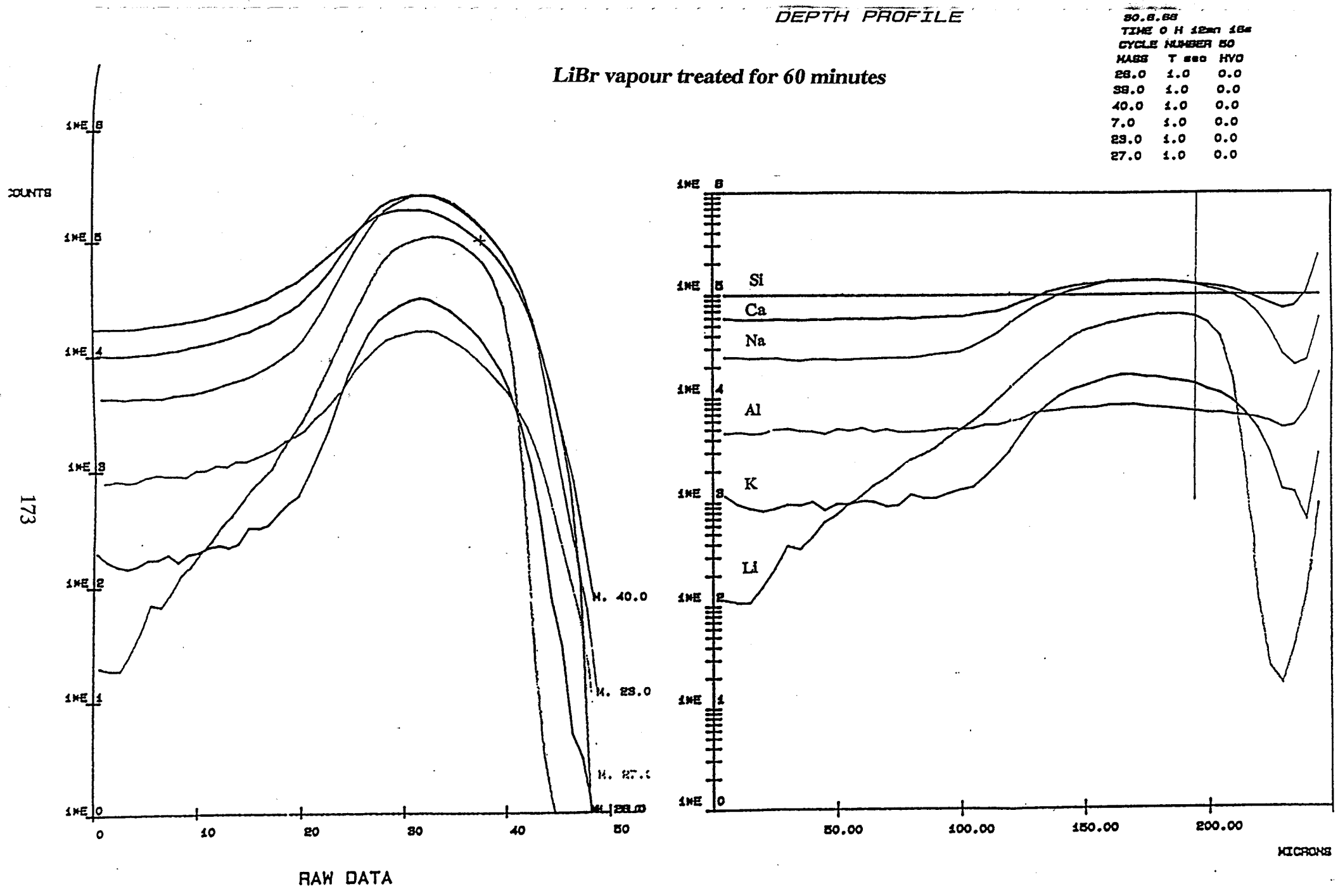

Figure 6.14(f) SIMS depth profile for Rockware R4795/10 glass treated by LiBr vapour for 60 minutes (Sample 3)

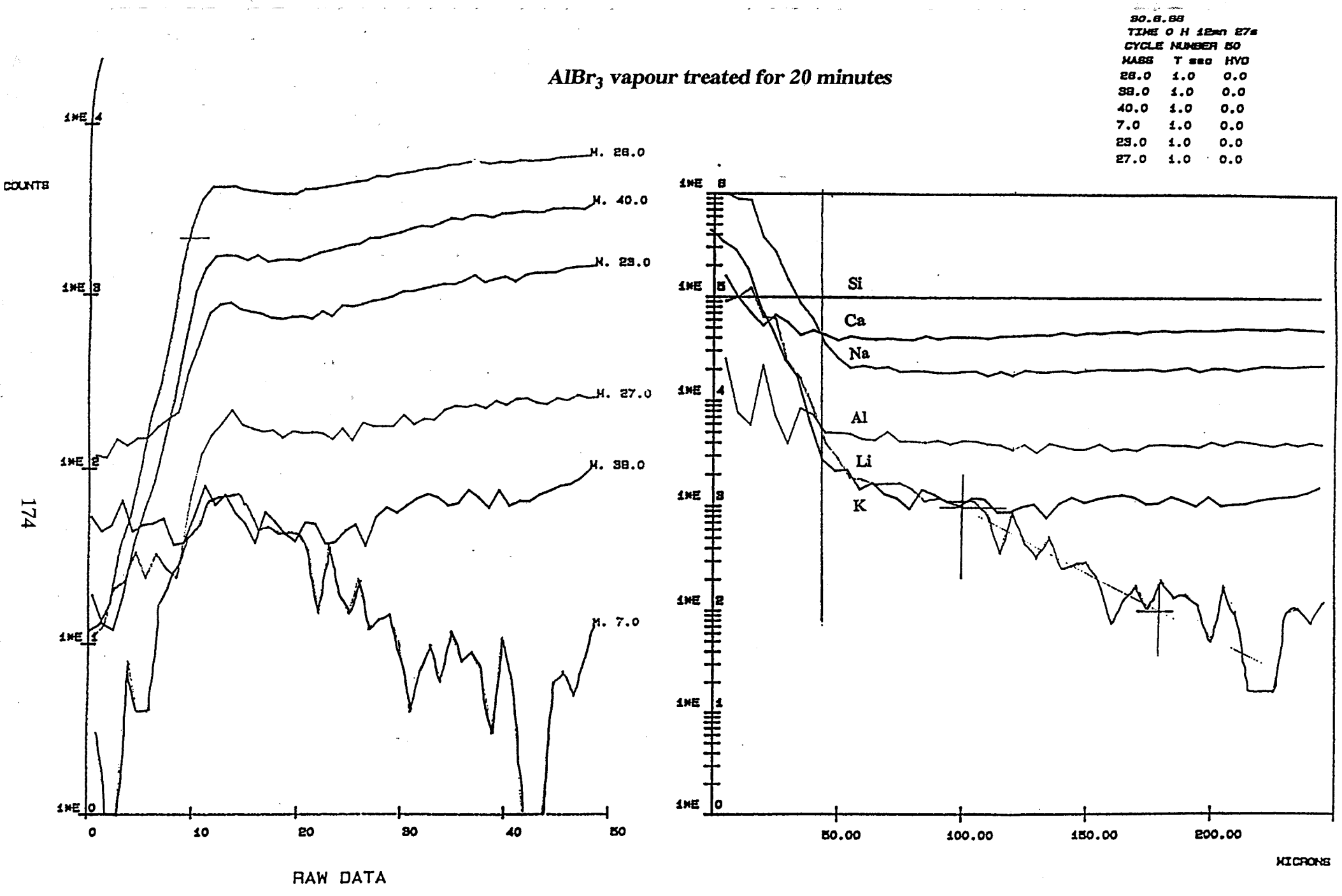

Figure 6.14(g) SIMS depth profile for Rockware R4795/10 glass treated by $AlBr_3$ vapour for 20 minutes (Sample 4)

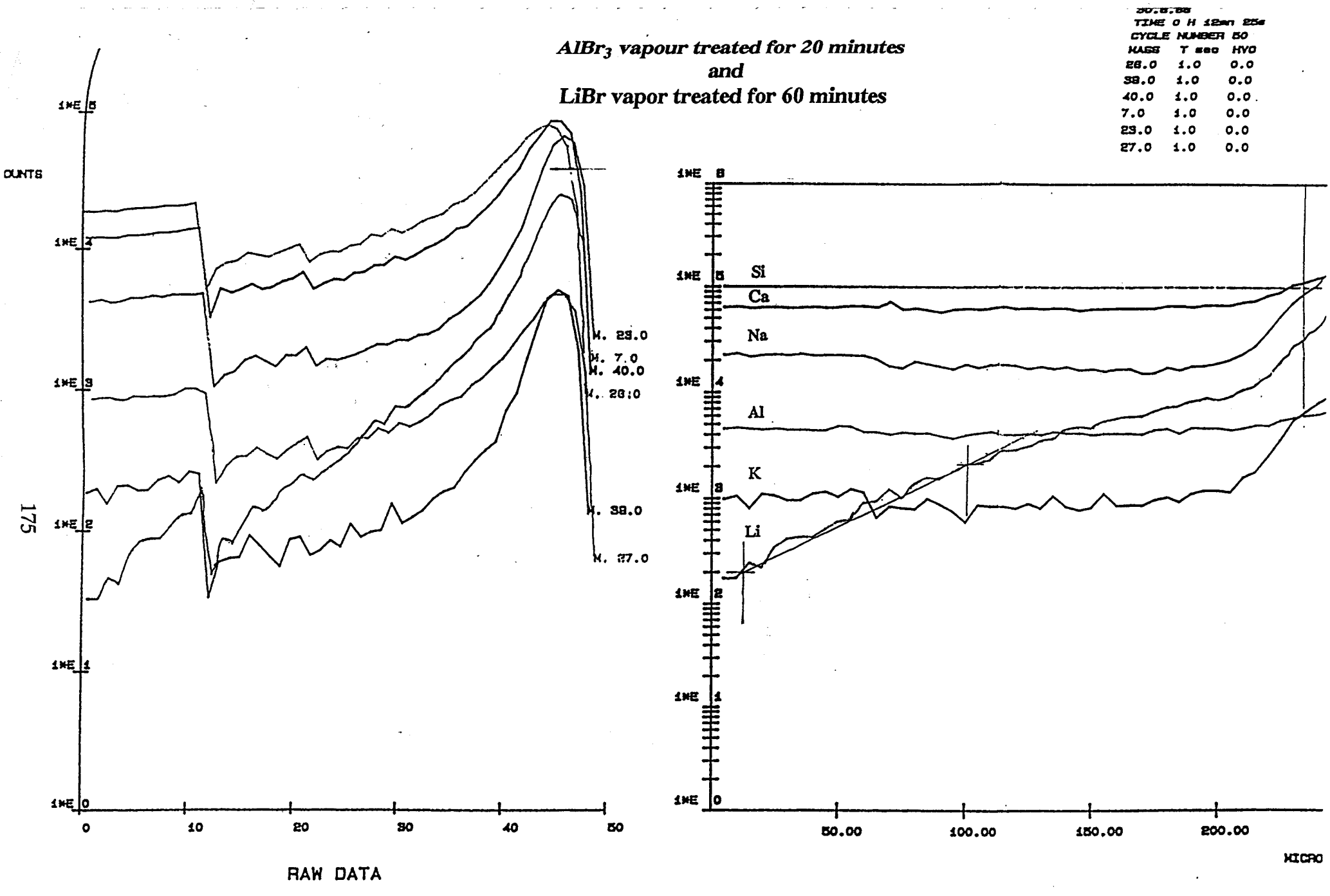

Figure 6.14(h) SIMS depth profile for Rockware R4795/10 glass treated by $AlBr_3$ and LiBr vapour (Sample 5)

value in the raw data profile. This criterion was applied to all the samples and this point has been marked on each normalised plot. The procedure shows the position of the surface to agree to within 10 μm between pairs of analyses carried out on each sample.

In the normalised plots, the relative levels of all the major elements monitored were consistent with the bulk levels. It is not possible to derive absolute concentrations from these profiles but only changes in the relative levels of specific elements between samples. The most noticeable differences that can be seen are in the Li content. Hence two parameters can be determined: (a) the relative concentration of the surface levels between the samples and (b) the decay rate of the Li signal with depth. The results of these analyses are summarised in Table 6.24.

The plots for the alumina modified Rockware R4795/10 glass rod, treated with LiBr vapour for 40 and 60 minutes respectively (samples 2 and 3) show the same decay rate despite different surface concentrations. The observed decay rate for the glass rod treated with $AlBr_3$ vapour and that with a follow-up LiBr treatment are also similar in both plots. However, the decay rate is, in this case, significantly different from those observed for Samples 2 and 3. Samples 2 and 5 show similar surface Li concentrations but markedly different diffusion parameters, suggesting different processing conditions. It is evident that the diffusivity of Li is modified by the prior presence of Al.

The analysis demonstrates that SIMS can usefully be used to understand the behaviour of Li in the ion exchange process in these glasses but there is scope for improvement in the experimental method. It would be advantageous, in any future analysis, to mount the samples in a conducting matrix for analysis so that the edge effect problem was not encountered.

6.8 GENERAL DISCUSSION AND CONCLUSIONS

Wide ranging methods, some of which are inter-related, have been successfully developed to strengthen container and related glasses. Several mechanisms, as discussed below, contributed to the strengthening effect observed.

In the case of two container glasses (Glass 1 and Glass 2 - one basically of high lime content and the other with MgO partially substituting CaO) with only 2 mole % CuO added, the strengthening arises from the precipitation of a blue translucent material containing tenorite crystals on the surface. The strengthening mechanism here relies on the effect of low solubility particles, which were dispersed in a glassy matrix in diverting or stopping cracks propagating through the material. Here, copper is sufficiently mobile in silicate glasses to cause the precipitation phenomenon and is better than those caused by alkali ions[147-149]. The effects of copper are complicated by its multivalent state (Cu^0, Cu^+ or Cu^{2+}), for Cu^+ acts like Na^+ and Cu^{2+} like Mg^+. This precipitation process, to some extent, is analogous to that observed by Stookey[150], who obtained colloidal metallic particles of Au and Ag precipitated by UV photochemical reduction of a glass containing a readily available source of electrons in Ce^{3+}. In the present work however the crystals are tenorite i.e. CuO and not metallic copper. One explanation is that metallic nuclei of copper, formed on the surface by the heat treatment, act as heterogeneous nuclei for crystallisation of tenorite on reoxidation in air. As evidenced by the XRD results, the improvement in the cross-breaking strength is assisted by the presence of extremely fine nanometer sized (~ 400 Å) crystallites in the abraded and heat treated sample of controlled flaw density. In comparison, samples heat treated but without any abrasion and having larger crystallites (~ 435 Å) showed proportionally less improvement in strength (Table 6.4). Although the samples were heat treated at temperatures which appeared to be slightly higher than T_s determined by the DTA there was no evidence of any sample deformation.

It is suggested that the presence and/or initial growth of tenorite crystals increased the viscosity of the surface structure and thereby prevented deformation whilst holding at temperature where surface flow may be expected.

Although heat treatment alone produced a modest strength increase (~ 27 %), promotion of surface crystallisation in these glasses was further assisted by abrasion of the surface, creating a uniform as well as high density of nucleation sites in a controlled manner. This observation is consistent with the literature data for zinc aluminosilicate glasses except that the 'airabrasion' technique developed in the present work was found to be more effective than those reported. It is significant that the strength also markedly improved to ~ 65 % over the pristine value.

Measurement of viscosity of the two glasses indicated that the T-η characteristics may be sufficiently close to those of industrial soda lime silica glass to allow the use of these in high speed production methods. However, as revealed by the DTA, the presence of the crystallisation peak of parawollastonite at higher temperature of 860 °C, means that it would be necessary to cool rapidly through this range to prevent troublesome devitrification of any undesirable phase.

The main strengthening mechanism involved in the vapour and associated treatments below the transformation temperature, T_g, is based on the development of a lithium rich outer shell, brought about by the diffusion of Li^+ ions from a metal vapour source. This places the surface of the glass skin in compression as a result of the differential thermal expansion between the glass skin and higher TCE glass interior. Since the stronger bond of Li^+ in glass is generally considered to result in a smaller coordination[82,151] compared to that of Na^+ ions[152], it is supposed that more Li^+ ions could diffuse into the glass surface than Na ions diffuse out and a lower coordination would be reached. The excess positive charge introduced this way could be compensated by $[AlO_4]^-$ anionic groups present on the surface of glass. Although not detected by XRD, in all cases

of vapour treatment investigated, a resulting surface crystallisation of low TCE phases such as β-eucryptite and/or β-spodumene is possible.

Using LiBr vapour only, a significant cross-breaking strength of ~ 400 MPa (104 %) has been achieved with comparable values for $AlBr_3$ (93 %) and a combined $AlBr_3$ and LiBr treatment (119 %), the correlation between flexural strength and treatment time being unity. The exact mechanism responsible for such a marked strength increase for the latter examples involving $AlBr_3$ vapour is not entirely clear although the explanation given above at least, in part, should be valid. The data from dynamic SIMS indicated different diffusion parameters involved for lithium and aluminium and it has been shown that prior presence of aluminium modifies the diffusivity of lithium. This is reflected in the marked overall strength increase of ~ 400MPa for the Rockware glass vapour treated by $AlBr_3$ and LiBr, exhibiting a maxima in the MOR-time relation. On the other hand, for single mode treatment (LiBr or $AlBr_3$ vapour) the correlation is linear and is attributed to the separate diffusion process.

The mechanism associated with the CVD involved primarily heterogeneous reaction and deposition of metal halide vapours at the heated glass surface. In this way, P_2O_5 and TiO_2 were successfully introduced to assist in nucleation and subsequent surface crystallisation of the glasses investigated. The results show that, in all cases including those combined with vapour treatments, it is the TiO_2 and/or P_2O_5 doping that was, at least in part, responsible for the significant strength enhancement (23-120 %) observed without any loss of transparency. However, it proved to be difficult to find meaningful explanation(s) to ascertain the exact role these catalysts play. For example, it is observed that TiO_2 gave a 58 % increase in strength in simple Float and NLS 1 glasses whereas P_2O_5 produced none. On the other hand, for commercial Rockware R4795 and RAM 4795, TiO_2 produced no discernible increase in strength. One possible explanation may lie in the marked compositional difference between these glasses. These have similar SiO_2

content but the Float contains high alkali R_2O (15 wt % Na_2O), similar RO (6 wt % CaO and MgO, each) and low R_2O_3 (2.5 wt % Al_2O_3) compared to Rockware series containing R_2O (~ 11 wt % Na_2O), RO (~ 11 wt % CaO) and R_2O_3 (1.17-10.15 wt % Al_2O_3). As a result, the local network structure of the latter glasses is thought to be less 'open' since viscosity-temperature profile indicates high annealing points (η = 13) of 571 and 610 °C compared to 536 and 549 °C for the Float and NLS 1. Thus the kinetic barrier for the nucleation step for Ti^{4+} ions may be lowered in the Float and NLS 1 glasses resulting in the detectable growth of surface crystals at the *drive-in* temperature. In addition, the nucleating agent TiO_2 might function as a surface active agent by reducing the interfacial free energy between the crystal and the amorphous matrix. Interestingly, simultaneous CVD doping of P_2O_5 and TiO_2 resulted in both surface crystallisation and upto 48 % strength increase in these glasses. It is suggested that the discrete TiO_2 particles would still be able to diffuse despite being dispersed in a glassy P_2O_5 coating which may otherwise inhibit the efficiency of the *drive-in* process as may have been the case when P_2O_5 was used alone.

In combination treatments i.e. CVD doping plus vapour, the role of high alumina content in the bulk, although producing an additional 18 % strength increase over that achievable by LiBr vapour treatment only, is not clear. It is postulated that this supplied additional ionic groups such as $[AlO_4]^-$, $[AlO_5]^{2-}$ or $[AlO_6]^{3-}$ on the surface which in the presence of an effective catalyst such as TiO_2 enhanced nucleation for any lithium aluminosilicate phase. However, the presence of P_2O_5 along with the TiO_2 produced lower strength, probably as a result of the reactivity of P^{5+} ions with Li^+ ions, thus depleting the surface of the lithium ions necessary to form a low TCE glass skin.

The mechanism for the strengthening effect observed in the ion-exchanged Rockware industrial glasses is very similar to that of vapour treatments. However, in this case, the kinetics of the process are accelerated in that the exchange between Na^+ and Li^+

ion is very effective particularly at the experimental temperatures marginally higher than T_g. Here, Li diffusion into the glassy network becomes easy and a compressive stress is induced upon cooling due to the lower thermal expansion coefficient of the Li rich glass layer compared to the interior of the glass. The excess alumina content in the glass enhanced the tendency to produce the low TCE β-eucryptite and/or β-spodumene on the surface. The ion-exchangeability is also enhanced by the effect of the high annealing (η = 13) and strain (η = 14.5) points of these glasses (see Tables 6.17) arising primarily from the increased Al_2O_3 content in the glass structure. Ion exchange above these points is particularly significant, since at a temperature below the strain point of the glass, the exchange of smaller Li ions for larger Na or K ions can establish a tensile stress resulting in minute cracks and checks. This potential problem for subsequent breakage is prevented in the present process provided the temperature is maintained above the strain point. Also, as a result of the displacement of Na_2O or K_2O by Li_2O (in terms of weight), the thermal expansion coefficient of the portion of the glass in which such exchange has occurred will be less than its original value and therefore less than that of the glass still untreated. Since the exchange process is progressive in nature and moves inwards from the surface, the glass body is provided with a surface layer having a lower thermal expansion coefficient than the interior. This argument, in terms of probable cause of the high level of strengthening achieved, is complimentary to that described earlier where further lowering of the thermal expansion coefficient occurred as a result of the formation, on the surface, of finely divided crystals of β-eucryptite and/or β-spodumene. The nature of the anion in the lithium salt also influenced this process. As described earlier, the presence and nature of Cl^-, or SO_4^{2-} anion additive in the halide salt baths used in the present work was shown to have a major influence on the transparency of the glass arising from the reactivity of glass surface with the salt. It is suggested that the radius of Cl^- ions electrolysed from the salt is smaller than SO_4^{2-} ions ($r\ Cl^-$ 181 pm < $r\ S^{2-}$ 184 pm < $r\ SO_4^{2-}$ 230 pm). Therefore

the polarisation ability of the Cl^- ions is the largest and, as a result, they will readily react with the glass surface in a molten salt bath at high temperature. Thus exchange in LiCl produced, as evidenced by XRD, reaction products, whilst it is quite important to stress here that glass treated in sulphate bath remained transparent. The alternative explanation of non-reactivity of sulphate ion may simply be due to the presence of more undissociated S^{6+}-O^{2-} rather than S^{2-} bond of the SO_4^{2-} group which would have penetrated in the glass.

The excellent transparency achieved for strengthened glasses either by vapour and related treatments or ion exchange can be explained from the consideration of light scattering ability or Rayleigh scattering[153,154] of the particulate phase involved. Referring to the experimental evidence from the XRD line broadening measurement of the surface crystallised phase, the size of the dispersed crystallites is sufficiently small (235-380 Å) to produce no effective scattering in the visible spectrum. There may also be optical isotropy involving a close match of the refractive index between the crystals and the glass coupled with small birefringence within the small crystals.

Although the distribution of compressive stress has not been determined experimentally, it is clear from the results that a surface crystallised layer of 20-70 μm can be successfully produced for only 10-120 second treatment with surface deformation beginning to be apparent only after 30 second (i.e. producing a 40 μm layer without deformation or any loss of transparency). This upper limit should permit the use of such a process for single service containers where the depth of abrasion is approximately 6-7 μm and therefore a 12-15 μm depth of compressive layer should easily cover such an abrasion. For the returnable containers, a 40-50 μm layer may also be adequate although only measurement of the actual level of compressive stress can properly establish this criterion. Furthermore, it is also evident that the economic benefits of the present method is attractive, particularly when compared to the widely used Na-K exchange process requiring longer time of about 20-30 hours to obtain a compressive layer of 50-60 μm.

The observed linear relationship between the duration of ion exchange and the thickness of β-eucryptite and/or β-spodumene layer is comparable to that found in normal ion exchange strengthening where the generation of compressive stress is directly proportional to the volume of ion exchange, which is directly proportional to the square root of treatment time. In the present work however, the volume of ion exchange is less important than the availability of mainly Al species on the surface, considered essential for the crystallisation of the low TCE phase. The Al content is provided by, in this case, bulk compositional change and clearly the economic constraint may arise from the cost of excess alumina addition (10 wt %) to container glass specification. However, the results in the present work also shows that the low TCE phase can indeed be produced for even lower (~ 3-5 wt %) alumina content thus making the process economically viable.

The structural information derived from the phase analysis for the surface crystallised alumina modified glass indicates that the arrangement of silica tetrahedra around the hexagonal axes of the β-eucryptite is such that one crystal direction expands whilst the other contracts. It is evident that the lattice parameter, *a* increases whereas *c* decreases as the duration of ion exchange is extended (see Table 5.5). A behaviour of this type has been previously observed for β-quartz and keatite or their stuffed derivatives and is related to the low thermal characteristics of the material[155].

Chapter 7

FIELD TRIALS

7.1 INTRODUCTION

A description of the very limited field trials and their results has been included in this Chapter. Although more comprehensive trials are desirable, this could not be achieved due to lack of time. However the results given below are expected to be useful in the event of any commercialisation of the methods developed in the present work.

7.2 IPGR MELTING STUDIES

A feasibility study of some of the glasses investigated by the author as a part of the overall IPGR programme (see Chapter 1) has been carried out by the GPD Laboratory Services of ACI, on a laboratory scale, to asses their melting properties, forming properties, refractory corrosiveness and physical properties.

7.2.1 RAW MATERIALS AND COMPOSITION

The compositions of the raw materials used are shown in Figure 7.1. They were of normal commercial glass/ceramic quality. For the purpose of calculation, the iron oxide has been included in the alumina, the potassia with soda and magnesia with the calcia.

Table 7.2 lists the glass and batch compositions. The reference glass used was a typical ACI flint composition containing slag saltcakes at levels typical of those used within ACI. Two glasses, namely NLS 7 and NCS 10 (see Table 3.1) were selected for this study. These glasses did not contain slag but saltcake was added at a level of 12 parts/1000 parts of sand.

7.2.2 MELTING

7.2.2.1 MELTING IN PLATINUM CRUCIBLE

Each batch of 150 g total weight was melted in a pure platinum crucible in an electric furnace at 1450 °C for periods of 1, 1.5 and 2 hours (selected batches only) followed by annealing. The glass for study was then drilled out using a diamond core drill. A description of each glass melted is shown in Table 7.3.

7.2.2.2 MELTING IN SILLIMANITE CRUCIBLE

Seven batches, each of 750 g of total weight, were melted in sillimanite crucibles (approximately 170 mm height and 900 ml brimful capacity) in a gas fired furnace at 1450 °C for 4 hours. The glasses were then poured into steel trays and annealed. A description of the glasses and that melting and pouring characteristics are shown in Table 7.3.

7.2.3 DISCUSSION AND CONCLUSION

As expected, the melting and other characteristics of the reference flint glass conformed to those normal to the industrial practice. For this reason, this glass also served as a reference point for other melts.

The melting characteristics of NLS 7 glass were found to be similar to those of the reference glass. In practice, however, it is thought that the lack of alumina may cause durability problems.

The glass NCS 10 showed very low viscosity and a tendency to devitrify. Attack on the refractory crucible was also observed. These factors, when taken into account in combination, would present problems during manufacture. If lowering the temperature to increase the viscosity and reduce refractory corrosion is employed, it would be likely to increase the possibility of devitrification. Wollastonite crystals were also observed in the glass melted in sillimanite.

The results on two other separate high alumina glasses showed that the very high alumina glasses (~ 8-12 wt %) are not as difficult to melt as was anticipated. Even when the major source of alumina was calcined alumina, the glass appeared to be only a little more viscous than the currently melted container glasses. This is an interesting observation since a number of high alumina glasses, investigated in the present work, showed very high flexural strength.

7.3 FRACTURE TEST OF GLASS CONTAINERS

The glass containers, in the form of milk bottles, were supplied by Rockware in an untitanised form. The bottles were electrostatically sprayed with ternary sulphate salt mixture. Some of these were given heat treatment at 550 °C for 1 hour. They were then subjected to a 'drop test' and, in some cases, to a 'burst test'. The empirical nature of the tests and the fact that they were not comprehensive means that the results should be considered only as a guide.

The drop test involved releasing the coated and sellotaped empty bottle from a fixed distance and allowing it to fracture on impact. Normal burst tests were carried out by Rockware which used a standard burst pressure.

TABLE 7.1
RAW MATERIAL COMPOSITIONS

Raw Material (wt %)	SiO_2	TiO_2	Al_2O_3	(Fe_2O_3)	Na_2O K_2O	CaO	MgO
Sand (dry)	99.6	0.1	0.1	0.02	-	-	-
Soda ash	-		-	-	58.0	-	-
Saltcake	-	-	-	-	43.6	-	-
Limestone	0.6	0.1	0.4	0.12	0.1	54.9	0.4
Calcined alumina	-	-	98.5	-	0.4	-	-
Feldspar	67.3	-	21.1	0.09	10.5	2.0	-
Slag	36.3	0.4	13.7	0.12	0.5	40.5	7.4

TABLE 7.2
GLASS AND BATCH COMPOSITIONS

Glass (wt %)	Reference	NLS 7	NCS 10
SiO_2	73.6	70.0	58.0
Al_2O_3	1.5	-	-
Na_2O	13.7	15	14
CaO	11.2	15	28
Fe_2O_3	0.04	0.05	0.07
Batch (100 g Total mol wt)			
Sand	717.3	701.2	579.3
Soda ash	229.0	251.2	235.3
Saltcake	8.6	8.4	7.0
Limestone	165.3	271.2	506.3
Calcined alumina	7.8	-	-
Slag	43	-	-

TABLE 7.3
GLASS MELTING AND POURING CHARACTERISTICS

Melting time in Platinum crucible at 1450 °C	**Reference Flint**	**NLS 7**	**NCS 10**
1 hour	Batch free Seedy Clear surface Flint colour	Batch free Seedy Clear surface Flint colour	Batch free Seed free Clear surface Flint colour Wollastonite inclusions on top and bottom surfaces (0.2 mm) Some devitrite on bottom Some surface silica
1.5 hours	Few seeds Clear surface Flint colour	Few seeds Clear surface Flint colour	Seed free Clear surface Flint colour Wollastonite inclusions on bottom surface after > 1 h Also some surface silica
2 hours	Seed free Flint colour	Few seeds Flint colour	Seed free Flint colour Many Wollastonite inclusions on bottom surfaces-large increase over 1-1.5 h Also some devitrite
Melting time in sillimanite crucible at 1450 °C	No foam during melting No attack on crucible No scum on surface	Not melted	No foam during melting Severe attack on refractory 3 mm flux line No scum on surface
Pouring characteristics	Glass poured normally Flint colour Very seedy		Glass poured like water Flint colour Seedy Wollastonite inclusions in glass

Although interpretation of the fracture surface proved to be difficult, the general features can be summarised as follows: (a) several radial cracks were observed originating from a number of points in the internal surface, particularly high above the base. These points were located at some distance from the point of impact at the base suggesting perhaps that there is a differential strengthening, with the base being strengthened the most. (b) burst tests showed a characteristic, fan shaped array of cracks with evidence of a few axial cracks. The fracture strength was considered to be higher-than-normal, indicating that some strengthening has occurred.

Chapter 8

OVERVIEW

The primary aim of this work, to strengthen container glassware, has been achieved by a number of differing methods, which were used either singly or in combination, as follows:

1. Surface crystallisation
2. Vapour treatment
3. Chemical vapour deposition (CVD)
4. Ion exchange

Various methods have been employed in the production of a surface crystalline layer which was designed to introduce a compressive stress into the glass surface. The results from one of these methods showed that it is possible to achieve surface crystallisation, accompanied by a modest increase in strength, by introducing a sparingly soluble species in the glass composition which can be precipitated out at the surface on subsequent heat treatment. This was demonstrated by the precipitation of a low solubility component, tenorite CuO, from a glass composition (Glass 2). This was related to container glass but with higher CaO and Al_2O_3, and surface crystallisation of CuO produced a MOR of ~ 300 MPa. This compares with ~ 200 MPa for the pristine strength. However, abrasion was necessary to produce the required nucleation density. Of all the

methods attempted, airabrasion proved to be the most effective in promoting a surface of highly dense nucleation sites most favourable for surface crystallisation to be induced.

It was found that surface crystallisation can also be induced by destabilising the glass by making quite large compositional changes. Examination of the devitrification behaviour of a number of soda lime silica glass compositions (NLS series) showed that several surface crystallisable glasses can be produced with viscosity characteristics similar to those of container glass. A majority of the compositions, without any nucleating agent added to the glass, exhibited significant crystallisation (50-500 μm layer thickness) without deformation or loss of transparency. The crystal phases identified, following heat treatment at 750-800 °C for a period of 1-2 hours were largely NC_3S_6, NC_2S_3 and β-CS. This process of surface crystallisation was further facilitated by a small additions of TiO_2, SnO_2 and P_2O_5; P_2O_5 addition of as little as 0.1 mole % was found to be the most effective. However, it is concluded that for P_2O_5 contents of more than 1 %, the increased growth rate would be compromised by an increased induction period for nucleation, further adding to the difficulty of maintaining a viscosity-temperature relationship suitable for forming operations. Although the crystal phases obtained, such as devitrite, cristobalite or tridymite are not known to produce a surface compressive layer, the use of such destabilised compositions may be possible in the surface crystallisation of low TCE phases, whilst still maintaining the desirable visual properties of the container glass and also retaining the forming characteristics.

The crystallisation behaviour of a series of soda lime silica glass compositions (NCS) with viscosity characteristics not necessarily conforming to those of container glasses showed that heat treatment at 600-1000 °C for a period upto 20 hours produced mostly bulk crystallisation, and surface crystallisation was restricted to only two compositions with noticeable deformation and loss of transparency.

The problem of maintaining transparency whilst inducing the crystallisation of suitable TCE phases led to consideration of the possibility of altering the surface composition only, by post- or mid-forming technique. This was achieved by LiBr vapour treatment which relied on diffusion of Li and Al from gas phase sources of LiBr and $AlBr_3$ into the glass, this being Float, soda-lime-silica glass (NLS 1) without any other added constituent and Rockware container glass as received or with additional Al_2O_3 added to the bulk. For all the glasses investigated for LiBr vapour exposure, overall percentile strength enhancements of 33-104 % were recorded. In particular, using only LiBr vapour treatment for 40 minutes at 585 °C, strengths of ~ 400 MPa were recorded for both the base and the alumina modified glasses, with no appreciable reduction in strength on follow-up heat treatments. Proportionally lower increases were obtained for shorter times. When the glasses were exposed to $AlBr_3$ vapour alone, strength increases of 49-95 % were obtained, with a maximum MOR value of 355 MPa being achieved for only a 30 minute treatment at 550 °C, again with no discernible decrease in strength on a follow-up heat treatment. Significantly, a combination of the two processes is highly effective in improving strength, giving a much higher level of over 400 MPa (119 %) if a 30 minutes $AlBr_3$ treatment is followed by a 10 minute LiBr vapour exposure. This suggests the importance of the presence of Al in the glass. The level of transparency following the treatments in all these glasses was generally excellent. It is concluded that it is possible to introduce either treatment at the hot or cold end of the forming operation. The time of treatment can be reduced significantly without sacrificing the strength enhancement if the process begins at the hot end immediately after the article leaves the mould on its travel to the annealing lehr. However, there still remains the question of the potential toxicity of gaseous LiBr. Although LiBr itself is not regarded as a dangerous chemical requiring special precautions, it may be possible that its decomposition products may present more serious hazards. Thermodynamic calculations suggests that such decomposition to give

solid Li_2O and Br_2 gas is likely only in an oxygen atmosphere and this becomes unfavourable if the temperature is increased to 1000 K.

Improvement of nucleation by CVD on container and other soda-lime silica glass compositions was examined for P_2O_5 and TiO_2. The initial problems were (a) achieving sufficient depth of diffusion and (b) producing crystallisation at a temperature sufficiently low to avoid deformation. This led to the formulation of a set of experiments where CVD was used to produce a surface chemistry suitable for the production of β-eucryptite or β-spodumene as the crystal phase. The surface chemistry was modified by surface doping of container glass with Li, Al and/or suitable nucleating agents, or by adjusting the container glass bulk composition so as to increase the Al content and also some Li in order that the "topping-up" process may be minimised. It is concluded from the former experiments, that P_2O_5 doping alone does not produce crystallisation but, when combined with TiO_2 followed by a "drive-in" heat treatment at 600 °C for 1 hour, it is highly effective in both promoting nucleation and crystallisation. There was a consequent increase in strength of 58 % over the pristine value without any deformation or loss of transparency. This process is limited only by the treatment temperature since deformation occurred above 600 °C for the glasses used. From the latter experiments, it was concluded that the strength enhancement of over 440 MPa (83-121 %) was dependent on prior doping of the glass with TiO_2 by CVD before being exposed to LiBr vapour since TiO_2 alone is ineffective for either base or alumina modified Rockware glass. It is also clear that the presence of added alumina in the modified container glass contributed an additional 21 % increase in strength over that obtained without TiO_2 but with LiBr vapour treatment only. However, when P_2O_5 was added as a second nucleating agent to TiO_2 prior to LiBr vapour exposure, no observable strength increase was noted for either glass. On the other hand, exposure to $AlBr_3$ resulted in a modest (36 %) increase in strength. However, a marked enhancement of an overall strength of over 400 MPa (121 %) was recorded if both $AlBr_3$ and LiBr

vapours were used consecutively. In all cases outlined, no sample deformation occurred and there was retention of full transparency and good surface finish. No evidence of β-eucryptite, β-spodumene or other crystal phase, detectable by XRD was found and thus the precise mechanism of the strength increase could not be established although reduction in surface TCE seems most likely.

It is concluded, from the results of the ion exchange strengthening using a molten salt bath route that surface composition changes, necessary for strengthening, can be achieved. Several baths have been assessed; those based on halides produced a problem with clouding of the glass surface but binary and ternary sulphate baths are capable of producing clear crystallised surface layers of β-eucryptite/β-spodumene solid solution. An increase in strength to over 500 MPa has been achieved for a 120 second treatment of rods of alumina enriched container glass. Overall, a level of strength enhancement from 16 to 163 % was achieved for treatment times from 10 to 120 seconds. A linear relationship between the surface crystallised layer and the MOR was observed. A uniform growth of the surface crystallised layer from 20 to 70 μm could be achieved for as low as 10 seconds to 120 seconds of treatment time in the sulphate bath for the glass with high alumina content. For glass with medium alumina content, a corresponding treatment time of 120 seconds produced a 10 μm surface crystallised layer. The flexural strength was found to be proportional to the depth of crystallised layer, which in turn was proportional to the square root of the duration of ion exchange. In addition, the dependence of strength increase was shown to be based on (a) alumina content of the glass, (b) temperature of treatment and (c) time of treatment. It appears therefore that a compromise of treatment time, alumina content and layer thickness has to be made to optimise the strength enhancement already achieved.

It is clear that significant increase in strength requires a higher alumina content in the surface. This can be achieved by a combination of (a) addition to the bulk composition

and (b) diffusion into the surface by CVD or vapour treatment or ion exchange. The required Li_2O content is easily achievable by diffusion or ion exchange. However, it should be appreciated that increased alumina content of the bulk has economic consequences, for the introduction of even 5 % alumina may increase the batch costs although this has to be set against the strength increase achieved and consequent reduction in container weight. For any practical application of these routes, it is therefore essential to minimise (a) and maximise (b).

In a comparison of the various methods investigated in this work, the vapour route for ion exchange appears to have advantages over the molten salt route, if a proper assessment of the toxicity related problems of the vapour route for lithium ion exchange can be made. Economic ways of optimising the alumina content of the glass surface which will give the best strengthening have also to be established. Any future scale up should involve two aspects, namely (a) provision of large scale vapour treatment facility and (b) use of an amenable source of lithium and aluminium. The arrangement can be introduced during annealing of the containers. However, the reaction enclosure should be capable of air or nitrogen operation and the choices of source should meet the criteria of their being able to provide reasonable partial pressure of the metal source at temperatures not exceeding the glass T_g; their being non-toxic; and if possible on their being useable in air without any reduction in their efficiency.

For base exchange above T_g, it is suggested that suitable lithium salts can be sprayed/coated onto the hot containers immediately after their release from the mould (or at parison stage). This is expected to crystallise β-eucryptite to a depth of 10 μm provided an optimised time-temperature protocol can be devised.

Table 8.1 summarises relative merits and demerits of the various techniques employed in the present investigation in terms of the level of strength enhancement, time, degree of deformation, optical quality, handling, cost and the potential.

TABLE 8.1
COMPARISON OF TECHNIQUES INVESTIGATED

Technique	Strength Enhancement MPa (%)	Temperature (°C)	Time (min)	Deformation	Optical Quality/ Opacity	Handling	Cost	Potential
Li -ion Base Exchange								excellent potential for container glass and other architectural glasses
Immersion in Sulphate Salt Bath	224 (16) 253 (32) 295 (54) 400 (108) 448 (133) 506 (163)	800	10 s 20 s 0.5 1 1.5 2	none none none slight noticeable vigorous	as pristine v. slight s.opaque opaque	medium	excellent	advantages include ease of application, cost saving, thin walled containers, lightweighting
Vapour Treatment								medium potential for container glass and other architectural glasses
LiBr	400 (104)	585	40	none		medium	excellent	
$AlBr_3$	355 (93)	550	30	none	as pristine	poor/ medium	medium	advantages include ease of application, cost saving, thin walled containers, lightweighting
LiBr + $AlBr_3$ + Heat Treat ment	328 (80) 376 (106) 400 (119)	550	10+60 20+60 30+60	none				toxicity may be a problem

TABLE 8.1 (contd)
COMPARISON OF TECHNIQUES INVESTIGATED

Technique	Strength Enhancement MPa (%)	Temperature (°C)	Time (min)	Deformation	Optical Quality	Handling	Cost	Potential
Surface Crystallisation by CVD Technique								
P_2O_5	205 (17)	600	60	none	as pristine	excellent/ medium	medium	poor potential for container glass and other architectural glasses - may be used for high value added products on a small scale
TiO_2	281 (58)							
$P_2O_5 + TiO_2$	215 (48)							
Combination Treatment								
TiO_2 (CVD) + LiBr	442 (121)	550	40	none	excellent	excellent/ medium	medium	poor/medium potential for container glass and other architectural glasses - may be used for high value added products on a small scale
$TiO_2 + P_2O_5$ + LiBr	370 (93)		40					
$TiO_2 + P_2O_5 + AlBr_3$	250 (36)		30					
$TiO_2+P_2O_5+AlBr_3+LiBr$	402 (120)		40					
Surface Crystallisation								
Airabrasion + Precipitation	300 (65)	670	180	none	mottled	excellent	medium	excellent to surface crystallise low TCE phase by surface destabilisation

In terms of manufacturing containers, the vapour treatment and the ion exchange are the most promising. From the standpoint of cost and efficiency, the primary constraints in both methods appear to be the difficulty in achieving a balance between the relative strength increase *versus* time and the reduction of wall thickness (20-30 % weight reduction). This should also include the appropriate stage where these methods can be introduced to the manufacturing process. In the case of vapour treatment, as mentioned earlier, since there is no loss of transparency or deformation, some of these objectives are easily achievable whilst the others are not. In particular, an overall time of 40 minutes, based on the temperature at the cold end (~ 650 °C), is not practicable in so far as the current container production methods are concerned. An effective time of 10-15 minutes is more realistic, since this is approximately the time required for the container to leave the mould at the hot end and travel to the cold end. This will obviously reduce the overall strength increase. However, if the base composition could be modified to higher level of alumina or lithia content and/or use may be made of nucleating agents such as P_2O_5 or TiO_2 to accelerate the formation of the low TCE phase, a comparable level of strength can still be achieved in a shorter time, provided the η -T is flexible for operational purposes. Also, if the exposure to vapour is possible at the hot end (but below the T_g) the rate of diffusion of Li into the glass will be faster and this will then reduce the time relative to strength enhancement. For $AlBr_3$ or a combined $AlBr_3$ and LiBr vapour treatment, the aspects described above would still apply.

For the method developed for base exchange using lithium salt, the time constraint can be eliminated altogether since the process takes place above the strain point of the glass and significant improvement in strength can be made in a relatively short time (i.e. 10-30 seconds). In contrast to the technique used in the present work, the time taken for normal ion exchange methods used in the container industry is between 10 and 20 hours for a comparable strength increase. Since the production methods are already available,

there should not be any problem in adapting the present process in the mainstream of container manufacturing. In this case, all the objectives outlined above could be met with the exception of handling of lithium based salts (LiBr, in particular) and associated possible toxicity problems; the use of other non-toxic lithium salt or variations thereof will minimise, if not eliminate, this concern. In case of dipping, it is suggested that the lithium salt is melted in a suitable container and the molten salt is maintained at a temperature above the annealing point but close to the softening point of the glass. If desired, compressional stress could be restricted to selected parts of the glass surface such as the rim or the base of the container. In this way, the process could be made cost effective since diffusion of lithium ions will occur, to a small extent, parallel with the surface as well as perpendicular to it and the boundary between the treated and untreated areas is not sharp enough to cause any splitting between the two regions. The spraying of the salt mixture, on the other hand, can be applied directly onto either the inner or the outer surface of the container, which will probably prove to be more convenient since the strengthening can be carried out at either the hot or the cold end.

Suggestion for further work

Some suggestions for future work are listed below:

- Future MOR measurements to be made on samples, with controlled abrasion following strength enhancement, to examine the effect of flaw sizes and simulate the handling characteristics of container glasses
- Further SIMS experiments to evaluate more fully the role of both lithium and aluminium diffusion in the LiBr and/or $AlBr_3$ vapour treated glasses

- MAS-NMR to provide insight into the role of phosphorus, added either to the bulk or as a surface destabiliser introduced by the CVD, in the P_2O_5 doped samples
- Following strengthening by vapour or ion exchange, regular 'Burst' testing of containers having diameter not less than 50 mm to be carried out to estimate the variability of strength data as well as to assess the mode of failure

REFERENCES

1. Rawson H, *IEEE Proc* **135** A 6 325
2. Staveley L.A.K 1955 Glass Delegacy of the University of Sheffield, p85
3. Turnbull D and Cohen M.H 1958 *J Chem Phys* **29** 1049
4. Turbull D 1956 in Solid State Physics vol 3 ed. F Seitz and D Turnbull Academic Press New York
5. Goldschmidt V M, *Skrifter Norske Videnskaps Akad* (Oslo) Math-Naturwiss. Kl 1926 **8** 7
6. Zachariasen W H, *J Amer Ceram Soc* **54** 3841
7. Warren B E, *J Appl Phys* 1937 **8** 645
8. Goodman C H L *Nature* **257** 1975 370; Glass Technology 28 1987 19
9. Tabata K *J Am Ceram Soc* **10** 1927 p6
10. Morey G W *J Amer Ceram Soc* **13** 1930 p683
11. Swift H R *J Amer Ceram Soc* **6** 1947 p165
12. Scott W D and Pask J A *J Amer Ceram Soc* **44** 1961 p181
13. Klingsberg C *J Amer Ceram Soc* **47** 1964 p97
14. Neely J E and Ernsberger F M *J Amer Ceram Soc* **49** 1966 p396
15. Bergeron C G and De Luca J P *J Amer Ceram Soc* **50** 1967 p116
16. Mattox D *J Amer Ceram Soc* **50** 1967 p683
17. Burnett D G and Douglas R W *Phys Chem Glasses* **12** 1971 p117
18. Stranad Z and Douglas R W *Phys Chem Glasses* **14** 1973 p33
19. Du P, Ding Z and Jiang Z *J Non-cryst Solids* **112** 1989 251
20. Bansal N D and Doremus R H *J Amer Ceram Soc* **66** 1983 p132
21. Zanotto E D, James PF and Craievich A F *J Mat Sc* **21** 1986 p305

22. Zanotto E D and Basso R *Ceramica* **32** 1986 117

23. Zanotto E D *J Non-cryst Solids* **129** 1991 183

24. Hishinuma A MSC dissertation MIT 1986

25. Stookey S D, Olcott J S, Garfinkel H M and Rothermel D L in Advances in Glass Technology VI Int. conf. Plenum NY 1962 p397

26. McMillan P W and Partridge G *UK Pat 1108 473*, 1968

27. McMillan P W and Partridge G *UK Pat 1322 796*, 1973

28. Partridge G and McMillan P W *Glass Technology* **15** 1974 p127

29. Adam R and McMillan P W *J Mat Sc* **17** 1982 2727

30. Donald I W *J Mat Sc* **24** 1989 4177

31. Kelly A in Strong Solids 2nd edn, Clarendon Press, Oxford 1973 p285

32. Inglis C E, *Trans Inst Nav Archit* **55** 219

33. Griffith A A, *Phil Trans Royal Soc* **A221** 163

34. Griffith A A, *Inst Int Cong Appl Mechanics*, Delft 1924 55

35. Stryjak A J Internal Report, Department of Physics, University of Warwick

36. Symmers C, Ward J B and Sugarman B *Phys Chem Glasses* **3** 1962 76

37. Brearley W Holloway D G *Phys Chem Glasses* **4** 1963 69

38. Proctor B R *Appl Mat Res* **3** 1964 28

39. Saha C K and Cooper A R *J Amer Ceram Soc* **67** 1984 C158

40. Mould R E *J Amer Ceram Soc* **43** 1960 160

41. Ray N H and Stacey M H *J Mat Sc* **4** 1969 73

42. Sozanski M R and Varshneya A K *Amer Ceram Soc Bull* **66** (11) 1987 1630

43. Longobardo A V, Sozanski M, Jain V and Varshneya A K Proc of the XIV International Congress on Glass vol 2, New Delhi, 1986 25-30

44. Longobardo A V, Jain V and Varshneya A K Proc of the ANSYS Conf, Pittsburgh 1987 7.78-7.86

45. Gardon R in Glass Science and Technology ed. D R Uhlmann and N J Kreidl Academic Press New York 1980 vol 5 145-216
46. Hirao K and Tomozawa M *J Amer Ceram Soc* **70** 1987 43
47. Sugarman M *J Mat Sc* **2** 1967 275
48. Davis M W, Smay G L and Wasylyk J S *Amer Ceram Soc Bull* **66**(11) 1987 1627-30
49. Smay G L *Amer Ceram Soc* **71**(4) 1988 C217-C219
50. Jackson J D J, Rand B and Rawson H *Verres Refract* **35**(2) 1981 257-61
51. Cunningham W C, Crouse K L and Telman RA *US Pat 91-708511 910531*
52. McCarthy L D and Rossell H *J Mat Sc* **28** 1993 6058
53. Ritter J E and Lin M R *Glass Technology* **32** (1) 1991
54. Daly P and Byers S *J Amer Ceram Soc* **73**(7) 1990 2111
55. Chen M, James P F, Jones F R, Dalton D A, Howard B H and Bedford B H *J Non Cryst Solids* **139**(3) 1992 185
56. James P F, Chen M and Jones F R *J Non Cryst Solids* **155** 1993 399
57. Wang T H and James P F *J Mat Sc* **26** 1991 354
58. Green D J *J Mat Sc* **19** 1984 2165-2171
59. Petticrew R W, Schott L E and Smith W E *US Patent 3490 984* 1970
60. Keifer W, Sack W and Krause D *US pat 3907 577,* 1975
61. Fine G J and Danielson P S *Phys Chem Glases* **29**(4) 1988 134
62. McMillan P W, Hodgson B P and Booth R E *J Mat Sc* **4** 1969 1029
63. McMillan P W, Partridge G and Darrant J G *Phys chem glasses* **10** 1969 153
64. Corning Glass Works *UK Patent 786 951* 1957
65. Philips Electronic and Associated Industries *UK Patent 1215 729* 1970
66. Kistler S S *J Amer Ceram Soc* **45** 1962 59
67. Bartholomew R F and Garfinkel H M in Glass Science and Technology ed. D R Uhlmann and N J Kreidl Academic Press New York 1980 vol 5 217-270

68. Corning Glass Works *UK Patent 966 732* 1964

69. Corning Glass Works *UK Patent 966 731* 1964

70. Marusak F J *US Patent 3301 649* 1967

71. PPG Company *UK Patent 1071 351* 1964

72. Zijlstra A L and Burgraaf A J *J Non Cryst Solids* **1** 49 1968

73. Zijlstra A L and Burgraaf A J *J Non Cryst Solids* **1** 163 1969

74. Saunders A E and Kubichan R E *US Patent 3433 611* 1969

75. Garfinkel H M and King C B *J Amer Ceram soc* **53** 1970 686

76. Donald I W and Hill M J C *J Mat Sc* **23** 1988 2797

77. Kobayashi K and Sato K *Glass technology* **19** 1978 66

78. Hill M J C and Donald W *Glass Technology* **30** 1989 123

79. Hood H P and Stookey S D *US Patent 2 779 136* 1957

80. Cornelissen J and Burgraaf A J in Proc VII Int Conf on Glass New York 1965 pp319.1-319.4

81. Ward J B, Sugarman B and Symmers C *Glass Technology* **6** 1965 90

82. Garfinkel H *Glass Industry* **50** 1969 28

83. Doyle C W and Marusak F J *US Patent 3524 737* 1970

84. Varshneya A K and Petti R J *J Amer Ceram Soc* **59** 1976 42

85. Rinehart D W *US Patent 4055 703* 1977

86. Kerper M J and Scuderi T G *J amer Ceram Soc* **49** 1966 613

87. Stroud J S *Glass Technology* **29** 1988108

88. Reinhart D W *US Pat 419 2689* 1980

89. Moiseev V V, Permyakov T V and Plotnikova *Glass Technology* **11** 1970 6

90. Glaverbel *UK Patent 1217 660* 1970

91. Yoko T, Kamiya K and Ishino Y and Sakka S *J Amer Ceram Soc* **69** 1984 C110

92. Capp J C and Shelby J E *J Amer Ceram Soc* **69** 1986 C110

93. Stookey S D in High Strength Materials ed. V F Zackay Wiley London 1965 669-681
94. Cheng Jijiian and Fang Zhi Yao *J Chinese silicate Soc* **4** 1965 160
95. Jiang Youmei and Jiang Linge *J Non Cryst Solids* **80** 1986 300
96. Zhang X, He Ouli, Xu C and Zheng Y *J Non Cryst Solids* **80** 1986 313
97. Manitz G, Finsterwald M, Heyn H and Rotermund H *German Patent DE 3729736 C2* 1988
98. Cheng Jiijan, Zhu Binfu, Jiang Youmei *J Non Cryst Solids* **80** 1986 317
99. *US Patent No 3,615,319*
100. Weber N *US Patent 3218 220* 1965
101. Surnes S *J Amer Ceram Soc* **56** 1973 514
102. Ohta H *J Non Cryst Solids* **24** 1977 61
103. Saha C K and Cooper A R *J Amer Ceram Soc* **67** 1984 C160
104. Abou-el-Leil M and Copper A R *Glass Technology* **21** 1980 57
105. Abou-el-Leil M and Copper A R *J Amer Ceram Soc* **64** 1981 141
106. Sane A Y and Cooper A R *J Amer Ceram Soc* **70** 1987 86
107. Rawson H *Glastech Ber* **61**(9) 1988 231-246
108. Stevels J M in Handbook der Physik vol XIII Springer 1962 pp510-645
109. Gehlhoff G and Thomas M Z *Tech Physik* **6** 1925 544
110. Gehlhoff G and Thomas M Z *Tech Physik* **7** 1926 105
111. Hlavac J in The Technology of Glass and Ceramics: An Introduction, Elsvier, 1983
112. Dietzel A and Bruckner R *Glastech Ber* **30** 1957 73
113. Lillie H R *J Amer Ceram Soc* **35** 1952 149
114. Littleton J T *J Soc Glass Tech* **24** 1940 176
115. Slavyanskii V T, Krestnikova E N and Boreyko V M *Steklo i Ker* **19** (11) 1962 18
116. Bruckner R and Demharter G *Glastech Ber* **48** 1975 12
117. Hagy H E *J Amer Ceram Soc* **46** 1963 95

118. Fulcher G S *J Amer Ceram Soc* **8** 1925339-355

119. Doremus R H Glass Science Wiley and Sons, NY 1973

120. Geiss E A and Knickerbocker S H *J Mat Sc Letters* **4** 1985 835

121. Gilman L and Rose A J in APL An interactive Approach 2nd edn Wiley New York1976 p249

122. Mackenzie J D *Trans Faraday Soc* **53** 1957 1488

123. Lakatos T, Johansson L-G and Simmingskold B, *Glass Technology* **13** (3)1972 p88

124. Shartsis L, Spinner S and Capps W 1952 *J Amer Ceram Soc* **35** 155-60

125. Scholze H Glas. Natur, Struktur und Eigenschaften 2nd edn, Springer, Berlin-Heidelberg-New York 1977

126. Morey G W 1954 The Properties of Glass 2nd edn Reinhold New York 591

127. Mazurin O V, Streltsina M V and Shvaiko-Shvaikovskya T P, in "The Properties of Glasses and Glass Forming Melts" Handbook of Glass Data 3 volumes, Elsevier 1983

128. Winter A *Verres refract* **13** (3) 1959 261

129. Winter A *Verres refract* **13** (6) 1959 293

130. Dingwall A G F and Moore H *J Soc Glass Tech* **37** 1953 316

131. Stryjak A J *unpublished work*

132. McMillan P W 1979 "Glass Ceramics" 2nd edition, Academic Press

133. George A G and Veasey J V *J Mat Sc* **7** 1972 1327

134. Pope M and Judd M D, Heyden Press London 1975

135. Klug H P and Alexander L E "X-ray Diffraction Procedures for Polycrystalline and Amorphous Materials" 2nd edition Wiley, New York 1974

136. Frank F C and Lawson B R *Proc Royal Soc* **A299** 1967 299

137. Stott, V H, Irvine E and Turner D *Proc Royal Soc* **A108** 1925 154

138. Napolitano A and Hawkins E G *J Researh National Bureau Standards* **68A** 1964 439-448

139. Napolitano A, Macedo P B and Hawkins E G *J Researh National Bureau Standards* **69A** 1965 449-455

140. Owens-Illinois Research Lab *J Amer Ceram Soc* **27** 1944 221

141. Lhota M *Private Communication*

142. Physical Properties Committee *J Soc Glass Tecnology* **40** 1956 83-104P

143 Volf M B in Chemical Approach to Glass, Glass Science and Technology 7, Elssevier 1984

144. Butaev A M, *Steklo i Keramika* **39** (8) 1982 15

145. Sendt A in Ion exchange and diffusion process in glass cited in Tober H *Glastech Ber* **33** 1960 33

146. Tober H *Glastech Ber* **33** 1960 33

147. White P *Phys Chem Glasses* **12** (1) 1971 11

148. Hoffman L and Weyl W *Glass Industry* **38** (2) 1957 81

149. Day D and Steinkamp W *J Amer Ceram Soc* **52** (11) 1969 571

150. Stookey S D *Ind Eng Chem* **51** (7) 1959 805

151. H Garfinkel *Glass Industry* **50** 1969 74

152. Hood H P and Stookey S D *US Patent 2 779 136* 1957

153. Rayleigh Lord *Phil Mag* **41** 1871 279, 497

154. Rayleigh Lord *Phil Mag* **47** 1899 375

155. Ostertag W, Fischer G R and Williams J P *J Amer Ceram Soc* **51** (11) 1968 651

Appendix I

PAGE NUMBERING AS ORIGINAL

SAFETY PROFILE: Contact with skin or living tissue can cause frostbite-like burns. This material is stable when very cold. Solid CO_2 goes directly (sublimes) to gaseous CO_2 which is mainly an asphyxiant. See also CARBON DIOXIDE.

LGM000 CAS:68476-85-7 *HR: 3*
LIQUEFIED PETROLEUM GAS
DOT: UN 1075

SYNS: LPG ◇ L.P.G. (OSHA, ACGIH) ◇ PETROLEUM GAS, LIQUEFIED

CONSENSUS REPORTS: Reported in EPA TSCA Inventory.

OSHA PEL: TWA 1000 ppm
NIOSH REL: TWA 350 mg/m³; CL 1800 mg/m³/15M
ACGIH TLV: TWA 1000 ppm
DOT Classification: Flammable Gas; Label: Flammable Gas.

SAFETY PROFILE: Olefinic impurities may lend a narcotic effect or it may act as a simple asphyxiant. A very dangerous fire hazard when exposed to heat or flame. Can react with oxidizing materials. To fight fire, use CO_2, dry chemical, water spray. Used as a fuel refrigerant, propellant, and raw material in chemical synthesis.

LGM200 *HR: 2*
LIQUIPRON

PROP: A yeast (CANDIDA MALTOSA) protein concentrate TOERD9 3,305,81

TOXICITY DATA with REFERENCE
orl-rat TDLo:15525 g/kg/3Y-C:CAR TOERD9 3,305,81
orl-rat TD:2628 g/kg/2Y-C:ETA,REP TOERD9 3,305,81

SAFETY PROFILE: Experimental reproductive effects. Questionable carcinogen with experimental carcinogenic and tumorigenic data. When heated to decomposition it emits acrid smoke and irritating fumes.

LGO000 CAS:7439-93-2 *HR: 3*
LITHIUM
DOT: UN 1415
SS: Li aw: 6.94

PROP: Silver-colored, light metal; mixture of isotopes Li^6 and Li^7. Mp: 179°, bp: 1317°, d: 0.534 @ 25°, vap press: 1 mm @ 723°. Sol in liquid ammonia. Keep under mineral oil or other liquid free from O_2 or water.

SYNS: LITHIUM METAL (DOT) ◇ LITHIUM METAL, IN CARTRIDGES (DOT)

CONSENSUS REPORTS: Reported in EPA TSCA Inventory.

DOT Classification: Flammable Solid; Label: Flammable Solid and Dangerous When Wet.

SAFETY PROFILE: See LITHIUM COMPOUNDS for a discussion of the toxicity of the lithium ion. See SODIUM for a discussion of the toxicity of metallic lithium.

A very dangerous fire hazard when exposed to heat or flame. The powder may ignite spontaneously in air. The solid metal ignites above 180°C. It will burn in oxygen, nitrogen, or carbon dioxide, and will continue to burn in sand or sodium carbonate. The use of most types of fire extinguishers (e.g., water, foam, carbon dioxide, halocarbons, sodium carbonate, sodium chloride, and other dry powders) may cause an explosion. Molten lithium is extremely reactive and attacks such inert materials as sand, concrete, and ceramics.

Explosive reaction with bromobenzene; carbon + lithium tetrachloroaluminate + sulfinyl chloride; diazomethane. Forms very friction- and impact-sensitive explosive mixtures with halogens [e.g., bromine; iodine (above 200°C)]; halocarbons (e.g., bromoform; carbon tetrabromide; carbon tetrachloride; carbon tetraiodide; chloroform; dichloromethane; diiodomethane; fluorotrichloromethane; tetrachloroethylene; trichloroethylene; 1,1,2-trichloro-trifluoroethane).

Violent reaction with acetonitrile; sulfur; mercury (potentially explosive); metal oxides [e.g., chromium (III) oxide (at 185°C); molybdenum trioxide (at 180°C); niobium pentoxide (at 320°C); titanium dioxide (at 200-400°C); tungsten trioxide (at 200°C); vanadium pentoxide (at 394°C)]; iron(II) sulfide (at 260°C); manganese telluride (at 230°C); hot water; bromine pentafluoride (may ignite with lithium powder); platinum (at about 540°C); trifluoromethyl hypofluorite (at about 170°C); arsenic; beryllium; maleic anhydride; carbides; carbon dioxide; carbon monoxide + water; chlorine; chromium; chromium trichloride; cobalt alloys; iron sulfide; diborane; manganese alloys; nickel alloys; nitric acid; nitrogen; organic matter; oxygen; phosphorus; rubber; silicates; $NaNO_2$; Ta_2O_5; Fe alloys; V; $ZrCl_4$; CHI_3; trifluoromethylhypofluorite.

Ignition on contact with carbon + sulfinyl chloride (when ground); nitric acid (becomes violent); viton (poly(1,1-difluorethylene-hexafluoropropylene); chlorine tri- and penta-fluorides (hypergolic reaction); diborane (forms a complex which is pyrophyoric); hydrogen (above 300°C).

Incandescent reaction with ethylene + heat; nitrogen + metal chlorides [e.g., chromium trichloride; zirconium tetrachloride; nitryl fluoride (at 200°C)]. Incompatible with atmospheric gases; bromine pentafluoride; diazomethane; metal chlorides; metal oxides; non-metal oxides.

When burned it emits toxic fumes of LiO_2 and hy-

droxide. Reacts vigorously with water or steam to produce heat and hydrogen. Can react vigorously with oxidizing materials. To fight fire, use special mixtures of dry chemical, soda ash, graphite. Note: water, sand, carbon tetrachloride and carbon dioxide are ineffective.

LGP875 CAS:1070-75-3 *HR: 3*
LITHIUM ACETYLIDE
mf: C_2Li_2 mw: 37.90

SAFETY PROFILE: Ignites and burns vigorously in fluorine; chlorine; phosphorus; selenium; or sulfur vapors. Ignites when heated in bromine or iodine vapors. When heated to decomposition it emits acrid smoke and fumes. See also LITHIUM COMPOUNDS and ACETYLIDES.

LGQ000 CAS:50475-76-8 *HR: 3*
LITHIUM ACETYLIDE COMPLEXED with ETHYLENEDIAMINE
DOT: NA 2813

SYN: LITHIUM ACETYLIDE-ETHYLENEDIAMINE COMPLEX

DOT Classification: Flammable Solid; Label: Flammable Solid and Dangerous When Wet.

SAFETY PROFILE: A very flammable, unstable mixture. When heated to decomposition it emits toxic fumes of NO_x. See also LITHIUM ACETYLIDE and 1,2-ETHANEDIAMINE.

LGS000 CAS:17476-04-9 *HR: 3*
LITHIUM ALUMINUM TRI-tert-BUTOXYHYDRIDE
mf: $C_{12}H_{18}AlLiO_3$ mw: 244.22

TOXICITY DATA with REFERENCE
ivn-mus LD50:32 mg/kg CSLNX* NX#00620

CONSENSUS REPORTS: Reported in EPA TSCA Inventory.

ACGIH TLV: TWA 2 mg(Al)/m^3

SAFETY PROFILE: Poison by intravenous route. When heated to decomposition it emits acrid smoke and irritating fumes. See also ALUMINUM and LITHIUM COMPOUNDS.

LGT000 CAS:7782-89-0 *HR: 3*
LITHIUM AMIDE
DOT: UN 1412
mf: H_2LiN mw: 22.97

PROP: White, crystalline solid or powder. Subl in NH_3 current. Insol in anhydrous ether, benzene, toluene. Mp: 380-400°. D: 1.178 @ 17.50.

SYNS: LITHAMIDE ◇ LITHIUM AMIDE, POWDERED (DOT)

CONSENSUS REPORTS: Reported in EPA TSCA Inventory.

DOT Classification: Flammable Solid; Label: Dangerous When Wet; Flammable Solid; Label: Flammable Solid.

SAFETY PROFILE: A powerful irritant to skin, eyes, and mucous membranes. Flammable when exposed to heat or flame. Ammonia is liberated and lithium hydroxide is formed when this compound is exposed to moisture. Reacts violently with water or steam to produce toxic and flammable vapors. Vigorous reaction with oxidizing materials. Exothermic reaction with acid or acid fumes. When heated to decomposition it emits very toxic fumes of LiO, NH_3, and NO_x. Used in synthesis of drugs, vitamins, steroids, and other organics. See also LITHIUM COMPOUNDS, AMIDES, AMMONIA, and LITHIUM HYDROXIDE.

LGU000 CAS:305-97-5 *HR: 3*
LITHIUM ANTIMONY THIOMALATE
mf: $C_{12}H_9O_{12}S_3Sb{\cdot}6Li$ mw: 604.78

SYNS: ANTHIOLIMINE ◇ ANTHIOMALINE ◇ LITHIUM ANTIMONIOTHIOMALATE ◇ MERCAPTOSUCCINIC ACID ANTIMONATE(III) HEXALITHIUM SALT ◇ MERCAPTOSUCCINIC ACID-S-ANTIMONY DERIVATIVE LITHIUM SALT ◇ MERCAPTOSUCCINIC ACID, THIOANTHIMONATE(III), DILITHIUM SALT ◇ 2,2',2''-STIBILIDYNETRIS(THIO)TRIS-BUTANEDIOIC ACID HEXALITHIUM SALT

TOXICITY DATA with REFERENCE
orl-hmn TDLo:11 mg/kg:GIT,MET JAMAAP 125,952,44
ivn-man TDLo:262 mg/kg/5W-I:CNS,SKN METRAZ 19,103,59
ipr-mus LD50:82 mg/kg AJTMAQ 25,263,45
ivn-mus LD50:181 mg/kg JPETAB 81,224,44

CONSENSUS REPORTS: Antimony and its compounds are on the Community Right-To-Know List.

OSHA PEL: TWA 0.5 mg(Sb)/m^3
ACGIH TLV: TWA 0.5 mg(Sb)/m^3
NIOSH REL: (Antimony) TWA 0.5 mg(Sb)/m^3

SAFETY PROFILE: Poison by intraperitoneal and intravenous routes. Human systemic effects by ingestion and intravenous routes: hallucinations, distorted perceptions, nausea or vomiting, skin dermatitis and fever. An anthelmintic agent. When heated to decomposition it emits very toxic fumes of SO_x, Sb, and LiO. See also ANTIMONY COMPOUNDS and LITHIUM COMPOUNDS.

LGV000 CAS:19597-69-4 *HR: 3*
LITHIUM AZIDE
mf: LiN_3 mw: 48.96

SAFETY PROFILE: The moist or dry salt explodes

when heated to 115-298°C. Forms very shock-sensitive explosive mixtures with alkyl nitrates or dimethylformamaide above 200°C. Incompatible with CS_2. When heated to decomposition it emits very toxic fumes of Li_2O and NO_x. See also AZIDES and LITHIUM COMPOUNDS.

LGV700 *HR: 3*
LITHIUM BENZENEHEXOXIDE
mf: $C_6Li_6O_6$ mw: 209.71

SAFETY PROFILE: Explodes on contact with water. When heated to decomposition it emits acrid smoke and irritating fumes. See also LITHIUM COMPOUNDS.

LGW000 CAS:553-54-8 *HR: 2*
LITHIUM BENZOATE
mf: $C_7H_5O_2 \cdot Li$ mw: 128.06

PROP: White, crystalline powder. Fairly sol in water. Somewhat sol in alc.

SYN: BENZOIC ACID, LITHIUM SALT

TOXICITY DATA with REFERENCE
orl-mus LD50:1198 mg/kg RPTOAN 33,266,70
scu-mus LD50:964 mg/kg RPTOAN 33,266,70

CONSENSUS REPORTS: Reported in EPA TSCA Inventory.

SAFETY PROFILE: Moderately toxic by ingestion and subcutaneous routes. When heated to decomposition it emits acrid smoke and irritating fumes. See also LITHIUM COMPOUNDS.

LGX000 CAS:4039-32-1 *HR: 3*
LITHIUM BIS(TRIMETHYLSILYL)AMIDE
mf: $C_6H_{18}LiNSi_2$ mw: 167.33

$$LiN[Si(CH_3)_3]_2$$

SAFETY PROFILE: Unstable in air. Ignites when compressed. Upon decomposition it emits toxic fumes of Li_2O and NO_x. See also LITHIUM COMPOUNDS, SILANE, and AMIDES.

LGY000 CAS:7550-35-8 *HR: 2*
LITHIUM BROMIDE
mf: BrLi mw: 86.85

PROP: White, hygroscopic, granular powder; sltly bitter taste. Mp: 549°, bp: 1265°, d: 3.46 @ 25°, vap press: 1 mm @ 748°. Very sol in alc, glycol; sol in ether, amyl alc. Keep well closed.

TOXICITY DATA with REFERENCE
scu-mus LD50:1680 mg/kg RPTOAN 33,266,70

CONSENSUS REPORTS: Reported in EPA TSCA Inventory.

SAFETY PROFILE: Moderately toxic by subcutaneous route. Large doses may cause central nervous system depression in humans. Chronic absorption may cause skin eruptions and central nervous system disturbances due to bromide. May also cause disturbed blood electrolyte balance. See also BROMIDES and LITHIUM COMPOUNDS.

LGZ000 CAS:554-13-2 *HR: 3*
LITHIUM CARBONATE (2:1)
mf: $CO_3 \cdot 2Li$ mw: 73.89

PROP: White, light alkaline, crystalline powder. D: 2.11 @ 17.5°; mp: 618°. Insol in alc. @ 17.5°.

SYNS: CAMCOLIT ◇ CANDAMIDE ◇ CARBOLITH ◇ CARBONIC ACID, DILITHIUM SALT ◇ CARBONIC ACID LITHIUM SALT ◇ CEGLUTION ◇ CP-15467-61 ◇ DILITHIUM CARBONATE ◇ ESKALITH ◇ HYPNOREX ◇ LIMAS ◇ LISKONUM ◇ LITHANE ◇ LITHICARB ◇ LITHINATE ◇ LITHIUM CARBONATE ◇ LITHOBID ◇ LITHONATE ◇ LITHOTABS ◇ NSC-16895 ◇ PLENUR ◇ PRIADEL ◇ QUILONUM RETARD

TOXICITY DATA with REFERENCE
dnd-hmn:fbr 500 mg/L MUREAV 169,171,86
msc-ham:lng 2 g/L MUREAV 169,171,86
orl-wmn TDLo:4256 mg/kg (1-38W preg):REP BMJOAE 3,233,73
orl-wmn TDLo:4900 mg/kg (1-35W preg):TER LANCAO 2,595,74
orl-wmn TDLo:3600 mg/kg/21W-C:CAR,BLD NEJMAG 302,808,80
orl-wmn TD:21 g/kg/3.5Y-C:CAR,END ANZJB8 10,62,80
orl-wmn TD:5940 mg/kg/47W-C:CAR,BLD AIMEAS 92,262,80
orl-man TD:6132 mg/kg/2Y-C:CAR,BLD HAEMAX 67,944,82
orl-man TDLo:8 mg/kg:GIT,SKN AJPSAO 141,909,84
orl-hmn TDLo:4111 mg/kg:CNS,GIT NEJMAG 287,867,72
orl-man TDLo:54 mg/kg NEMJAX 97,23,84
orl-wmn TDLo:120 mg/kg/12D-I JCLPDE 48,81,87
orl-man TDLo:1080 mg/kg/13W-I:SKN JCLPDE 47,330,86
unr-wmn TDLo:556 mg/kg/32D JAMAAP 213,865,70
orl-rat LD50:525 mg/kg KSRNAM 7,1273,73
ipr-rat LD50:156 mg/kg KSRNAM 7,1273,73
scu-rat LD50:434 mg/kg KSRNAM 7,1273,73
ivn-rat LD50:241 mg/kg KSRNAM 7,1273,73
orl-mus LD50:531 mg/kg RPTOAN 33,266,70
ipr-mus LD50:236 mg/kg KSRNAM 7,1273,73
scu-mus LD50:413 mg/kg RPTOAN 33,266,70
ivn-mus LD50:497 mg/kg KSRNAM 7,1273,73
orl-dog LD50:500 mg/kg 27ZQAG -,436,72

CONSENSUS REPORTS: Reported in EPA TSCA Inventory.

SAFETY PROFILE: Human carcinogenic data. Poison by intraperitoneal and intravenous routes. Moderately toxic by ingestion, and subcutaneous routes. Human systemic effects by ingestion: toxic psychosis, tremors, changes in fluid intake, muscle weakness, increased urine volume, nausea or vomiting, allergic dermatitis. Human reproductive effects by ingestion: effects on newborn including apgar score changes and other neonatal measures or effects. Human teratogenic effects by ingestion: developmental abnormalities of the cardiovascular system, central nervous system, musculoskeletal and gastrointestinal systems. An experimental teratogen. Experimental reproductive effects. Questionable carcinogen producing leukemia and thyroid tumors. Human mutation data reported. Used in the treatment of manic-depressive psychoses. Incompatible with fluorine. See also LITHIUM COMPOUNDS.

LHA000 CAS:12772-56-4 ***HR: D***
LITHIUM CARMINE
mf: $C_{22}H_{20}O_{13}$•Li mw: 499.36

TOXICITY DATA with REFERENCE
ipr-mus TDLo:100 mg/kg (female 8D post):TER
NNAPBA 270,56[illegible]
ipr-mus TDLo:100 mg/kg (female 8D post):REP
NNAPBA 270,56[illegible]

SAFETY PROFILE: An experimental teratogen. Experimental reproductive effects. When heated to decomposition it emits acrid smoke and irritating fumes. See also LITHIUM COMPOUNDS.

LHB000 CAS:7447-41-8 ***HR: 3***
LITHIUM CHLORIDE
mf: ClLi mw: 42.39

PROP: Cubic, white, deliquescent crystals. Mp: 605°, bp: 1350°, d: 2.068 @ 25°, vap press: 1 mm @ 547°.

SYNS: CHLORAT. LITU (POLISH) ◇ CHLORURE de LITHIUM (FRENCH)

TOXICITY DATA with REFERENCE
skn-rbt 500 mg 24H SEV 28ZPAK -,7,72
eye-rbt 100 mg 24H MOD 28ZPAK -,7,72
mrc-smc 9 mmol/L MUTAEX 1,21,86
dni-hmn:hla 70 mmol/L MUREAV 92,427,82
ipr-mus TDLo:320 mg/kg (female 6-7D post):REP
JPETAB 101,362,51
ipr-rat TDLo:1 g/kg (female 7-11D post):TER
CRSBAW 167,[illegible],73
ipr-mus TDLo:882 mg/kg/7D-I:NEO PWPSA8 22,343,79
orl-hmn LDLo:200 mg/kg/3D JAMAAP 139,688,49
orl-hmn TDLo:243 mg/kg/13D:CNS,GIT JAMAAP 139,688,49
orl-rat LD50:526 mg/kg APTOA6 47,351,86
ipr-rat LD50:514 mg/kg PetKP# 22DEC[illegible]
scu-rat LD50:499 mg/kg PetKP# 22DEC[illegible]
ice-rat LD50:4800 µg/kg PJPPAA 26,399[illegible]
orl-mus LD50:1165 mg/kg RPTOAN 33,[illegible]70
ipr-mus LD50:600 mg/kg JTBIDS 6,87,81
scu-mus LD50:828 mg/kg OYYAA2 7,413[illegible]
ivn-mus LD50:363 mg/kg OYYAA2 7,413[illegible]
ipr-cat LD50:492 mg/kg RPTOAN 42,9[illegible]9
scu-cat LDLo:450 mg/kg EQSSDX 1,1,75
orl-rbt LD90:850 mg/kg BEXBAN 74,914[illegible]
scu-rbt LDLo:531 mg/kg EQSSDX 1,1,75
scu-gpg LDLo:620 mg/kg EQSSDX 1,1,75
scu-pgn LDLo:513 mg/kg HBAMAK 4,[illegible]35
orl-qal LD50:422 mg/kg AECTCV 12,355,82

CONSENSUS REPORTS: Reported in EPA TSCA Inventory. EPA Genetic Toxicology Program.

SAFETY PROFILE: Human poison by ingestion. Experimental poison by intravenous and intracerebral routes. Moderately toxic by subcutaneous and intraperitoneal routes. Experimental teratogenic and reproductive effects. Human systemic effects by ingestion: somnolence, tremors, nausea or vomiting. An eye and severe skin irritant. Human mutation data reported. Questionable carcinogen with experimental neoplastigenic data. This material has been recommended and used as a substitute for sodium chloride in "salt-free" diets, but cases have been reported in which the ingestion of lithium chloride has produced dizziness, ringing in the ears, visual disturbances, tremors and mental confusion. In most cases, the symptoms disappeared when use was discontinued. Prolonged absorption may cause disturbed electrolyte balance, impaired renal function. Reaction is violent with BrF_3. When heated to decomposition it emits toxic fumes of Cl^-. Used for dehumidification in the air conditioning industry. Also used to obtain lithium metal. See also LITHIUM COMPOUNDS.

LHC000 CAS:6180-21-8 ***HR: 3***
LITHIUM CHLOROACETYLIDE
mf: C_2ClLi mw: 66.41

$$LiC{\equiv}CCl$$

SYN: LITHIUM CHLOROETHYNIDE

SAFETY PROFILE: Violently explosive when dry. When heated to decomposition it emits very toxic fumes of Li_2O and Cl^-. See also LITHIUM COMPOUNDS and ACETYLIDES.

LHD000 ***HR: 3***
LITHIUM CHROMATE
mf: $CrH_2O_4 \cdot 2Li$ mw: 131.90

PROP: Yellow, crystalline, deliquescent powder. Mp: $-2H_2O$ @ 150°.

SYNS: CHROMIC ACID, DILITHIUM SALT ◇ CHROMIUM LITHIUM OXIDE ◇ DILITHIUM CHROMATE

CONSENSUS REPORTS: Chromium and its compounds are on the Community Right-To-Know List.

ACGIH TLV: TWA 0.05 mg(Cr)/m³. Confirmed Human Carcinogen.

SAFETY PROFILE: A toxic material. Combustible when exposed to heat or flame. An oxidizer. It can react with reducing materials. Potentially explosive reaction with zirconium at 450-600°C. When heated to decomposition it emits toxic fumes of Li_2O. See also LITHIUM COMPOUNDS and CHROMIUM COMPOUNDS.

LHD099 ***HR: 3***
LITHIUM CHROMATE(VI)
mf: $CrLi_2O_4$ mw: 129.87

CONSENSUS REPORTS: Chromium and its compounds are on The Community Right-To-Know List.

SAFETY PROFILE: Potentially explosive reaction with zirconium when heated above 400°C. See also LITHIUM COMPOUNDS and CHROMIUM COMPOUNDS.

LHE000 ***HR: D***
LITHIUM COMPOUNDS

SAFETY PROFILE: Lithium oxide, hydroxide, carbonate, etc., are strong bases and their solutions in water are very caustic. Otherwise, toxicity of lithium compounds is a function of their solubility in water. The halide salts, except the fluoride, are highly soluble in water. The carbonate, phosphate, oxalate, and fluoride are relatively insoluble in water. Lithium ion has central nervous system toxicity. In industry, the most hazardous lithium compound is the hydride. It produces large amounts of hydrogen gas when exposed to water; this reaction can cause severe damage to exposed tissue. Some lithium compounds, particularly the carbonate, are used in psychiatry. The difference between therapeutic levels of lithium and toxic levels is small. Plasma lithium concentrations of 2 mmol/L are associated with toxic symptoms. Concentrations of 4 mmol/L can be fatal.

The initial effects of lithium exposure are tremors of the hands, nausea, micturition, slurred speech, sluggishness, sleepiness, vertigo, thirst, and increased urine volume. Effects from continued exposure are apathy, anorexia, fatigue, lethargy, muscular weakness, and changes in ECG. Long-term exposure leads to hypothyroidism, leukocytosis, edema, weight gain, polydipsia/polyuria (increased water intake leading to increased urinary output), memory impairment, seizures, kidney damage, shock, hypotension, cardiac arrhythmias, coma, death. Have been implicated in development of aplastic anemia. See also specific compounds, LITHIUM, and POTASSIUM COMPOUNDS.

LHE450 CAS:57880-27-7 ***HR: 3***
LITHIUM DIAZOMETHANIDE
mf: $CHLiN_2$ mw: 47.97

SAFETY PROFILE: The dry material is very explosive when exposed to air. When heated to decomposition it emits toxic fumes of NO_x. See also LITHIUM COMPOUNDS.

LHE475 CAS:816-43-3 ***HR: 3***
LITHIUM DIETHYL AMIDE
mf: $C_4H_{10}LiN$ mw: 79.07

$$LiN(CH_2CH_3)_2$$

SAFETY PROFILE: Ignites spontaneously in air. When heated to decomposition it emits toxic fumes of NO_x. See also LITHIUM COMPOUNDS and AMIDES.

LHE525 CAS:13529-75-4 ***HR: 3***
LITHIUM-2,2-DIMETHYLTRIMETHYLSILYL HYDRAZIDE
mf: $C_5H_{15}LiN_2Si$ mw: 138.21

$$LiN[Si(CH_3)_3]N[CH_3]_2$$

SAFETY PROFILE: Explosive reaction with 1:1 mixture of nitric and sulfuric acids; liquid ozone + oxygen. Hypergolic reaction with fuming nitric acid. Ignites on contact with fluorine. When heated to decomposition it emits toxic fumes of NO_x. See also LITHIUM COMPOUNDS and HYDRAZINE.

LHF000 CAS:7789-24-4 ***HR: 3***
LITHIUM FLUORIDE
mf: FLi mw: 25.94

PROP: Fine, white powder. Mp: 845°, bp: 1681°, d: 2.635 @ 20°, vap press: 1 mm @ 1047°. Sol in acids.

SYNS: LITHIUM FLUORURE (FRENCH) ◇ TLD 100

TOXICITY DATA with REFERENCE
orl-gpg LDLo:200 mg/kg MEIEDD 10,793,83
scu-frg LDLo:280 mg/kg CRSBAW 124,133,37

CONSENSUS REPORTS: Reported in EPA TSCA Inventory.

route. Experimental reproductive effects. When heated to decomposition it emits toxic fumes of NO_x and SO_x.

SJW475 CAS:127-58-2 ***HR: 2***
SODIUM SULFAMERAZINE
mf: $C_{11}H_{11}N_4O_2S{\cdot}Na$ mw: 287.32

PROP: Crystals; bitter, caustic taste. Hygroscopic. On prolonged exposure to humid air, it absorbs CO_2 with the liberation of sulfamerazine and becomes incompletely sol in water. Its solns are alkaline to phenolphthalein (pH 10 or more). One gram dissolves in 3.6 mL water. Slty sol in alc; insol in ether, chloroform.

SYNS: 4-AMINO-N-(4-METHYL-2-PYRIMIDINYL)-BENZENESULFONAMIDE MONOSODIUM SALT ◇ N^1-(4-METHYL-2-PYRIMIDINYL) SULFANILAMIDE SODIUM SALT ◇ SODIUM SULPHAMERAZINE ◇ SOLUBLE SULFAMERAZINE ◇ SOLUMEDINE ◇ SULFAMERAZINE SODIUM

TOXICITY DATA with REFERENCE
orl-mus LD50:2800 mg/kg AIPTAK 94,338,53
ipr-mus LD50:1522 mg/kg JPETAB 81,17,44
scu-mus LD50:1739 mg/kg JPETAB 81,17,44
ivn-mus LD50:900 mg/kg AIPTAK 94,338,53

CONSENSUS REPORTS: Reported in EPA TSCA Inventory.

SAFETY PROFILE: Moderately toxic by ingestion, subcutaneous, intraperitoneal, and intravenous routes. When heated to decomposition it emits toxic fumes of SO_x, NO_x, and Na_2O.

SJW500 CAS:1981-58-4 ***HR: 2***
SODIUM SULFAMETHIAZINE
mf: $C_{11}H_{11}N_4O_2S{\cdot}Na$ mw: 301.35

SYNS: 4-AMINO-N-(4,6-DIMETHYL-2-PYRIMIDINYL)BENZENESULFONAMIDE, MONOSODIUM SALT ◇ N^1-(4,6-DIMETHYL-2-PYRIDINYL)-SULFANILAMIDE, MONOSODIUM SALT ◇ (N^1-(4,6-DIMETHYL-2-PYRIMIDINYL)SULFANILAMIDO)SODIUM ◇ SODIUM SULFAMETHAZINE ◇ SODIUM SULFAMETHAZINE ◇ SODIUM SULFAMEZATHINE ◇ SULFADIMIDINE SODIUM ◇ SULFAMETHAZINE SODIUM ◇ SULMET ◇ VESADIN

TOXICITY DATA with REFERENCE
orl-mus LD50:2057 mg/kg JPETAB 81,17,44
ipr-mus LD50:974 mg/kg JPETAB 81,17,44
scu-mus LD50:1191 mg/kg JPETAB 81,17,44
ivn-mus LD50:728 mg/kg RPOBAR 2,329,70

CONSENSUS REPORTS: Reported in EPA TSCA Inventory.

SAFETY PROFILE: Moderately toxic by ingestion, intravenous, intraperitoneal, and subcutaneous routes. When heated to decomposition it emits very toxic fumes of NO_x, SO_x, and Na_2O.

SJY000 CAS:7757-82-6 ***HR: 2***
SODIUM SULFATE (2 : 1)
mf: $O_4S{\cdot}2Na$ mw: 142.04

PROP: White crystals or powder; odorless. Mp: 888°, d: 2.671. Sol in water, glycerin; insol alc.

SYNS: DISODIUM SULFATE ◇ NATRIUMSULFAT (GERMAN) ◇ SALT CAKE ◇ SODIUM SULFATE anhydrous ◇ SODIUM SULPHATE ◇ SULFURIC ACID, DISODIUM SALT ◇ THENARDITE ◇ TRONA

TOXICITY DATA with REFERENCE
orl-mus TDLo:14 g/kg (female 8-12D post):REP
TCMUD8 6,361,86
par-mus TDLo:60 mg/kg (female 8D post):TER
JPMSAE 62,1626,73
scu-mus TDLo:806 mg/kg/26W-I:ETA IVIVE4 1,39,87
orl-mus LD50:5989 mg/kg SKEZAP 4,15,63
ivn-mus LDLo:1220 mg/kg CLDND-

CONSENSUS REPORTS: Reported in EPA TSCA Inventory. EPA Genetic Toxicology Program.

SAFETY PROFILE: Moderately toxic by intravenous route. Mildly toxic by ingestion. An experimental teratogen. Experimental reproductive effects. Questionable carcinogen with experimental tumorigenic effects. Violent reaction with Al. When heated to decomposition it emits toxic fumes of SO_x and Na_2O. See also SULFATES.

SJY500 CAS:1313-82-2 ***HR: 3***
SODIUM SULFIDE (anhydrous)
DOT: UN 1385
mf: Na_2S mw: 78.04

PROP: Amorph, yellow-pink or white, deliq crystals. Mp: 1180°, d: 1.856 @ 14°.

SYNS: SODIUM MONOSULFIDE ◇ SODIUM SULPHIDE

CONSENSUS REPORTS: Reported in EPA TSCA Inventory.

DOT Classification: Label: Flammable Solid

SAFETY PROFILE: Flammable when exposed to heat or flame. Unstable and can explode on rapid heating or percussion. Reacts violently with carbon; diazonium salts; n,n-dichloromethylamine; p-nitroaniline diazonium salt; water. When heated to decomposition it emits toxic fumes of SO_x and Na_2O. See also SULFIDES.

SJZ000 CAS:7757-83-7 ***HR: 3***
SODIUM SULFITE (2 : 1)
mf: $O_3S{\cdot}2Na$ mw: 126.04

PROP: Hexagonal prisms or white powder; odorless with salty, sulfurous taste. Bp: decomp, d: 2.633 @ 15.4°. Sol in water; sltly sol in alc.

CONSENSUS REPORTS: Reported in EPA TSCA Inventory.

SAFETY PROFILE: Poison by intravenous route. Moderately toxic by ingestion. When heated to decomposition it emits very toxic fumes of Cl^- and NO_x.

CDT500 CAS:14007-07-9 *HR: 3*
CHLORHEXIDINE GLUCONATE
mf: $C_{22}H_{30}Cl_2N_{10}•7C_6H_{12}O_7$ mw: 1878.78

SYN: CHLORHEXIDIN GLUKONATU (CZECH)

TOXICITY DATA with REFERENCE
orl-mus LD50:1800 mg/kg CESTAT 74(5),392,74
ipr-mus LD50:22 mg/kg CESTAT 74(5),392,74

SAFETY PROFILE: Poison by intravenous route. Moderately toxic by ingestion. When heated to decomposition it emits very toxic fumes of NO_x and Cl^-.

CDT750 CAS:96-24-2 *HR: 3*
CHLORHYDRIN
DOT: UN 2689
mf: $C_3H_7ClO_2$ mw: 110.55

$ClCH_2CHOHCH_2$

PROP: Colorless liquid. Bp: 213° decomp, d: 1.326.

SYNS: α-CHLORHYDRIN ◇ CHLORODEOXYGLYCEROL ◇ 1-CHLORO-2,3-DIHYDROXYPROPANE ◇ 3-CHLORO-1,2-DIHYDROXYPROPANE ◇ α-CHLOROHYDRIN ◇ 1-CHLOROPROPANE-2,3-DIOL ◇ 1-CHLORO-2,3-PROPANEDIOL ◇ 3-CHLORO-PROPANE-1,2-DIOL ◇ 3-CHLORO-1,2-PROPANEDIOL ◇ 3-CHLORO-PROPYLENE GYLCOL ◇ 3,3'-DIHYDROXYISOPROPYL CHLORIDE ◇ 2,3-DIHYDROXYPROPYL CHLORIDE ◇ EPIBLOC ◇ GLYCERIN-α-MONOCHLORHYDRIN ◇ GLYCEROL CHLOROHYDRIN ◇ GLYCEROL-α-CHLOROHYDRIN ◇ GLYCEROL-α-MONOCHLOROHYDRIN ◇ GLYCERYL-α-CHLOROHYDRIN ◇ MONOCHLORHYDRIN ◇ MONOCHLOROHYDRIN ◇ α-MONOCHLOROHYDRIN ◇ U-5897

TOXICITY DATA with REFERENCE
eye-rbt 27 mg JRPFA4 24,267,71
mmo-ssp 100 mmol/L MUREAV 118,213,83
mma-ssp 300 mmol/L MUREAV 118,213,83
ipm-rat-orl 600 mg/kg/24D-C CUSCAM 44,193,75
mic-mus:lym 10 mmol/L PAACA3 21,74,80
orl-mky TDLo:1260 mg/kg (male 42D pre):REP JRPFA4 21,275,70
orl-rat TDLo:34580 mg/kg/72W-C:ETA JJIND8 67,75,81
orl-rat TDLo:26 mg/kg IPCLBZ 24,20,82
ihl-rat LCLo:125 ppm/4H JIHTAB 31,343,49
ipr-rat LDLo:10 mg/kg NCNSA6 5,9,53
orl-mus LD50:160 mg/kg AMIHAB 14,250,56
ipr-mus LD50:73 mg/kg JMCMAR 18,116,75
orl-bwd LD50:23700 μg/kg AECTCV 12,355,83

CONSENSUS REPORTS: Reported in EPA TSCA Inventory. EPA Genetic Toxicology Program.

DOT Classification: Poison B; Label: St. Andrews Cross.

SAFETY PROFILE: Poison by ingestion and intraperitoneal routes. Moderately toxic by inhalation. Experimental reproductive effects. An eye irritant. Questionable carcinogen with experimental tumorigenic data. Mutation data reported. A chemosterilant for rodents. Combustible when exposed to heat or flame. Reaction with perchloric acid forms a sensitive explosive product more powerful than glyceryl nitrate. When heated to decomposition it emits toxic fumes of Cl^-.

CDU000 CAS:7790-93-4 *HR: 3*
CHLORIC ACID
DOT: UN 2626/NA 2626
mf: $ClHO_3$ mw: 84.46

PROP: Colorless solution. Mp: $< -20°$, bp: decomp @ 40°, d: 1.282 @ 14.2°.

SYN: CHLORIC ACID, solution, containing not more than 10% acid (DOT)

CONSENSUS REPORTS: Reported in EPA TSCA Inventory.

DOT Classification: Oxidizer; Label: Oxidizer and Poison (NA2626); Oxidizer; Label: Oxidizer (UN2626)

SAFETY PROFILE: A poison. A strong irritant by ingestion and inhalation. Dangerous fire hazard; ignites organic matter upon contact. A very powerful oxidizing agent. Violent or explosive reaction with oxidizable materials. Aqueous solutions decompose explosively during evaporation. Solutions greater than 40% are unstable. Reacts violently with NH_3; Sb; Sb_2S_3; As_2S_3; Bi; CuS; PHI_4; SnS_2; SnS. Reaction with cellulose causes ignition after a delay period. Dangerous reaction with metal sulfides and metal chlorides (e.g., incandescent reaction with antimony trisulfide; arsenic trisulfide; tin(II)sulfide; tin(IV) sulfide; explosion on contact with copper sulfide). Reaction with metals (e.g., antimony; bismuth; iron) forms explosive products. When heated to decomposition it emits toxic fumes of Cl^-. See also CHLORATES and CHLORINE.

CDU250 *HR: D*
CHLORIDES

SAFETY PROFILE: Varies widely. Sodium chloride (table salt) has very low toxicity, while carbonyl chloride (phosgene) is lethal in small doses. Therefore, see specific entries. When heated to decomposition or on contact with acids or acid fumes, they evolve highly toxic chloride fumes. Some organic chlorides decompose to yield phosgene.

orl-rat LD50:1950 mg/kg KSRNAM 7,2413,73
ipr-rat LD50:1660 mg/kg OYYAA2 17,115,79
scu-rat LD50:8800 mg/kg OYYAA2 17,115,79
orl-mus LD50:879 mg/kg OYYAA2 17,115,79
ipr-mus LD50:200 mg/kg JDGRAX 16,7,85
scu-mus LD50:6870 mg/kg OYYAA2 17,115,79
orl-rbt LD50:1690 mg/kg 27ZQAG -,158,72

SAFETY PROFILE: Poison by intraperitoneal route. Moderately toxic by ingestion. An experimental teratogen. Other experimental reproductive effects. Human skin irritant. A tranquilizer. When heated to decomposition it emits very toxic fumes of NO_x and HBr.

BMO000 CAS:9001-00-7 ***HR: 3***
BROMELAIN

PROP: From pineapples *Ananas comosus* and *Ananas bracteatus* L. White to tan amorphous powder. Sol in water; insol in alc, chloroform, ether.

SYNS: ANANASE ◇ BROMELAINS ◇ BROMELIN ◇ E.C. 3.4.4.24 ◇ EXTRANASE ◇ INFLAMEN ◇ PLANT PROTEASE CONCENTRATE ◇ TRAUMANASE

TOXICITY DATA with REFERENCE
ipr-rat LD50:85200 µg/kg AIPTAK 145,166,63
ipr-rat LD50:85 mg/kg AIPTAK 145,166,63
ipr-mus LD50:37 mg/kg AIPTAK 145,166,63
ivn-mus LD50:30 mg/kg AIPTAK 145,166,63

CONSENSUS REPORTS: Reported in EPA TSCA Inventory.

SAFETY PROFILE: A poison via intraperitoneal and intravenous routes. When heated to decomposition it emits acrid smoke and fumes.

BMO250 CAS:15086-94-9 ***HR: 1***
BROMEOSIN
mf: $C_{20}H_8Br_4O_5$ mw: 647.92

SYNS: BROMOEOSIN ◇ BROMOFLUORESCEIC ACID ◇ C.I. 45380:2 ◇ C.I. SOLVENT RED 43 ◇ D&C RED No. 21 ◇ EOSIN ◇ EOSINE ◇ 2,4,5,7-TETRABROMO-3,6-FLUORANDIOL ◇ TETRABROMOFLUORESCEIN ◇ 2',4',5',7'-TETRABROMOFLUORESCEIN

TOXICITY DATA with REFERENCE
mrc-bcs 2 mg/disc TRENAF 27,153,76
scu-mus LDLo:450 mg/kg HBAMAK 4,1289,35
scu-frg LDLo:1 g/kg HBAMAK 4,1289,35

CONSENSUS REPORTS: IARC Cancer Review: Group 3 IMEMDT 7,56,87, Animal Inadequate Evidence IMEMDT 15,183,77. Reported in EPA TSCA Inventory.

SAFETY PROFILE: Mutation data reported. Incompatible with reducing agents. When heated to decomposition it emits very toxic fumes of Br^-. See also BROMIDES.

BMO325 CAS:611-75-6 ***HR: 3***
BROMHEXINE CHLORIDE
mf: $C_{14}H_{20}Br_2N_2 \cdot ClH$ mw: 412.64

SYNS: 2-AMINO-3,5-DIBROMO-N-CYCLOHEXYL-N-METHYLBENZENEMETHANAMINE MONOHYDROCHLORIDE (9CI) ◇ BISOLVON ◇ BISOLVON HYDROCHLORIDE ◇ BROMHEXINE HYDROCHLORIDE

TOXICITY DATA with REFERENCE
orl-rat LD50:6 g/kg GNRIDX 3,259,69
ipr-rat LD50:1680 mg/kg GNRIDX 3,259,69
orl-mus LD50:4800 mg/kg GNRIDX 3,259,69
ipr-mus LD50:2210 mg/kg GNRIDX 3,259,69
ivn-mus LD50:44 mg/kg GNRIDX 3,259,69

SAFETY PROFILE: Poison by intravenous route. Moderately toxic by other routes. When heated to decomposition it emits toxic fumes of Br^-, NO_x, and HCl.

BMO750 ***HR: 3***
BROMIDES

SAFETY PROFILE: The most common inorganic bromides are Na, K, NH_4, Ca and Mg bromides. Methyl and ethyl bromides are among the most common organic bromides. The inorganic bromides produce depression, emaciation, and, in severe cases, psychosis and mental deterioration. Bromide rashes (bromoderma), especially of the face and resembling acne and furunculosis, often occur when bromide inhalation or administration is prolonged. Organic bromides, such as methyl bromide and ethyl bromide, are volatile liquids of relatively high toxicity. See also specific compounds. When strongly heated they emit highly toxic fumes of Br^-.

BMO825 ***HR: D***
BROMINATED VEGETABLE (SOYBEAN) OIL

PROP: Pale yellow to dark brown viscous, oily liquid; bland or fruity odor and bland taste. Sol in alc, chloroform, ether, hexane, fixed oils; insol in water.

SYN: VEGETABLE (SOYBEAN) OIL, brominated

TOXICITY DATA with REFERENCE
orl-rat TDLo:9 g/kg (2W male 2W pre-14D post):REP TJADAB 28,309,83

SAFETY PROFILE: Experimental reproductive effects. When heated to decomposition it emits toxic fumes of Br^-.

BMP000 CAS:7726-95-6 ***HR: 3***
BROMINE
DOT: UN 1744
mf: Br_2 mw: 159.82

PROP: Rhombic crystals or dark red liquid. Fp: −7.3°,

SAFETY PROFILE: Poison by ingestion and intraperitoneal routes. A strong alkali. A severe eye, skin, and mucous membrane irritant.

Ignites in air above 288°C when exposed to spark. Potentially explosive reaction with aluminum chloride + bis(2-methoxyethyl) ether. Reacts with ruthenium salts to form a solid product which explodes when touched or on contact with water. Reacts to form dangerously explosive hydrogen gas on contact with alkali: water and other protic solvents (e.g., methanol; ethanol; ethylene glycol; phenol); aluminum chloride + bis(2-methoxyethyl)ether. Reacts violently with anhydrous acids (e.g., sulfuric; phosphoric; fluorophosphoric) to form diborane. Violent exothermic reaction with dimethyl formamide has caused industrial explosions. Mixtures with sulfuric acid may ignite. Incompatible with palladium; diborane – bis(2-methoxyethyl) ether; polyglycols; dimethylacetamide; oxidizers; metal salts; finely divided metallic precipitates of cobalt; nickel; copper; iron and possibly other metals. Emits flammable vapors on contact with acid fumes. Materials sensitive to polymerization under alkaline conditions, such as acrylonitrile, may polymerize upon contact with sodium borohydride. Avoid storage in glass containers. When heated to decomposition it emits toxic fumes of Na_2O. See also HYDRIDES, BORON COMPOUNDS, and SODIUM COMPOUNDS.

SFG000
SODIUM BROMATE CAS:7789-38-0 *HR: 3*
DOT: UN 1494
mf: $BrO_3 \cdot Na$ mw: 150.90

PROP: White crystals or crystalline powder. Odorless. Mp: 381°, d: 3.339 @ 17.5°.

SYNS: BROMATE de SODIUM (FRENCH) ◇ BROMIC ACID, SODIUM SALT ◇ DYETONE

TOXICITY DATA with REFERENCE
ipr-mus LD50:140 mg/kg COREAF 257,791,63
scu-dog LDLo:120 mg/kg SAPHAD 30,337,13
orl-rbt LDLo:250 mg/kg SAPHAD 30,337,13
ivn-rbt LDLo:360 mg/kg SAPHAD 30,337,13
scu-gpg LDLo:100 mg/kg SAPHAD 30,337,13

CONSENSUS REPORTS: Reported in EPA TSCA Inventory.

DOT Classification: Oxidizer; Label: Oxidizer

SAFETY PROFILE: Poison by ingestion, intravenous, subcutaneous, and intraperitoneal routes. A powerful oxidizer. Violent reactions with Al, As, C, Cu, oil, F_2, metal sulfides, organic matter, P, S. Mixtures with grease are shock-sensitive explosives at 120°C. When heated to decomposition it emits toxic fumes of Na_2O and Br^-. See also BROMATES.

SFG500 CAS:7647-15-6 *HR: 2*
SODIUM BROMIDE
mf: BrNa mw: 102.90

PROP: White crystals, granules or powder; saline bitter taste. D: 3.21, mp: 755°, volatilizes at higher temp.

SYNS: BROMIDE SALT of SODIUM ◇ BROMNATRIUM (GERMAN) ◇ SEDONEURAL

TOXICITY DATA with REFERENCE
orl-rat TDLo: [illegible] mg/kg (female 3-20D post): REP JOPSAM 19,1[illegible]
orl-rat LD50:3500 mg/kg JPETAB 55,200,35
orl-mus LD50:7000 mg/kg SMWOAS 85,305,55
scu-mus LD50:5020 mg/kg JPMSAE 50,858,61
orl-rbt LDLo:580 mg/kg 27ZIAQ -,243,73

CONSENSUS REPORTS: Reported in EPA TSCA Inventory.

SAFETY PROFILE: Moderately toxic by ingestion. Experimental reproductive effects. Incompatible with acids, alkaloidal and heavy metal salts. When heated to decomposition it emits toxic fumes of Br^- and Na_2O. See also BROMIDES.

SFG600 *HR: 3*
SODIUM BROMOACETYLIDE
mf: C_2BrNa mw: 126.92

$$NaC \equiv CBr$$

SAFETY PROFILE: An extremely shock-sensitive explosive. When heated to decomposition it emits toxic fumes of Br^- and Na_2O. See also ACETYLIDES.

SFJ500 CAS:64048-05-1 *HR: 3*
SODIUM BUTYLMERCURIC THIOGLYCOLLATE
mf: $C_6H_{11}HgO_2S \cdot Na$ mw: 370.81

SYN: S-(BUTYLMERCURIC)-THIOGLYCOLIC ACID, SODIUM SALT

TOXICITY DATA with REFERENCE
ipr-rat LDLo:[illegible] mg/kg JPETAB 35,343,29
ivn-rbt LDLo:[illegible] mg/kg JPETAB 35,343,29

CONSENSUS REPORTS: Mercury and its compounds are on the Community Right To Know List.

OSHA PEL: (Transitional: CL 1 mg/10m³) CL 0.1 mg(Hg)/m³ (skin)
ACGIH TLV: TWA 0.1 mg(Hg)/m³ (skin)
NIOSH REL: (Inorganic Mercury) TWA 0.05 mg(Hg)/m³

SAFETY PROFILE: Poison by intraperitoneal and intravenous routes. When heated to decomposition it emits very toxic fumes of Hg, SO_x, and Na_2O. See also MERCURY COMPOUNDS.

LHP000 CAS:68348-64-6 ***HR: 3***
LITHIUM SILICON
DOT: UN 1417

PROP: Solid. Composition: Li + Si.

DOT Classification: Flammable Solid; Label: Flammable Solid and Dangerous When Wet.

SAFETY PROFILE: A very dangerous fire hazard in the form of dust when exposed to heat or flame or by chemical reaction with moisture or acids. In contact with water, silane and hydrogen are evolved. Slightly explosive in the form of dust when exposed to flame. Will react with water or steam to produce flammable vapors; on contact with oxidizing materials, can react vigorously; on contact with acid or acid fumes, can emit toxic and flammable fumes. To fight fire, use CO_2, dry chemical. See also LITHIUM, SILICON, and POWDERED METALS.

LHQ000 ***HR: 3***
LITHIUM SODIUM NITROXYLATE
mf: $LiNNaO_2$ mw: 75.94

SAFETY PROFILE: Decomposes violently. When heated to decomposition it emits very toxic fumes of Li_2O, NO_x, and Na_2O. See also LITHIUM COMPOUNDS.

LHR000 CAS:10377-48-7 ***HR: 2***
LITHIUM SULFATE (2:1)
mf: $O_4S \cdot 2Li$ mw: 109.94

SYNS: LITHIUM SULPHATE ◇ SULFURIC ACID, DILITHIUM SALT ◇ SULFURIC ACID, LITHIUM SALT (1:2)

TOXICITY DATA with REFERENCE
mmo-smc 100 mmol/L MUREAV 117,149,83
mrc-smc 100 mmol/L MUREAV 117,149,83
orl-mus LD50:1190 mg/kg RPTOAN 33,266,70
scu-mus LD50:953 mg/kg RPTOAN 33,266,70

CONSENSUS REPORTS: Reported in EPA TSCA Inventory.

SAFETY PROFILE: Moderately toxic by ingestion and subcutaneous routes. Mutation data reported. When heated to decomposition it emits toxic fumes of SO_x. Used in photographic developer compositions and special high strength glass. See also LITHIUM SALTS and SULFATES.

LHR650 CAS:67849-02-9 ***HR: 3***
LITHIUM TETRAAZIDOALUMINATE
mf: $AlLiN_{12}$ mw: 202.00

SAFETY PROFILE: A shock-sensitive explosive. When heated to decomposition it emits toxic fumes of NO_x. See also AZIDES, LITHIUM COMPOUNDS, and ALUMINUM COMPOUNDS.

LHR675 ***HR: 3***
LITHIUM TETRAAZIDOBORATE
mf: $BLiN_{12}$ mw: 185.83

$$Li[B(N_3)_4]$$

SAFETY PROFILE: A powerful explosive sensitive to heat, impact, and friction. When heated to decomposition it emits toxic fumes of NO_x. See also AZIDES, LITHIUM COMPOUNDS, and BORON COMPOUNDS.

LHR700 CAS:14128-54-2 ***HR: 3***
LITHIUM TETRADEUTEROALUMINATE
mf: AlD_4Li mw: 41.99

SAFETY PROFILE: Ignites spontaneously in moist air. See also LITHIUM COMPOUNDS and ALUMINUM COMPOUNDS.

LHS000 CAS:16853-85-3 ***HR: 3***
LITHIUM TETRAHYDROALUMINATE
DOT: UN 1410/UN 1411
mf: $AlH_4 \cdot Li$ mw: 37.96

PROP: White, microcrystalline lumps.

SYNS: ALUMINUM LITHIUM HYDRIDE ◇ LITHIUM ALANATE ◇ LITHIUM ALUMINOHYDRIDE ◇ LITHIUM ALUMINUM HYDRIDE (DOT) ◇ LITHIUM ALUMINUM HYDRIDE, ETHEREAL (DOT) ◇ LITHIUM ALUMINUM TETRAHYDRIDE

CONSENSUS REPORTS: Reported in EPA TSCA Inventory.
ACGIH TLV: TWA 2 mg(Al)/m^3

DOT Classification: Flammable Solid; Label: Flammable Solid & Danger When Wet (UN1410); DOT Class: Flammable Liquid; Label: Flammable Liquid (UN1411); DOT Class: Flammable Solid; Label: Danger When Wet, Flammable Liquid (UN1411)

SAFETY PROFILE: Stable in dry air at room temperature. It decomposes above 125° forming Al, H_2 and lithium hydride. Very powerful reducer. Can ignite if pulverized even in a dry box. Reacts violently with air; acids; alcohols; benzoyl peroxide; boron trifluoride etherate; 2-chloromethyl furan + ethyl acetate; diethylene glycol dimethyl ether; diethyl ether; 1,2-dimethoxyethane, dimethyl ether; methyl ethyl ether; (nitriles − H_2O); perfluoro-succinamide; (perfluoro-succinamide + H_2O); tetrahydrofuran; water. To fight fire, use dry chemical, including special formulations of dry chemicals as recommended by the supplier of the lithium aluminum hydride. Do not use water, fog, spray or mist. Incompatible with bis(2-methoxy-ethyl)ether;

Appendix II

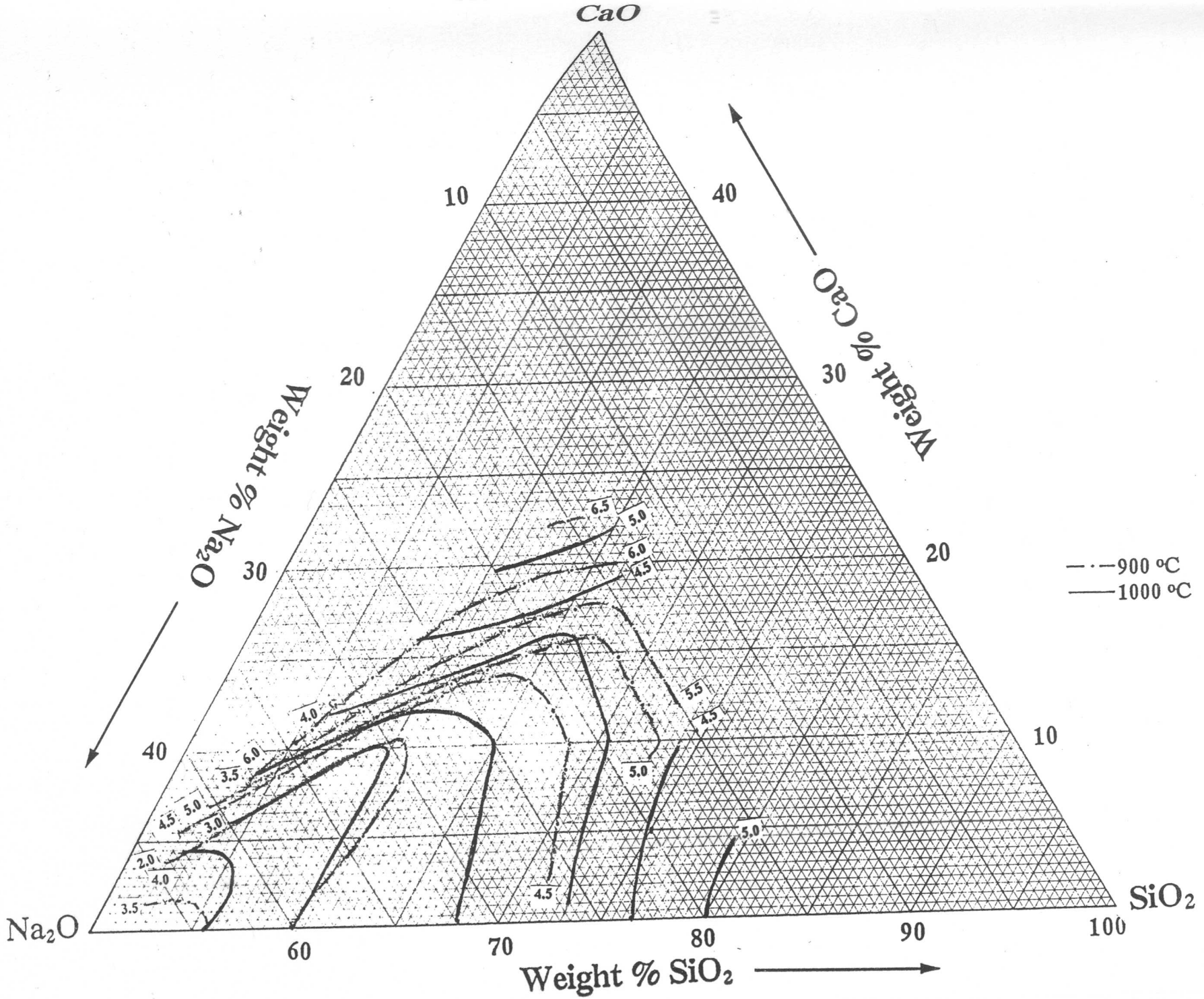
CaO
Weight % CaO
Weight % Na2O
Na2O
SiO2
Weight % SiO2
10
20
30
40
60
70
80
90
100
—·—900 °C
——1000 °C
6.5
5.0
6.0
4.5
4.0
5.5
3.5
5.0
4.5
3.0
2.0
4.0
3.5
4.5
5.0

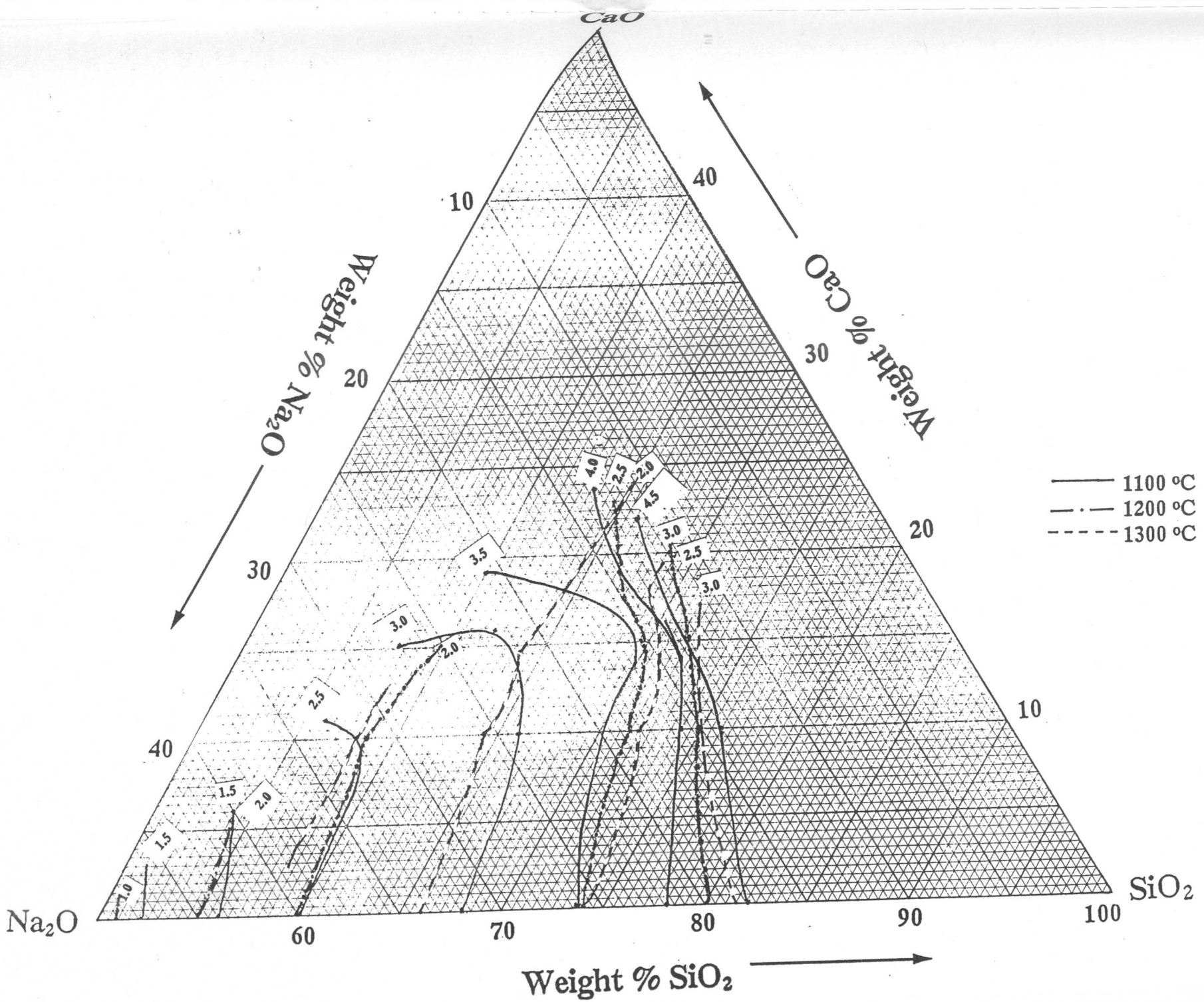
CaO
Weight % Na2O
Weight % CaO
Na2O
SiO2
Weight % SiO2
10
20
30
40
60
70
80
90
100
1100 °C
1200 °C
1300 °C
4.0
2.5
2.0
4.5
3.0
2.5
3.0
3.5
3.0
2.0
2.5
1.5
2.0
1.5
1.0

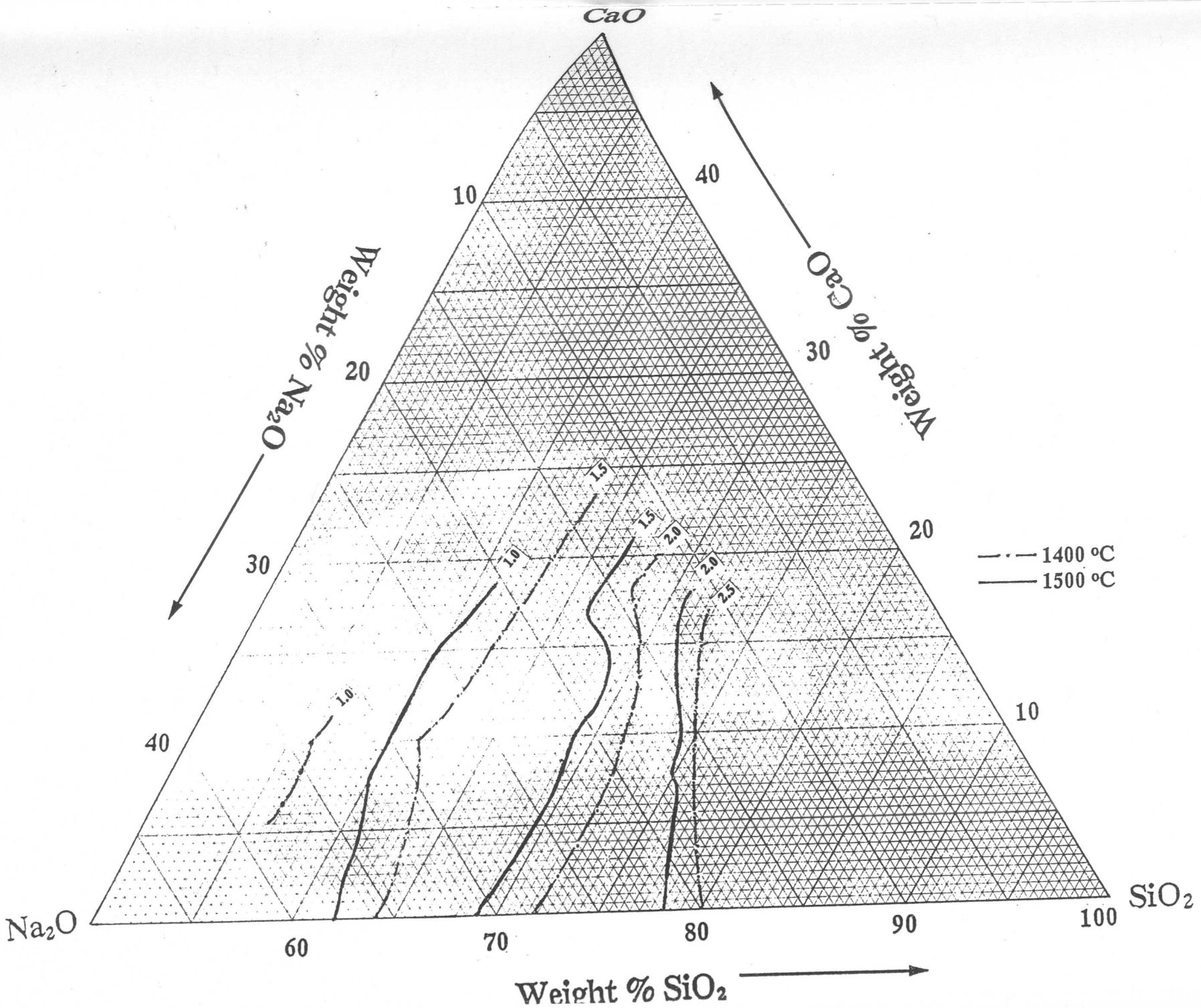
CaO
Weight % Na₂O
Weight % CaO
Na₂O
SiO₂
Weight % SiO₂
10
20
30
40
60
70
80
90
100
1.0
1.5
2.0
2.5
1400 °C
1500 °C

Appendix III

Sodium Bromide (NaBr)

(Ideal Gas) Mol. Wt. = 102.907

T, °K.	C_p°	S°	$-(F^\circ-H^\circ_{298})/T$	$H^\circ-H^\circ_{298}$	ΔHf	ΔFf	Log K_f
	cal. mole^{-1}deg.$^{-1}$			kcal. mole^{-1}			
0	.000	.000	INFINITE	- 2.344	- 32.276	- 32.276	INFINITE
100	7.475	48.726	65.090	- 1.637	- 32.278	- 35.880	78.412
200	8.255	54.221	58.413	- .838	- 32.396	- 39.684	43.056
298	8.681	57.628	57.628	.000	- 34.600	- 42.491	31.149
300	8.685	57.681	57.628	.016	- 34.612	- 42.548	30.989
400	8.833	60.203	57.971	.893	- 39.000	- 44.496	24.261
500	8.915	62.103	58.672	1.781	- 39.294	- 45.722	19.984
600	8.970	63.814	59.356	2.675	- 39.565	- 46.983	17.113
700	9.010	65.298	60.044	3.574	- 39.818	- 48.288	15.048
800	9.043	66.605	60.809	4.477	- 40.059	- 49.588	13.489
900	9.072	67.672	61.491	5.383	- 40.292	- 50.931	12.270
1000	9.096	68.678	62.138	6.291	- 40.523	- 51.655	11.269
1100	9.121	69.597	62.758	7.202	- 40.760	- 52.759	10.482
1200	9.144	70.092	63.327	8.115	- 44.238	- 53.382	9.722
1300	9.166	70.825	63.878	9.031	- 44.272	- 52.476	8.822
1400	9.187	71.505	64.399	9.948	- 44.304	- 51.568	8.050
1500	9.208	72.139	64.894	10.868	- 44.335	- 50.656	7.380
1600	9.228	72.736	65.369	11.790	- 44.363	- 49.743	6.796
1700	9.248	73.294	65.814	12.714	- 44.392	- 48.827	6.277
1800	9.268	73.823	66.266	13.639	- 44.419	- 47.911	5.813
1900	9.287	74.325	66.658	14.567	- 44.444	- 46.993	5.403
2000	9.307	74.802	67.053	15.497	- 44.470	- 46.076	5.035
2100	9.328	75.256	67.443	16.428	- 44.492	- 45.155	4.699
2200	9.349	75.691	67.799	17.362	- 44.516	- 44.233	4.394
2300	9.366	76.106	68.151	18.297	- 44.536	- 43.311	4.119
2400	9.383	76.505	68.491	19.235	- 44.556	- 42.386	3.868
2500	9.402	76.889	68.819	20.174	- 44.575	- 41.465	3.639
2600	9.421	77.258	69.137	21.115	- 44.595	- 40.539	3.427
2700	9.440	77.614	69.444	22.058	- 44.615	- 39.615	3.236
2800	9.459	77.957	69.742	23.003	- 44.635	- 38.688	3.020
2900	9.478	78.290	70.031	23.950	- 44.655	- 37.760	2.866
3000	9.497	78.611	70.312	24.900	- 44.676	- 36.832	2.683
3100	9.515	78.923	70.585	25.848	- 44.699	- 35.904	2.531
3200	9.534	79.225	70.850	26.802	- 44.722	- 34.973	2.388
3300	9.553	79.519	71.108	27.756	- 44.749	- 34.045	2.255
3400	9.572	79.805	71.360	28.713	- 44.776	- 33.117	2.129
3500	9.590	80.082	71.605	29.671	- 44.808	- 32.188	2.009
3600	9.609	80.353	71.844	30.631	- 44.844	- 31.258	1.897
3700	9.628	80.616	72.077	31.592	- 44.883	- 30.317	1.791
3800	9.647	80.873	72.304	32.556	- 44.926	- 29.378	1.690
3900	9.665	81.124	72.529	33.522	- 44.977	- 28.445	1.594
4000	9.684	81.369	72.747	34.489	- 45.033	- 27.509	1.503
4100	9.703	81.608	72.960	35.459	- 45.096	- 26.567	1.416
4200	9.721	81.842	73.169	36.430	- 45.169	- 25.628	1.333
4300	9.740	82.071	73.373	37.403	- 45.250	- 24.683	1.254
4400	9.759	82.296	73.573	38.378	- 45.342	- 23.745	1.179
4500	9.777	82.515	73.770	39.355	- 45.446	- 22.793	1.107
4600	9.796	82.730	73.962	40.333	- 45.564	- 21.846	1.038
4700	9.815	82.941	74.151	41.314	- 45.697	- 20.894	.972
4800	9.833	83.148	74.336	42.296	- 45.847	- 19.943	.908
4900	9.852	83.351	74.518	43.280	- 46.016	- 18.991	.847
5000	9.871	83.550	74.697	44.267	- 46.205	- 18.038	.788
5100	9.889	83.746	74.872	45.255	- 46.418	- 17.085	.731
5200	9.908	83.938	75.045	46.244	- 46.655	- 16.085	.676
5300	9.926	84.127	75.214	47.236	- 46.919	- 15.109	.623
5400	9.945	84.312	75.381	48.230	- 47.213	- 14.126	.572
5500	9.964	84.495	75.545	49.225	- 47.540	- 13.142	.522
5600	9.982	84.675	75.707	50.222	- 47.901	- 12.153	.474
5700	10.001	84.852	75.865	51.222	- 48.298	- 11.153	.428
5800	10.019	85.026	76.022	52.223	- 48.734	- 10.146	.382
5900	10.038	85.197	76.176	53.225	- 49.213	- 9.127	.338
6000	10.057	85.366	76.329	54.230	- 49.734	- 8.108	.295

Sept. 30, 1964

SODIUM BROMIDE (NaBr) (IDEAL GAS) MOL. WT. = 102.907

Ground State Configuration $^1\Sigma^+$

$\Delta H^\circ_{f\ 0}$ = -32.27 ± 0.50 kcal. mole^{-1}

$S^\circ_{298.15}$ = 57.628 cal. deg.$^{-1}$ mole^{-1}

$\Delta H^\circ_{f\ 298.15}$ = -34.40 ± 0.50 kcal. mole^{-1}

Electronic Levels and Quantum Weight

ϵ_i, cm.$^{-1}$	g_i
0	1

ω_e = 302.1 ± 4 cm.$^{-1}$ $\omega_e x_e$ = 1.50 cm.$^{-1}$ σ = 1

B_e = 0.1495 cm.$^{-1}$ α_e = 0.000859 cm.$^{-1}$ r_e = 2.5020 ± 0.0001 Å

Heat of Formation.

The heat of formation ($\Delta H^\circ_{f\ 298.15}$) was calculated from $\Delta H^\circ_{f\ 298.15}$ and $\Delta H^\circ_{s\ 298.15}$ for NaBr(c). The latter was derived from six sets of corrected vapor pressure data, due to the presence of dimeric species in the vapor, by both the second and third law methods. The results are listed as follows.

Investigator	Reaction	$\Delta H^\circ_{f\ 298.15}$, kcal. mole^{-1} Third Law Value	Second Law Value	$\Delta H^\circ_{f\ 298.15}$, kcal. mole^{-1}
Niwa[1]	NaBr(c) → NaBr(g)	51.97	50.31	-35.24
Cogin and Kimball[2]	NaBr(c) → NaBr(g)	52.26	52.14	-34.18
Mayer and Wintner[3]	NaBr(c) → NaBr(g)	52.89	65.30	-33.79**
Ruff and Mugdan[4]	NaBr(l) → NaBr(g)	46.45	47.48	-34.15
Vartenberg and Albrecht[5]	NaBr(l) → NaBr(g)	46.38	47.56	-34.15
Bloom et al.[6]	NaBr(l) → NaBr(g)	46.23	51.53	-34.88**

*Based on the average of the second and third law values.

**Only the third law value being used.

1 K. Niwa, J. Fac. Sci., Hokkaido Univ., Ser. III, 2, 201 (1938).

2 G. E. Cogin and G. E. Kimball, J. Chem. Phys. 16, 1035 (1948).

3 J. E. Mayer and I. H. Wintner, J. Chem. Phys., 9, 301 (1938).

4 O. Ruff and S. Mugdan, Z. anorg. allgem. Chem., 117, 147 (1921).

5 H. von Vartenberg and P. Albrecht, Z. Electrochem., 27, 162 (1921).

6 H. Bloom, J. O'M. Bockris, M. E. Richards and R. G. Taylor, J. Am. Chem. Soc. 80, 2044 (1958).

The value of $\Delta H^\circ_{f\ 298.15}$ for NaBr(g) adopted is the average value of the six $\Delta H^\circ_{f\ 298.15}$ values listed in the above table. The dissociation energy (D°_0) was calculated to be 88.28 kcal. mole^{-1} or 3.74 e.v. which is in good agreement with the values, D°_0 = 3.84 ± 1 and 3.85 e.v., reported by A. G. Gaydon, "Dissociation Energies", Chapman and Hall Ltd., London, 1953 and G. Herzberg, "Spectra of Diatomic Molecules", D. Van Nostrand Company, New York, 1950, respectively. According to L. Brewer, private communication, October 23, 1964, Gaydon's original reported value, D°_0 = 3.8, is an average of the value of 3.84 e.v. from atomic fluorescence and the value of 3.75 e.v. calculated for Gaydon by Brewer from pressure data available at that time.

Heat Capacity and Entropy.

The values of ω_e, $\omega_e x_e$, B_e and α_e were taken from S. A. Rice and W. Klemperer, J. Chem. Phys. 27, 573 (1957). The adopted bond distance (r_e) was reported by A. Honig, M. Mandel, M. L. Stitch and C. H. Townes, Phys. Rev. 96, 629 (1954), which was derived from microwave spectrum. By electron-diffraction method, the Na-Br bond distance was determined as 2.64 ± 0.01 Å by L. R. Maxwell, S. B. Hendricks and V. M. Mosley, Phys. Rev. 52, 968 (1937). The discrepancy may be due to the presence of a large proportion of dimer at the higher pressures used in the electron-diffraction determination. The ground state configuration was reported by G. Herzberg, loc. cit.

BrNa

Sodium Monoxide (Na_2O)

rystal) GFW = 61.979

T, °K	Cp°	S°	−(G°−H°298)/T	H°−H°298	ΔHf°	ΔGf°	Log Kp
	gibbs/mol			kcal/mol			
0	.000	.000	INFINITE	0.000	99.780	99.780	INFINITE
100	7.938	3.978	36.237	0.685	99.652	99.662	211.212
200	14.533	11.761	19.387	1.529	99.815	99.655	102.341
298	16.516	17.935	17.935	.000	99.900	99.600	64.418
300	16.550	18.038	17.936	.031	99.900	99.550	63.446
400	18.111	23.017	18.604	1.765	101.209	97.329	47.719
500	19.278	27.219	19.017	3.666	101.174	93.858	36.654
600	20.165	30.854	21.163	5.648	100.993	88.618	29.189
700	21.236	34.073	23.092	7.735	100.787	77.063	24.041
800	21.819	36.968	24.586	9.869	100.362	73.668	20.118
900	22.251	39.566	26.168	12.005	99.923	70.327	17.078
1000	22.686	41.915	27.576	14.145	99.467	67.062	14.654
1100	23.026	44.064	29.004	17.051	98.572	63.879	12.692
1200	23.334	46.021	30.305	19.365	144.536	59.433	10.697
1300	23.611	50.883	31.795	24.567	146.783	52.938	8.680
1400	23.867	52.652	33.205	26.681	139.835	46.217	7.215
1500	24.106	54.347	34.547	28.339	138.806	39.564	5.768
1600	24.336	55.976	35.819	31.762	137.478	32.875	4.504
1700	24.554	57.552	37.031	34.206	136.860	26.468	3.490
1800	24.765	59.541	38.188	36.672	135.837	19.983	2.474
1900	24.969	59.906	39.296	39.159	134.792	13.574	1.561
2000	25.169	61.192	40.359	41.666	133.731	7.224	.748

June 30, 1962; June 30, 1968

SODIUM MONOXIDE (Na_2O) (CRYSTAL) GFW = 61.979

$S^\circ_{298.15}$ = 17.935 gibbs/mol

$T_t(\gamma \rightarrow \beta)$ = 1023.2°K

$T_t(\beta \rightarrow \alpha)$ = 1243.2°K

T_m = 1405.2°K

ΔHf°_0 = -98.74 ± 1.0 kcal/mol

$\Delta Hf^\circ_{298.15}$ = -99.90 ± 1.0 kcal/mol

$\Delta Ht^\circ(\gamma \rightarrow \beta)$ = 0.42 kcal/mol

$\Delta Ht^\circ(\beta \rightarrow \alpha)$ = 2.85 kcal/mol

ΔHm° = 11.4 kcal/mol

Heat of Formation

The enthalpy change of the reaction $Na_2O(c) + H_2O(l) = 2NaOH(aq)$ has been determined by Matsui (1, 2), Roth (3, 4) and Rengade (5). Based on their reported ΔHr° values, the corresponding ΔHf°_{298} for $Na_2O(c)$ are calculated, using $\Delta Hf^\circ_{298}(H_2O, l)$ = -68.315 kcal/mol obtained from U. S. Natl. Bur. Std. Tech. Note 270-1, 1965, and $\Delta Hf^\circ_{298}(NaOH, nH_2O)$ derived from JANAF $\Delta Hf^\circ_{298}(NaOH, c)$ and ΔH_{soln} and ΔH_{dil} reported by V. B. Parker, U. S. Natl. Bur. Std. NSRDS-NBS 2, 1965. The sample employed by Matsui was prepared by the method of Rengade (7) and contains $Na_2O_2(c)$ and Na(c) as impurities. The sample used by Roth also contains 3.96 per cent (by weight) $Na_2O_2(c)$. Corrections in the reported results for such impurities have been made by the authors. However, in order to obtain better results, more measurements using purer samples are necessary. The enthalpy change of the reaction $2Na(c) + H_2O(l) = Na_2O(c) + H_2(g)$ was calculated by Rengade (5) from his measurements (5) incorporating with ΔHr = -85.2 kcal/mol for the reaction $2Na(c) + 2H_2O(l) = 2NaOH(aq) + H_2(g)$ determined by Joannis (8). The value ΔHf°_{298} = -94.9 kcal/mol is derived from the data of Forcrand (6) using $\Delta Hf^\circ_{298}(Na_2O_2, c)$ = -122.66 kcal/mol. The results are presented in the table below.

Brewer (11) determined the equilibrium constants, 918-1467°K, for the vaporization of $Na_2O(c)$, using an effusion method. The Na_2O vapor consists predominately of Na(g) and $O_2(g)$ molecules with any oxide molecules being not important. The Na/O ratio was not measured and assumed to be 2/1 in all calculations on Na_2O. Based on the reported data, we derive the equilibrium constants for the reaction $Na_2O(c) = 2Na(g) + 1/2O_2(g)$ and evaluate the third law ΔHr°_{298} as 117.1 ± 10 kcal/mol. From this ΔHr°_{298} value, we obtain $\Delta Hf^\circ_{298}(Na_2O, c)$ = -65.6 ± 10 kcal/mol, employing ΔHf°_{298} = 25.75 kcal/mol for Na(g). The value -65.6 kcal/mol is not consistent with the other values described above. This may be caused by an invalid assumption used in the calculation.

The heat of formation at 298°K for $Na_2O(c)$ is tentatively selected as -99.90 ± 1.0 kcal/mol.

Investigator	Reaction	ΔHr°, kcal/mol	ΔHf°_{298}, kcal/mol
1. Matsui (1929)	$Na_2O(c)+H_2O(l) = 2NaOH(7890\ H_2O)$	-56.61 ± 0.16	-100.08
2. Matsui (1929)	$Na_2O(c)+H_2O(l) = 2NaOH(4600\ H_2O)$	-56.70 ± 0.07	-99.89
3. Roth (1947)	$Na_2O(c)+H_2O(l) = 2NaOH(825\ H_2O)$	-56.03 ± 0.13	-100.55
4. Roth (1948)	$Na_2O(c)+H_2O(l) = 2NaOH(825\ H_2O)$	-55.98 ± 0.13	-100.60
5. Rengade (1907)	$Na_2O(c)+H_2O(l) = 2NaOH(aq)$	-56.50	-100.09
	$2Na(c)+H_2O(l) = Na_2O(c)+H_2(g)$	-28.70	-97.07
6. Forcrand (1900)	$Na_2O(c)+1/2O_2(g) = Na_2O_2(c)$	-27.76	-94.90

Heat Capacity and Entropy

The low temperature heat capacities, 15-380°K, were obtained from Furukawa (9). We make the corrections in the reported Cp values for impurity $Na_2CO_3(c)$ 2.33 per cent (by weight), analyzed by Grimley (10). The effect on heat capacity due to the presence of Na_2O_2(0.91 per cent) impurity is insignificant. Using the smoothed low temperature Cp data the $S^\circ_{298.15}$ is calculated, based on S°_{15} = 0.0122 eu.

Grimley (10) measured the high temperature enthalpies, 380.1-1174.6°K, with a copper block drop-type calorimeter. The enthalpies for the γ phase, 380.1-980.4°K, are joined smoothly with the low temperature data and extrapolated to 1023.2°K (the γ → β transition temperature). The enthalpies above 1023.2°K are obtained by extrapolation. The enthalpies measured at 1078.3 and 1174.6°K by Grimley are unreasonably large, and are not adopted.

Transition Data

The transition temperature and heats of transition were determined calorimetrically by Bouasis (12) who used a very pure sample. The adopted ΔHt° = 0.42 and 2.85 kcal/mol, are averages of the derived values, 0.38 - 0.48 and 2.7 - 3.0 kcal/mol, respectively.

Melting Data

T_m and ΔHm° were obtained from Bouasis (12). The adopted ΔHm° is an average of the reported 10.8-12.0 kcal/mol. T_m has been reported as 1193 and 1190 ± 10°K by Bunzel (13) and Brewer (11), respectively, which are not adopted.

References

1. M. Matsui and S. Oka, J. Soc. Chem. Ind. (Japan) 32, 78 (1929).
2. M. Matsui and S. Oka, J. Soc. Chem. Ind. (Japan) 32, 83 (1929).
3. W. A. Roth and M. L. Kaule, Z. Anorg. Chem. 253, 382 (1947).
4. W. A. Roth, Z. Anorg. Chem. 256, 324 (1948).
5. E. Rengade, Compt. Rend. 144, 236 (1907).
6. de Forcrand, Compt. Rend. 130, 1465 (1900).
7. E. Rengade, Compt. Rend. 147, 1152 (1908).
8. Joannis, Ann. Chim. Phys. 12; 376 (1887).
9. G. T. Furukawa, private communication, National Bureau of Standards, November 13, 1967.
10. R. T. Grimley and J. L. Margrave, J. Phys. Chem. 64, 1703 (1960).
11. L. Brewer and J. Margrave, J. Phys. Chem. 59, 921 (1955).
12. E. Bouasis, G. Papin and A. P. Rollet, Compt. Rend. Ser. C 262, 1051 (1966).
13. E. G. Bunzel and E. J. Kohlmeyer, Z. Anorg. Chem. 241, 1 (1947).